Mineralogy and Trace Element Variations in Cu-(Fe) sulphides of the Munda Resource, Prominent Hill:
Application for mine scale exploration and ore genesis

Todd Williams – a1185081

School or Earth and Environmental Science, University of Adelaide, South Australia, 5005

Phone: 0422225211

Email: Todd.williams@student.adelaide.edu.au

Supervisors

Cristiana L. Ciobanu, Nigel J. Cook

School or Earth and Environmental Science, University of Adelaide, South Australia, 5005

ABSTRACT

The Prominent Hill Iron-Oxide Copper-Gold deposit is situated on the southern margin of the Mount Woods Inlier, South Australia. The western Munda Au ± Cu resource is an extensional ore body governed by a subvertical, N-dipping, E-W-striking terrane-boundary. Since its discovery, debate has been focused on the distribution of principal ore components throughout the deposit, with Munda containing endowments of Au not present elsewhere at Prominent Hill. The present study attempts to unravel a complex history of source-fluid chemistry from trace/minor element concentrations in bornite-chalcocite determined by *in situ* laser-ablation ICP mass spectroscopy (LA-ICP-MS). One goal of the work was to establish if distinctions could be made between the mineralogy and textures present in the high-grade Munda gold resource with those elsewhere in the deposit.

By integrating microscopy and electron probe microanalysis with the minor element geochemistry it has been determined that formation of purple bornite predates steely hematite alteration and thus represents stage I of mineralisation. The LA-ICP-MS data shows important concentrations of Au (up to 12 ppm) reside in purple bornite in solid solution or as submicroscopic inclusions. Experimental data also suggest gold saturation occurred at temperatures <400˚C. Concentrations of >1 wt.% Se and Pb, 3208 ppm Te, 974 ppm Bi and 114 Ag have also been documented. Exsolution of clausthalite (PbSe) from purple bornite provides textural evidence for simultaneous deposition favouring a single fluid for the input of exotic elements (i.e. Pb and Se) and metal elements (Au and Ag).

Two principal sequences are constrained by textural analysis. Sequence (1a) Type-A purple bornite → Type-B purple bornite → chalcopyrite illustrates the remobilisation of Cu and crystal lattice-bound Au from mineral-fluid interaction via dissolution. Alternatively sequence (2a) purple bornite → blue chalcocite → white chalcocite shows proximal-to-breccia Cu enrichment via coupled dissolution-reprecipitation reactions (stage II). Microprobe data show that significant fluorine concentrations (0.36 a.p.f.u; total negative charge of 22) are present in Munda sericite and suggest alkali-fluoride complexes have played a role in ore transportation and formation, as well as the development of pervasive sericitization in hydrothermal alteration profiles. Concentrations of Ag in chalcocite show promise for distal-to-source vectoring and suggest grey chalcocite formed during stage III.

Investigations on gold mineralogy show two assemblages are present; native gold forms with chalcopyrite-loellingite and occurs with various Co-Ni-Fe-arsenides, bismuth, Y-bearing coffinite and coffinite. In addition three phases in the system Au-Cu are identified; symplectic intergrowths of unnamed Au_3Cu and Au_9Cu form an assemblage with chalcocite and minor bornite, and tetraauricupride (AuCu) forms homogeneous grains. All three phases rarely occur in nature and have implication for a S-deficient ore forming system.

INTRODUCTION

Prominent Hill is a hematite-rich Cu-Au deposit consistent with the Iron-Oxide-Copper-Gold (IOCG) *sensu stricto* classification as introduced by Hitzman (1992) and later reviewed by Hitzman (2008) and Groves *et al.* (2010). The deposit is located in southern extension of the Mount Woods Domain (MWD) and is situated approximately 650 km northwest of Adelaide, South Australia (Freeman & Tomkinson 2010). Its discovery in 2001 was based on a conceptual model developed from geological, geophysical and petrophysical data pertaining to the Olympic Dam deposit (Belperio & Freeman 2004).

Prominent Hill consists of three ore bodies that are governed by terrane- to province-scale faults and crustal dilations. The current total resource of 283 Mt @ 0.9% Cu and 0.8g/t Au comprises the Malu Cu-Au deposit, the western Ankata Cu- resource and the western Munda Au ± Cu resource. The Munda resource comprises an extensional ore body that delineates the structural corridor joining the proximal Malu Cu-Au deposit to the western Ankata Cu deposit.

Since its discovery, collaboration studies began on the mine scale encompassing structural setting (Belperio & Freeman, 2004) metallogenesis (Belperio *et al.* 2007); structural analysis of the host sequence (Walsh 2010) and of the mine tenement (Holcombe 2010); fluid inclusion (Schlegel 2010); and paragenesis (Benavides 2010). Despite this, there is still uncertainty on the source of principal ore components (i.e. Cu, Au, and U) and the metallogenic processes leading to ore formation. Regarding the Munda resource, there still remains a dearth of knowledge on; (1) the mineralogy and (2) the processes that have permitted enrichments of Au that are not present elsewhere at Prominent Hill.

The purpose of this contribution is two-fold. Firstly, the mineralogical framework of the Munda resource is reported in accordance to sampled intervals of recent exploration drill core. This includes an inventory of sulphides and other ore minerals, their distribution, and textural properties reported via optical and scanning electron microscopy (SEM). Secondly, using Laser Ablation-Inductively Coupled-Mass Spectroscopy (LA-ICP-MS) we aim to classify the trace element geochemistry of major Cu-carries bornite and chalcocite to elucidate the fluid chemistry relating to ore formation. From the electron microprobe technique, we also present a comprehensive and systematic study of mica geochemistry at the Munda resource. The halogen content of mica permits the estimation of the fluorine fugacity. The combined results contribute to our understanding of metal transportation and deposition at the Munda resource.

GEOLOGICAL SETTING

The Gawler Craton

The Gawler craton is a poorly exposed Mesoarchaean to Mesoproterozoic terrain comprising fourteen geological domains that are characterised by their tectono-stratigraphic history and geophysical signatures (Hayward & Skirrow 2010). The composite geology (Figure 1a) and tectonic evolution of the craton is comprehensively covered within Hand *et al.* (2007). Hand *et al.* (2007) broadly attribute two episodes of major magmatism and crustal mantle evolution to the development of the Gawler Craton. An interval within the Archean (ca. 2550 – 2500 Ma) is coeval with the development of the central-western craton and representative metasedimentary sequences and banded iron formations (BIF) of the Mulgathing and Sleaford Complexes. The remaining units are composed of Paleo- to Mesoproterozoic (ca. 2000 – 1580 Ma) rocks that flank the northern- and eastern-extensions of the craton. Within this interval, two periods of basin development (2000 to 1690 Ma and 1690 to 1500 Ma) and the 1730 to 1690 Ma Kimban and 1570 to 1540 Ma Karan orogenies define the regional fabric and emplacement of batholithic complexes.

The emplacement of the ca. 1590 Ma Hiltaba suite granitoids and co-magmatic bimodal Gawler Range volcanics (GRV) temporally and spatially overlap the formation of the Olympic IOCG province and associated Cu-Au±U±REE alteration and mineralisation (Skirrow *et al.* 2002; Hayward & Skirrow 2010). The Hiltaba Suite comprises highly fractionated granite to granodiorite (>70% SiO_2), with accompanying minor, but spatially widespread coeval mafic to ultramafic intrusions (Porter 2010b). Hiltaba suite plutons are predominantly A-type, are more oxidised, and geochemically enriched in uranium and fluorine compared to other granites of the Gawler Craton (Hayward & Skirrow 2010).

The GRV comprise a lower sequence of texturally and compositionally varied volcanic units that amount to 0.5–3 km in thickness, and are gently to moderately dipping (10°–30°). These units are best exposed on the western and southern margin of the GRV (Figure 1a). These lower GRV units range in composition from basalt to rhyolite and comprise lavas, ignimbrites and other minor volcaniclastic facies (Allen *et al.* 2008).

The Olympic IOCG province

The Olympic IOCG province extends ~500 km along the eastern margin of the cratons nucleus and defines a world-class terrain for IOCG metallogeny. First described by Skirrow (2002), the province includes the supergiant Olympic Dam Cu-Au-U-REE deposit (9.09 Gt @ 0.87% Cu, 0.32 g/t Au, 0.27 kg/t U_3O_8; Porter 2010a), Carrapateena (203 Mt @ 1.3% Cu, 0.56 g/t Au, 0.27 kg/t U; Porter 2010c), Prominent Hill, and weakly mineralized subeconomic iron-oxide rich deposits (Oak Dam, *in* Davidson *et al*. 2007; Acropolis, Wirrda Well, Emmie Bluff, Torrens, and Titan *in* Bastrakov *et al*. 2007). The recent discovery of the Hillside Cu-Au deposit (170 Mt @ 0.7% Cu, 0.2 g/t Au: Conor 2010) within the southern extension of the Olympic IOCG Province, Yorke Peninsula, validates the potential for further discoveries.

A synthesis of province to sub-province scale alteration and mineralisation is presented in Skirrow (2002) and later revised by Skirrow (2007) and Hayward & Skirrow (2010). IOCG mineralisation formed mostly during a short-lived episode of NNW-SSE extension that approximately coincided with eruption of the GRV, but was preceded by a protracted NW-SE to NNW-SSE contraction (Hayward & Skirrow 2010). Iron-oxide/alkali alteration assemblages demonstrate no spatial relation with batholithic complexes; rather, intersections of major transcrustal structures coincident with terrane boundaries and supracrustal deformation place first control on district- to deposit scale ore location.

Bastrakov *et al.* (2007) favoured two stages of hydrothermal activity in the Olympic province, with the first a hypersaline high-temperature (>400˚C) hydrothermal fluid responsible for accumulations of magnetite. Although fluids carried significant credits of Cu (>500ppm), inefficient deposition of ore components is ascribed to low S and accompanied high Fe and Cl activity. Ore deposition only occurred where mixing or overprinting occurred with lower temperature, more oxidised, SO_4-rich brines derived from either playa lake (bitten) sources or evolved from cooled and extensively equilibrated magmatic brines (Hayward & Skirrow 2010)

The Mount Woods Domain

The Mount Woods Domain (MWD) is an aeromagnetically defined extension of the northeastern Gawler Craton. The composite geology comprise three main Proterozoic units; (1) The Mount Woods metamorphics (2) the Engenina Adamellite and the (3) Balta granite suite (Freeman & Tomkinson 2010).

The tectonic evolution of the MWD comprise a history of polyphase deformation, high-temperature metamorphism and syn- to post-orogenic magmatism spanning ca. 1736 to 1584 Ma (Betts *et al.* 2003). The Mesoproterozoic is characterised by the emplacement of unmetamorphosed voluminous, bimodal, subaerial, and submarine volcanism of the GRV, and Hitaba Suite equivalents, and pyroxenite, norite and gabbro of White Hill complex. Regionally, a Neoproterozoic dyke swarm cuts all terranes and serves as a local anisotropy. The regional geochronology is reviewed in Belperio *et al.* (2007) and U-Pb ages of 1742±27 Ma and 1736±14 Ma for metamorphic zircons and 1587±4 Ma and 1584±28 Ma for unmetamorphosed granites (Hiltaba Suite/GRV equivalents) are reported.

Prominent Hill

Prominent Hill (Figure 1b) lies on the southern margin of the MWD and is concealed by 90-150 metres of flat-lying Permo-Carboniferous sandstone and diamictite (Boorthana Formation), and Cretaceous sandstone and black claystone (Cadna-owie Formation and Bulldog Shale respectively) (Freeman & Tomkinson 2010). Lithological units and mineralized hematite-sericite breccias are broadly subvertical, north dipping and controlled by a crustal-scale domain boundary delineating the contact between the ca. 1792-1762 Ma greenschist-facies metasediments and ca. 1609-1603 Ma sandstones, conglomerates and intercalated flow basalts (Holcombe 2010).

The host sequence consists of unmetamorphosed lithic quartz sandstone, conglomerate, argillite and dolomite, intercalated with mafic to felsic volcanic rocks. Copper-Au bearing heterolithic hematite-matrix breccias form discrete tabular sheet-like bodies and represent the most voluminous unit. Controversy regarding the breccia development remains unresolved. Explosive hydrothermal milling of the wall rock (Belperio *et al.* 2007) is tested by Freeman & Tomkinson (2010) and alternately proposed is the passive infiltration and replacement of primary fragmental sedimentary strata. In mineralised breccias magnetite is absent, however to the north of the deposit, and separated by its components in the hangingwall fault, is a body of massive "magnetite skarn" and associated, pyrite, actinolite, phlogopite, chlorite, serpentinite, carbonate and talc (Freeman & Tomkinson 2010).

A much broader iron-oxide sericite alteration system overprints all Mesoproterozoic units over an area of ~2km^2 around breccias (Belperio *et al.* 2007). Hydrothermal fluids have altered volcanic units (basalts and andesites) to sericite-chlorite-earthy hematite-leucoxene-carbonate. Host breccia units are intensively altered to hematite + sericite + chlorite + carbonate (± quartz ± barite ± fluorite ± REE

phosphates) (Freeman & Tomkinson 2010). Bornite, chalcocite and chalcopyrite are the most common Cu-sulphides at PH and occur as very fine disseminations or irregular aggregates as infillings in specular hematite. Less commonly Cu-sulphides are hosted by altered wall rocks such as silicified dolomites, sericitized sedimentary rocks or sericitized dacite intrusions (Benavides 2010).

SAMPLE SUITE DESCRIPTION

Fieldwork was conducted in March 2011. To comprehensively characterise the mineralisation of the Munda resource, a suite of one inch polished block samples (Figures A2-A6) were selected from 39 intervals of 8 diamond drill holes (Table 2). Drill holes were selected on an E-W orientation at equal spacing consistent with the strike of the main ore bearing breccia unit. Samples were selected on the basis of variable Cu/Au ratios consistent with whole rock assay data, and from intervals that encompass grains of visible gold or bornite and/or chalcocite.

Host Lithology and alteration

At the Munda resource (Figure 2a) lithological units comprise intercalated dolomite, limestone, quartzo-feldspathic sandstone, siltstone, bimodal volcanics and heterolithic to monolithic hematite-matrix breccias. Plotting log Zr/Ti against log Nb/Y (Figure 4a) from whole-rock data (*after*; Winchester & Floyd 1977) demonstrates that volcanic rocks comprise subalkaline to alkaline rhyodacite-dacite, trachyandesite-andesite, and subalkaline-alkaline basalt. All lithological packages are dismembered by a series of brittle-ductile shear zones that conform to the major E-W striking Hanging Wall Fault (Figure 2a).

Consistent with elsewhere at Prominent Hill, the dominant alteration assemblage within representative drill core is hematite + sericite (± chlorite ± quartz ± calcite ± barite). The development of alteration minerals is highly variable and ranges from vein-form, to incipient replacement, to the complete destruction of all primary textures.

Intercalated dolomite and siltstone sequences are commonly overprinted by weak silicification, chloritization and earthy hematization. Original styolitic textures in dolomite are commonly replaced by earthy hematite and/or provide a first order control for the precipitation of well-formed calcite crystals. The pervasive development of sericite + chlorite alteration is distinctive in zones peripheral to intercalated bimodal volcanic rocks (i.e. basalts and andesites). In such sequences, localised evidence of flow banded plagioclase laths and silica-hematite vesicle infill are observed on bleached contact margins.

The lower footwall of the host sequence comprises dominantly Cu-Au bearing hematite-matrix breccias and a dacitic intrusion. Pervasive hematitic alteration spatially coincides with the dacitic unit

leaving the interpretation of volcanic textures to bleached relict fragments. The 'psuedobrecciation' of host lithologies by Fe-metasomatism is a salient feature at Prominent Hill and completely obliterates primary igneous textures.

Mineralisation

COPPER-GOLD BEARING HEMATITE BRECCIAS

At the Munda resource, discrete subvertical hematite-matrix breccia units and dolomitic sequences are the principle host to Cu and Au mineralisation. Breccia hosted mineralisation can be broadly sub-divided into four packages; (1) steely hematite + calcite ± Au crackle breccia, (2) hematite + sericite + chalcocite matrix supported breccia, (3) iron-oxide + silica + bornite ± chalcocite volcaniclastic breccia and (4) earthy hematite ± chlorite ± sericite poorly sorted to megaclastic breccias.

Steely hematite breccias (Figure 2b) are volumetrically significant within the host sequence and comprise intervals pervasively overprinted by silica + iron-oxide alteration. Intervals range from massive to clast supported and comprise late stage veins of calcite + speculate ± barite alteration. Within intervals copper mineralisation is generally absent and minor Au credits (< 2 g/t) are present in whole rock assays (Figure 3b; sample 15TW).

Matrix supported hematite + sericite breccias (Figure 2*c*) are significant carries of disseminated chalcocite ± bornite mineralisation. A well-developed matrix (30 - 60 vol.%) of crystalline hematite and bleached sericitic halos on breccia fragments is characteristic of these units. In localised intervals the preferential replacement of fine-grained interbeds by earthy hematite is suggestive of an original graded sedimentary sequence. Within sampled intervals Cu values range from 1 - 3 % and Au is generally <1 g/t in whole rock assays (Figure 3b; sample 17-21TW).

Volcaniclastic iron oxide + silica breccias range from matrix supported (~30% vol.%) to clast supported breccias with igneous fabrics preserved in minor bleached fragments. Bornite ± chalcocite mineralisation is chiefly present as disseminations within the crystalline hematite matrix or as veinlets in fractures.

Earthy hematite ± chlorite ± sericite breccias are located distal to principal *sensu stricto* mineralised breccias, and where hematite + sericite alteration is poorly developed. Units encompass a broad spectrum of atypical breccia fabrics that range from chaotic, megaclastic and matrix supported. Units

are generally absent of visual mineralisation and were chiefly sampled to investigate the distal-from-source transition in mineralogy. This is supported in whole rock assays where Cu grades are generally low (<0.3 %) and Au is present in concentrations <1.5 g/t.

COPPER BEARING DOLOMITE

At the Munda resource dolomitic units (Figure 2d) are major Cu-carriers and host discrete m-scale intervals of massive vein-form chalcocite mineralisation. Although present as narrow intervals, these intersections are major Cu-carries with up to 20 wt.% Cu (Figure 3a) in whole rock assays. Two main alteration assemblages overprinting dolomitic sequences are recognised in sampled intervals. At a depth of 320 m chloritization is well developed and pyrite forms as 'styolitic' veins. When present, chalcocite ± bornite occurs as mm-scale veinlets cross cutting the original assemblage. At greater depths the alteration assemblage comprises earthy hematite + crystalline hematite + chalcocite, which observably overprints a peripheral of chlorite + pyrite alteration.

VISIBLE GOLD

Two intervals encompassing visible gold mineralisation were sampled. The first interval (Figure 3d) comprises intercalated volcano-sedimentary units overprinted by incipient to pervasive iron-oxide and silica alteration (Figure 3d). Plotting Zr/Ti on Nb/Y from the representative lithogeochemical data shows that the interval is andesitic in composition. The single grain of Au was hosted in an open fracture and coincided with Au concentrations of 179 g/t in whole rock assays.

The second interval (Figure 3c) comprised a 10 m unit of hematite-breccia with gold grains homogeneously distributed and present in interstitial cracks of the matrix (Figure 2e). The clast-supported breccia (5 vol.%) comprised rounded fragments overprinted by earthy hematite alteration. The occurrence of gold in this interval is directly correlative to elevated permeability and the absence of sericitic alteration. From whole rock assays the entirety of the interval is consistent with average Au grades of 33 g/t.

MASSIVE PYRITE

Massive pyrite mineralisation has been intercepted in recent drill-core at the footwall dacite unit. Pyrite is developed on a meter scale and varies from pervasive to a localized incipient overprint. Peripheral to the massive pyrite mineralisation, plagioclase phenocrysts are selectively replaced to sericite and weak hematitic alteration is present. Although this interval in not represented in the drill core from this study, acknowledging this alteration assemblage is of interest, as it is not found elsewhere.

Lithogeochemical trends

MASS ELEMENT EXCHANGE FROM HYDROTHERMAL ALTERATION

Hydrothermal alteration records the effects of fluid-rock interaction, and these effects are expressed as compositional changes that can be recognised in the geochemistry of the rocks (Warren *et al*. 2007). An understanding of hydrothermal alteration is of value because it provides an insight into the chemical attributes and origins of ore fluids and the physical conditions of ore formation (Barnes 1997). To evaluate metasomatic process and mass-element exchange intimately associated with mineralisation, lithogeochemical data from sampled intervals is plotted in log K/Na vs. K/Al compositional space (Figure 4b).

On a whole, all stratigraphic units demonstrate a clear trend towards sericitization, with a majority of data plotting within the relative compositional field. In contrary, deviations above ideal K/Al ratios demonstrate that sericite to phengite substitution is favoured. The continuation of this trend concludes that that biotite and/or feldspar alteration opposed to muscovite is unquestionable for localized intervals. Of further interest is the distribution of compositional points for high-grade Au and Cu intervals. Interestingly, mineralisation hosted in shallow dolomitic sequences and Au-bearing hematite rocks are not altered to sericite, whereas the high-grade Au hosted in volcano-sedimentary units is indisputably sericitized.

WHOLE ROCK ASSAY DISTRIBUTION

Whole-rock Au-Cu concentrations (Figure 4c) show a strong negative correlation and define a wedge shape in log-log space. As anticipated, the distribution of values is bias towards elevated Cu in favour of gold. Interestingly, when data points are discriminated by sampled intervals (central to the plot) a weak positive correlation in Au and Cu can be determined.

ANALYTICAL METHODOLGY

Optical Microscopy

Ore microscopy was conducted on a Leitz Laborlux-12-Pol polarizing microscope operating in reflected light mode. The microscope was equipped with a digital camera.

Scanning Electron Microscope

The Philips XL30 scanning electron microscope (SEM) with energy dispersive X-ray spectrometry (EDAX) and back-scattered electron (BSE) imaging at Adelaide Microscopy was used operating at 20 eV. Backscatter imaging coupled with semi-quantitative EDAX facilities allowed rapid identification of trace minerals (down to 1-2 micron) and identification of the alteration silicates. Analysis was performed on a majority of the sample suite and used to produce a sub-suite of one inch polished blocks for EMPA and LA-ICP-MS.

Electron Microprobe Analysis

Microprobe analysis was performed at Adelaide Microscopy, University of Adelaide, using a CAMECA SX-51 electron microprobe (EPMA) with wavelength dispersion spectrometers. For silicates operating conditions were an accelerating voltage of 20 KV and a beam current of 20 nA. Standards used were; fluorite (F), albite (Na), almandine (Mg, Al, Si, Fe), apatite (Ca, P), tugtupite (Cl), sanidine (K), rutile (Ti), pyrope (Cr), rhodonite (Mn), monitoring following spectral lines F Kα, Na Kα, Mg Kα, Al Kα, Si Kα Fe Kα, Ca Kα, P Kα, Cl Kα, K Kα, Si Kα, Ti Kα, Cr Kα and Mn Kα. Count times were 10 seconds for all elements. Operating conditions for Cu-(Fe)-sulphides and Au phases were an accelerating voltage of 20kV and a beam current of 20nA. Standards used were; Marcasite (S, Fe), Co metal (Co), Pentlandite (Ni), Chalcopyrite (Cu), Gallium Arsenide (As), Bismuth Selenide (Bi, Se), Silver Telluride (Ag, Te), Galena (Pb), Stibnite (Sb), Au, Hg (pure metals), monitoring the following spectral lines: Bi Mα, Se Lα, Ag Lα, Cu Kα, Fe Kα and S Kα. Count times were 20 s for all elements. For Rare Earth Element (REE) phases, standards used were Y, La, Ce, Pr, Nd, Sm, Dy, Er (pure single element glasses), Tb, Ho, Yb, Lu (pure metals), K227 glass (Pb), Huttonite (Th), UO_2 (U), zircon (Zr), Nb (pure metal), monitoring the following lines; Y Lα, La, Ce Lα, Pr Lβ, Nd Lα, Nd Lβ, Sm Lβ, Dy

Lβ, Er Lβ, Tb, Ho Lβ, Yb Lα, Lu Lα, Pb Lβ, Th Mβ, U Mβ, Zr Lα, Nb Lα. Count times were 20 s for all elements.

Laser-Ablation Inductively-Coupled Mass Spectrometry

LA-ICP-MS analysis was conducted using the Agilent HP-7500 Quadrupole ICPMS instrument at Adelaide Microscopy. The instrument is equipped with a New Wave UP-213 Nd:YAG laser ablation system equipped with MeoLaser 213 software. Data reduction was performed using Glitter software. Pre-defined areas of the polished blocks were ablated. The methodology governing the in analysis of copper-(iron)-sulphide is based upon the Cook *et al.* (2011; in prep). The following isotopes were monitored; ^{23}Na, ^{29}Si, ^{34}S, ^{43}Ca, ^{51}V, ^{55}Mn, ^{57}Fe, ^{59}Co, ^{60}Ni, ^{65}Cu, ^{66}Zn, ^{69}Ga, ^{75}As, ^{77}Se, ^{93}Mo, ^{107}Ag, ^{111}Cd, ^{115}In, ^{118}Sn, ^{121}Sb, ^{125}Te, ^{137}Ba, ^{182}W, ^{193}Ir, ^{197}Au, ^{202}Hg, ^{205}Tl, ^{208}Pb, ^{209}Bi. Total analysis time for each analysis (30-seconds pre ablation and 60 s ablation time) was 90 seconds. The calibration of representative isotopes was performed using USGS sulphide standard Mass-1. This is a sulphide matrix, trace element-doped precipitated powder fused to a glass disc that has been specially developed for trace element analysis of sulphides. Mass-1 (previously known as PS-1; Wilson *et al.* 2002) is certified for a broad range of trace elements including all those listed in the tables. Analytical accuracy is expected to be better than 20%.

PETROGRAPHY

Gangue minerals

From SEM investigation of sampled intervals, the dominant gangue minerals are quartz, sericite and hematite, with the development of all minerals often constituting <90% of host units (Table 3). Present as a minor phase, chlorite is generally absent, with development restricted to samples peripheral to mineralised hematite-matrix breccias. The distributions, texture and morphology of gangue minerals were evaluated under BSE to enable comparisons with observations made on the specimen scale. For simplicity, all intercalated phases of K-mica with variable [Na + K] occupancy are referred to as sericite.

Under BSE, sericite is present with comparable texture and morphology. Sericite (I) (Figure 5a) is coarse-grained, chemically homogeneous and abundant within samples corresponding to earthy hematite + chlorite breccias. On a specimen scale sericite (I) has a white colouration and weakly overprints breccia fragments (Figure 5b). Under BSE, apatite and fluorapatite (Figure 5c) are abundant and occur as coarse-grained (<200 μm) interstitial aggregates crosscut by lamellae of sericite (I). In a majority of samples the replacement of quartz by sericite (I) is readily observed and well developed on fragment margins (Figure 5a). Present in sample 5TW are hexagonal grains (10 – 15 μm) of a fibrolite mineral (Figure 5d) with occupancy of Mg and Na depicted in EDAX. Such fibrolite minerals share mutual boundaries with sericite (I), with grain boundaries of the former crosscut by the later.

Sericite (II) is comparatively fine-grained and occurs as intercalations of variable [Na + K] occupancy (Figure 5e). The development of sericite (II) is elevated proximal to the main Cu-bearing breccias, commonly constituting up to 50% of the sample volume. On a specimen scale, samples are associated with matrix-supported hematite + sericite breccias (Figure 5f) characterised by a profound sericitized halo overprinting earthy hematite fragments.

Under BSE, samples containing sericite (II) commonly show elevated development of REE minerals. Florencite ($CeAl_3(PO_4)_2(OH)_6$) and fluocerite ($(CeLa)F_3$) are present as euhedral aggregates forming as open space infill, or more commonly, as fine-grained inclusions (<2 μm) within lamellae of sericite (II) (Figure 5g). Monazite ((Ce, La, Nd, Th)(PO_4)) (Figure 5h) is also abundant, and forms fine- to coarse-grained aggregates (2 – 60 μm) that are encompassed within channels of sericite (II). On grain boundaries of monazite, <4 μm grains of hematite are readily observed encapsulated in overgrowth

textures. In representative samples, silicate minerals containing U and Cu were also noted; U-bearing mica (Figure 6a) is present as fine-grained (< 2 μm) lamellae interlayered with sericite, while a Cu-silicate (Figure 6b) was observed bordering chalcocite. Although the mineral chemistries of the two phases could not be validated with the microprobe method, compositional data depicted in EDAX shows the two respective phases could be torbernite ($Cu\ (UO_2)_2(PO)_2$ - $12H_2O$) and spangolite ($Cu_6Al(SO_4)(OH)_{12}Cl – 3H_2O$).

In selected samples there is compelling mineralogical and textural evidence to suggest that sericite (II) has replaced a mafic precursor, with skeltal grains of rutile (Figure 6c) and euhedral xenoblasts of hematite (Figure 6d) with ilmenite lamellae commonly observed encapsulated in channels of sericite (II) alteration.

Quartz is the second most abundant gangue mineral and can constitute <80 % sample volume. Observations made on a specimen scale often invalidate the pervasive development quartz as depicted in BSE. From sampled intervals with iron oxide + quartz alteration (Figure 6e), under BSE hematite is minor (<2 vol.%) and occurs as fine impregnations within quartz. Quartz is major (<80 vol.%) and comprises elevated micro-porosity and concentrically zoned overgrowth textures. To a lesser extent, such inclusions comprise spherules (<5 μm) of native copper and domeykite (Cu_3As) (Figure 6f). Quartz is also present as well-formed euhedral fragments (50 – 300 μm) constituting the matrix of breccia sequences. Such grains have little to no micro-porosity and commonly host fine- to coarse-grained (10 – 200 μm) Cu-(Fe)-sulphides (Figure 10a-b), coffinite and Co-Ni arsenides.

In sampled intervals distal to hematite-matrix Cu-bearing breccias the textural aspects of sericite (II) is largely comparable. In such samples, the development of sericite (II) replacement on quartz fragments is poor (Figure 6g), and rather, sericite (II) is present as radial growths (Figure 6h) interstitial to breccia fragments. Chlorite, when present, mimics the textural aspects of sericite (II) and forms mutual boundaries. Hematite occurs as long radial blades (<50 μm) propagating into open cavities (Figure 7a), or more intriguingly, as 200-300 μm euhedral psuedomorphic grains that have replaced a porous fibrolitic mineral (Figure 7b-c). Within such grains, concentrically zoned pores are commonly host to <3 μm inclusions of U-bearing minerals (Figure 7d) and monazite.

Calcite is present in BSE images as a minor phase that correlates to hand specimens with pervasive steely hematite alteration and late stage calcite veins (Figure 7e). In BSE images samples calcite is developed as box-form veins replacing a dolomite precursor (Figure 7f).

For samples representing shallow dolomitic mineralisation, the development of alteration phases is distinct from elsewhere. Chlorite is profoundly coarse-grained (figure 7g) and occurs as long stringy bands within voids of pyrite mineralisation. Hematite is also present as both granular aggregates in chalcocite mineralisation, or more extensively as fine-grained needles (Figure 7h) impregnated in the host sequence. These observations are corroborated by weak hematitic alteration peripheral to chalcocite veins on a specimen scale (Figure 2d).

Copper-(Iron)-Sulphides

The main Cu-carrying minerals observed in sampled intervals are chalcocite and bornite accompanied by minor chalcopyrite. From observation made on mineral associations and textural aspects (Table 3), the common Cu-(Fe)-sulphides are discriminated herein by colour properties.

WHITE CHALCOCITE

White chalcocite is the most important Cu-carrier of the Munda resource and is present as fine disseminations within the matrix of monolithic hematite + sericite breccias. These intervals show a strong correlation with Ce and up to 10,000 ppm (Table 2) is present in whole-rock assays.

Under reflected light white chalcocite is isotropic and present as μm- to mm-scale monomineralic grains (Figure 8a). Chalcocite occurs dominantly as open space infill and is volumetrically abundant in samples with elevated porosity. To a lesser extent, chalcocite forms 50 – 150 μm interstitial veinlets within the matrix (Figure 8b). In samples where chalcocite grains are well formed in the matrix, <20 μm rounded inclusions of quartz are often present as inclusions.

In representative samples sericite (II) is the abundant mica (Figure 8a-f) and is depicted crosscutting grain boundaries of white chalcocite (Figure 8d). Also present are Ce-rich REE's (Figure 8e-h) such as fluorencite and fluocerite, with both phases occurring as <5 μm aggregates in the matrix hosted by lamellae of sericite (II) (Figure 8e). Of all REE phases, fluocerite is the most abundant and

forms on grain boundaries of white chalcocite or as <4 μm inclusions (Figure 8h), validating a complex mineralogical association between the two phases.

BROWN BORNITE

Second to white chalcocite, intervals of brown bornite are present as disseminations within heterolithic hematite + silica breccias. Compared to intervals encompassing white chalcocite, concentrations of Ce are far lower, with up to 500 ppm present in whole-rock assays.

Under reflected light brown bornite is isotropic and present as polymineralic aggregates (Figure 9a) that range from hundreds of μm to mm in scale. Quartz is abundant in selected samples, and restricts the precipitation of bornite to open fractures (Figure 9b). Within xenoblastic bornite, hematite occurs as orientated lamellae with porous contacts. To a lesser extent, <60 μm grains of concave pyrite (Figure 9c) and monazite (Figure 9d) are present central to bornite grains and conversely form sharp contact at phase boundaries. Fluocerite (Figure 9e) and chalcocite (Figure 9f) are present as minor phases on grain boundaries and forms complex intermingling textures.

In representative samples both sericite (I) and sericite (II) are moderately developed and have comparable mineralogical associations, with sericite (I) present (Figure 9g-h) in domains occupied by pyrite, whereas sericite (II) forms mutual boundaries with brown bornite (Figure 9e).

PURPLE BORNITE – BLUE CHALCOCITE

Purple bornite and blue chalcocite often coexist as fine- to coarse (10 - 200 μm) grains hosted in the cavities of silicate fragments (Figure 10a-b). The identification of this assemblage spatially coincides with breccias peripheral to major Cu-bearing intervals, and where weak chloritization or pervasive steely hematization is present (Figure 10d). Intervals are poorly mineralised and comprise minor Cu (~ 0.3 wt. %) and elevated credits of Au (~1.5 g/t) in whole rock assays (Figure 3b; sample 15TW).

Under reflected light blue chalcocite (Figure 10c) forms monomineralic viens in the breccia's matrix. Such grains are present with white chalcocite and commonly show exsolution lamellae of deep blue to white $Cu_{2-x}S$ phases. When coexisting with blue chalcocite (Figure 10b-c), purple bornite is often the dominant phase and comprise exsolution of clausthalite (PbSe) (Figure 10f). Under reflected light grains are anisotropic with colour properties ranging from purple to orange-brown (Figure 10e)

depending on the presence of exsolution or replacement. At higher resolution, grains are readily observed with homogenously distributed lamellae of chalcopyrite (Figure 10g) or minor spindle lamellae of chalcocite (Figure 10h).

Forming a Co-Ni-Fe-As-U association, 5 – 10 μm grains of loellingite, coffinite and safflorite are present as complex intergrowths that crosscut grains of blue chalcocite or coexisting purple bornite (Figure 11c-g). Also observed are blades of xenotime (<40 μm) (Figure 11a-b) encapsulated within puffy aggregates of hematite. The tabular morphology of xenotime grains is preserved as cavities in hematite, providing evidence for the partial dissolution of the former. Sericite (I) and (II) are present in representative samples; lamellae of sericite (II) share mutual boundaries with bornite (Figure 11h), while textural aspects suggest that sericite (I) (Figure 11j) is crosscut by grains of coexisting purple bornite and blue chalcocite. More commonly, sericite (II) occurs as radial lamellae occupying voids in the matrix (Figure 11i).

Chalcopyrite, when present, occurs as 5 - 300 μm monomineralic aggregates hosted in quartz cavities to polymineralic aggregates coexisting with brown bornite. In such grains, chalcopyrite occurs principally as crosscutting veinlets (Figure 11f) or as an intergranular film encompassing brown bornite (Figure 11g). Present as a trace mineral, altaite occurs as submicroscopic to <4 μm inclusions in chalcopyrite, and along phase boundaries between bornite and chalcopyrite (Figure 12d-e). To a lesser extent, altaite also occurs as coarse-grained (<7 μm) inclusions invariably hosted by monomineralic grains of chalcopyrite (Figure 12j).

GREY CHALCOCITE – RED BORNITE

Grey chalcocite is developed in samples derived from major Cu-bearing dolomitic sequences where Cu concentrations of up to 20 wt.% are present in whole rock assays. Under reflected light, grey chalcocite occurs as isotropic compact that encapsulates 50 -100 μm concave inclusions of pyrite (Figure 13a-c). In localised samples, red bornite in present as veins (Figure 13g-h) crosscutting grey chalcocite, with such veins commonly preceded by neo-crystallisation of chalcopyrite. In shallow samples encompassing pyrite + chlorite alteration, grey chalcocite is absent under reflected light. In such samples pyrite (Figure 13) is abundant (~50 vol.%) and occurs as “symplectic” intergrowths with the host minerals. In comparison, chalcocites is blue under reflected light and occurs as 1 – 15 μm veins accompanied by minor bornite crosscutting pyrite (Figure 13g-h).

Gold Mineralogy

From petrography two main gold assemblages have been investigated from the Munda Resource. Native gold occurs with chalcopyrite-loellingite and forms a complex mineral association with Ni-Co-Fe arsenides, Y-U-bearing phases and native bismuth (Figure 14; Figure A1). Also observed in this study are Au-Cu alloys (Figure 15) that are present as polymineralic aggregates comprising bornite-chalcocite. Native gold was sampled in drill core PH11D576 (Figure 3c) while Au-Cu alloys represent visible gold observed in drill core PH10D550 (Figure 3d).

Under reflected light native gold is present as coarse-grained (up to mm scale) interstitial aggregates that coexist with chalcopyrite and loellingite (Figure 14a-b). Gold grains are very porous with chalcopyrite (Figure 14c) present as anastomosing veinlets (up to 3 μm) or homogenously distributed submicroscopic to <30 μm equigranular inclusions. Chalcopyrite is abundant in represented samples, and occurs as open space infill that mediates the contact between gold boundaries of gangue minerals (Figure 14d). Present in only minor amounts, loellingite is observed as equigranular blebs that occur on the boundary of gold grains.

From BSE images, the host gangue consists predominantly of dolomitic (Figure 14c) domains replaced by calcite veins. Encapsulated in calcite veins are polymineralic aggregates of loellingite, co-safflorite, coffinite, Y-bearing coffinite and native bismuth. Loellingite and coffinite form complex intergrowths textures and often demonstrating phase zonation on grain boundaries (Figure 14d-j). From compositional data depicted in EDAX, coffinite is also present with exsolutions of a complex Y-bearing coffinite (Figure 14d). Present as a trace mineral, native bismuth is present as crustations on all minerals or forms fibrous aggregates in intragranular pores (Figure 14j). To a lesser extent, blades (<5 μm) of bismuth minerals (i.e. bismuthinite and native bismuth) occur as isolated blades suspended in calcite veins.

In representative samples, blue chalcocite is present coexisting with purple bornite, with both phases hosted within calcite viens. Interestingly, submicroscopic to <2 μm grains of Au occur as inclusions hosted in discrete zones of all phases forming a mineral association (Figure 14i).

Au-Cu alloys are present as mm-scale grains with serrate boundaries. From ore microscopy phases of Au-Cu composition are discriminated from native gold by its rose gold reflective property (Figure 15a). Within representative samples, Au-Cu occurs as both homogenous grains (Figure 15b) or as coarse-grain symplectoids (Figure 15c-d) of variable compositions as determined by colour impurities.

Symplectic grains are highly porous and comprise 1 - 50 μm blebby inclusions of grey chalcocite. Observable at higher resolution are fine-grained lamellae of hessite (AgTe) (Figure 15e) hosted within chalcocite. Symplectic grains are also consistent with an intergranular film of dominantly grey chalcocite with minor red bornite (Figure 15). In contrary, chemically homogenous grains of Au-Cu contain small rounded inclusions of quartz and are spatially dissociated from Cu-(Fe)-sulphides. Minor Au-Cu is depicted intergrown with chalcocite and with bushels aggregates of coffinite (Figure 16g-h) nucleating on grain boundaries.

In represented samples, sericite (II) is the dominant mica (figure 15h) and forms along grain boundaries of Au-Cu alloys or in the matrix intergrown with florencite. Au-Cu alloys were also recognised from various locations as <5 μm grains encompassed in florencite dominant veins (Figure 15i).

MINERAL CHEMISTRY

Sulphide mineral chemistry

Electron microprobe analysis was performed on eighteen samples to quantifying the stoichiometric proportions and minor element concentration of Munda Cu-(Fe)-sulphides. Chalcocite and bornite were chiefly investigated due to the existence of intermediate solid solutions and composition variation associated with order-disorder transformation and vacancy clustering. The selected microprobe data from all point analysis is present in table 4 and the complete data set is provided in the electronic appendix (Table A1-A2). Histograms showing representative M/S ratios and simplified distribution of point analysis are shown in Figure 16. For simplification all phases with composition $Cu_{2-x}S$ are described herein as chalcocite.

THE COPPER-(IRON)-SULPHIDE SYSTEM

Our understanding of the Cu-S system is based chiefly on the work of Roseboom (1966), Rau (1967), Morimoto & Koto (1970), and Porter (1977). At high temperature (>435°C), the system is dominated by the high digenite solid solution (Cu_2S – $Cu_{1.73}S$). Below such temperatures the digenite-solid solution persists only in its more sulfur-rich composition range. Most natural systems, however, are dominated by the low temperature system (<100°C) with compositions of $Cu_{2-x}S$. Identification of discrete phases by ore microscopy is hindered by complex order and disorder transformations and chemical inhomogeneities.

Monoclinic low-T chalcocite (<103°C) and djurleite ($Cu_{1.93-1.96}S$) are structurally related to high-T chalcocite (<435°C). In comparison low-T digenite ($Cu_{1.75-1.8}S$) is metastable below 83°C and decomposes to mixtures of anilite ($Cu_{1.74}S$) and djurleite (Morimoto & Koto, 1970).

Contributions on the ternary Cu-Fe-S system provide the greatest insight into IOCG-systems where bornite (Cu_5FeS_4) and Chalcocite are major Cu-carriers. Bornite exists in three polymorphic forms defined by transitions at 200 and 265°C (Grguric *et al.* 1998). The high temperature polymorph, stable above approximately 270°C, consists of a random distribution of six metal cations and two vacancies in the eight tetrahedral interstices of a cubic close-packed sulfur framework (Morimoto & Kullerud 1961; Kanazawa *et al.* 1978; in Grguric *et al* 1998). The intermediate polymorph exists over the temperature

range 200 to 270°C, with some variation induced by minor deviations from stoichiometry (Grguric & Putnis 1998). Below 200°C the low form involves a doubling of the intermediate unit cell in the b direction, resulting in an orthorhombic pseudo-tetragonal 2*a*4*a*2*a* superstructure (Grguric *et al.* 1998). At temperatures >80°C bornite and digenite form a broad solid solution known as the digenite-type or 1a solid solution (Morimoto & Kullerud 1966, Morimoto Gyobu 1971, Grguric *et al*. 2000), which becomes complete at the consolute point of 265°C. Cubic low digenite *sensu stricto* has an integer 5a superstructure is stabilized by small amounts of Fe (Morimoto & Gyobu 1971).

COPPER-(IRON)-SULPHIDE PHASES

Of all point analyses grey chalcocite has a formula closest to ideal with a mean occupancy of $Cu_{1.98}S_{1.01}$. Associated metal/sulfur (M/S) ratios fall between 1.95 and 2.00 on the histogram (Figure 17b) suggesting intergrowths of djurleite and chalcocite are present. Grey chalcocite intergrown with Au-Cu is discriminated herein as a subpopulation due to the variation in mineral association. This grey chalcocite demonstrated deviation from stoichiometry with a mean occupancy of $Cu_{1.95}S_{1.03}$ consistent with a range of M/S ratios that range from 1.71 to 1.97. This corresponds to a population that plots near djurleite-digenite, and a second subpopulation that plots near anilite on the histogram. Of the minor elements this grey chalcocite has elevated Te with concentrations of up to 0.88% present. Such levels were anticipated by ore microscopy with inclusions of hessite identified in chalcocite. Also present are minor credits of Se (up to 0.48 wt %) and Bi (up to 0.14 wt %) with the remainder below detection limits.

Microprobe analysis was performed on blue chalcocite (Figure 17d) from two mineral assemblages. Blue chalcocite coexisting with bornite + clausthalite demonstrated the widest range of non-stoichiometry illustrated by M/S ratios that range from 1.69 to 2.05 on the histogram. This comprises Pb occupancy in both the Cu-rich ($Cu_{2.00}Pb_{0.01}S_{0.97}$) and Cu-poor equivalent ($Cu_{1.88}Pb_{0.02}S_{1.10}$). The broad non-stoichiometry is supported by an elevated enrichment in trace elements when compared to other chalcocites. Sample 15TW contained the highest enrichment of all trace elements, however due to analytical errors only one point analysis was accepted. From the single analysis, minor element populations include 3.55 wt.% Se, 1.32 wt.% Fe, 0.58 wt.% Pb, 0.17 wt.% Te and 0.12 wt.% Bi. Trace element concentrations in other blue chalcocite were comparably lower, and include <0.83 wt.% Se, <0.13 wt % Ag, < 0.14 wt % Pb, <0.37 wt % Bi, and <0.12 wt % Te.

In samples containing native gold, blue chalcocite has a mean occupancy of $Cu_{1.97}S_{1.02}$ and non-stoichiometry that ranges from $Cu_{1.97}S_{1.01}$ to $Cu_{1.88}Pb_{0.02}S_{1.06}$. On the histogram, two discrete populations of M/S values cluster at ~1.8 and ~1.93 suggesting djurleite and digenite, if present, are chemically homogenous. Vacancy populations are comparable to other blue chalcocites, with microprobe data showing lower Se-concentrations (<0.12 wt %) and both higher and more consistent occupancy of Pb (<0.24 wt %).

White chalcocite (Figure 17f) is poorly represented by microprobe data as majority of M/S exceeded 2.1 and were subsequently rejected due to analytical errors. From the remaining point analysis the mean occupancy for white chalcocite is $Cu_{1.98}S_{1.02}$ and M/S ratios plot between 1.89 and 2.05 suggesting the presence of djurleite and digenite is favoured. It is hard however to quantify the true range of white chalcocite from probe analysis because grains are often observed in ore microscopy to coexist with interstitial grains of blue chalcocite. Broadly speaking, trace element occupancy is below detection limits, with exceptions of Ag and Bi recorded at concentrations of 0.17 wt.% and 0.12 wt.% respectively.

Microprobe data shows that red bornite (Figure 17c) is broadly stoichiometric with the mean formula $Cu_{5.03}Fe_{0.96}S_{4.00}$ (M/S = 1.5). Red bornite is also low in detectable trace elements with Pb (< 0.20 wt. %) and Ag (< 0.15 wt %) present in rare concentrations.

Of all Cu-Fe-sulphides, purple bornite (Figure 17e) has the broadest non-stoichiometry, with M/S values ranging from 1.7 to 1.2. High Se occupancy was noted in the Cu-rich composition ($Cu_{5.29}Fe_{0.79}S_{3.88}Se_{0.04}$) and is comparably absent in the Cu-poor ($Cu_{4.36}Fe_{1.04}S_{4.26}$) end member. Representative M/S populations are noted at ~1.4 and ~1.3 validating the presence of chalcopyrite intergrowths. With visible inclusions of clausthalite, purple bornite is enriched in Pb and Se with respective concentrations of 4.04 wt.% and 4.10 wt.% present. Concentration of up to 0.10 wt % Ag, 0.24 wt % Bi and 0.35 wt % Te were also noted. From samples containing native gold, purple bornite is comparably Cu-rich and has a mean occupancy of $Cu_{5.14}Fe_{0.85}S_{3.96}$. This is further validated by M/S ratios that range from 1.5 to 1.6. With exceptions of Pb (up to 1.12 wt %) and Se (0.23 wt %) all trace elements were below detection limits.

Only three point analyses were acquired for bornite in association with Au-Cu alloys. The mean composition of $Cu_{5.00}Fe_{0.98}S_{1.49}$ shows occupancy of such bornites is close to the theoretical. With inclusions of pyrite, microprobe shows that brown bornite (Figure 17g) is invariably Cu-deficient

represented by the empirical formula $Cu_{4.96}S_{0.99}S_{4.06}$ (M/S = 1.46). Present in minor concentrations were Bi (up to 0.23 wt %), Pb (up to 0.16 %) and Ag (up to 0.12 wt %).

Gold mineral chemistry

Electron microprobe analysis was performed on four samples to quantify the stoichiometric proportions and minor element concentrations of visible gold grains identified in petrography. In addition to native gold, three discrete phases of the binary system Au-Cu were recognised in SEM. The selected microprobe data from all point analysis are present in table 5 and the complete dataset is provided in the electronic appendix (Table A3-A4).

THE BINARY AU-CU SYSTEM

The most comprehensive review of the synthetic Au-Cu system is provided in Okamoto *et al* (1987). From the Au-Cu phase diagram, a continuous series is found only at temperatures above 400˚C. Below this however, the resultant Au-Cu phases consist: Au, Cu, two polymorphs of AuCu, Au_3Cu, and two polymorphs of $AuCu_3$. The phases auricupride (AuCu) and tetra-auricupride ($AuCu_3$) are well characterised in both synthetic and natural systems (Ramdohr 1969; Knipe & Fleet 1997). In comparison, the phase Au_3Cu is not well characterised due to the difficulty in attaining a full equilibrium state at low transformation temperatures (<240˚C) (Okamoto *et al.* 1989). What is known however is that the Cu concentration of Au_3Cu phase decreases as the temperature is lowered (Okamoto *et al.* 1989).

AU-CU PHASES

Microprobe analysis shows that (Figure 17a) tetra-auricupride (AuCu) and unnamed Au_3Cu and Au_9Cu are present within the Munda resource. Under BSE tetra-auricupride was present as homogenous monomineralic grains. Microprobe analysis has shown that tetra-auricupride is stoichiometric with a mean occupancy of $Au_{1.00}\,Cu_{1.00}$. Both Au_3Cu and Au_9Cu were identified coexisting as symplectoids. The mean occupancy for each phase is $Au_{2.96}Cu_{1.03}$ and $Au_{8.85}Cu_{0.93}$ respectively. From respective Au/Cu values shown in Figure 17a, it is clear that phases of higher Au occupancy illustrate the broadest non-stoichiometry. Total Au/Cu ratios range from 8.1 to 9.7 for Au_9Cu and are comparatively invariable for

AuCu. All Au-Cu alloys are broadly free of impurities with only minor credits of Ag (up to 0.11 %) recorded.

NATIVE GOLD

Native gold was observed under SEM to contain microscopic to submicroscopic inclusions of chalcopyrite. When conducting microprobe analysis we sought to avoid surfaces with microscopic heterogeneities to minimize analytical errors. Even so, data shows concentrations of up to 0.10 Cu, 0.12 Fe and 0.15 S a.p.f.u are present. This validates observations made in petrography and suggests both minerals coexist on a submicroscopic scale.

Other Minerals

ARSENIDES

Selected compositional data for arsenide phases are presented in Table 6 and the complete dataset is provided within the electronic appendix (Table A5-A6). Microprobe analysis shows that loellingite and safflorite are the two main arsenide phases present within the Munda resource. Loellingite (As_2Fe) has composition represented by $As_{2.00}Fe_{0.94}$ to $As_{1.91}Fe_{0.92}S_{0.05}$ with minor occupancy of S (up to 0.79 wt.; mean 0.26 wt.%) and Se (up to 0.7 wt.%; mean 0.57 wt.%). Safflorite ((Co, Fe, Ni)As_2) is present both Co-saffrolite and an intermediate Co-Fe-variety with average empirical formulae of $Co_{0.99}As_{1.99}$ to $Co_{0.52}Fe_{0.43}As_{1.99}$ respectively.

RARE EARTH PHASES

Microprobe was used to characterise the major and minor element concentrations in the REE minerals xenotime, florencite, monazite and fluocerite. Selected compositions for Munda REE phases are presented in Table 7 and the complete dataset is provided within the electron appendix (Table A7-A9) For this study a -15 % error in totals was accepted to avoid a blanket rejection of all data. Unfortunately Eu, As and V are not included in the element set, possibly introducing some errors into the formula calculation for xenotime.

Analysed monazite grains occur as <50-µm euhedral grains encapsulated within coarse-grained polymineralic aggregates comprising dominantly brown bornite. In comparison, analysed florencite was present as puffy aggregates interstitial to a network of hematite. Based on these textural aspects it can be speculated that monazite developed concurrently with brown bornite mineralisation and florencite is broadly a later stage alteration. The single grain of xenotime analysed in this study was recognised in association with purple bornite. Within this assemblage xenotime (Figure 11a-b) occurs as < 50 µm blades with textural aspects suggestive of partial dissolution.

Adapted from Boynton (1985), Chondrite-normalised patterns (Figure 17b) illustrate the LREE-rich and HREE-rich patterns expected for monazite and xenotime, respectively, reflecting the pronounced fractionation of LREE/HREE between the two minerals. Monazite is enriched in Ce and La when compared to florencite. Significant Fe was noted in both monazite and florencite (mean 4.77 wt.% and 5.5 wt.%, respectively) validating the presence of hematite as sub-microscopic intergrowths. Xenotime is particularly rich in the HEE Gd, Dy and Er. U and Th concentrations in xenotime are 0.4 and 0.15 wt.%, respectively.

GANGUE MINERALS AND FLUORINE DISTRIBUTION

Introduction

Fluorine is a common volatile component present in volcanic emissions that can affect melt properties, phase relations and ligands (Hedenquist and Lowenstern, 1994; Aiuppa *et al.* 2009). Fluid inclusion studies conducted on F-rich granites have demonstrated magmatic-hydrothermal fluids emitted during the final stages of magma differentiation may achieve extreme enrichments in alkali-fluorides (Auippa *et al* 2009). This process permits the enrichment in elements such as U, Th, Zr, Hf, Nb, Ta, Ti, Sn, Mo, W and REE (Congdon & Nash 1988; *in* Ehrig & Green 2009). The presence of fluorine in magma also causes High Field Strength (HFS) elements to become highly incompatible (Keppler 1993).

Copper-gold mineralisation within the Gawler craton is closely related to the magmatic emplacement of the Gawler Range Volcanics (GRV). Melt inclusion studies have shown that important contents of fluorine (up to 1.3 wt.%) were exsolved on crystallisation of the GRV (Ehrig & Green, 2009). The fluorine content of hydrothermal mica in mineralized porphyry copper and intrusion related systems have been subject to numerous investigations (Gunow *et al.* 1980; Idrus *et al.* 2007, Ehrig & Green 2009). This is because hydroxly-bearing minerals, such as micas, are convenient indicators of halogen activities as they can be used to estimate the fugacities of HCl and HF in coexisting fluids (Yavuz 2003).

Despite this, there remains a paucity of published data investigating the geochemistry of F-bearing mica within the Gawler craton. Current knowledge is based chiefly on the contributions of Tappert *et al.* (2011) for the Olympic Dam deposit and the unpublished report of Williams & Duckworth (2010) concerning the Prominent Hill deposit. The aim of this investigation is thus two-fold. Firstly, data systematically quantifying mica geochemistry are present. Secondly, the deposits scale variation between F-enrichment and the distribution of ore minerals and alteration is investigated and the implications discussed.

Background information

Micas are phyllosilicates in which the unit structure consists of one *octahedral sheet* (Os) between two opposing *tetrahedral sheets* (Ts) (Rieder, 2001). Micas have a simplified formula $IM_{2-3}\square_{1-2}T_4O_{10}A_2$, where I is commonly Cs, **K**, Na, NH_4, Rb, Ba, Ca; M is usually Li, **Fe** (Fe^{3+} or Fe^{2+}), **Mg**, Mn (Mn^{3+} or Mn^{2+}),

Zn, **Al**, Cr, V, Ti; □ represents a vacancy; T is usually Be, **Al**, B Fe^{3+}, **Si**, and A is usually Cl, **F**, OH, O (oxy-micas), and S (Rieder 2001). Micas are subdivided into two groups, respectively *true micas* or *brittle mica* based on the I cation, or moreover, they can be dismembered as dioctahedral (if M < 2.5) and trioctahedral (if M > 2.5) (Yavuz 2003).

The mica end-members chiefly investigated in this study are muscovite and phengite, which are the dominant mica reported at the Olympic Dam deposit (Tappert *et al.* 2011). Dioctahedral muscovite has the generalised formula $KAl_2\square AlSi_3O_{10}(OH)_2$, whereas the phengite series represents solid solution between muscovite, aluminoceladonite (ideal formula; $KAl(Mg, Fe^{2+})\square Si_4O_{10}(OH)_2$) and celadonite (ideal formula; $KFe^{3+}(Mg, Fe^{2+})\square AlSi_3O_{10}(OH)_2$) (Rieder 2000).

F and OH are known to represent one third of anions in the octahedral sheet, and in individual octahedral they arrange as *trans*- or *cis*- configuration. The microprobe method allows quantitative measurements of F content in sericite and permits an evaluation of exchange equilibrium between sericite and the hydrothermal fluid.

Our understanding of F=OH exchange for mica in hydrothermal systems is based on the contributions by Munoz (1984). It was designated that the substitution of F for OH markedly increases the physical properties of trioctahedral micas (i.e. M cations > 2.5). From this, Munoz (1984) introduced the iron-fluoride avoidance rule applicable to Fe-Mg micas and noted a positive correlation between an increase in F and [Mg+Fe] occupancy.

Results

MICA MINERAL CHEMISTRY

Microprobe analyses of sericites from the Munda resource are presented in table 8. Due to the intercalated nature and occupancy of OH in the mica formula, totals with –10 wt. % errors were accepted in this study to avoid blanket rejections and maintain deposit-scale representation of the mica chemistry. The total point analyses are subdivided by depth, with interval selection based (broadly) on equal point density. The mean and standard deviation for the representative formulae are calculated for a total negative charge of 22. The complete dataset is provided in the electronic appendix (Table A10).

All point analyses are plotted against the sum [Si+Fe+Mg] on [Al] to characterise the level of phengite substitution (Figure 18a). The plot shows that mica within the Munda resource is broadly muscovite with variable substitution to the phengite series. From preliminary analysis it appears that the distribution of phengite substitution is homogeneous and independent of depth. Noteworthy is a small subpopulation of data from sample 13TW that trend towards the composition control line of phlogopite.

The microprobe data shows that all mica analysis are predominantly dioctahedral with about two thirds of the octahedral sites occupied. With variation in phengite substitution, both Mg^{+2} and Fe (Fe^{3+} or Fe^{2+}) occupy some of the octahedral positions normally occupied by Al^{+3}. From represented samples there is a weak increase in Si and decrease in Al^{iv} present at depth, with respective values ranging from 3.26 and 0.74 at 700 m, to 3.37 and 0.63 at 950 m.

In consideration of the iron-fluoride avoidance rule, the [F] content for all K-mica are plotted against the parameter [Si+Mg+Fe] to mediate the effect of phengite substitution (Figure 18b). It is clear that fluorine is detectable in all point analyses with F-in mica values ranging from 0.35 to 0.05 a.p.f.u. The distribution of point analysis in compositional space further shows that a high-F trend is defined by analyses between 850 to 950 m. In contrary, the low-F trend limit is defined by the distribution of analyses from both 700 to 800 m, and 950 to 1020 m. Independent of [Si+Fe+Mg] occupancy, it can be further added that the approximate F-in mica threshold for the Munda resource anomaly is represented by values that range from 0.1 to 0.15 a.p.f.u

FLUORINE INDEX

To further simplify the interpretation of fluorine trends in the Munda resource, all microprobe data has been recalculated to the Fluorine Index (FI) (Figure 19c). The generalised formula presented below is based on unpublished work of Williams & Duckworth (2010) and produces a single numerical ranking that accounts for both the F-content and the quantified phengite substitution.

The FI is based on the generalised calculation;

$$\textbf{Fluorine Index (FI)} = c[F]^n / f[Si]+[Fe]+[Mg]$$

Where:

C is an arbitrary constant selected to fix the index to a convenient numerical range

[F] is the atomic proportion of fluorine in the mica structure formulae

^{n} is the power term that applies weight to both the fluorine content and its ratio to the phengite content

f[Si]+[Fe]+[Mg] is a function of the phengite substitution

Fluorine Index values used in this study are derived from the calculation

$$\textbf{Fluorine Index (FI)} = 50*[F]^{1.2} / [Si]+[Fe]+[Mg]$$

From calculated values, the FI thresholds for all point analyses range from 0.47 to 3.99 with a mean of 2.34. The distribution of FI values in consideration to depth clearly validates the upper- and lower-F trends previously defined in compositional [F] vs. [Si+Fe+Mg] space. The highest single FI value is consistent with point analyses from depths 850 to 950 m and conversely the lowest from 950 to 1012 m. Comparisons in the spread of values for each respective interval can also be made, with the high F-in mica anomalies consistent with the lowest range of FI values, and alternatively, the low F-in mica anomaly comprising broad FI values. Presenting the microprobe data in FI format therefore outlines the heterogeneities in F-enrichment that cannot be quantified by geochemical parameters in compositional space.

Application of the Fluorine Index to alteration and mineral zonation

FI values for individual samples were calculated in order to assess trends in F-enrichment in the light of lithology, Cu-Au grade distribution and mineral zonation. Two drill cores were selected for this study based on spatial representation from microprobe analysis and mineralogical variations.

LITHOLOGY, MINERALOGY AND WHOLE-ROCK ASSAYS

PH10D549: The main unit sampled at depths 950 to 972 m consists of a silica + hematite breccia hosting visible bornite mineralisation. At shallower depths the host sequence comprise (Figure19b) a matrix supported sericite-altered monolithic breccia with high matrix volume (40-60 vol.%). In contrary, at lower depths the host geology (Figure 19c) is a clast supported volcaniclastic breccia with less matrix volume (10-25 vol.%). The breccia fragments are replaced to chlorite ± sericite and the matrix is altered to earthy hematite. Gold concentration for upper and lower intervals are relatively constant, fixed at ~0.1 g/t in whole rock assays (Figure 19h). In contrary, Cu concentrations fluctuate between 0.4 and 1.05 wt.%, with the highest vales corresponding to depth 959 m. Brown bornite + pyrite are the dominant ore minerals; at shallow depths brown bornite is present as veinlets associated with specular hematite or as an intergranular film that weakly replaces euhedral grains of pyrite (Figure 19f). At depth 972 m overgrowth textures in bornite are observed with inclusions of euhedral monazite (Figure 19g) and chalcocite occurs on grain boundaries intermingling with inclusions of bornite (Figure 19e). Two sub-types of sericite are present in all samples; sericite (I) is commonly associated with pyrite grains incipiently replaced by bornite, while sericite (II) shares mutual boundaries to well developed xenoblasts of bornite (Figure 19d).

PH10D551: The investigated intervals 720 to 832 m have comparable lithology and mineralogy. The host sequence (Figure 20b) sampled at 720 m is a clasts supported monolithic breccia with low (<10 %) matrix volume. Fragments are weakly altered to chlorite and the matrix is dominantly fine-grained earthy hematite. In contrary, at depth 832 m the host sequence (Figure 20c) comprise a hematite + sericite monolithic breccia with high matrix volume (40-70 %). The matrix is invariably altered to crystalline hematite, while bleached halos are present on breccia fragments and overprint an earlier earthy hematite alteration. Whole rock assays (Figure 20h) show that Au content increases at depth, from 0.0 g/t at 720 m to 0.71 g/t at 832 m. The reverse is apparent for Cu grades, with whole rock values of 0.22 wt.% and 0.06 wt.% respectively.

Under SEM the mineral assemblage identified at the depth of 759 m is chalcopyrite (Figure 20f) plus minor altaite. Bornite is a trace mineral, and when present, chalcopyrite is well developed at grain boundaries as replacement. Sericite (I) is the dominant mica (Figure 20d) and replaces quartz at fragment boundaries and crosscuts aggregates of the F-mineral fluorapatite. In contrary, the dominant mineral assemblage at depth 832 m is sericite (II) and REE's minerals fluocerite and florencite (Figure 20e). Fluocerite is present as euhedral grains that form large (<200 μm) mineral aggregates which mediate the contact between quartz and sericite (II). Florencite is present as fine-grained intercalations within sericite (II) and also forms 20 μm euhedral grains in the matrix. Bornite (Figure 20g) is the main ore mineral and is present as <100 μm grains coexisting with chalcopyrite. In comparison, at depth 832m chalcopyrite is present as fine submicroscopic impregnations or rare concave (<15μm) fragments central to bornite grains (Figure 20g).

FLUORINE INDEX TRENDS

From Figure 19a, it is clear that the F-enrichment in drill core PH10D549 systematically decrease with depth, with mean FI values that ranging from 3.37 at 950m, 2.33 at 959m and finally 1.68 at 972 m. On a specimen scale, the decrease in FI values strongly correlates to a decrease in both matrix volume and the development of sericitic alteration in the host breccia unit. The broadest range is present for point analyses from sample 34TW, and in contrary, the respective distribution of FI values for samples peripheral are relatively narrow.

From mineralogical and texture evidence, it is clear that the development of pyrite to bornite replacement is negatively correlated to increasing FI values. For point analyses that define the upper FI threshold, euhedral grains of pyrite are observed with only incipient replacement to bornite at grains boundaries. In comparison, the observed replacement sequence for Cu-(Fe)-sulphides spatially coincident with lower FI values is appreciably pyrite → bornite → chalcocite.

From Figure 20a it is clear that the spatial trend in FI values for drill core PH10D551 is comparable to drill core PH10D549. Mean FI values for respective intervals range from 1.83 at 720 m, 1.93 at 751 m and finally 2.71 at 832 m. When corroborating the trend in F-enrichment to observations made on a specimen scale, a strong positive correlation between increasing FI values and the development of sericitic alteration and breccia matrix volume is consistent with drill core PH10D549. Also noteworthy is the positive correlation between F-enrichment and Au content from whole rock assays grades,

which range from 0.0 g/t at 720m to 0.7 g/t at 832 m. In contrary, whole rock Cu-concentrations shows a weak negative correlation, decreasing from 0.3 wt.% at 720 m to 0.06 wt.% at 832m.

From SEM observations it can be further noted that the development of sericite (II) spatially coincides with pervasive sericitization and a high F-in mica anomaly. In comparison, sericite (I) was abundant at depth 720 m and coincided with white mica alteration on a specimen scale. Also associated with elevated FI values is the development of the F-REE mineral fluocerite. Florencite is also abundant as fine intercalations with sericite (II).

Interesting comparisons can also be made between the spatial variation of the F-in mica anomaly and coincident Cu-(Fe)-sulphide paragenesis. From SEM the sequence of replacement depicted in sample 7TW is appreciably bornite → chalcopyrite. In contradistinction, the paragenesis observable in sample 10TW is chalcopyrite → bornite.

Implications

The geochemical data from this paper represent the first attempt to constrain the distribution of fluorine in sericite from the Munda resource. From the selected suite we have aimed to represent both spatial and mineralogical variation throughout the deposit with consideration to the presence of discrete fluorine minerals. The geochemical data from this study can be compared to the fluorine data for Malu deposit at Prominent Hill (Williams & Duckworth 2010) and the Olympic Dam deposit (Tappert *et al.* 2011). We also evaluate the zonation of mineralogy observed in this study and make comparisons to experimental work constraining the geochemical behaviour of F-enriched hydrothermal fluids.

COMPARISONS WITH PUBLISHED WORK

The Olympic Dam IOCG-deposit represents a world-class enrichment in Cu, Au, and U, but it is also a fluorine anomaly in a crustal setting (Ehrig & Green, 2009). Within the deposit fluorite is a major mineral and present as crosscutting veins or as fragments within the mineralised breccias. Fluorine also occurs as F-chlorite, F-sericite along with REE phases such as bastnaesite, britholite and florencite. Microprobe data collected by Tappert *et al.* (2011) shows that the chemical composition of K-mica from Olympic dam is broadly phengitic and that the sum of [Si+Fe+Mg] present in octahedral

sites strongly increases with depth. The distribution of the F-in mica anomaly also shows strong depth dependence, with the average F-content ranging from 0.0 wt.% at 38m to 1.41 wt.% at 245 m.

At Prominent Hill, understanding of mica geochemistry is based on unpublished data from Williams & Duckworth (2010). Using the microprobe technique, the results show that micas are predominantly sericite with significant phengite substitution, which is concordant to the findings of this study. The author also validates a positive correlation between the phengite substitution and F-enrichment. The F-in mica anomaly for Prominent Hill is stated at 0.15 - 0.20 fluorine a.p.f.u (calculated for a total negative charge of 44) with a maximum F-enrichment of 0.68. The distribution of point analyses in [F] verses [Si+Mg+Fe] compositional space is also highly variable and defines an upper and lower F-threshold.

For discussion on fluorine enrichment, all point analysis presented by Williams & Duckworth (2010) are subdivided by host lithology and therefore no preliminary spatial trends were concluded. For this study, dismembering the point analyses by drill core depth has shown that F-enrichment in strongly depth dependent, with a high F-in mica anomaly corresponding to intervals comprising mineralised hematite-sericite breccias. There is also a pronounced vertical zonation, with breccias peripheral to these intervals marked by pronounced low F-in mica anomalies.

PETROGRAPHIC CONSTRAINTS ON MICA PARAGENESIS

Developing an understanding of the mica paragenesis in the context of the Cu-(Fe)-sulphide formation is of value when evaluating the role F-complexes have played in metallogenetic processes.

From cross cutting relationships depicted in SEM, it is clear that at least two generations of sericite are present in the Munda resource. Sericite (I) was been previously defined as coarse-grained and chemically homogenous and present in hand specimens where white mica alteration is developed. From cross cutting relationships depicted in BSE, the development of sericite (I) can be constrained to predate all forms of Cu-(Fe)-sulphides. This statement is based on textural evidence showing chalcocite grains crosscutting the fabric of sericite (I) (Figure 11h). Further evidence can be drawn from this study where sericite (I) is depicted in close association with euhedral pyrite (Figure 19f). Although unclear, it can be further added that these grains of pyrite, which are subsequently replaced by bornite, also crosscut the fabric of sericite (I).

In comparison, sericite (II) is invariably fine grained and comprises fine intercalations of mica with chemical heterogeneity. Sericite (II) also has an indisputable relationship with Cu-(Fe)-sulphide development, forming mutual boundaries with brown bornite and white chalcocite. Further evidence can be draw from SEM images that show lamellae of sericite (II) clearly crosscutting the grain boundaries of Cu-(Fe)-sulphides (Figure 8d). Based on these observations it is unequivocal to interpret the development of sericite (II) as both syn- and post-major Cu mineralisation in the Munda resource. Moreover, sericite (II) has been characterised with complex associations with REE minerals such as fluocerite and fluorencite. This mineralogical association would suggest the development of sericite (II) and deposition of REE minerals occurred in equilibrium.

FLUORINE DISTRIBUTION AND ALTERATION MINERALOGY

From petrographic investigations there is a clear vertical zonation in alteration and REE minerals that coincides with the F-in mica anomaly defined in this study. From microprobe analysis, the high F-in mica threshold for the Munda resource was defined by an upper FI value of 4 for the interval 850 to 950m. Breccia sequences spatially coincident comprise a high matrix volume (<60 %) and well-developed sericite + crystalline hematite alteration. The textural aspects of this alteration are distinct to elsewhere at the Munda resource with breccia fragments comprising a distinct sericitic halo that overprints an earlier earthy hematite alteration.

To the peripheral of these intervals, and coinciding with the low F-in mica thresholds, sericite (I) is well developed and the main F-bearing mineral present is fluorapatite. The microprobe data collected from representative intervals show that sericite (II) has a higher occupancy of F then sericite (I). Evidence can be drawn from point analyses acquired from sample 5TW and 10TW. In sample 5TW, where sericite (I) was the dominant phase, mean F content per formula unit was 0.19. This is comparable to 0.26 for sample 10TW, from which sericite (II) was the dominant phase. However based on textural relationships, a temporal disconnection between the development of sericite (I) and sericite (II) is favored, therefore rejecting the significance of F-enrichment from point analyses taken on the former.

FLUORINE DISTRIBUTION AND MINERALISATION

The investigation of whole-rock assay grades in relation to fluorine trends is inconclusive in defining any potential correlations. From the unified study conducted on drill core PH10D551, whole rock data show that the Cu-content decreased proximal to zones with high F-in mica anomalies. In contrary, whole rock Au grades increased from 0.0 g/t distal-to- and 0.7 g/t proximal-to the main F-in mica anomaly.

The most intriguing observation was the variation in the Cu-(Fe)-sulphide paragenesis for intervals of comparable F-enrichment. At depth 759 m, and coinciding with low FI values, bornite to chalcopyrite replacement is developed and suggests Cu-removal via mineral-fluid reaction is present in the paragenesis. At depth 832 m, and coinciding with high FI values, the replacement of chalcopyrite to bornite is conversely representative of Cu-enrichment. The contradiction in the Cu-(Fe)-sulphide paragenesis can be best explained when considering the complex geochemical nature of F-enriched hydrothermal fluids.

Numerous authors have demonstrated that the presence of F in aqueous fluids is instrumental in the dissolution and transportation of metals and REEs in a hydrothermal solution (Keppler 1993, Hedenquist and Lowenstern, 1994; Aiuppa et al., 2009). Extrapolating this to the Munda resource; hydrothermal alteration profiles may exhibit strong vertical zonation, whereby Cu leached in the upper and lower sequences may be subsequently redeposited in central breccia units. This hypothesis would thereby simplify what may appear as a complex ore forming system comprising the interplay of multiple fluids with comparable chemistries.

Gold enrichment (<2 g/t) proximal to high F-in mica anomalies warrants further investigation. No discrete Au mineral were recognised in represented samples. From other samples however, fine-grained (<4 μm) Au-Cu phases were present in florencite-dominant veins. Florencite is also well developed in samples where (<1 mm) of Au-Cu phases are present, validating this mineral association. Elsewhere in the Munda resource, the REE phase was either absent or minor. An equivocal interpretation is that the fluid responsible for the precipitation of florencite contains dissolved Au and Cu. Upon change in physiochemical conditions during alteration - including pH, Eh, fluid rock/ratios, and F-concentrations - Au-Cu alloys may be deposited in equilibrium with florencite. Due to the highly chalcophile nature of Cu, this would also suggest that the fluid chemistry is depleted in S.

LA-ICP-MS: TRACE ELEMENT STUDY

Introduction

Bornite and chalcocite are major Cu-carriers in IOCG deposits such as Olympic Dam, Carrapateena and Prominent Hill in the Gawler Craton (Hayward & Skirrow 2010). Understanding the Cu-(Fe)-sulphide geochemistry has implications for both processing and fluid source vectoring. This is because knowledge of trace/minor elements in sulphides is fundamental for evaluation of the distributions of economic by-products such Au and Ag, particularly where the host bornite and chalcocite are volumetrically significant. The populations and distribution of exotic elements, such as Se, Bi and Ag also show promise for near-mine exploration and proximal-to-source vectoring (Cook *et al.* 2011; in prep). Information on trace element distributions within key minerals can also be used to optimize processing and thus ensure improved recoveries of by-product elements (Cook *et al.* 2011; in prep).

This study represents the first attempt to determine the trace element geochemistry of bornite and chalcocite from the Munda resource. Twelve one-inch sections were selected for the LA-ICP-MS study based on their spatial and textural variation. The methodology and conceptual framework for this study is adapted from Cook *et al.* (2011; in prep). This study demonstrated that hypogene bornite and chalcocite are favourable hosts for exotic elements such as Bi, Pb, Se and Te. Furthermore, bornite and chalcocite displayed systematic fractionation of Bi and Ag, and that trace element variation might offer insights into ore genesis and have potential value in near-mine exploration. These ideas have been tested at Prominent Hill (Cook & Ciobanu, unpublished) with some degree of success, using drillcore material from the Munda deposit and western Ankata resource, but not from Munda.

Insight into replacement processes

In contrast to the single-stage hypogene Cu-Fe-sulphides investigated by Cook *et al.* (2011; in prep), Prominent Hill display substantial evidence of replacement and remobilisation processes. The Cu-(Fe)-sulphide paragenesis (*sensu lato*) thus needs to be carefully evaluated with respect to genetically related or superimposed textures before the LA-ICP-MS data can be correctly interpreted to aid understanding of fluid geochemistry, the sequence of mineralising events and identification of potentially useful trace element distribution patterns.

THE COPPER-IRON-SULPHIDE PARAGENESIS

Evidence of crosscutting relationships, mineral zonation and exsolution suggest a complex history of Cu-enrichment coupled with localised Cu-depletion has been superimposed on a proto-ore system consisting pyrite and an early Pb-Se enriched bornite.

Purple bornite with a Type-A fabric represents the first Cu-(Fe)-sulphide assemblage. Such bornites form symplectoids with clausthalite (Figure 12a-b) and commonly coexist with blue chalcocite. Based on mineralogical studies conducted on synthetic sulphide systems (Brett, 1964; Barnes, 1997; Grguric & Putnis, 1999) it can be proposed that this texture is the product of exsolution from a high temperature (>350^{o}C) bornite$_{ss}$ containing anomalous credits of Pb and Se. Grains with preserved Type-A fabrics are invariably hosted within cavities of silicate fragments or are encapsulated within networks of fine-grained (<2 μm) hematite gangue (Figure 10d).

Purple bornite with a Type-B fabric (Figure 12c) is orange to red under reflected light and rarely observed coexisting with chalcocite. The presence of fractures, serrate boundaries and coalescence of clausthalite inclusions provides evidence for decomposition of these grains. Unlike the perfect symplectic textures observed in Type-A bornites, clausthalite forms irregular emulsions that disperse at grain boundaries. Considering bornite crystal structure, this observation could correlate to any of the three temperature dependent polymorphs transitions that may result in release and subsequent remobilization of impurities. This is validated from microprobe analysis where it is shown that Type-A purple bornites have elevated impurities of Pb and Se in comparison to Type-B purple bornites.

Further evidence for the Cu-(Fe)-sulphide paragenesis can be drawn from petrographic observation where brown bornite is replaced by chalcopyrite (Figure 12d-g). Evidence of this replacement can be drawn from Type-B purple bornite with crosscutting neo-crystallisation of chalcopyrite. Within the same sample the development of this transformation is varied, and for Cu-(Fe)-sulphide grains where chalcopyrite is the dominant phase, bornite always appears brown under reflected light. Irregular, μm-scale grains of altaite (PbTe) (Figure 12d-e) are commonly seen precipitating at the contact between brown bornite and chalcopyrite. In the final stage of the paragenesis, chalcopyrite forms porous monomineralic aggregates (Figure 12h) with open fractures providing evidence of replacement by dissolution. Altaite (Figure 12i-j) is present as both submicroscopic and coarse-grained <4 μm aggregates validating the Se-Pb-Te affinity throughout the mineral assemblages.

Interestingly, textural aspects of Cu-(Fe)-suphides also suggest that replacement processes permitting the enrichment of Cu are present proximal to major mineralised breccia sequence. The early stage of replacement is depicted in Figure 10g, where purple bornite hosted within a silicate cavity is replaced by blue chalcocite. Within the same sample the magnitude of this replacement varies from incipient to pervasive and always occurs on grain boundaries or along crystallographic planes. Of further interest is the transformation in Cu-(Fe)-sulphide morphology toward major Cu-bearing breccias, with a proximal-to trend of firstly cavity hosted blue chalcocite followed by interstitial veined blue chalcocite (Figure 10c). In such breccias white chalcocite is the dominant Cu-sulphide and occurs principally as open space infill. Round inclusions of quartz hosted in white chalcocite also suggest that the replacement of host gangue by the former has permitted the precipitation of coarse-grained xenoblasts.

From textural and mineralogical aspects of brown bornite and grey chalcocite mineralisation it is favored that pyrite has provided a first order control on the development of these Cu-(Fe)-sulphides. Euhedral grains of pyrite are crosscut and rimmed by brown bornite in poorly mineralised intervals (Figure 9h). Within the same drill core the evolution of this process becomes clearer, with bornite forming large xenoblastic grains encapsulating concave grains of pyrite (Figure 9c). This replacement sequence is further supported by microprobe analysis that shows brown bornite is invariably Cu-poor (Figure 17g), raising the possibility that submicroscopic intercalations of pyrite are still present.

In the shallow dolomitic sequences, major pyrite mineralisation is crosscut by neo-veinlets of blue chalcocite with minor blebs of red bornite (Figure 13h). Such pyrite-dominant mineralisation is distinct as it is hosted in weak chloritic alteration. At lower depths chloritic alteration is overprinted by earthy hematite and the replacement of pyrite is well developed, with grey chalcocite comprising ~50 vol.% of the sample (Figure 13a). Within the same sample, veinlets of (Figure 13f) chalcopyrite preceding red bornite are depicted crosscutting grey chalcocite. Such textures provide evidence for the final stage in the Cu-(Fe)-sulphide paragenesis.

Results

Selected data on the trace element concentration in both bornite and chalcocite are provided in Table 9-10. The complete dataset is given in the electronic appendix (Table A11-A12). Selected time-resolved depth (TRD) profiles are given in Figure 21-22. Purple bornite grains were typically <60 μm in diameter and are present with intergrowths of chalcocite, with minor exsolution of clausthalite (Figure 21a-c). Grey chalcocite also contains inclusions of hessite and Au-Cu phases. Obtaining 'clean' ablations with sufficient sample volume was often difficult for the two phases due to small size and intergrown character. The remaining bornites and chalcocites are coarse-grained and free of inclusions minimizing analytical errors.

SILVER

Concentrations of silver were present in all spot analyses with values ranging from 0.47 ppm to 192 ppm. Chalcocite typically carries more Ag than bornite and is the major carrier of Ag in the Munda resource. For all chalcocite varieties, time resolved depth (TRD) profiles are invariably flat and mimic Cu-concentrations, implying that silver resides within solid solution. This is also true for bornite although concentrations are commonly an order of magnitude lower than in coexisting chalcocite.

Concentrations of Ag in blue chalcocite were also among the lowest (6-13 ppm). White chalcocite and grey chalcocite (Figure 22f) are comparably enriched in Ag (mean concentrations of 50 and 78 ppm, respectively). Values for grey chalcocite are also highly variable and range from the dataset minimum (0.47 ppm) to the maximum (192 ppm). There is also a noteworthy comparison in the distribution of Ag throughout the chalcocite dataset. White chalcocite shows a Gaussian distribution whereas grey chalcocite is bimodal (Figure 23a); subpopulations in grey chalcocite correspond to individual samples.

In purple bornite enrichments of Ag are highly variable (5-114 ppm). Typical values are narrower for brown bornite (8-42 ppm). Grey bornite values are also highly variable (~5 to ~80 ppm).

BISMUTH

Bismuth concentrations are commonly an order of magnitude higher than Ag and range from 0.5 ppm to 1406 ppm. Bornite shows the strongest enrichment in Bi, with values displaying a bimodal

distribution on the histogram (Figure 23b). For bornite, representative TRD profiles depicting Bi concentrations are flat and correlative to Fe suggesting Bi resides in solid solution (Figure 21e). TRD profiles for chalcocite are not always flat; spikes appear to be correlative to contamination from bornite inclusions. Purple bornite has the highest Bi-enrichment coupled with highly variable values (ranging from 0.87 ppm to the highest single analysis of 1,406 ppm). In contrast, brown bornite demonstrates a narrow range of Bi-enrichment (44-104 ppm). Concentrations of Bi in red bornite were the lowest of all bornite (only 0.79 to ~7 ppm). Concentrations of Bi in all chalcocite varieties are within the same order of magnitude and the distribution of values are represented by the left hand peak on the respective histogram plot. The lowest value of 0.5 ppm was measured in blue chalcocite whereas the highest single value (31 ppm) was from grey chalcocite in association with Au-Cu phases.

GOLD

Concentrations of gold in most point analyses were below detection limit. Among the exceptions, purple bornite with a Type-A fabric (Figure 21f-g) appears to host significant Au, with six of the seven point analyses showing detectable concentrations. In sample 15TW, Au concentrations in bornite ranged from 1.9 to 65.6 ppm, with a sample mean of 16 ppm. Purple bornite (sample 8TW) gave the highest single value (~130 ppm). From TRD profiles, Au concentrations in bornite are either flat or display marked spikes, demonstrating that Au resides in both solid solution and as submicroscopic inclusions. Coexisting with purple bornite; blue chalcocite registered only a single value (~0.6 ppm) above *mdl*. This measurement is likely to be an analytical artifact, the high Fe concentration in the analysis suggesting that admixtures of bornite are present.

As anticipated, grey chalcocite intergrown with Au-Cu alloys registered highly variable Au concentrations. The two highest values (5,027 ppm and 836 ppm) were rejected due to the likelihood of contamination from associated free gold. The three remaining values (12-29 ppm) are conceived as submicroscopic inclusions, as evidenced by spikes in the TRD profiles.

LEAD AND THALLIUM

Lead concentrations in Cu-(Fe)-sulphides are among the highest of all represented elements, consistent with the observation of fine-grained clausthalite. The highest single value (97,232 ppm) was obtained from purple bornites with Type-A fabrics (Figure 21f). The distribution of values is

largely skewed for bornite, with mean values of 8,313 ppm for purple bornite, 92 ppm for red bornite and 24 ppm for brown bornite (Figure 32e). Interestingly, TRD profiles for Pb were generally flat for grains with and without visible inclusions of clausthalite. This presents two possible interpretations; (1) Pb resides as solid solution within purple bornite in concentrations comparable to the inclusions of clausthalite; or (2) that submicroscopic inclusions are sufficiently fine-grained to produce an artificial homogeneity. Coexisting blue chalcocite had values ranging from 4 to 2,832 ppm. Lead concentrations in white and blue chalcocite are considerably lower (mean ~8 ppm and ~6 ppm, respectively); TRD profile spikes suggest Pb resides within submicroscopic inclusions.

Bornite also hosts thallium at concentrations an order of magnitude below that of Pb. TRD profiles show that Tl mimics Pb. Thallium concentrations range from 0.04 to 254 ppm in bornite and 0.1 ppm to 4 ppm in chalcocite.

SELENIUM AND TELLURIUM

Detectable concentrations of selenium are noted in all point analyses, with the relative distribution showing no preference for either chalcocite or bornite. Due to the widespread visible exsolution of clausthalite, Se-enrichment in purple bornite is highly variable (25 to 78,951 ppm). On the histogram (Figure 23c) three discrete subpopulations are noted and are directly correlative to the development of replacement textures in purple bornite. This highest mean Se enrichment (54,241 ppm) is present in purple bornites with a Type-A fabric. With the presence of replacement textures, the concentration of Se in bornites with a Type-B fabric is considerably lower (mean 6,775 ppm). From TRD profiles Se signals are invariably flat for all Cu-(Fe)-sulphides suggesting concentrations reside in solid solution. Similar to Pb, this is irrespective of the presence of discrete selenide minerals or not.

On average, blue chalcocite contained half the Se content of coexisting bornite, with values ranging from 804 to 33,522 ppm (mean 8,832 ppm). Red bornite had higher enrichments in Se when compared to brown bornite (mean values of 85 ppm and 54 ppm, respectively). In contrary to their bornite correlatives, white chalcocite has, on average, higher Se enrichment then grey chalcocite, (mean values 281 and 77 ppm, respectively).

Tellurium was present in all spot analyses, broadly correlative to Se but present at concentrations an order of magnitude less. In all TRD profiles Te signals are broadly flat and mimic Se, illustrating that Te also resides as solid solution in all Cu-(Fe)-sulphide phases. The broadest range of Te-enrichment is

present in purple bornite (19 to 3,274 ppm). Blue chalcocite has, on average, half the Te concentration of coexisting bornite, with concentrations ranging from 8 to 1,300 ppm. With visible inclusions of hessite, grey chalcocite in association with Au-Cu phases is highly enriched in Te. Values range from 6 to 2,967 ppm with the higher values correlative to submicroscopic hessite inclusions as demonstrated by peaks on the TRD profiles. Both red and brown bornites are conversely poor hosts for Te (means 7 and 3 ppm, respectively). White chalcocite is Te-rich (32 to 101 ppm).

OTHER ELEMENTS

Detectable concentrations of Co and Ni are present in Cu-(Fe)-sulphides from samples that contain Co-Ni-bearing phases. In other samples, concentrations are below *mdl*. The identification of Co-safflorite in sample 15TW validates discrete spikes in TRD profiles for both Co and Ni.

Elevated levels of As in purple bornite and blue chalcocite are consistent with inclusions of loellingite and minor Co-bearing arsenides. In sample containing white chalcocite and brown bornite, As concentrations are generally <28 ppm and are present as submicroscopic inclusions in TRD profiles. Red bornite replacing grey chalcocite is generally more enriched in As (mean 25 and 6 ppm, respectively). Tin concentrations are variable, with irregular TRD profiles suggesting the presence of submicroscopic Sn-bearing phases. Concentrations of Sb (<134 ppm) are typically higher in samples with Ni-Co-bearing mineral inclusions. It is therefore likely that Sb occurs as fine dustings on Co-Ni-arsenides such as Co-safflorite.

Data Trends

Silver and Bi are two chalcophile elements present at elevated concentrations in all spot analyses. The element pair shows an antithetic behaviour, with Ag showing a preference for chalcocite and Bi for bornite. The log-log plot of Ag vs. Bi (Figure 24a) clearly shows a systematic partitioning of the two elements between chalcocites and bornites with a mineral association are present. The highest Ag values associated with grey chalcocite cluster in the top left corner of the diagram since corresponding Bi-concentrations are < *mdl* (if the subpopulation of grey chalcocite associated with Au-Cu phases that was sampled at greater depths is excluded). Red bornite occurring as veins within chalcocite clearly displays higher enrichment in Bi and a lower enrichment in Ag. The relationship between white chalcocite and brown bornite further validates this trend.

Less clear however is the partitioning of Ag and Bi between purple bornite and blue chalcocite. The recognition of purple bornite Type-A and Type-B textures must be acknowledged when trying to interpret this data trend. From petrography it was concluded that purple bornites have undergone varying magnitudes of phase transformation and replacement, more so then elsewhere in the deposit. This observation may explain why purple bornite shares a geochemical affinity with both brown and red bornites when discriminated by Ag and Bi enrichment.

There are a number of element pairs that show positive correlations that are to be expected because of their geochemical affinity between the elements concerned and the mineralogy of exsolutions observed. As anticipated from the identification of clausthalite inclusions, Pb and Se is one element pair where there is a strong positive correlation (r = 0.66). From the log-log plot (Figure 24b) it is clear that purple bornite shows the strongest correlation coefficient for this pair. However for Cu-(Fe)-sulphides where evidence of replacement is present there are two distinct populations, with Se-enrichment favouring chalcocites and Pb favouring bornites.

A good correlation between Se and Te (Figure 24e) is seen (r=0.6). Upon further interrogation of the data it is clear that both Te and Se systematically decrease throughout the Cu-(Fe)-sulphide paragenesis.

A strong correlation between Co and Ni (Figure 24f) is observed (r=0.52). From the log-log plot it is clear that Ni shows a preference for bornite while Co is elevated in white chalcocite. Also noteworthy is a weak positive correlation (r = 0.16) between Pb and Tl (Figure 25a). From the log-log plot it is clear that Pb and Tl enrichment shows a preference for bornite, with a majority of values plotting along the regression line. Conversely the cluster of values along the y-axis shows that chalcocite is a poor host of Tl irrespective of Pb enrichment.

With evidence for element leaching and remobilising present the in the Munda ore genesis, warranting investigation is the element pair Ag and As. Experimental data in literature has shown that Ag and As concentrations are strongly correlative in supergene digenite defining a wedge-shaped zone in log-log space (Reich *et al.* 2010). In this study however, correlations between As and Ag are poor for all chalcocites, with a weak negative correlation between the two elements best observed in bornite.

For Munda Cu-(Fe)-sulphides, some clear spatial trend in Ag- and Bi-enrichment are present. Silver concentrations in all chalcocites increase away-from-source (distal) in respect to depth (figure 25e) and displacement towards the western Ankata deposit (Figure 25c). Conversely, Bi-enrichment in all

increase closer-to-source (proximal) and are elevated at lower depths (Figure 25f) and along strike toward the Mula deposit (Figure 25e). However, in saying this, there are nevertheless a number of exceptions to this trend. Of the grey chalcocites, Ag-enrichment is an order of magnitude higher at depth 508 m when compared to depth 320 m. This outlier does show however that there is a stronger distal-to-source dependency for Ag-enrichment in chalcocite, as the highest vales where sourced from a sample further along strike towards the Ankata deposit.

Implications

The multi-element LA-ICP-MS data represent the first attempt at classifying the geochemical signature of the Munda Cu-(Fe)-sulphides. From petrographical studies conducted on the represented samples it is evident that the Cu-(Fe)-sulphide paragenesis comprises multiple stages of element recycling and redeposition. We have therefore sought to sample all phases based on textural and spatial variations to ensure the dataset is representative. Below we evaluate the dataset in the light of (i) published experimental work on relevant phase systems; and (ii) published data for bornite and chalcocite from other natural systems.

INSIGHT INTO EXPERIMENTAL WORK

Understanding of the system Au-Cu-Fe-S is based chiefly on the contributions of Simon *et al.* (2000). From experiments carried out at temperatures of 400 to 700˚C, Simon *et al.* (2000) quantitatively determined Au partitioning between bornite and chalcopyrite. Results show that high-temperature bornite ($bornite_{ss}$) can be a major host of Au and contains one order of magnitude more Au than chalcopyrite. The range of Au concentrations in bornite decreases markedly with decreasing temperature from 1,280 to 8,200 ppm Au in bornite at 600˚C, to 235 to 364 ppm Au in bornite at 500˚C, and 13 to 80 ppm Au in bornite at 400˚C (Simon *et al.* 2000). The amount of gold in bornite is also phase dependent, with the highest enrichments present in stoichiometric phases, followed by Cu-rich varieties, and lowest in Cu-poor varieties (Simon *et al.* 2000). In our LA-ICP-MS data we have shown that concentrations of up to ~12 ppm Au reside in purple bornite in solid solution. From the experimental work conducted by Simon *et al.* (2000) it is possible to place a tentative constraint on the temperatures permitting the substitution of Au in Munda purple bornites. The averages and ranges of Au concentrations for respective bornite Cu/Fe ratios determined by EMPA are shown in Figure 26a

(Simon *et al.* 2000). The relative field shows Au saturation temperatures of <400˚C are favored. Although this temperature estimation does not account for Au removal from low-T alterations, it does coincide with the >350˚C temperatures required for $bornite_{ss}$ containing anomalous credits of Pb and Se.

COMPARISONS WITH NATURAL COPPER-(IRON)-SULPHIDES

Quantitative trace element data for bornite and chalcocite is largely incomplete for IOCG systems. Applicable to this study is a small dataset provided by Cook *et al.* (2010; *in prep*) on the trace element populations of bornite and chalcocite from the Olympic Dam deposit. The results show that bornite is a major host of Ag and Bi, with enrichments present at 70.5 and 204 ppm. Chalcocite in comparison is a poor host, with concentrations of 3.0 and 7.1 present. This is comparable to the distribution of the element pair in this study, with Ag showing a strong preference for chalcocite, particularly for grey chalcocite.

Silver and Bi at concentrations of >1 wt.% has been documented in hypogene bornite by Cook *et al.* (2010; *in prep*). Cook *et al.* (2010; *in prep*) also contends that Ag and Bi show a systematic partitioning, with Ag showing preference for chalcocite and Bi for coexisting bornite. From our LA-ICP-MS data the partitioning of the two elements is most pronounced for bornites and chalcocites that coexist (i.e. red bornite and grey chalcocite). With no textural evidence to suggest hypogene development of these Cu-(Fe)-sulphides, the systematic fractionation of this element pair must also occur for low-T phases precipitating from a comparable ore fluid. Of interest here is that textural properties of purple bornite coexisting with blue chalcocite are conceivable via hypogene formation. However, our LA-ICP-MS data shows that enrichments of Ag are higher in purple bornite (up to 192 ppm) then coexisting blue chalcocite (up to 13 ppm). This provides geochemical evidence to suggest that blue bornite has formed via the replacement of purple bornite.

Cook *et al.* (2010; *in prep*) also comments that bornite is a poor host of Au, which mimics Ag by being typically richer in coexisting chalcocite. In contradistinction, concentrations of up to 12 ppm Au are present in Munda bornites in solid solution or as submicroscopic inclusions. With the highest single value of 0.6 ppm, chalcocite coexisting with bornite is comparably a poor host of Au.

DISCUSSION

This study represents the first micro-analytical classification of gold and Cu-(Fe)-sulphides from Munda diamond drillcore. Current understanding on the Prominent Hill mineralogy is based on Belperio *et al*. (2007) and the unpublished report of Benavides (2010) concerning the paragenesis. From our LA-ICP-MS data we contribute the trace/minor element geochemistry of Munda Cu-(Fe)-sulphides and have evaluated the relative distributions in a paragenetic framework. Furthermore, a unified study on the distribution of F-bearing mica has evaluated the role fluoride-complex in the leaching and transportation of principal ore products Cu, Au and U. Below we evaluate our findings in the light controversial topics concerning both Prominent Hill and the broader IOCG genetic model.

Controversies in IOCG ore genesis

On a global scale, the classification of a prototypical IOCG deposit has been continuously revisited (Hitzam 1992; Hitzam 2000; Pollard 2010a, Groves *et al*. 2010). Many aspects of the model remain enigmatic or somewhat equivocal. It has been recognised in literature that; (1) IOCG deposits can form in numerous terrains, all of which are explained by geologically 'reasonable' models (Hitzam 2000; Barton & Johnson 2000); that (2) fluids transporting ore constituents (Fe, Cu, Au, U, S) are inherently complex, demonstrating both magmatic and/or meteoric origins and involving multiple phases of hydrothermal injection (Gow et al. 1994); and (3) no clear spatial, other than a temporal, relationship is required within a batholithic complex other than the preservation of a temperature flux (Pollard 2010a).

From current literature at Prominent Hill there is no textural evidence to suggest that uranium and major Cu-mineralisation (i.e. bornite-chalcocite) formed in equilibrium. Uraninite is the principal U-bearing mineral of the Malu deposit and occurs as discrete grains encapsulated in iron oxides or chalcopyrite (Belperio *et al*., 2007). Also of interest is the distribution and enrichment of Au and Cu ore at Prominent Hill, with the Munda resource endowed in Au while the western Ankata deposit Cu only. At the Munda resource, current near mine exploration has shown that Au and Cu mineralisation is distinctively zoned, with either low-Cu concentrations peripheral to Au, or low-Au concentrations peripheral to Cu.

RECONSTRUCTION OF THE MUNDA RESOURCE ORE SYSTEM

Evidence for a proto-ore system

The present study contributes to the mineral inventory at Prominent Hill in that clausthalite, safflorite, Co-safflorite, loellingite and xenotime are reported for the first time. Based on textural relationships we provide compelling evidence to suggest these phases form a mineralogical association with purple bornite and coexisting blue chalcocite. From petrographic investigations we have also shown that chalcocite and coffinite (Figure 11f) occur as complex polymineralic aggregates, and furthermore, that textural aspects of these grains are suggestive of simultaneous deposition. This observation contributes to a genetic model for Prominent Hill, as it provides textural evidence to suggest concentrations of uranium have precipitated broadly coeval with purple bornite.

From analytical work we have constrained the geochemical and textural aspects of purple bornite. The LA-ICP-MS data shows that maximum concentration of ~7 wt.% Se, ~10 wt.% Pb, 3,208 ppm Te, 974 ppm Bi, and 114 ppm Ag reside, in solid solution within this bornite generation. Of interest here are the wt.% levels of Pb and Se, even for point analyses where clausthalite is absent. More importantly, purple bornite hosts significant concentrations of Au, with up to ~12 ppm in solid solution and 129 ppm detected as nano-scale inclusions. Based on these lines of evidence it is favoured that this input of exotic elements (i.e. Pb and Se) and important precious metal concentrations (i.e. Au and Ag) have been sourced from a single fluid. From trace element data on major Cu-(Fe)-sulphide phases (i.e. white chalcocite - brown bornite) it can be also added that the fluid-source is comparable to that responsible for major Cu mineralisation at the Munda resource.

Based on the contribution of Simon *et al.* (2002), we have estimated gold saturation temperatures for purple bornite to be <400°C. This temperature aligns with the extensive literature on sulphide systems that favour high-T processes (>350˚C) for the formation of symplectic textures (Brett 1864; Augustithis, 1997). The presence of clausthalite in purple bornite also carries physiochemical constraints, with Simon *et al.,* (1997) showing that $fSe_{2(g)}/fS_{2(g)}$ ratios higher than unity are required to permit precipitation of selenide minerals within a sulphide.

From petrography, there is strong textural evidence to suggest that formation of purple bornite predates the development of steely hematite alteration. Under BSE Type-A bornite grains invariably occur within fine-grained networks of hematite lamellae. Based on the absence of sericite in selected samples it is also clear that this steely hematite alteration has placed a mineralogical buffer permitting the preservation of this assemblage. Interestingly, Benavides (2010) provides evidence to suggest that steely hematite alteration represents stage IV in the paragenesis and the first pulse of Fe metasomatism at Prominent Hill. The implications of this observation would suggest that the formation of purple bornite and associated Co-Ni-Fe-arsenides and uranium minerals represents the first stage in the Prominent Hill ore genesis and a temporal disconnection between major Cu mineralisation.

Although it is beyond the scope of this project to place spatial constraints on the formation of this assemblage, some interesting observations can nevertheless be noted. From this present study we have identified purple bornite in sampled depths from 720 to 1007 m and in poorly mineralised (<0.3 Cu wt.%) rocks peripheral to Cu-bearing breccias. From studies on the textural and mineralogical aspects we provide compelling evidence to suggest that formation of associated gangue minerals (i.e. hematite and sericite) occurred under conditions permitting open space infill and colloidal fabrics. Also interesting is the dearth of petrographic evidence, at least in the present study, to suggest that purple bornite has formed in original volcanic precursors. Rather, the host sequence generally comprises rounded fragments of quartz and poorly sorted fibrolitic hematite grains. Although equivocal, there is some evidence to suggest that the precipitation of purple bornite occurred within the quartz fragments of an original sedimentary package.

Evidence for element remobilisation

In petrographic investigations we introduced the term Type-B bornites (Figure 12c), and suggest that fabric properties or these grains are typomorphic to replacements, and furthermore, that these replacements resulted in the remobilisation of impurities (i.e Pb and Se) via processes of diffusion. From textural studies, microprobe analysis, and LA-ICP-MS we have shown important contents of Cu are remove from breccias adjacent to major-Cu intervals via the replacement sequence (1a).

(1a) Type-A purple Bn + PbSe → Type B purple Bn ± PbSe → Cp ± PbTe

From the LA-ICP-MS method we have shown trace element enrichments in Type-B purple bornites are far lower, with mean concentrations of 6775 ppm Se, 2844 ppm Pb, 16 ppm Ag, and 41 ppm Bi detected in point analyses. Of interest here, is that no concentrations of Au were detectable in any point analyses where replacement processes are evident. This observation speculates that important concentrations of Au have been leached from purple bornites and remobilized in the system. From microprobe analysis we have shown that purple bornite grains are broadly non-stoichiometric as a reflection of replacement processes; Type-A purple bornites are Cu-rich and have a noted occupancy of Se represented by the empirical formula $Cu_{5.29}Fe_{0.79}S_{3.88}Se_{0.04}$. Conversely, type-B bornites are Cu-poor ($Cu_{4.36}Fe_{1.04}S_{4.26}$) and Se is only present in minor concentrations.

Intriguing, is the commonality of altaite (PbTe); present as in inclusions in host chalcopyrite, or more so, at phase boundaries where bornite is replaced by chalcopyrite (Figure 12d-e). Due to the greater atomic radius of the telluride ion relative to that of the selenide and sulphide ion, telluride minerals will form in sulphide ore deposits during later stages of mineralisation when $fTe_{2(g)}/fSe_{2(g)}$ ratios have increased (Simon *et al.,* 1997). With important credits of Te present in purple bornite (up to 3208 ppm), the presence of altaite therefore represent the final stages of element remobilization, whereby Se is preferentially leached from the crystal structure of bornites and incompatible elements Pb and Te remain in concentrations permitting the formation of altaite (Figure 12 j).

Evidence for element redeposition

From textural studies we concluded that replacement processes governing the enrichment of Cu are present for Cu-(Fe)-sulphides proximal to major Cu-bearing breccias. Two principle sequences of replacement have been constrained from textural aspects.

(2a) Type-A purple Bn + PbSe → blue Cc → white Cc

(2b) Pyrite → brown Bn → Cc

From microprobe analysis we have shown that blue chalcocite has a broad range of non-stoichiometry and occupancy of Pb in Cu-poor ($Cu_{1.88}Pb_{0.02}S_{1.10}$) and Cu-rich ($Cu_{2.00}Pb_{0.01}S_{0.97}$) phases.

In comparison, point analyses illustrate that white chalcocite is broadly stoichiometric, with a mean occupancy of $Cu_{1.98}S_{1.02}$. Corroborating the microprobe data to textural aspects concludes that Type-A bornites have undergone progressive 'djurleitization' (Figure 10g) by mineral-fluid reaction via coupled dissolution-reprecipitation. For purple bornite coexisting with chalcocite, the enrichments of the element pair Ag and Bi (Figure 24a) provide geochemical evidence to suggest that textural aspects are superimposed in contrary to genetic (i.e. result of exsolution).

Furthermore, our LA-ICP-MS data has shown that Se and Te are non-essential elements present in solid solution for all Cu-(Fe)-sulphides. A strong correlation (r = 0.6) between Se and Te in log-log space proposes that the ore fluid has undergone fractionation of the element pair throughout the sequence (2a-b). This provides geochemical evidence to suggest element recycling is present in the Munda resource, whereby the leaching of ore constituents from purple bornite in sequence (1a) has provided a source permitting the precipitation of white chalcocite and brown bornite. With evidence of open space infill, it can further be noted that the precipitation of blue chalcocite and white chalcocite has occurred at temperatures below 250^{o}C (Barnes, 1997). Therefore it is favored that $Cu_{2-x}S$ phases defined in sequence (2a-b) are derivatives of the low-T (<103^{o}C) CuS system, providing further physiochemical constraints on the formation of major Cu-carrying copper-sulphides at the Munda resource.

From microprobe analysis we have shown that brown bornite is invariably Cu-poor (Figure 16g), with mean occupancy of $Cu_{4.96}S_{0.99}S_{4.06}$ (M/S = 1.46). This is coherent with textural evidence that strongly suggests bornite has formed via the replacement of pyrite. The precipitation of Cu-(Fe)-sulphides on preexisting pyrite has been document for numerous Andean IOCG such as La Candelaria and Mantoverde in Chile (Marschik and Fontbote, 2001; Benavides *et al.*, 2007; *in* Benavides 2010). This replacement theoretically requires the intercoupled dissolution of Fe and reprecipitation of Cu (Augustithis 1995). The preservation of euhedral grains (Figure 9h) would imply that pyrite has not been partly dissolved prior to the formation of bornite.

From analytical studies on mica geochemistry we have shown that sequence (2a) and (2b) spatially and paragenetically coincides with the developments of sericite (II) (Figure 8d) and also REE minerals fluocerite, florencite and monazite (Figure 8e-h). Of interest here is that sericite (II) contains important enrichments of F (up to 0.36 a.p.f.u; calculated for a total negative charge of 22) validating

the role of alkali fluoride complexes in the leaching, transport and redeposition of Cu, Au, and REE and U minerals (Barnes, 1997; Keppler and Wyllie 1991; Bau and Dulski 1995).

From investigations focused on mineral zonation and fluorine distribution, we have shown that high-F in mica anomalies are not necessarily spatially coincident with economic mineralisation, and rather, white chalcocite and brown bornite principally developed in adjacent intervals. Lottermoser (1992) attributes REE and ore formation from a F-enriched hydrothermal solution to abrupt changes in fluid temperature, pressure, pH, Eh, alkalinity and ligand concentrations. With this in consideration, we contend that brown bornite and white chalcocite formation occurs peripheral to high-F in mica anomalies as abrupt changes in fluid-rock ratios or physiochemical parameters permit the precipitation of dissolved constituents. Intervals comprising high F-in mica anomalies therefore represent solution channelways where important concentrations of metals have been transported in the alteration profile. The geochemical nature of F-enriched hydrothermal fluids would also permit the simultaneous development of sequence (1a) and sequence (2a-b), whereby Cu is leached from adjacent breccias and dissolved constituents are transported and redeposition in proximal mineralised breccias (Lottermoser 1992).

From our LA-ICP-MS data the relative concentrations of Ag in chalcocite show promise for fluid-source vectoring. We have shown that such enrichments systematically increasing along strike toward the western Ankata deposit. With concentrations of up to 192 ppm present in grey chalcocite it is therefore favored that the development of this phase occurred from an evolving hydrothermal fluid late in the paragenesis.

Formation of gold in the Munda resource

This study represents the first textural and mineralogical classification of gold in the Munda resource. The recognition of three phases of the binary system Au-Cu contributes to the Prominent Hill mineral inventory and has implications for ore genesis.

REFRACTORY GOLD

Using the LA-ICP-MS technique, we have shown that concentrations of up to 129 ppm Au reside as nano-scale inclusions in purple bornite. When comparing the bulk *in situ* Cu/Au ratio to the whole-rock Cu/Au quantities for this sampled interval, some interesting comparisons can be made.

The respective Cu/Au values are derived from the following equations;

$$Cu/Au_{(LA\text{-}ICP\text{-}MS)} = 629{,}998 \text{ ppm} / 129 \text{ ppm} = 4859$$

$$Cu/Au_{(whole\text{-}rock)} = 7430 \text{ ppm} / 2.2 \text{ ppm} = 3377$$

Comparing the two respective Cu/Au ratios demonstrates that refractory Au in bornite does contributes to the distribution of Au in Munda resource. Interestingly, Belperio *et al.* (2007) has commented on gold only steely hematite breccias, with low grades of Au (<1 g/t) and minor Cu present in whole rock assays. In our study we have shown that gold bearing purple bornites are preserved in the network of steely hematite alteration. Although tentative, there is some evidence to suggest that refractory gold may be of economic importance to the Prominent Hill deposit.

NATIVE GOLD

Native gold investigated in this study occurred as coarse-grained (up to mm scale) aggregates that coexist with chalcopyrite and loellingite. From studies conducted on mineralogy of native gold we contribute to the mineral inventory at Prominent Hill with bismuth, bismuthinite, and Y-bearing coffinite reported for the first time. Also present were phases of Co-safflorite, loellingite and coffinite.

The textural aspects of native gold and coexisting chalcopyrite are suggestive of co-precipitation (Figure 14a-b). This is supported by microprobe data that has shown impurities of up to 0.1 Cu, 0.12 Fe and 0.15 S (based on 1 a.p.f.u) are present in native gold. Mineral associations include polymineralic

aggregates of loellingite, Co-safflorite, safflorite, Y-bearing coffinite, coffinite and bismuth. Textural evidence strongly suggests that all minerals, excluding bismuth, formed in equilibrium. This conclusion is drawn from BSE images depicting phase zonations in single grains (Figure 14d) and complex guest-host relationships. In such grains, <3 μm of Au (Figure 14i) were observed as inclusions validating a complex history of Au formation accompanied by the development of exotic Co-Ni-Fe arsenides and Y-bearing coffinite. From textural aspects, the development of native bismuth can be constrained to late in the gold paragenesis as native bismuth invariably occurs as crustations on all minerals in the assemblage.

Of interest here are comparisons made between the mineralogy of Munda gold and the mineralogy concerning purple bornites. In such samples xenotime, loellingite, Co-safflorite and coffinite all occur as trace mineral. Furthermore, from textural and geochemical characterisation of purple bornites we have shown that concentrations of Au and exotic elements (i.e. Bi) have been leached via mineral-fluid reactions and remobilized.

In porphyry copper deposits gold is found in solid solution in Cu-(Fe)-sulphides and as small grains of native gold, usually at the grains of bornite (Kesler *et al.,* 2002). Kesler *et al.* (2002) attributes the economic content of Au in porphyry systems to; (i) the Cu/Au ratio of the ore forming fluid permitting the absolute quantities of Au incorporated as solid solution in the Cu-(Fe)-sulphide, and (ii) the presence of superimposed low-temperature (300^{o}C) alteration permitting the leaching and remobilization of Au in solid solution. Interesting parallels can be drawn from the formation of gold at the Bell Copper deposits, British Columbia, and the assemblage observed from this present study. At the Bell Copper deposit, it is advocated that an early potassic bornite-chalcopyrite ore was destroyed by a pervasive, high-temperature, quartz-sericite alteration (Carson et al., 1976; Wilson et al., 1980). This resulted in the complete destruction of bornite and the deposition of a new chalcopyrite – pyrite assemblage in which gold is associated with both minerals (Carson et al, 1976).

Also of interest is the mineralogical association gold has with Y-bearing coffinite. Understanding of the tetragonal thorite-xenotime-zircon-coffinite solid solutions is based on the contributions of Forster (2006), wherein the author suggests intermediate solid solutions of this system are likely to be unstable. The single process permitting the formation of such phases require the leaching and dissolution of preexisting accessory phases during interaction with F-bearing hydrous fluids enriched in Th, Y(HREE), Zr, and or U (Forster 2006). Interestingly, xenotime associated with purple bornite is

the only Y-bearing phases recognised in this study. Although equivocal, it favoured that the decomposition of purple bornite and associated trace elements by a superimposed F-enriched fluid has contributed the source of dissolved constituents for this exotic mineral assemblage. Tentatively, the same F-enriched fluid responsible for the remobilisation and formation of major Cu-mineralisation may have leached, transported and redeposited important concentrations of Au at the Munda resource. To validate this hypothesis, further study focused on the Malu gold mineralogy and geochemical behaviour of remobilised Au and Cu in hydrothermal systems is required.

GOLD-COPPER ALLOY

For natural systems, the conditions permitting formation of Au-Cu alloys have been comprehensively reviewed in Knipe & Fleet (1997) and Knight & Leitch, (2001). Reviewing the intermetallic compounds auricupride ($AuCu_3$) and tetraauricupride (AuCu), Ramdohr (1969) suggest that known occurrences belong to hydrothermal veins and have formed below the stability field of AuCu, i.e. below 390˚C. In a recent literature review, Knight & Leitch (2001) provide evidence to suggest Au-Cu alloys are also associated with differentiated mafic magmas, serpentinites, rodingite and other altered ultramafic rocks, usually associated with ophiolite complexes. Regarding the highly chalcophile nature of Cu, Ramdohr (1969) also suggests that the ores system must be very low in sulfur.

From textural aspects of Au-Cu at the Kerr Mine, Ontario, Knipe & Fleet, (1997) favors mechanisms of replacement for the formation of this compound. The presence of hydrothermal or weathering-related alteration in other known occurrences of Au-Cu alloys (Ramdohr, 1967) is also suggestive that the copper was derived from remobilization. From studies on fluid inclusion in healed quartz grains associated with Au-Cu alloy, Channer & Spooner (1991) contends that the fluids responsible have salinities of 4-4.7 wt.% eq, NaCl, moderate CO_2, and formation temperatures of ~130˚C. In regard to exsolution-induced intergrowths concerning Au-Cu alloys, our understanding is based on contributions by Murzin & Sustavov (1989). The authors demonstrate that true eutectic textures comprise laths of varying thickness, length and taper, arranged in subparallel to net-like configurations within the host.

From this study, whole rock immobile element data from has shown Munda Au-Cu alloys are hosted in andesitic rocks and are therefore comparable in geoenvironment to documented natural alloys. Two

principal assemblages have been determined from textural aspects; Au_3Cu and Au_9Cu coexist as symplectic grains, with these grains hosting inclusions of chalcocite and rim of chalcocite + bornite. In contradistinction, grains of AuCu are compositionally homogenous and only contain minor inclusions of rounded quartz. The compositions of Au-Cu alloy phases from the Munda resource (determined by EMPA) are shown in Figure 26b in relation to the phase diagram for the binary Au-Cu system (Okamoto et al. 1897). Microprobe data has shown that tetraauricupride is stoichiometric, with a mean empirical formula of $Au_{1.0}Cu_{1.0}$. Conversely, the unnamed Au_9Cu phases are broadly non-stoichiometric, with Au/Cu ratios ranging from 8.6 to 9.5 (ideal 9.0). All Au-Cu phases are free of impurities with only minor Ag documented (up to 0.11 wt.% Ag). The phase diagram for the Au-Cu system illustrates temperatures of <390˚C are required to permit the formation of tetraauricupride. Constrains on the Au-rich phases Au_3Cu and Au_9Cu are less clear, however it can be broadly stated that temperatures <200˚C are required.

From textural aspects of all Au-Cu phases there is no evidence, in this study at least, to suggest the exsolution of phases Au_9Cu and Au_3Cu has occurred. This assumption is based on the textural descriptions from Murzin & Sustavov (1989) concerning exsolution for Au-Cu alloys. The presence of fine-grained (<5 μm) Au-Cu phases in mineral assemblage with florencite-dominant veins (Figure 15i) provides mineralogical evidence to favour Au-Cu formation occurred in a low-temperature aqueous system i.e. below 390˚C. To permit formation this ore fluid requires a low sulphur fugacity. This is validated by the presence of native Cu and domeykite (Figure 6f), with the two phases occurring as concentrically zoned spherules trapped in silicate pores. It is therefore favored, however not certain, that the formation of Munda Au-Cu alloys has occurred from the replacement of preexisting Au by remobilized Cu. Low S-fugacities in the ore fluid could best explain the complex distribution of Cu ore in the Munda resource, whereby preexisting pyrite has provided the source of S required for high-grade Cu mineralisation.

Multisystem analogy: Stratiform hosted uranium

From literature, interesting comparisons can be made between different types of selenide-bearing ore deposits, and more importantly, the genetic implications of their formation.

Simons *et al.,* (1997) advocates that selenide-bearing hydrothermal deposits are restricted mainly to four types; “telethermal” selenide vein-type deposits, unconformity-related deposits, sandstone-

hosted uranium deposits and Au-Ag epithermal volcanic-hosted deposits. When reviewing the mineralogy and paragenesis of these preferred genetic models there are noteworthy comparisons between the Munda mineralogy and unconformity-related uranium deposits.

In the Bohemian Massif of western Moravia, the Czech Republic, unconformity-related uranium deposits contain dominantly Cu, Co, and Ni selenides associated with uraninite, hematite, Cu, Co and Ni sulphides and arsenides, and carbonate minerals (Simons *et al.,* 1997). The paragenesis of these stratiform related uranium deposits broadly comprise the precipitation of an early sulphide phase followed by an oxide, arsenide- and sulphide rich phase (Simons *et al.,* 1997). From this study we have observed Co-Ni arsenides developing as an intergranular film (Figure 11g) on purple bornite-blue chalcocite mineralisation. Crosscutting relationships would also imply that the development of Co-Ni arsenides was broadly syn-, to post-formation of purple bornite.

Of further interest is the development of alteration proximal to stratiform-hosted uranium deposit. At the Jabilku stratiform-hosted uranium deposit, Northern Territory, alteration dominantly comprises widespread chlorite and minor white mica, tourmaline and apatite alteration (Nutt, 1989). The development of chlorite alteration is also the favoured mechanism for lowering the pH of the circulating hydrothermal fluid, thereby permitting the precipitation of uranium minerals (Nutt, 1989). At the Munda resource chlorite alteration is constrained to the upper volcano-sedimentary sequences, and when present, overprinting textures would suggest that the development of chlorite pre-dates pervasive sericitization.

Also intriguing is the mineral association purple bornite has with xenotime. Diagenetic xenotime is a common accessory mineral in stratabound uraniferous deposits, as associated metallogenetic processes are favored for the development of the xenotime crystal structure (Vallini *et al*. 2007). Of interest to this study is that U-Pb dating conducted on uraniferous xenotime is applicable to constraining the formation age of unconformity-hosted deposits (Vallini *et al.* 2007). Therefore, the use of U-Pb dating methods on Munda resource xenotime would provide a reliable timeframe for uranium mineralisation and have implications for ore genesis.

Conclusions

- Formation of minor purple bornite predates steely hematite alteration and thus represents stage I of ore formation

- The LA-ICP-MS data shows important concentrations of Au (up to 12 ppm) reside in purple bornite in solid solution or as submicroscopic inclusions. Concentrations of >1 wt.% Se and Pb, 3208 ppm Te, 974 ppm Bi and 114 Ag have also been documented. Exsolution of clausthalite (PbSe) from purple bornite provides textural evidence for simultaneous deposition favouring a single fluid for the input of exotic elements (i.e. Pb and Se) and metal elements (Au and Ag).

- Two principal sequences are constrained by textural analysis. Sequence (1a) Type-A purple bornite → Type-B purple bornite → chalcopyrite illustrates the remobilisation of Cu and crystal lattice-bound Au from mineral-fluid interaction via dissolution. Sequence (2a) purple bornite → blue chalcocite → white chalcocite shows proximal-to-breccia Cu enrichment via coupled dissolution-reprecipitation reactions (stage II).

- A second, superimposed ore fluid enriched in alkali-fluoride complexes has permitted ore transportation and formation, as well as the development of pervasive sericitization in hydrothermal alteration

- Concentrations of Ag in chalcocite show promise for distal-to-source vectoring and suggest grey chalcocite formed during stage III.

- Investigations on gold mineralogy show two assemblages are present; native gold forms with chalcopyrite-loellingite and occurs with various Co-Ni-Fe-arsenides, bismuth, Y-bearing coffinite and coffinite.

- Three phases in the system Au-Cu are identified; symplectic intergrowths of unnamed Au_3Cu and Au_9Cu form an assemblage with chalcocite and minor bornite, and tetraauricupride (AuCu) forms homogeneous grains. All three phases rarely occur in nature and have implication for a S-deficient ore system.

ACKNOWLEDGEMENTS

Thanks go to OZ Minerals for their financial and logistical support of this project, to all the crew from the resource and exploration team for support in obtaining data throughout the year. Special thanks go to Jorge Benavides for his support and level-minded contributions. Thanks also to the crew from Adelaide Microscopy for assistance with the analytical work, especially to Angus Netting and Benjamin Wade. Lastly to my supervisors, thanks go to Cristiana Ciobanu for inspiring me to never lose my curiosity, and Nigel Cook for your contributions and support.

REFERENCES

AIUPPA A., BARKER D.R., WEBSTER J.D. 2009. Halogens in volcanic systems. *Chemical Geology , 263*, 1-18.

ALLEN S.R., MCPHIE J. FERRIS G. SIMPSON C. 2008. Evolution and architecture of a large felsic igneous province in western Laurentia: the 1.6 Ga Gawler Range Volcanics, South Australia. *Journal of Volcanology and Geothermal Research , 172*, 132-147.

BARTON M.D., JOHNSON D.A. 2000. Alternative brine sources for Fe oxide-(REE-Cu-Au-Ag) mineralisation. *Geology , 1*, 43-60.

BASTRAKOV E.N., SKIRROW R.G., DAVIDSON G.J. 2007. Fluid Evolution of Iron Oxide Cu-Au Prospoects in the Olympic Dam District, Gawler Craton, South Australia. *Economic Geolgoy , 102*, 1413-1440.

BELPERIO A., FLINT R., FREEMAN H. 2007. Prominent Hill: A hematite-dominated iron oxide copper-gold system. *Economic Geology , 102*, 1499-1510.

BELPERIO A., FREEMAN H. 2004. Common geological characteristics of Prominent Hill and Olympic Dam - implications for iron oxide copper-gold exploration models: . *Australian Institute of Mining and Metallurgy, PACRIM* , 115-125.

BENAVIDES J., KEYSLER T.K., CLARK A.H., OATES C., ZAMORA R. 2007. The Mantoverde iron oxide-copper-gold district, III region, Chile; the role of regionally derived, non-magmatic fluid contributions to chalcocpyrite mineralisation. *Economic Geology , 102*, 415-440.

BENAVIDES J. 2010. *Paragensis and genetic model for Prominent Hill IOCG deposit. Implications on exploration.* Oz Minerals.

BOYTON W.V. 1985. Cosmochemistry of the rare earth element: Meteoric studies. *Rare Earth Element Geochemistry* , 115-1522.

BRETT R. 1964. Experimental data from the system Cu-Fe-S and their bearing on exsolution textures in ores. *Economic Geology , 59*, 1241-1269.

CONGDON R.D., NASH W.P. 1988. High Fluorine Rhyolite - an eruptive pegmatite magma at the Honeycomb Hills, Utah. *Geology , 16*, 1018-1021.

CONNOR C., RAYMOND O.L., BARKER T., LOWE G. 2010. Aspects of structural control on alteration and mineralisation in the Moonta-Wallaroo Cu-Au Mining Field, Olympic Dam Domain, South Australia: *in Porter, T.M., (ed), Hydrothermal Iron Oxide Copper Gold and Related Deposits; A Global Perspective - Advances in the Understanding of IOCG Deposits.* PGC Publishing, Adelaide *, 3*, 147-170.

COOK N.J., CIOBANU C.L., DANYUSHEVSKY L.V., GILBERT S. 2011. Minor and trace elements in bornite and associated Cu-(Fe)-sulphides: A LA-ICP-MS study. *Cosmochim Acta* .

DAVIDSON G.J., PATERSON H.L., MEFFRE S., BERRY R.G. 2007. Characteristics and Origin of the Oak Dam East Breccia-Hosted Iron Oxide Cu-U-(Au) Deposit: Olympic Dam Region, Gawler Craton, South Australia. *Economic Geology , 102*, 1471-1498.

EHRIG K.E., GREEN N. 2009. The Olympic Dam Cu-Au-U deposit, South Australia: Was fluorine a key in forming this giant. *Smart Science for Exploration and Mining* . (E. P. Christie A.B., Ed.)

FORSTER H.J., 2006. Composition and origin of intermediate solid solutions in the system thorite-xenotime-zircon-coffinite. *Lithos , 88*, 35-55.

GOW P.A., WALL V.J., OLIVER N.H.S., VALENTA R.K. 1994. Proterozoic iron oxide (Cu-U-Au-REE) deposits: further evidence of hydrothermal origins. *Geology , 22*, 633-636.

GRGURIC B.A., HARRISON R.J., PUTNIS A. 2000. A revised phase diagram for the bornite-digenite join from in-situ neutron diffraction and DSC experiments. *Mineralogical Magazine , 64*, 213-231.

GROVES D.I., MEINERT L.D., HITZMAN M.W. 2010. Iron oxide copper-gold (IOCG) deposits through Earth history: implications for origin, lithospheric setting, and distinction from other epigenetic iron oxide deposits. *Economic Geology , 105* (641-654).

GUNOW A., LUDINGTON S., MUNOZ J.L. 1980. Fluorine in micas from the Henderson molybdenite deposit, Colorade. *Eoncomic Geology , 75*, 1127-1137.

HAND M., REID A., JAGODZINSKI L. 2007. Tectonic framework and evolution of the Gawler Craton, Southern Australia. *Economic Geology , 102*, 1377-1395.

HAYWARD N., SKIRROW R.G. 2010. Geodynamic setting and controls on iron-oxide Cu-Au(+U) ore in the Gawler craton, South Australia. *Porter, T.M., (ed) Hydrothermal Iron Oxide Copper-Golf and Related Deposits: A Global Perspective v.3* , 116-146.

HENDQUIST J.W., LOWENSTERN J.B. 1994. The role of magmas in the formation of hydrothermal ore deposits. *Nature , 370*, 519-527.

HITZAM M.W., ORESKES N., EINAUDI M.T. 1992. Geological characteristics and tectonic setting of Proterozoic iron oxide (Cu-U-Au-LREE) deposits. *Precambrian Research , 58*, 241-287.

HITZAM M.W. 2000. Iron oxide-Cu-Au deposits: what, where, when and why; *in Porter T.M., (ed.), Hydrothermal Iron Oxide Copper-Gold and Related Deposits: A Global Perspective*. PGC Publishing, Adelaide, *1*, 1-17.

HOLCOMBE R. 2010. *Prominent Hill basement map & 3D geology model, Explanatory Notes and Synthesis*. Oz Minerals interval report prepared by Holcombe, Couglin Oliver .

IDRUS A., KOLB J., MEYER M. 2007. Chemical composition of rock-forming minerals in copper-gold bearing tonalite porphyries at the Batu Hijau deposit, Sumbawa Island, Indonesia: implications for crystallisation conditions and fluorine-chlorine fugacity. *Resource Geology , 57* (102-113).

KANAZAWA Y., KOTO K., MORIMOTO N. 1978. Bornite (Cu_5FeS_4): stability and crystal structure of the intermediate form. *Canadian Mineralogist , 16*, 397-404.

KEPPLER H. 1993. Influence of fluorine on the enrichment of high field strength trace elements in granitic rocks. *Contrib Mineral Petrol , 114*, 479-488.

KNIPE S.W., FLEET M.E. 1997. Gold-copper alloy minerals from the Kerr mine, Ontario. *The Canadian Mineralogist*, 35, 573-586

LOTTERMOSER B.G. 1992. Rare earth elements and hydrothermal ore formation processes. *Ore Geology Reviews , 7*, 25-41.

MORIMOTO N., KULLERUD G.1961. Polymorphism in bornite. *Americal Mineralogist , 46*, 1270-1282.

MORIMOTO N. 1971. The composition and stability of digenite. *American Mineralogist , 56*, 1889-1909.

MORIMOTO N., KOTO K. 1970. Phase relations in the Cu-S system at low temperature: stability of anilite. *Am. Minerals , 55*, 106-117.

MUNOZ J.L. 1984. F-OH and Cl-OH exchange in micas with application to hydrothermal ore deposits. *Mineralogical Society of America , 13*, 469-493.

MURZIN V.V., SUSTAVOV S.G. 1989. Solid-phase transformation in native cupriferous gold. *Izv. Akad. Navk SSSR, Ser. Geol. , 11*, 94-104.

NUTT C.J. 1989. Chloriziation and associated alteration at the Jabiluka unconformity-type uranium deposit, Northern Territory, Australia. *Candian Mineralogist , 27*, 41-58.

OKAMOTO H., CHAKRABARTI D.J., LAUGHLIN D.E., MASSALSKI T.B. 1987. The Au-Cu (gold-copper) system. *Bulletin of Alloy Phase Diagrams , 8*.

POTTER R. 1977. An electrochemical investigation of the system copper-sulfur. *Economic Geology , 72*, 1524-1542.

PORTER T.M. 2010a. Current Understanding of IOCG-alkali altered mineralised systems: Part I - A review: *in Porter, T.M., (ed), Hydrothermal Iron Oxide Copper Gold and Related Deposits: A Global Perspective - Advances in the Understanding of IOCG Deposits.* PGC Publishing Adelaide , *3*, 33-106.

PORTER T.M. 2010b. Current Understanding of IOCG-alkali altered mineralised systems: Part II - A review: *in Porter, T.M., (ed), Hydrothermal Iron Oxide Copper Gold and Related Deposits: A Global Perspective - Advances in the Understanding of IOCG Deposits.* PGC Publishing Adelaide , *3*, 5-32.

PORTER T.M. 2010c. The Carrapateena iron oxide copper gold deposit, Gawler craton, South Australia: i*n Porter, T.M., (ed), Hydrothermal Iron Oxide Copper Gold and Related Deposits: A Global Perspective - Advances in the Understanding of IOCG Deposits.* PGC Publishing, Adelaide , *3*, 191-200.

RAMDOHR P. 1980. The ore minerals and their intergrowths. 2nd ed. New York: Pergamon Press.

RIEDER M. 2001. Mineral nomenclature in the mica group: the promise and the reality. *Eur. J. Mineral , 13*, 1009-1012.

ROSEBOOM, E. 1966. An investigation of the system Cu-S and some natural copper sulphides between 25˚C and 700˚C. *Economic Geology , 61*, 642-672.

SCHLEGEL T.U. 2010. Ore-fluid history of Prominent Hill iron oxide copper gold deposit, South Australia: A reconnassance fluid inclusion study. MSc Thesis. *ETH Zurich* .

SKIRROW R.G 2009. "Hematite-group" IOCG-U ore systems: tectonic setting, hydrothermal characteristics, and Cu-Au and U mineralizing processes. *Geological Association of Canada* , 39-57.

SKIRROW R.G., BASTRAKOV E., DAVIDSON G., RAYMOND O.L., HEITHERSAY P. 2002. The geological framework, distribution and controls of Fe oxide Cu-Au mineralisation in the Gawler craton, South Australia: Part II: Alteration and Mineralisation: *in Porter T.M., (ed), Hydrothermal*

iron Oxide Copper-gold and Related Deposits: A Global Perspective. PGC Publishing, Adelaide , *2*, 33-47.

TAPPERT M., RIVARD B., GILES D., TAPPERT R., MAUGER A. 2011. Automated drill core logging using visible and near-infrared reflectance spectroscopy: a case study from the Olympic Dam IOCG deposit, South Australia. *Economic Geologist , 106*, 289-296.

VALLINI D.A., GROVES D.I. 2007. Uraniferous diagenetic xenotime in northern Australia and its relationship to unconformity-associated uranium mineralisation. *Mineralium Deposita , 42*, 51-64.

WALSH M.K. 2010. Structural based timing constraints on the evolution of the hanging wall sequence, Prominent Hill IOCG (Iron-Oxide Cu-Su) deposit: implications for mineralisation. Hons Thesis. *Monash University*.

WARREN I., SIMMON S.F., MAUK J. 2007. Whole-rock geochemical techniques for evaluating hydrothermal alteration, mass changes, and compositional gradients associated with epithermal Au-Ag minerlisation. *Economic Geology , 102*, 923-948.

WILLIAMS P., DUCKWORTH R. 2010. *Electron microprobe study of sericites from Prominent Hill and Regional Prospects, Mount Woods Inlier: Development of a fluorine-in-muscovite Index for exploration.* Clump Mountain Report for Oz Minerals Ltd, 14p

WINCHESTER J.A., FLOYD P.A. 1997. Geochemical discrimination of different magma series and their differentiation products using immobile elements. *Chemical Geolgoy , 20*, 325-343.

YUVAZ F. 2003. Evaluating micas in petrological and metallogenic aspects: I-definitions and structure of teh computer program MICA. *Computers & Geosciences , 29*, 1203-1213.

FIGURE CAPTIONS

Figure 1: (a) Geology of the Gawler craton (Neoproterozoic, and excluding the Mesoproterozoic Pandurra formation), regional fault zones and principle IOCG±U and prospects in the Olympic IOCG Province. Regional faults: ECFZ: Elizabeth Creek Fault Zone, KSZ: Kalinjala Shear Zone, KRFZ: Karari Fault Zone, PPFZ: Pine Point Fault Zone, YaSZ: Yarlbrinda Shear Zone, YeSZ: Yerda Fault Zone. IOCG deposit abbreviations, CH: Cairn Hill, A: Acropolis, WW: Wirra Well, OD: Oak Dam, E: Emmie Bluff, Modified after Skirrow (2009). (B) Simplified geological map of Prominent Hill deposit area below the Phanerozoic cover. The main copper-gold ore is hosted by the hematite matrix supported breccias, while the steely hematite breccias contain variable gold. The location of the Mula deposit (Cu-Au), the Munda resource (Au-Cu) and the western Ankarta deposit (Cu) are based on Freeman & Tomkinson (2010).

Figure 2: Down-hole simplified lithology logs, sample location and the distributions of Cu (ppm), Au (ppm), U (ppm) and Ce (ppm) in representative whole rock data. (a) From drill core PH11D554, chalcocite occurs as massive veins replacing dolomite. Note the high concentrations of Cu (up to 20 wt.%) present in whole rock assays. (b) From drill core PH10D554, sampled intervals in steely hematite were selected due to high Au values in whole rock assays (up to 3 g/t). Note the spike in Au correlative to pervasive hematite alteration. Samples encompassing chalcocite mineralisation are sampled between 900 to 930 m comprising sericite + hematite alteration. Grains of visible gold were sampled from two intervals in this study; (c) Ten m-interval of hematite breccia encompassing homogeneously distributed mm-scale visible gold in breccia matrix. From whole rock assays, high Au (up to ~90 g/t) shows a strong correlation to hematite alteration U (up to 300 ppm). (d) Visible gold was present as a single grain hosted in an open fracture of a iron-oxide + sericite altered volcano-sedimentary sequence. Note for both Au intervals high Ce concentrations in whole rock assays peripheral to intervals.

Figure 3: (a) Schematic cross section Munda resource showing the distribution of lithological under the Phanerozoic cover sequence; *from* Holcomb (2010). The main copper-gold ore is hosted by the hematite-matrix breccias (b), while steely hematite (c) breccias contained variable gold. The metamorphic represents the contact between 1792-1762 Ma greenschist-facies metasediments ca. 1609-1603 Ma conglomerates and intercalated flow basalts (Holcomb 2010).

Figure 4: Bi-plots of lithogeochemical data from sampled drill core intervals. (a) Zr/Ti versus Nb/Y classification diagram (Winchester & Floyd 1977); (a) data points in K/Na on K/Al compositional

space shows that sericite alteration is well developed in all diamond drill core. (c) In log-log space Cu wt.% on Au ppm show a strong negative correlation and define a wedge shape in log-log space

Figure 5: Back-scatter electron images showing aspects of gangue mineralogy; sericite (I) is present in samples with (a) white mica alteration (5TW) and is (b) coarse-grained and chemically homogeneous. Apatite and fluorapatite and quartz are abundant, with boundaries crosscut by sericite (I) (5TW). Sericite (II) occurs proximal to Cu-mineralisation and coincides with (e) 'yellow' sericitization on a specimen scale (10TW). Sericite (II) is fine-grained, commonly interlayered with variable [Na + K] occupancy from EDAX (19TW). REE-bearing phases are present. Fluocerite (f) and florencite (g) occur as fine-grained inclusions in sericite (II) lamellae and monazite (h) is present with overgrowth textures encompassing grains of hematite (28TW).

Figure 6: Back-scatter electron images showing mineral association with sericite (I); (a) U-bearing mica occur interlayered in lamella (19TW). In the same sample, a Cu-bearing silicate is present near fractured grains of Chalcopyrite (19TW). Skeletal grains of rutile (c) and xenoblasts of hematite with ilmenite lamellae provide mineralogical evidence for a mafic precursor that has been replaced by sericite (II) (10TW). Note the presence of fine-grained monazite grains encapsulated in channels of sericite (II). On a specimen scale, hematite breccias with 'red rock' alteration (e) correlate to samples where quartz is abundant (up to 80 vol.%) and hematite occurs principally as fine-grained impregnations (f) (26TW). Note the concentrically zoned inclusions of domeykite and native Cu in porous quartz sheets (26TW). Distal to mineralisation, breccias comprise euhedral quartz fragments and sericite (II) is present as radial growths in the matrix (6TW).

Figure 7: Back-scatter electron images illustrating textural aspects of gangue mineralogy; hematite is occurs as ;(a) tabular lamellae propagating into open cavities; (a) colloidal psuedomorphs; (c) puffy grains with concentrically zoned porosity hosting (d) U-bearing minerals (11TW). Textural and mineralogical aspects of lithologies with steely hematite alteration (27TW); (e) dolomite is abundant and calcite is present in box-form veins. Textural aspects of gangue minerals in mineralised shallow dolomite samples; (g) chlorite is coarse-grained and forms stringy lamellae (38TW); (h) under reflected hematite occurs as fine lamellae impregnated in the host dolomite (40TW). This style of alteration correlated with 'earthy hematite' on specimen scale

Figure 8: Reflected light and backscatter electron images depicting textural and mineralogical aspects of white chalcocite. White chalcocite occurs as (a) isotropic monomineralic grains, or as (b) interstitial veinlets within the matrix (28TW). (c) Sericite (II) is abundant and (d) crosscuts grains of white

chalcocite. REE-minerals are well developed (18TW); (e) florencite and fluocerite occurs as aggregates or encapsulated in sericite (II) (19TW). Fluorencite forms in open cavities (10TW), (g) and at the grain margins of white chalcocite. (h) Fluocerite also occurs as inclusions within chalcocite (18TW).

Figure 9: Reflected light and backscatter electron images depicting textural and mineralogical aspects of brown bornite; (a) bornite present as polymineralic with orientated hematite lamellae, concave pyrite and monazite, (b) vein-form bornite in open fractures (32TW). Images depicting bornite mineral assemblage with (c) grains of concave pyrite and (d) monazite central to bornite grains (31TW). (e) Fluocerite and (f) chalcocite is present intermingling at grain boundaries of brown bornite (31TW). Sericite (I) present (g) in domains distal to bornite mineralisation or occupied by pyrite (h).

Figure 10: Reflected light and backscatter electron images depicting textural aspects of purple bornite and blue chalcocite; (a) Grains occur in the cavities of silicate fragments and are (b) anisotropic under reflected light (15TW). (c) Blue chalcocite forms monomineralic veins in the breccias matrix (37TW) or forms on (d) grain boundaries of purple bornite (15TW). Note the nature of steely hematite development around grains with no evidence of partial dissolution. For (e) orange-red purple bornites (8TW), (f) chalcopyrite lamellae are present (8TW). Conversely, when (g) blue chalcocite (18TW) is present (h) spindle lamellae of chalcocite occur in purple bornite grains.

Figure 11: Backscatter electron images depicting mineral associations of purple bornite and blue chalcocite; (a) xenotime occurs in puffy aggregates of hematite and grains (b) show evidence of partial dissolution (15TW). (c) Loellingite crosscutting barite. (d) Coffinite with irregular inclusions of chalcocite (15TW). (e) Skeletal Co-safflorite hosted in bornite (7TW). (f) Chalcocite hosting and crosscutting coffinite (7TW). (g) Chalcocite rimmed and crosscut by loellingite. (h) Sericite (II) forms mutual boundaries with coexisting bornite-chalcopyrite; (i) sericite (II) is cross cut by coexisting bornite-chalcocite (8TW).

Figure 12: Backscatter electron and reflected light images showing; (a-b) symplectic textures of clausthalite in host purple bornite (15TW). (c) Coalescence of clausthalite and open fractures in purple bornite provide evidence of grain decomposition (6TW). (d) Brown bornite rimmed by chalcopyrite; (d-e) altaite is commonly observed precipitating in chalcopyrite at phase boundaries (7TW). Evidence bornite to chalcopyrite replacement; (f) brown bornite coexisting with blue bornite and neo-crystallisation of crosscutting chalcopyrite (6TW); (g) bornite replaced by chalcopyrite on grain boundaries and along crystallographic planes (7TW); altaite is present in porous (g) grains of chalcopyrite as (i) submicroscopic or (j) coarse-grained inclusions (7TW).

Figure 13: Reflected light images showing textural aspects of Cu-(Fe)-sulphides hosted in shallow dolomitic sequences; (a) Grey chalcocite with concave inclusions of pyrite and (b) irregular 'emulsions' of red bornite preceding blue chalcocite (40TW). (c) Hematite is present as well-formed lamellae; note that chalcocite mediates the contact between hematite and pyrite (40TW). (d) Irregular grain of anisotropic blue chalcocite coexisting with red bornite. (e) Red bornite is present on fracture planes replacing grey chalcocite; (f) veinlets chalcopyrite preceding red bornite crosscutting grey chalcocite (39TW). Where abundant, pyrite forms (g) "symplectic" intergrowths with host gangue; (h) pyrite is crosscut by veins of blue chalcocite + bornite (38TW).

Figure 14: Backscatter electron and reflected light images showing textural and mineralogical aspects of native gold (41TW); (a-b) gold is present in a chalcopyrite-loellingite assemblage and forms coarse interstitial grains. (c) Host dolomite is replaced by calcite. (d) Phase zonation in polymineralic grain comprising chalcopyrite, coffinite, Y-bearing coffinite and coffinite. (e) Chalcopyrite and gold forming if fractured gangue minerals. (f-g) Images showing coffinite; rimming loellingite, (h) coexisting with Y-coffinite, and hosting (i) gold. (j) Fibrous aggregates of native bismuth forming in coexisting safflorite and chalcopyrite.

Figure 15: Backscatter electron and reflected light images showing textural and mineralogical aspects of Au-Cu alloys showing (3TW); (a) two discrete Au-Cu phases coexisting as symplectic aggregates; chalcocite forms and rim with bornite or is hosted as blebby inclusions. (b) Au-Cu is compositionally homogeneous with irregular serrate boundaries. (c) Chalcocite inclusions in Au-Cu alloys with symplectic intergrowths. (d) The relationship between bornite and chalcocite on grain boundaries of Au-Cu alloys, with bornite hosted in chalcocite. (e) Polymineralic aggregate of Au-Cu with chalcocite; (f) coffinite forms as radial growths on grain of Au-Cu. (i) AuCu (3TW) also occurs as a host within (j) florencite-dominant viens (26TW)

Figure 16: (a) Simplified down-hole log showing distribution of Cu-(Fe)-sulphides and host lithology of selected samples, and histograms showing the M/S ratios (determined by EMPA) for (b) grey chalcocite, (b) red bornite, (c) blue chalcocite, (d) purple bornite, (f) white chalcocite, (g) brown bornite. Note that purple bornite and blue chalcocite show the broadest non-stoichiometry and are distributed peripheral to white chalcocite-bearing breccias.

Figure 17: (a) Ternary plot of atom.% Cu-Au-Ag for Au-Cu alloys and native gold determined by EMPA. Note that AuCu is broadly stoichiometric while Au9Cu is non-stoichiometric. Native gold shows minor variation due to impurities of chalcopyrite. (b) Chondrite-normalised patterns (Boynton, 1985) for

xenotime, monazite and florencite. Note the fractionation in L-REEs Ce and La between monazite and florencite, with monazite comparably enriched.

Figure 18: Bi-plots (atomic proportions calculated for a total negative charge of 22) illustrating the composition of micas determined by EMPA. (a) The plot molar Al vs. [Si+Fe+Mg] shows that Munda micas are broadly sericite with variable phengite substitution; while (b) fluorine is detectable in all point analyses and ranges from 0.35 to 0.05 a.p.f.u. (c) Box and whisker plot showing the distribution Fluorine Index values verses depth; FI values (*from* Williams 2010) are calculated based on F-content and [Si+Fe+Mg] determined from EMPA. Note that the high F-in mica for the Munda is at the depth interval 850 to 950 m and spatially coincides with Cu-Au mineralised hematite-matrix breccias.

Figure 19: Selected data for PH10D549 at depths 950 to 972 m; (a) Box and whisker plot showing calculated FI values determined by EMPA point analysis and selected photographs of lithologies (b-c) for samples analysed by EMPA; Backscatter electron images depicting textural and mineralogical aspects of gangue and ore minerals for selected samples; (d) Sericite (II) forming at grain boundaries of brown bornite (33TW; 950 m). (e) Chalcocite intergrown with brown bornite on grain boundaries (31TW; 972). (f) Pyrite grains incipiently replaced by bornite at grain boundaries (33TW; 950 m). (g) Monazite as puffy aggregates encompassed in pores of brown bornite (33TW; 950 m). (h) Down-hole assays showing the distribution of Cu (ppm), Au (ppm) and Ce (ppm) in relation to sampled intervals.

Figure 20: Selected data for PH10D551 at depths 720 to 832 m; (a) Box and whisker plot showing calculated FI values determined by EMPA point analysis and selected photographs of lithologies (b-c) for samples analysed by EMPA; Backscatter electron images depicting textural and mineralogical aspects of gangue and ore minerals for selected samples; (d) Sericite (I) is well developed and replaces the boundaries of quartz fragments (5TW; 720 m). (e) Sericite (II) is abundant and is host to fine-grained fluocerite and florencite (10TW; 832). (f) Chalcopyrite replacing bornite on grain boundaries (7TW; 750m). (g) Under reflected light; chalcopyrite is replaced on fracture margins by bornite and occurs as concave inclusions (10TW; 832 m). (h) Down-hole assays showing the distribution of Cu (ppm), Au (ppm) and Ce (ppm) in relation to sampled intervals.

Figure 21: (a-c) Backscatter electron images showing LA-ICP-MS spot analysis with visible inclusions of clausthalite in bornite. (d-i) Representative LA-ICP-MS depth profiles for bornite and chalcocite. From left, the background count is 30 s, followed by 60 s ablation time, which is integrated. (d) Type B purple bornite (6TW); note flat spectra for Pb, Se, Te, Tl and divergence of Ag. (e) Type B purple bornite (8TW); note flat spectra from Pb, Tl, Bi, Ag, and minor divergence in Se and Te. (f) Bornite

from sample 15TW; note flat spectra for Se, Tl, Te, Sb while Pb, Bi, Ag, Au are divergent with Fe. (g) Type-A purple bornite (15TW); note flat signals for Se, Fe, Tl, Te, Ag, Au increasing Pb and Bi and minor spikes in Sb. (h) White chalcocite (17TW); note flat signals for Ag, Se, and Bi. (h) White chalcocite from sample 17TW; note minor spikes in Se, Ag, Te, Pb, Bi that otherwise are broadly flat

Figure 22: Reflected light images showing LA-ICP-MS spot analysis for (a) white chalcocite (28TW) and brown bornite (31TW). Representative LA-ICP-MS depth profiles for bornite and chalcocite. From left, the background count is 30 s, followed by 60 s ablation time, which is integrated. (c) Brown bornite (32TW); note flat signals for Fe, Ag, Pb, Bi. (b) Brown bornite (33TW); note flat signals for Fe, Bi, Ag and spike in Zn. (c) Grey chalcocite (39TW); note flat signals for Ag and Se, minor spikes of Fe, Mn and Pb. (d) Grey chalcocite (40TW); note flat signal for Ag, and minor signal spike in Pb and Co.

Figure 23: Histograms (log-scale) illustrating variations in concentrations of (a) Ag, (b) Bi, (c) Se, (d) Te, (e) Pb, (f) Tl and (g) Au in bornite and chalcocite.

Figure 24: Log-log plots showing relationships and correlations between different pairs of trace/minor elements in Cu-(Fe)-sulphides. (a) Ag vs. Bi, (b) Se vs. Pb, (c) Ag vs. Se, (d) Ag vs. Te, (e) Te vs. Se and (f) Co vs. Ni. See text for addition explanation.

Figure 25: Log-log plots showing relationships and correlations between different pairs of trace/minor elements in Cu-(Fe)-sulphides.; (a) Pb vs. Tl, (b) Ag vs. As. Bi-plots showing the spatial distribution of trace element proportions for chalcocite and bornite; (c) Ag vs. easting, (d) Ag vs. depth, (e) Bi vs. easting and (f) Bi vs. depth.

Figure 26: (a) Averages and ranges of gold contents and Cu/Fe ratios (shown as bars) in bornite with different chemical compositions obtained in salt-fluxed experiments at temperatures of 400˚C, 500˚C and 600˚C. The composition and Au content of Purple bornites from the Munda resource are shown in the relative field. (b) Schematic phase-diagram for the system Au-Cu (after Okamoto et al., 1987), with suggested fields of stability at very low temperatures. The compositions of Au-Cu alloy phases from the Munda resource (determined by EMPA) are shown along the axis.

Figure 1

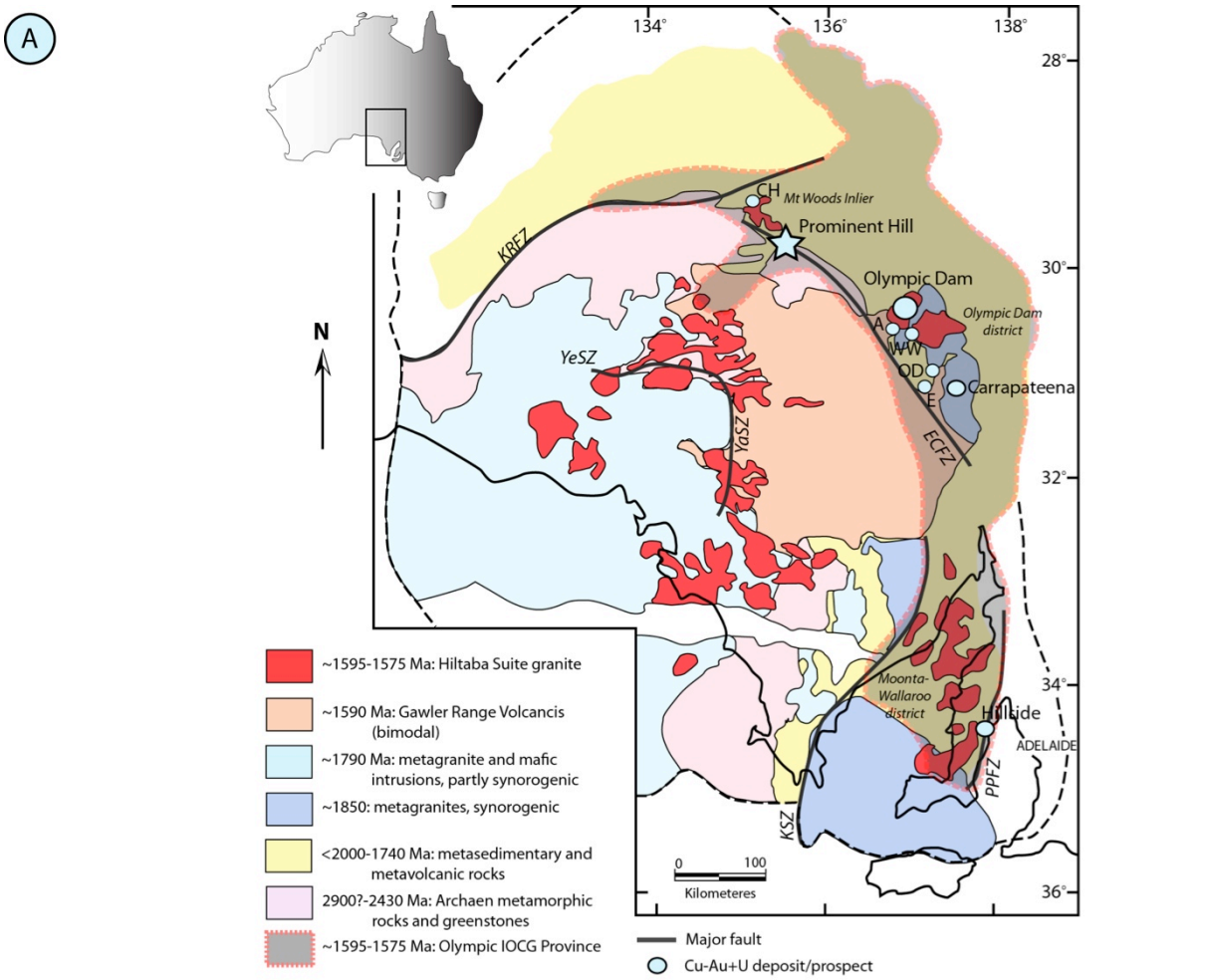
A
134°
136°
138°
28°
30°
32°
34°
36°
CH
Mt Woods Inlier
Prominent Hill
Olympic Dam
Olympic Dam district
A
WW
OD
E
Carrapateena
KREZ
YeSZ
YaSZ
ECFZ
PPFZ
KSZ
N
Moonta-Wallaroo district
Hillside
ADELAIDE
0
100
Kilometeres
~1595-1575 Ma: Hiltaba Suite granite
~1590 Ma: Gawler Range Volcancis (bimodal)
~1790 Ma: metagranite and mafic intrusions, partly synorogenic
~1850: metagranites, synorogenic
<2000-1740 Ma: metasedimentary and metavolcanic rocks
2900?-2430 Ma: Archaen metamorphic rocks and greenstones
~1595-1575 Ma: Olympic IOCG Province
Major fault
Cu-Au+U deposit/prospect

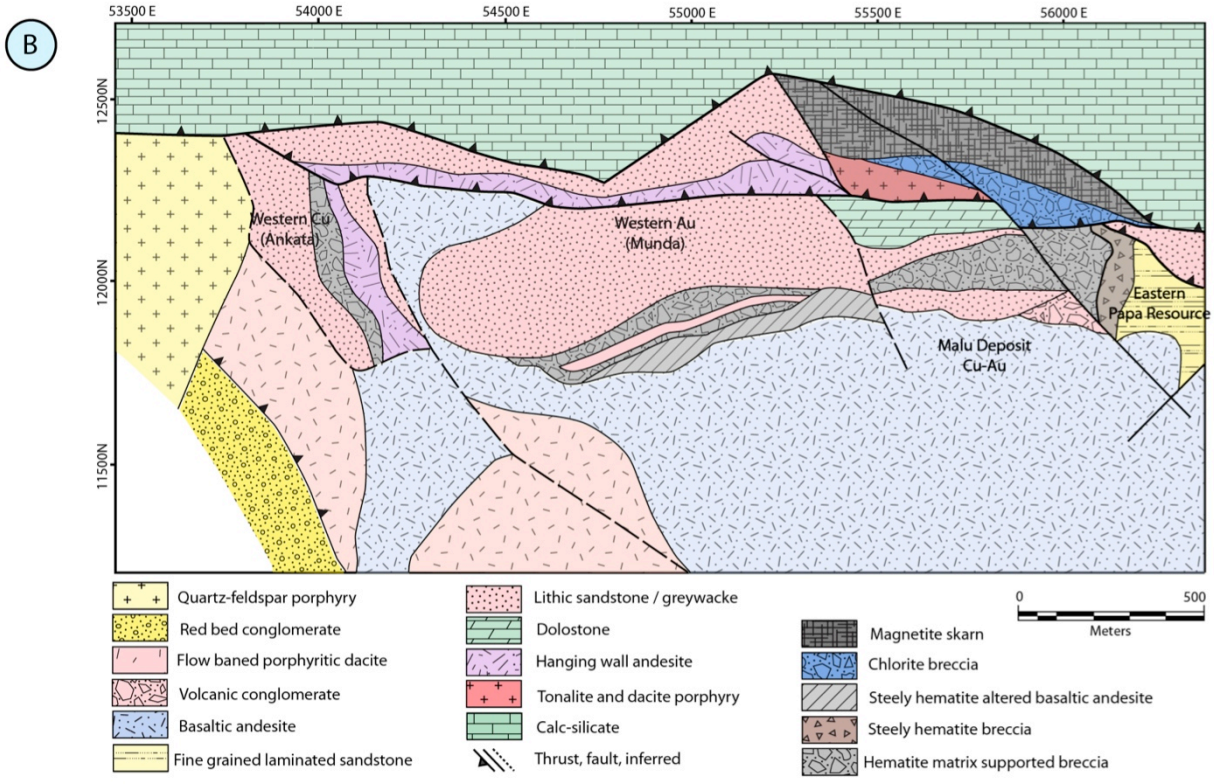
B
53500 E
54000 E
54500 E
55000 E
55500 E
56000 E
12500N
12000N
11500N
Western Cu (Ankata)
Western Au (Munda)
Eastern Papa Resource
Malu Deposit Cu-Au
0
500
Meters
Quartz-feldspar porphyry
Red bed conglomerate
Flow baned porphyritic dacite
Volcanic conglomerate
Basaltic andesite
Fine grained laminated sandstone
Lithic sandstone / greywacke
Dolostone
Hanging wall andesite
Tonalite and dacite porphyry
Calc-silicate
Thrust, fault, inferred
Magnetite skarn
Chlorite breccia
Steely hematite altered basaltic andesite
Steely hematite breccia
Hematite matrix supported breccia

Figure 2

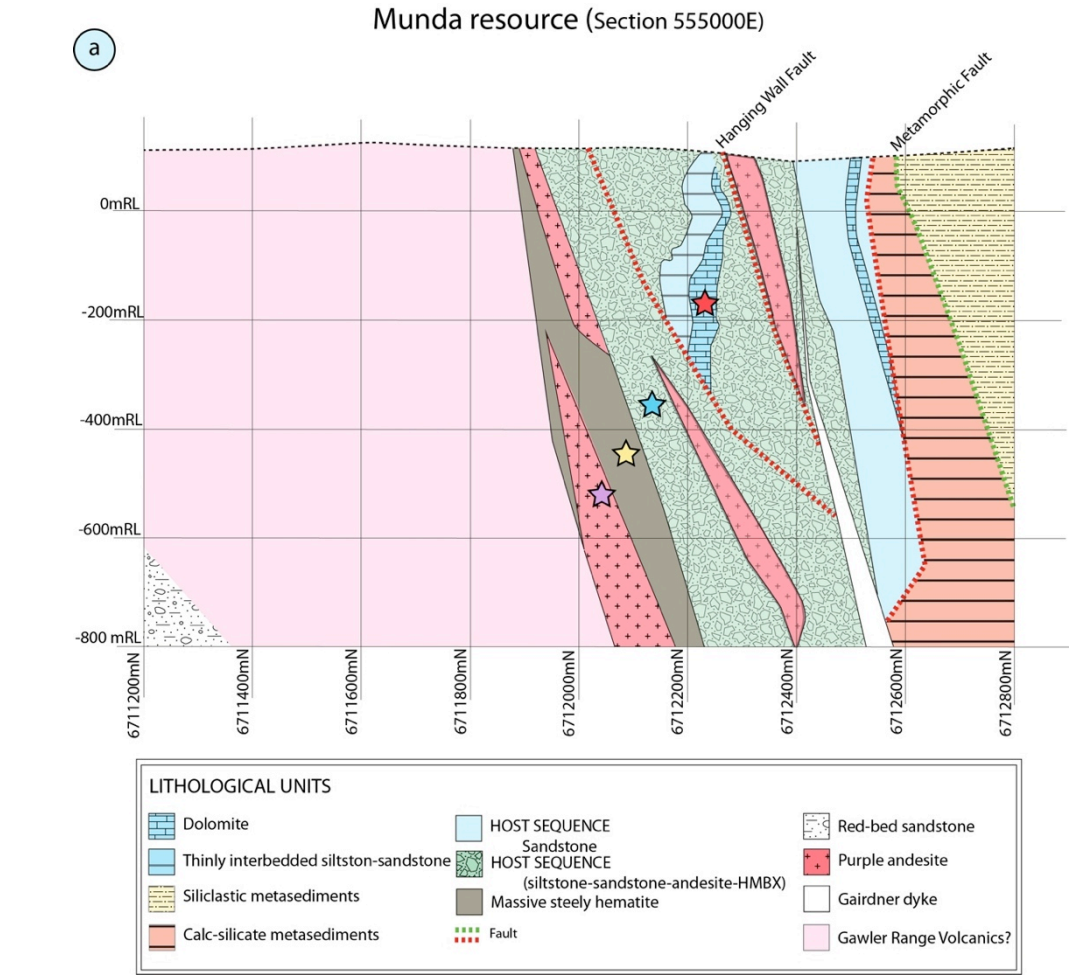
a
Munda resource (Section 555000E)
Hanging Wall Fault
Metamorphic Fault
0mRL
-200mRL
-400mRL
-600mRL
-800 mRL
6711200mN
6711400mN
6711600mN
6711800mN
6712000mN
6712200mN
6712400mN
6712600mN
6712800mN
LITHOLOGICAL UNITS
Dolomite
Thinly interbedded siltston-sandstone
Siliclastic metasediments
Calc-silicate metasediments
HOST SEQUENCE Sandstone
HOST SEQUENCE (siltstone-sandstone-andesite-HMBX)
Massive steely hematite
Fault
Red-bed sandstone
Purple andesite
Gairdner dyke
Gawler Range Volcanics?


b

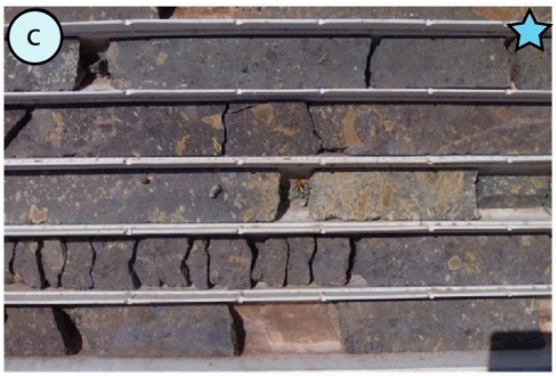
c

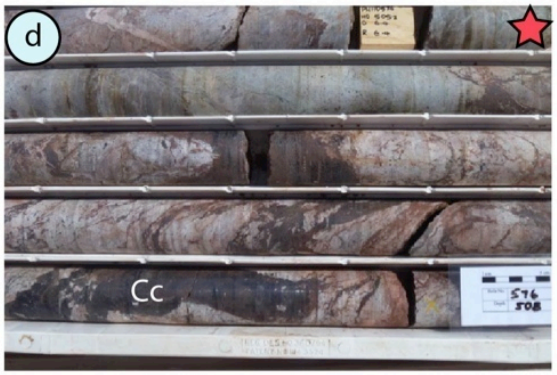
d
Cc

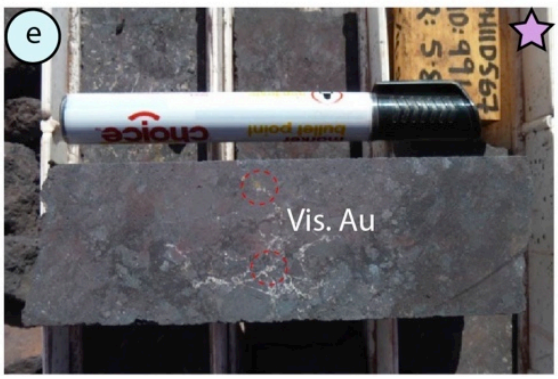
e
Vis. Au

Figure 3

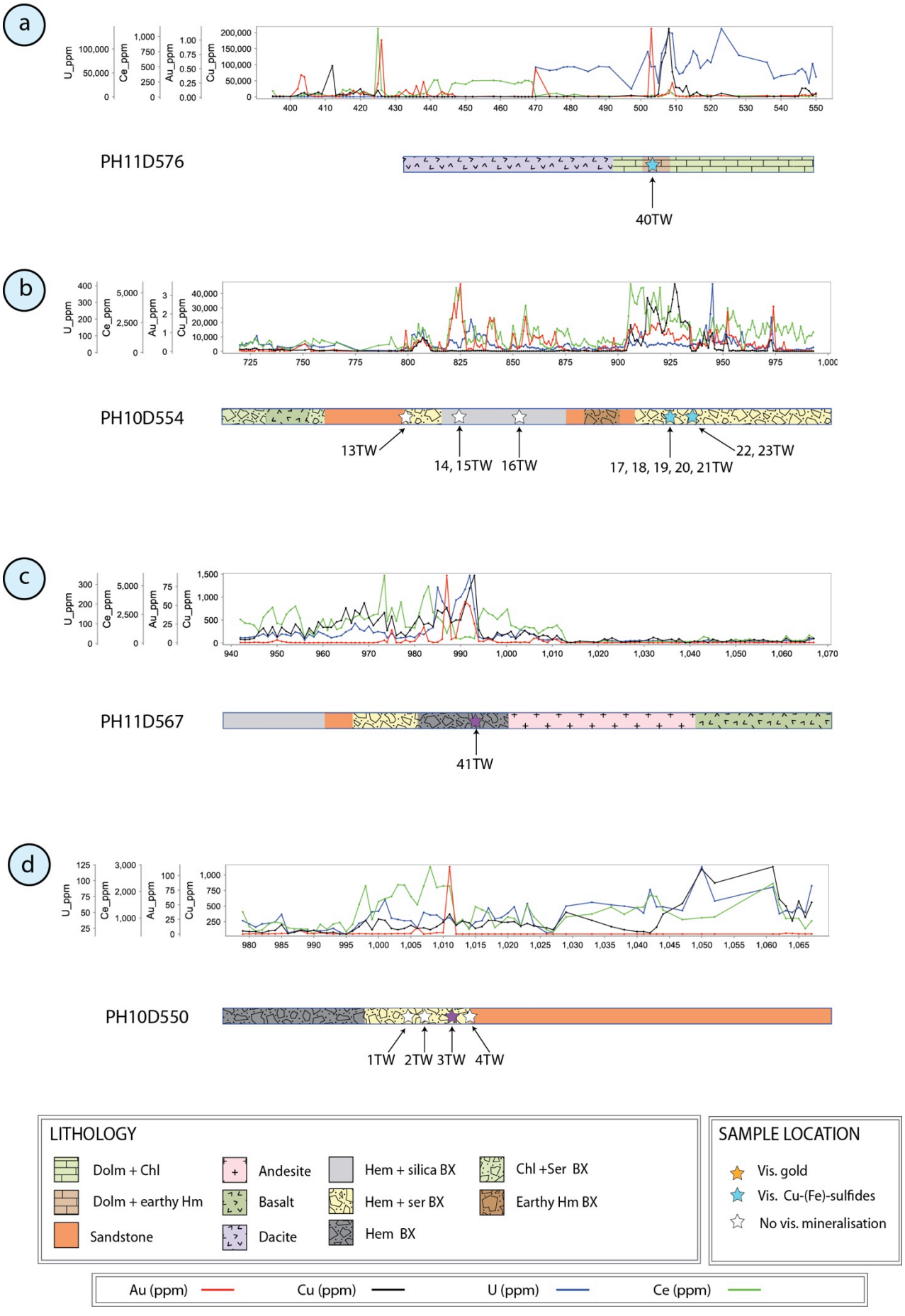
a
U_ppm
Ce_ppm
Au_ppm
Cu_ppm
PH11D576
40TW
b
PH10D554
13TW
14, 15TW
16TW
17, 18, 19, 20, 21TW
22, 23TW
c
PH11D567
41TW
d
PH10D550
1TW
2TW
3TW
4TW
LITHOLOGY
Dolm + Chl
Dolm + earthy Hm
Sandstone
Andesite
Basalt
Dacite
Hem + silica BX
Hem + ser BX
Hem BX
Chl +Ser BX
Earthy Hm BX
SAMPLE LOCATION
Vis. gold
Vis. Cu-(Fe)-sulfides
No vis. mineralisation
Au (ppm)
Cu (ppm)
U (ppm)
Ce (ppm)

Figure 4

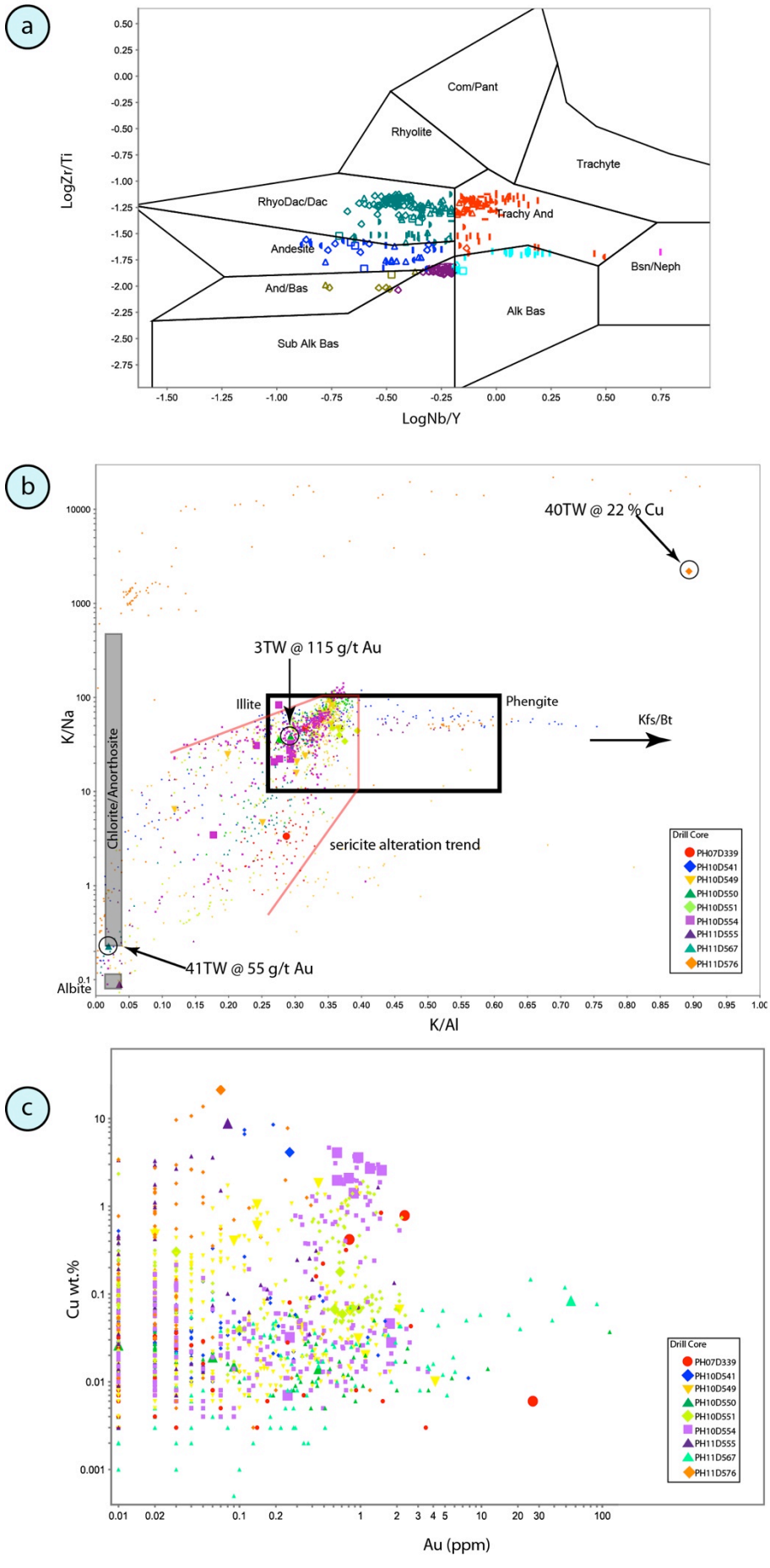
a
Com/Pant
Rhyolite
Trachyte
RhyoDac/Dac
Trachy And
Andesite
Bsn/Neph
And/Bas
Alk Bas
Sub Alk Bas
LogZr/Ti
LogNb/Y
b
40TW @ 22 % Cu
3TW @ 115 g/t Au
Illite
Phengite
Kfs/Bt
Chlorite/Anorthosite
sericite alteration trend
41TW @ 55 g/t Au
Albite
K/Na
K/Al
Drill Core
PH07D339
PH10D541
PH10D549
PH10D550
PH10D551
PH10D554
PH11D555
PH11D567
PH11D576
c
Cu wt.%
Au (ppm)

Figure 5

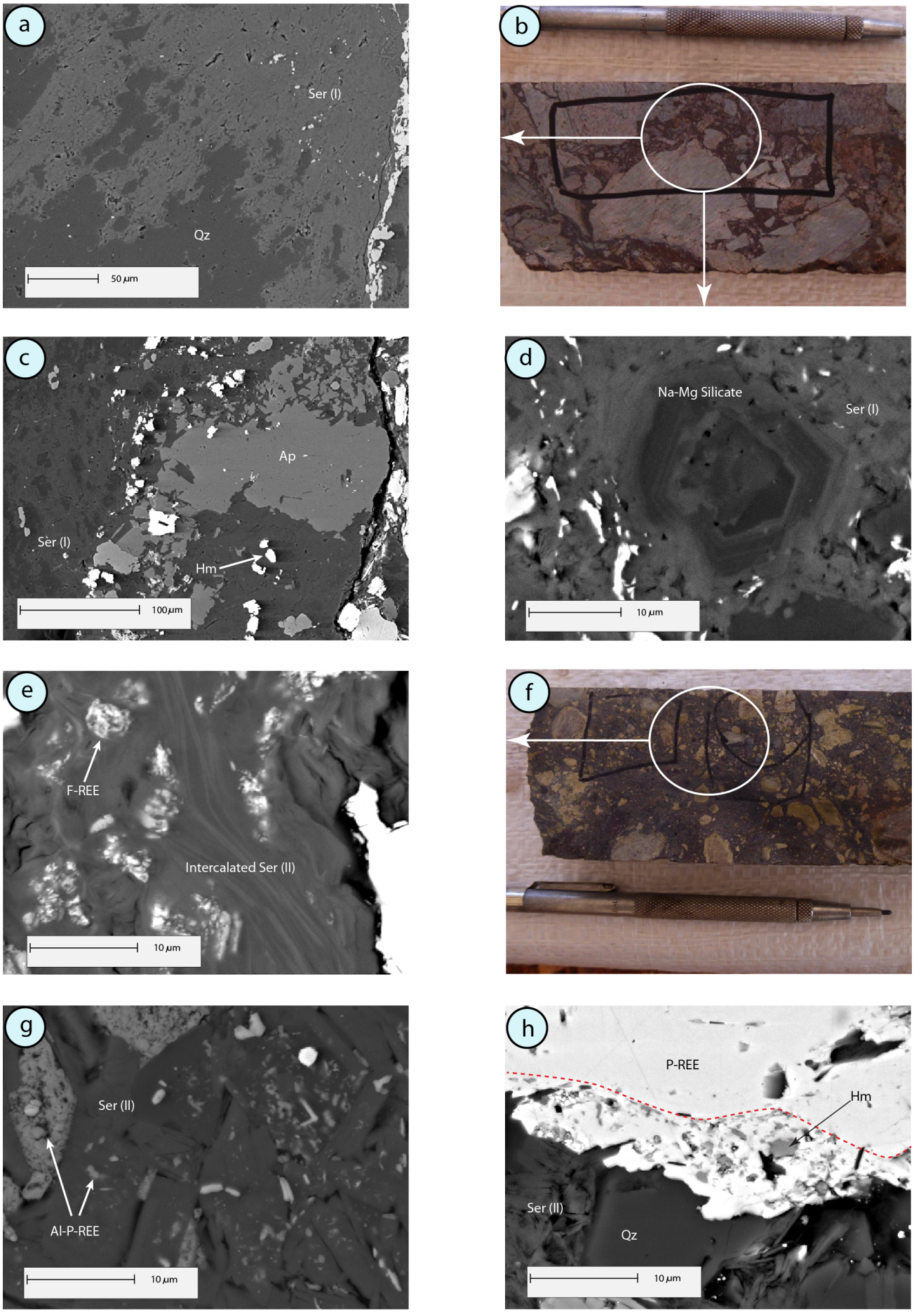
a
Ser (I)
Qz
50 µm
b
c
Ap
Ser (I)
Hm
100µm
d
Na-Mg Silicate
Ser (I)
10 µm
e
F-REE
Intercalated Ser (II)
10 µm
f
g
Ser (II)
Al-P-REE
10 µm
h
P-REE
Hm
Ser (II)
Qz
10 µm

Figure 6

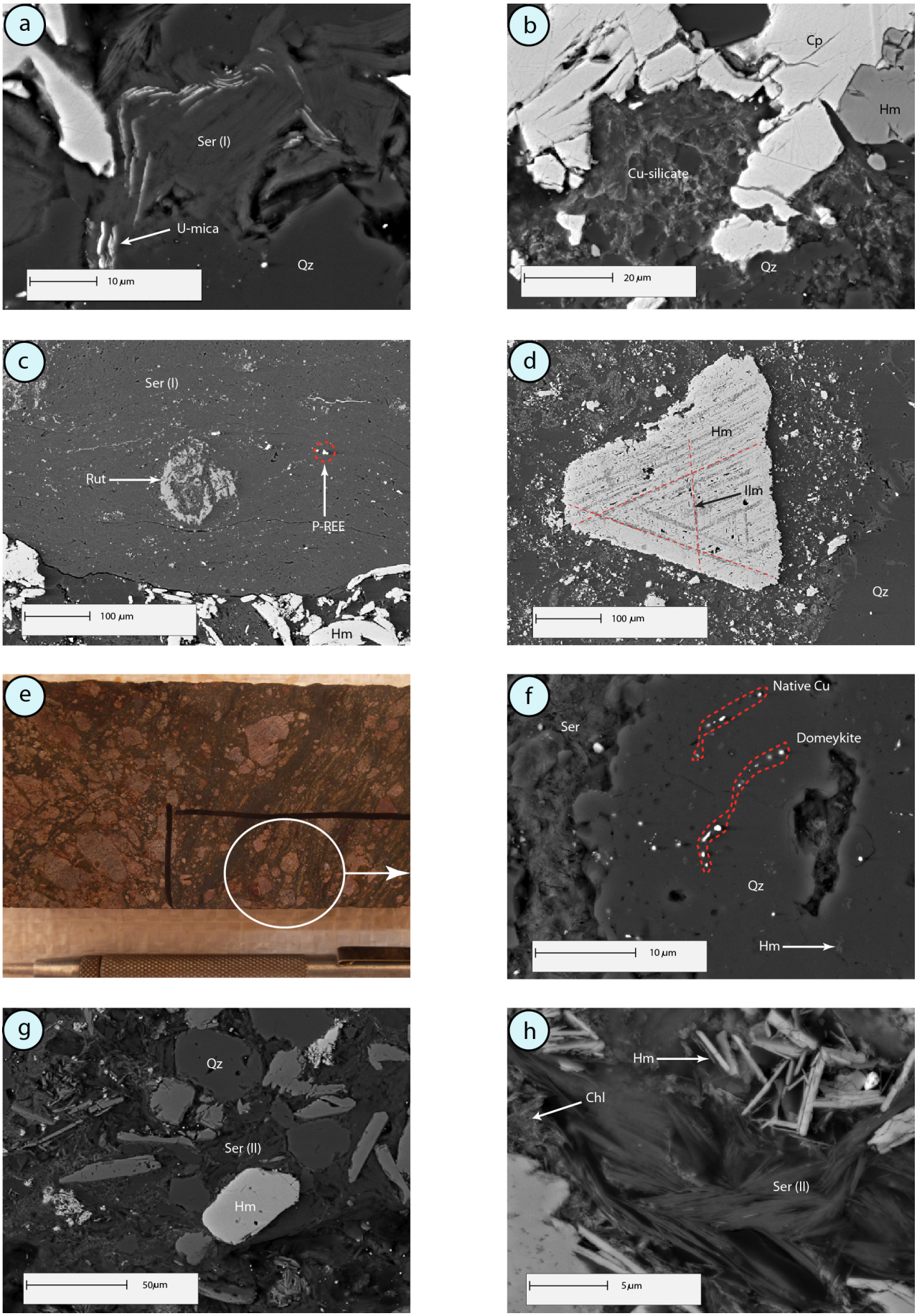
a
Ser (I)
U-mica
Qz
10 µm
b
Cp
Hm
Cu-silicate
Qz
20 µm
c
Ser (I)
Rut
P-REE
100 µm
Hm
d
Hm
Ilm
Qz
100 µm
e
f
Native Cu
Ser
Domeykite
Qz
10 µm
Hm
g
Qz
Ser (II)
Hm
50µm
h
Hm
Chl
Ser (II)
5µm

Figure 7

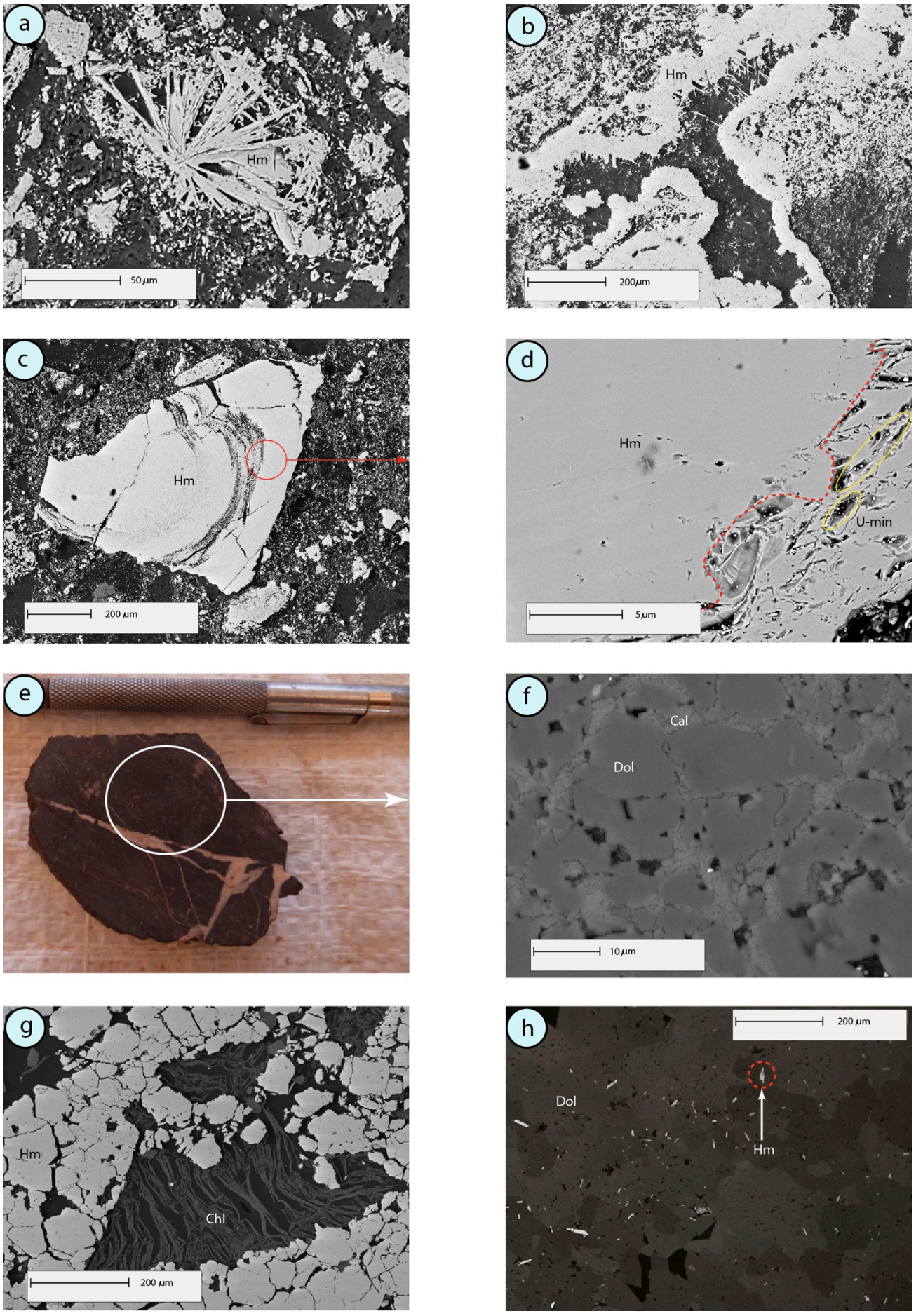
a
Hm
50 µm
b
Hm
200µm
c
Hm
200 µm
d
Hm
U-min
5µm
e
f
Cal
Dol
10 µm
g
Hm
Chl
200 µm
h
200 µm
Dol
Hm

Figure 8

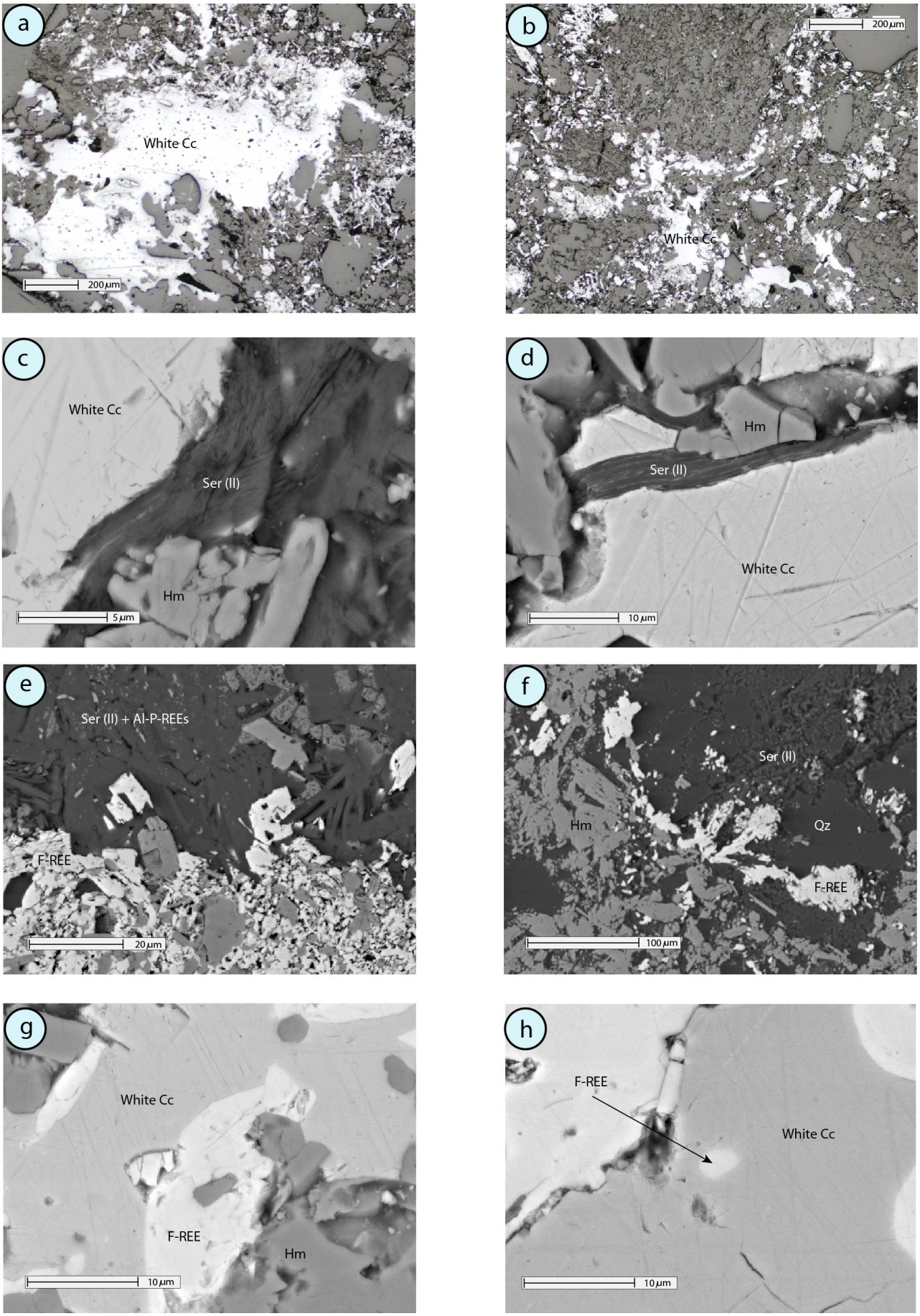
a
White Cc
200 µm
b
200 µm
White Cc
c
White Cc
Ser (II)
Hm
5 µm
d
Hm
Ser (II)
White Cc
10 µm
e
Ser (II) + Al-P-REEs
F-REE
20 µm
f
Ser (II)
Hm
Qz
F-REE
100 µm
g
White Cc
F-REE
Hm
10 µm
h
F-REE
White Cc
10 µm

Figure 9

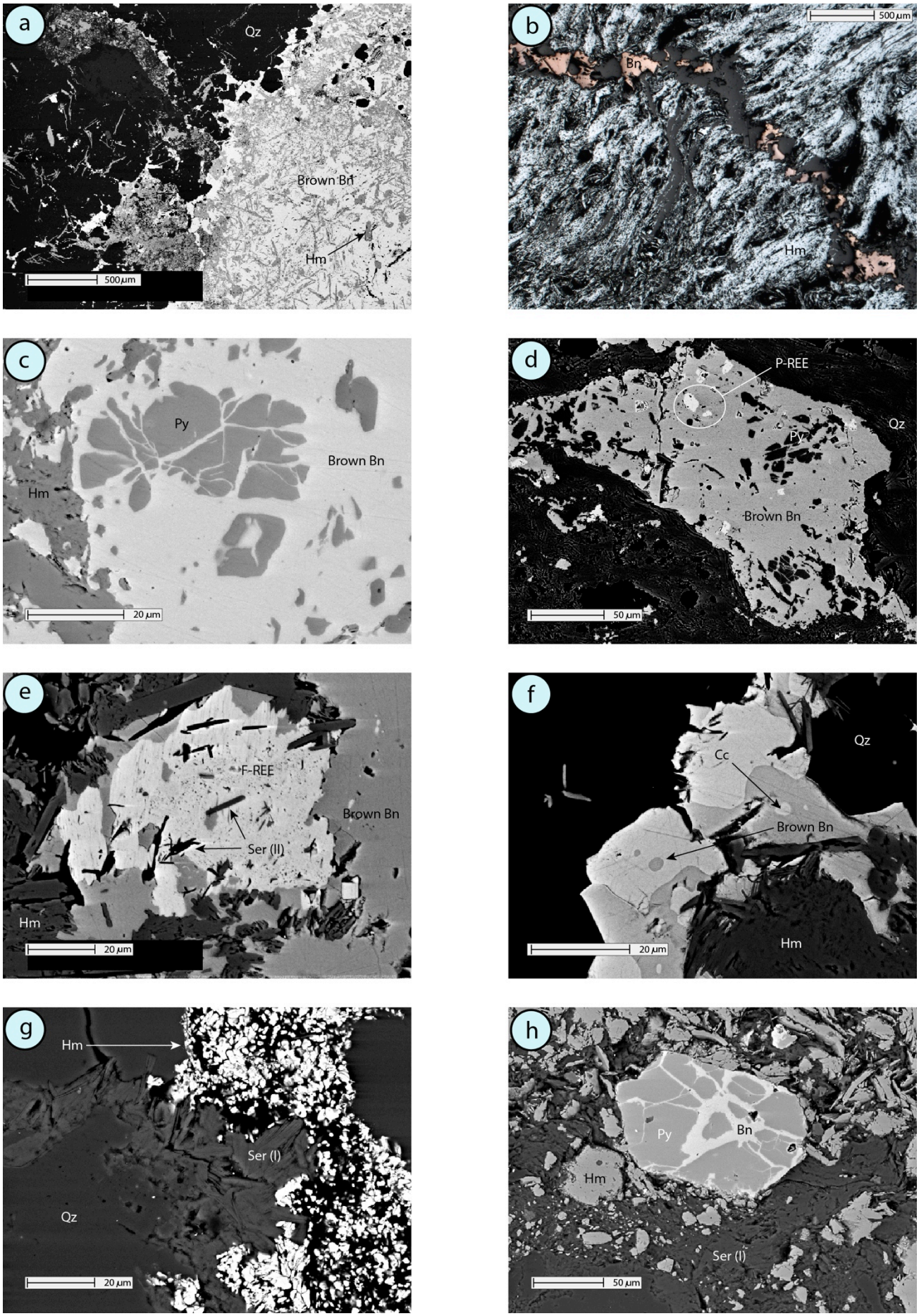
a
Qz
Brown Bn
Hm
500 µm
b
500 µm
Bn
Hm
c
Py
Brown Bn
Hm
20 µm
d
P-REE
Qz
Py
Brown Bn
50 µm
e
F-REE
Brown Bn
Ser (II)
Hm
20 µm
f
Qz
Cc
Brown Bn
20 µm
Hm
g
Hm
Ser (I)
Qz
20 µm
h
Py
Bn
Hm
Ser (I)
50 µm

Figure 10

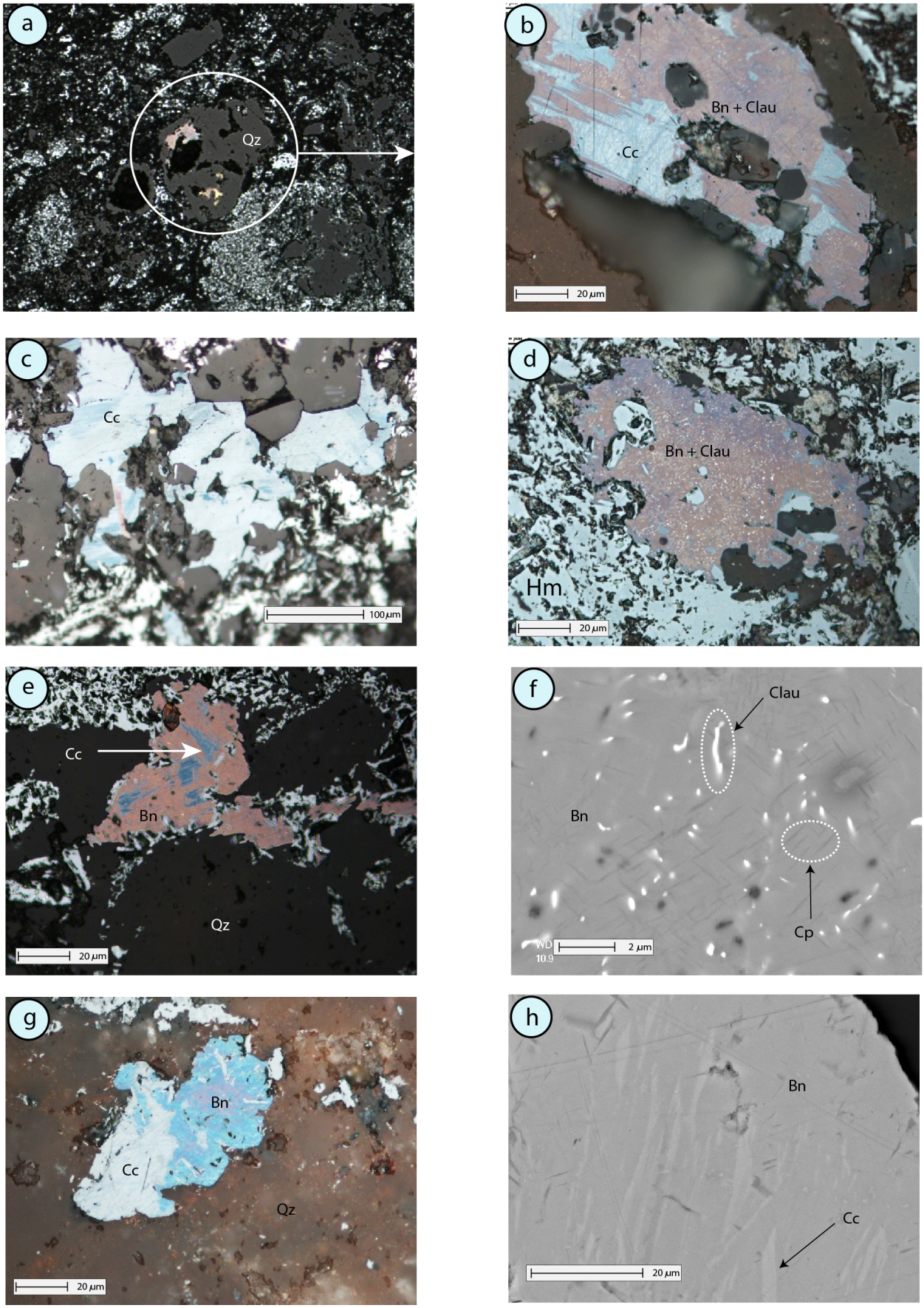
a
Qz
b
Bn + Clau
Cc
20 µm
c
Cc
100 µm
d
Bn + Clau
Hm
20 µm
e
Cc
Bn
Qz
20 µm
f
Clau
Bn
Cp
WD
10.9
2 µm
g
Bn
Cc
Qz
20 µm
h
Bn
Cc
20 µm

Figure 11

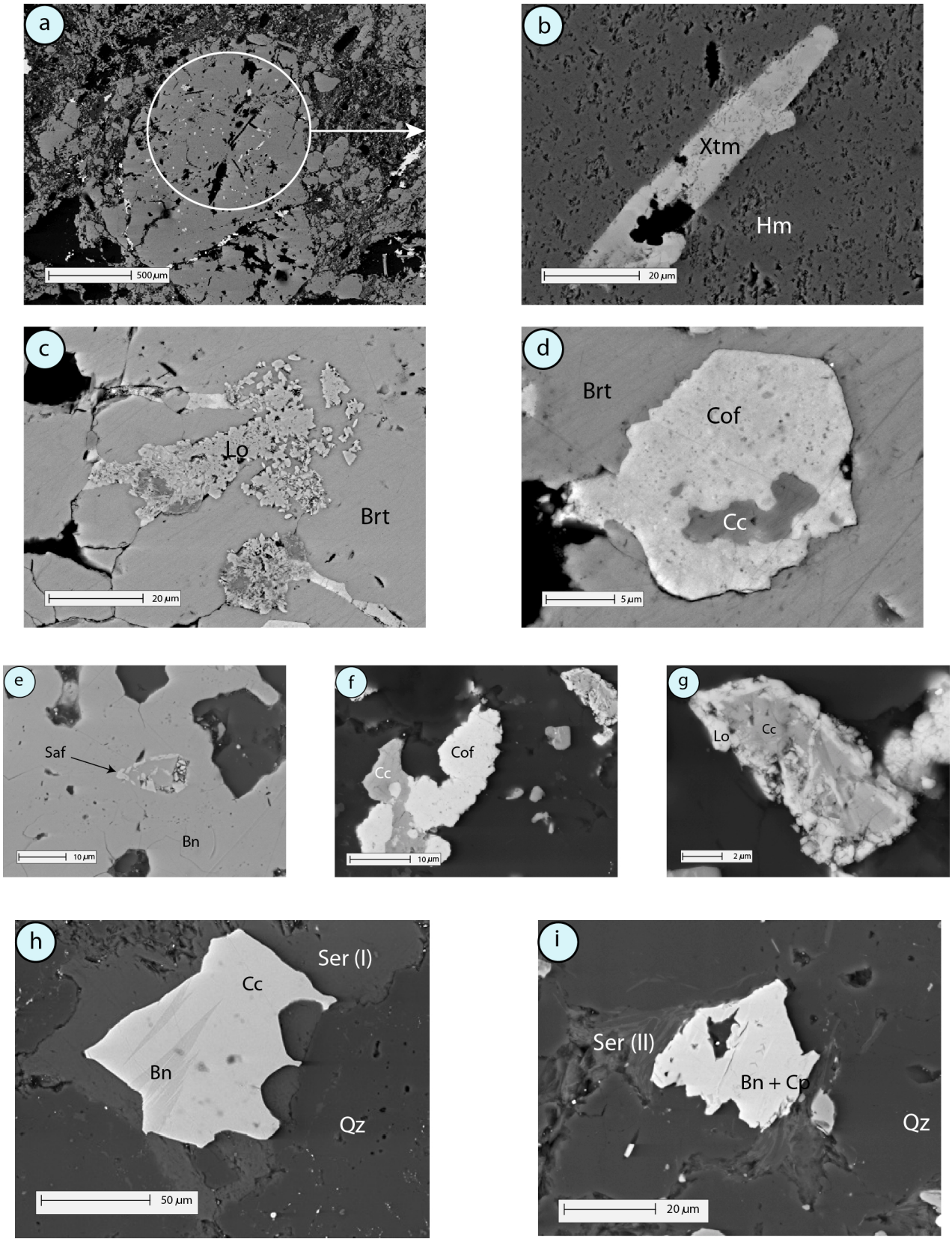
a
500 µm
b
Xtm
Hm
20 µm
c
Lo
Brt
20 µm
d
Brt
Cof
Cc
5 µm
e
Saf
Bn
10 µm
f
Cof
Cc
10 µm
g
Lo
Cc
2 µm
h
Ser (I)
Cc
Bn
Qz
50 µm
i
Ser (II)
Bn + Cp
Qz
20 µm

Figure 12

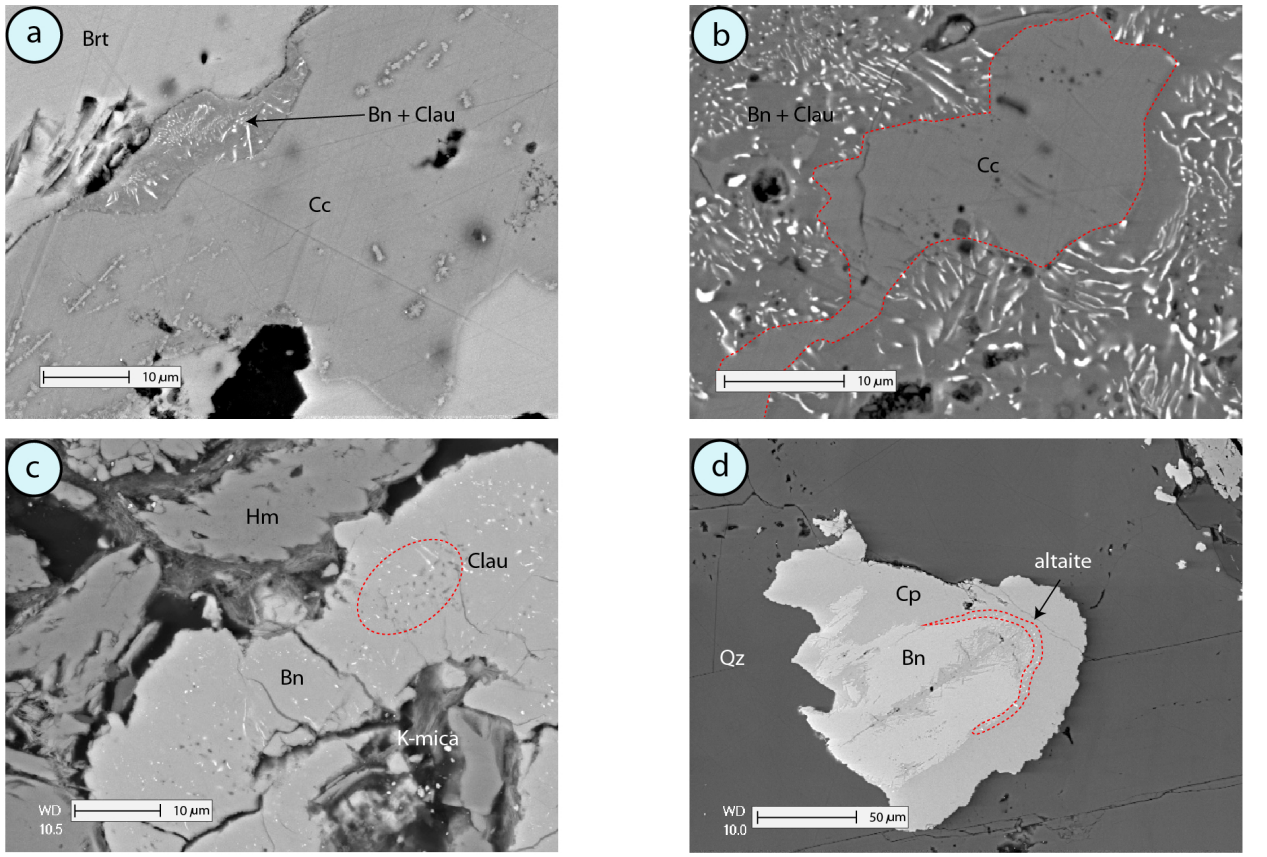
a
Brt
Bn + Clau
Cc
10 µm
b
Bn + Clau
Cc
10 µm
c
Hm
Clau
Bn
K-mica
WD 10.5
10 µm
d
altaite
Cp
Qz
Bn
WD 10.0
50 µm
e
Bn
Cp
altaite
WD 9.9
5 µm
f
100 µm
Cc
Bn
Cp
g
10 µm
Cp
Bn
h
100 µm
Qz
Cp
i
Cp
altaite
WD 9.9
10 µm
j
Cp
altaite
WD 9.9
10 µm

Figure 13

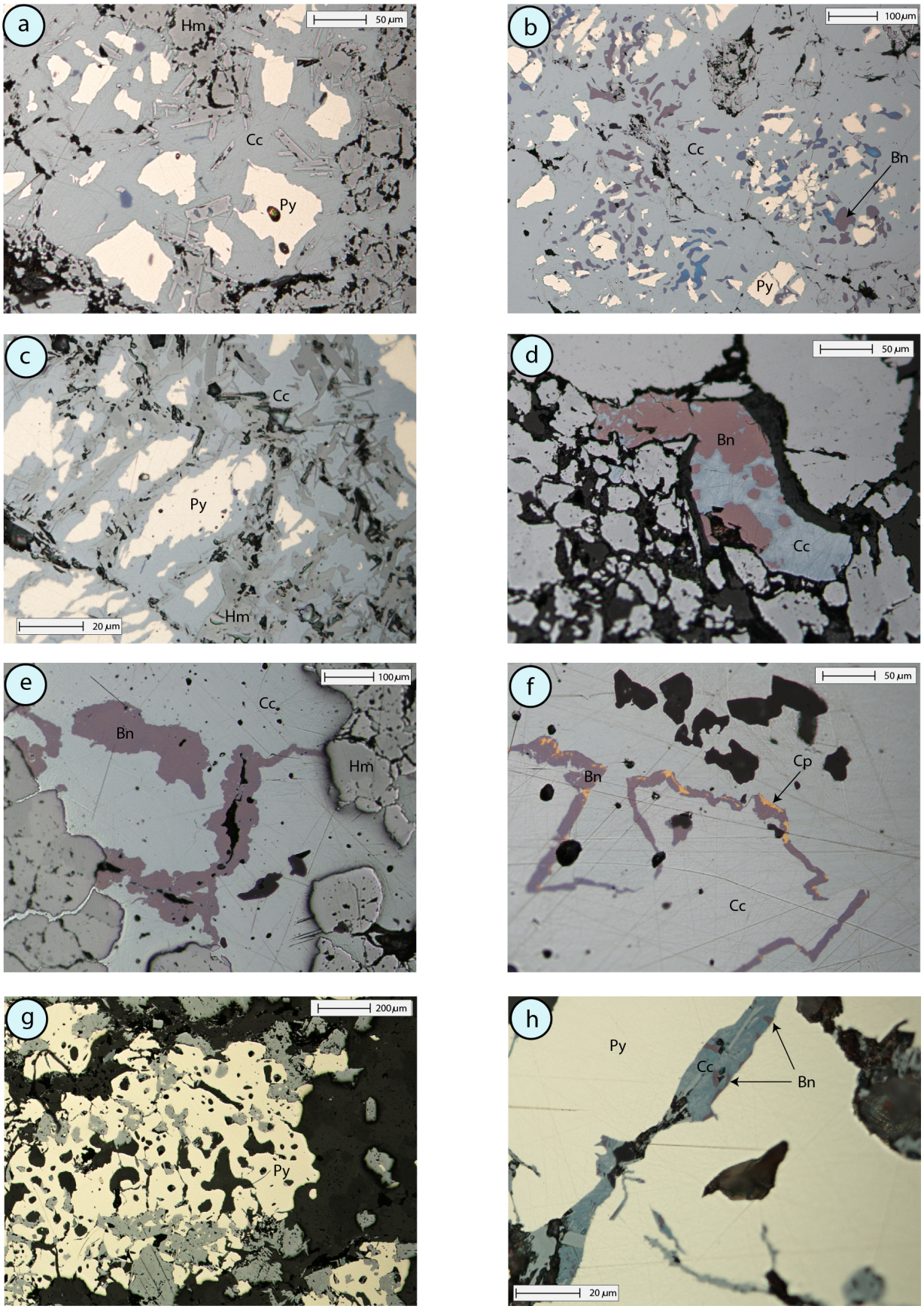
a
Hm
50 µm
Cc
Py
b
100µm
Cc
Bn
Py
c
Cc
Py
20 µm
Hm
d
50 µm
Bn
Cc
e
100µm
Cc
Bn
Hm
f
50 µm
Cp
Bn
Cc
g
200µm
Py
h
Py
Cc
Bn
20 µm

Figure 14

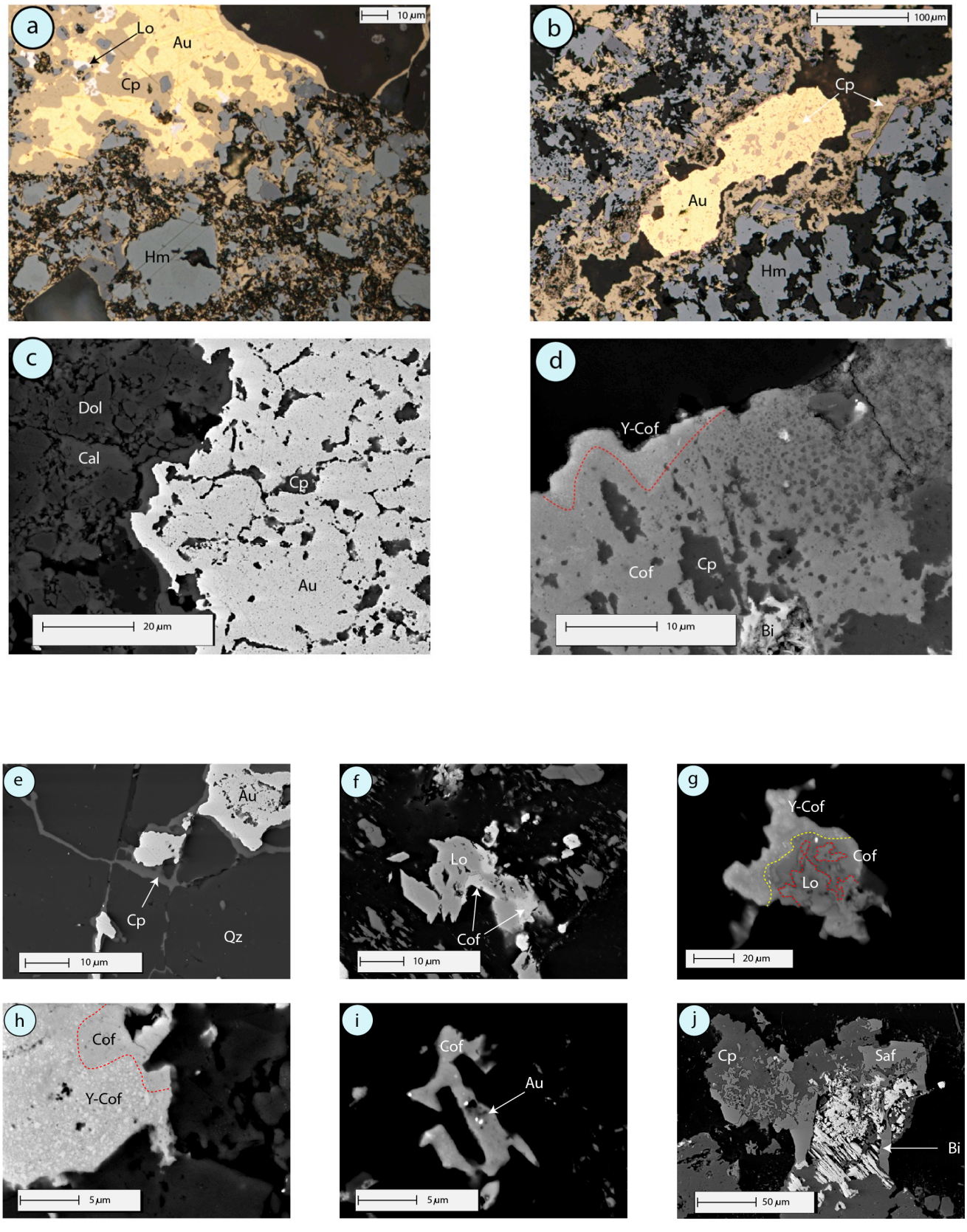
a
Lo
Au
Cp
Hm
10 µm
b
Cp
Au
Hm
100 µm
c
Dol
Cal
Cp
Au
20 µm
d
Y-Cof
Cof
Cp
Bi
10 µm
e
Au
Cp
Qz
10 µm
f
Lo
Cof
10 µm
g
Y-Cof
Cof
Lo
20 µm
h
Cof
Y-Cof
5 µm
i
Cof
Au
5 µm
j
Cp
Saf
Bi
50 µm

Figure 15

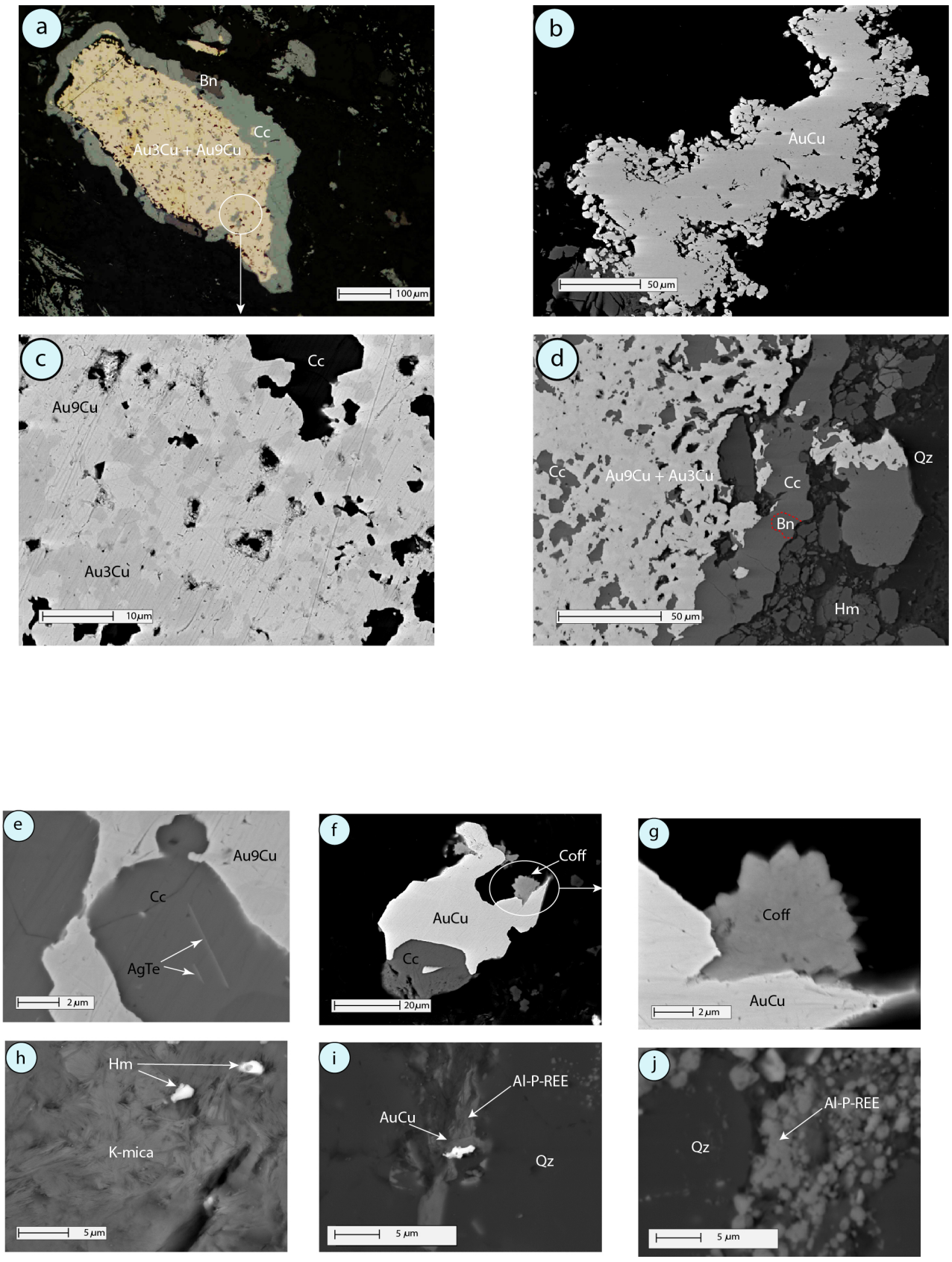
a
Bn
Cc
Au3Cu + Au9Cu
100 µm
b
AuCu
50 µm
c
Cc
Au9Cu
Au3Cu
10µm
d
Cc
Au9Cu + Au3Cu
Cc
Qz
Bn
Hm
50 µm
e
Au9Cu
Cc
AgTe
2 µm
f
Coff
AuCu
Cc
20µm
g
Coff
AuCu
2 µm
h
Hm
K-mica
5 µm
i
Al-P-REE
AuCu
Qz
5 µm
j
Al-P-REE
Qz
5 µm

Figure 16

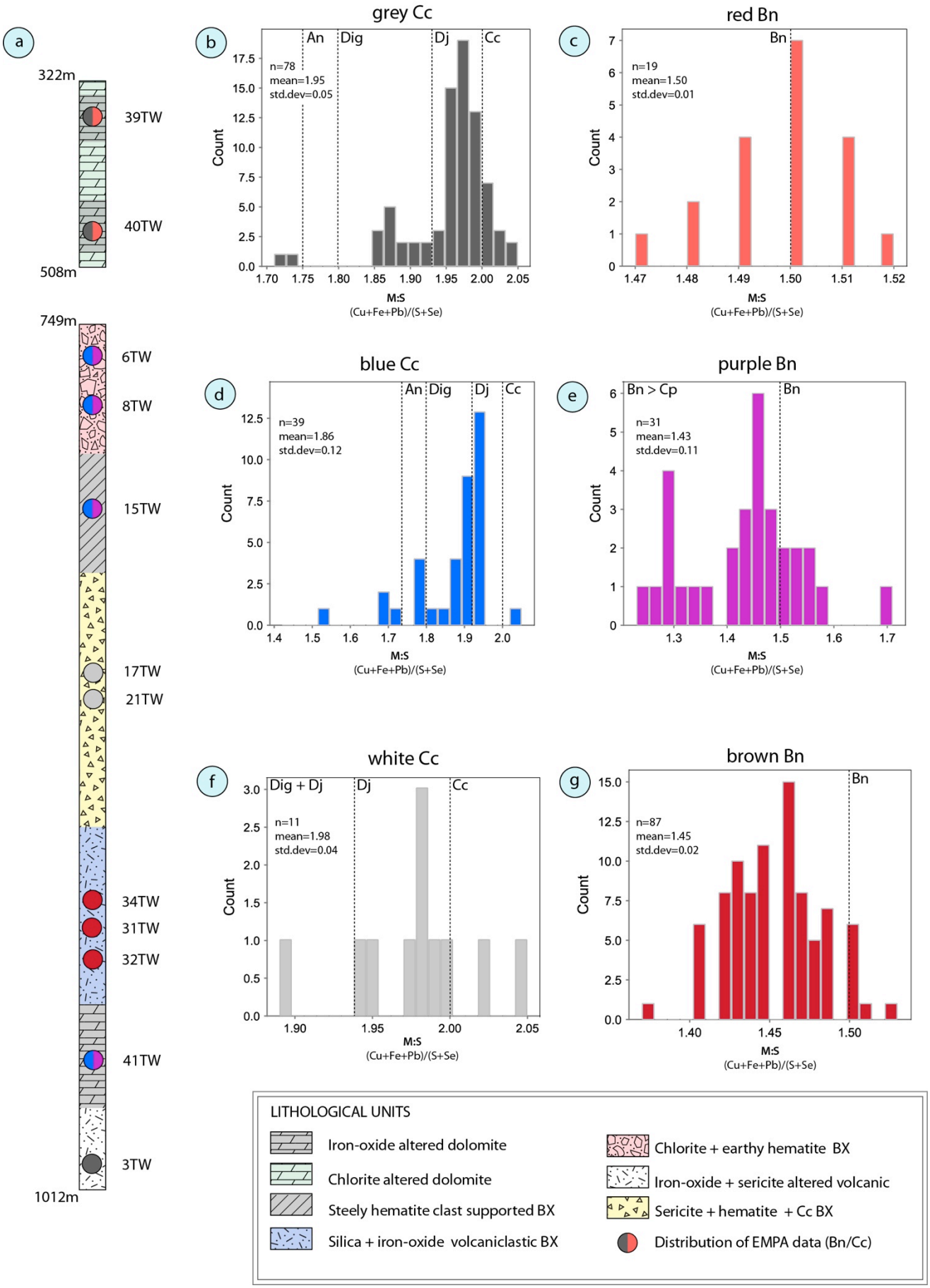
a
322m
39TW
40TW
508m
749m
6TW
8TW
15TW
17TW
21TW
34TW
31TW
32TW
41TW
3TW
1012m
b
grey Cc
An
Dig
Dj
Cc
n=78
mean=1.95
std.dev=0.05
Count
M:S
(Cu+Fe+Pb)/(S+Se)
c
red Bn
Bn
n=19
mean=1.50
std.dev=0.01
d
blue Cc
n=39
mean=1.86
std.dev=0.12
e
purple Bn
Bn > Cp
n=31
mean=1.43
std.dev=0.11
f
white Cc
Dig + Dj
n=11
mean=1.98
std.dev=0.04
g
brown Bn
n=87
mean=1.45
std.dev=0.02
LITHOLOGICAL UNITS
Iron-oxide altered dolomite
Chlorite altered dolomite
Steely hematite clast supported BX
Silica + iron-oxide volcaniclastic BX
Chlorite + earthy hematite BX
Iron-oxide + sericite altered volcanic
Sericite + hematite + Cc BX
Distribution of EMPA data (Bn/Cc)

Figure 17

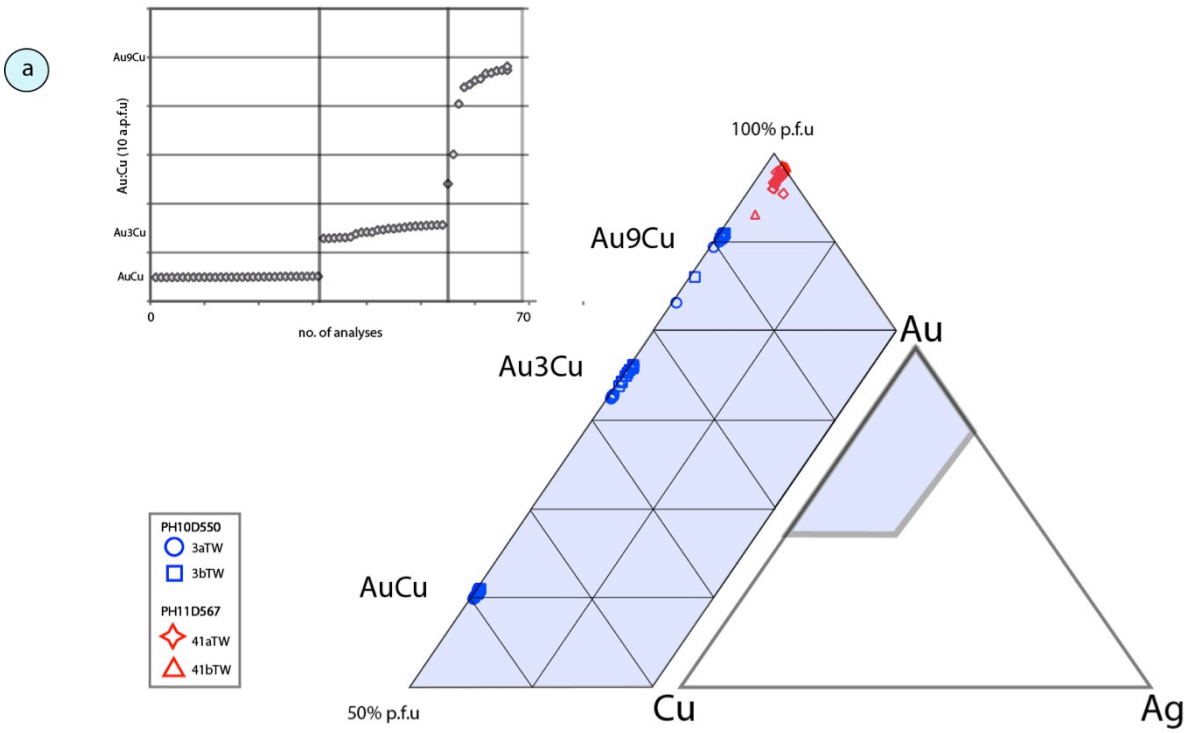
a
Au9Cu
Au3Cu
AuCu
Au:Cu (10 a.p.f.u)
0
70
no. of analyses
100% p.f.u
Au9Cu
Au
Au3Cu
AuCu
50% p.f.u
Cu
Ag
PH10D550
3aTW
3bTW
PH11D567
41aTW
41bTW

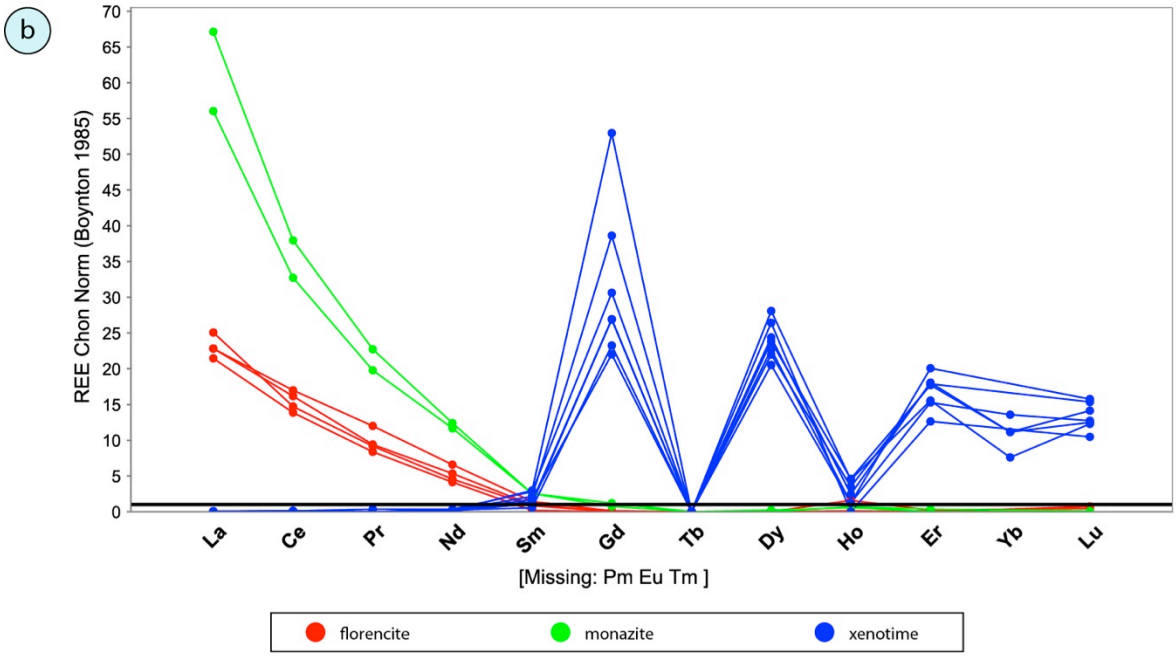
b
REE Chon Norm (Boynton 1985)
70
65
60
55
50
45
40
35
30
25
20
15
10
5
0
La
Ce
Pr
Nd
Sm
Gd
Tb
Dy
Ho
Er
Yb
Lu
[Missing: Pm Eu Tm]
florencite
monazite
xenotime

Figure 18

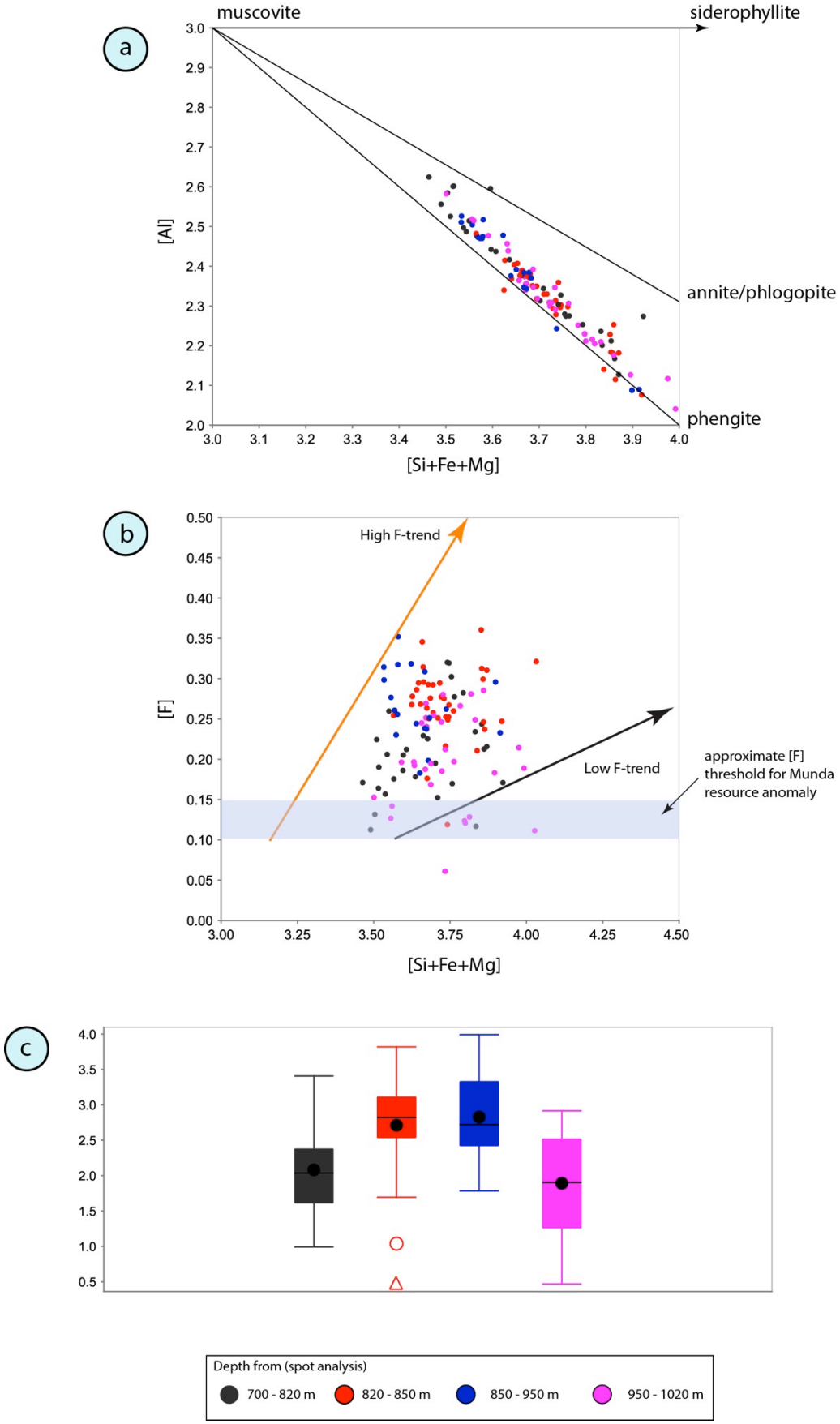
a
muscovite
siderophyllite
annite/phlogopite
phengite
[Al]
[Si+Fe+Mg]
b
High F-trend
Low F-trend
approximate [F] threshold for Munda resource anomaly
[F]
[Si+Fe+Mg]
c
Depth from (spot analysis)
700 - 820 m
820 - 850 m
850 - 950 m
950 - 1020 m

Figure 19

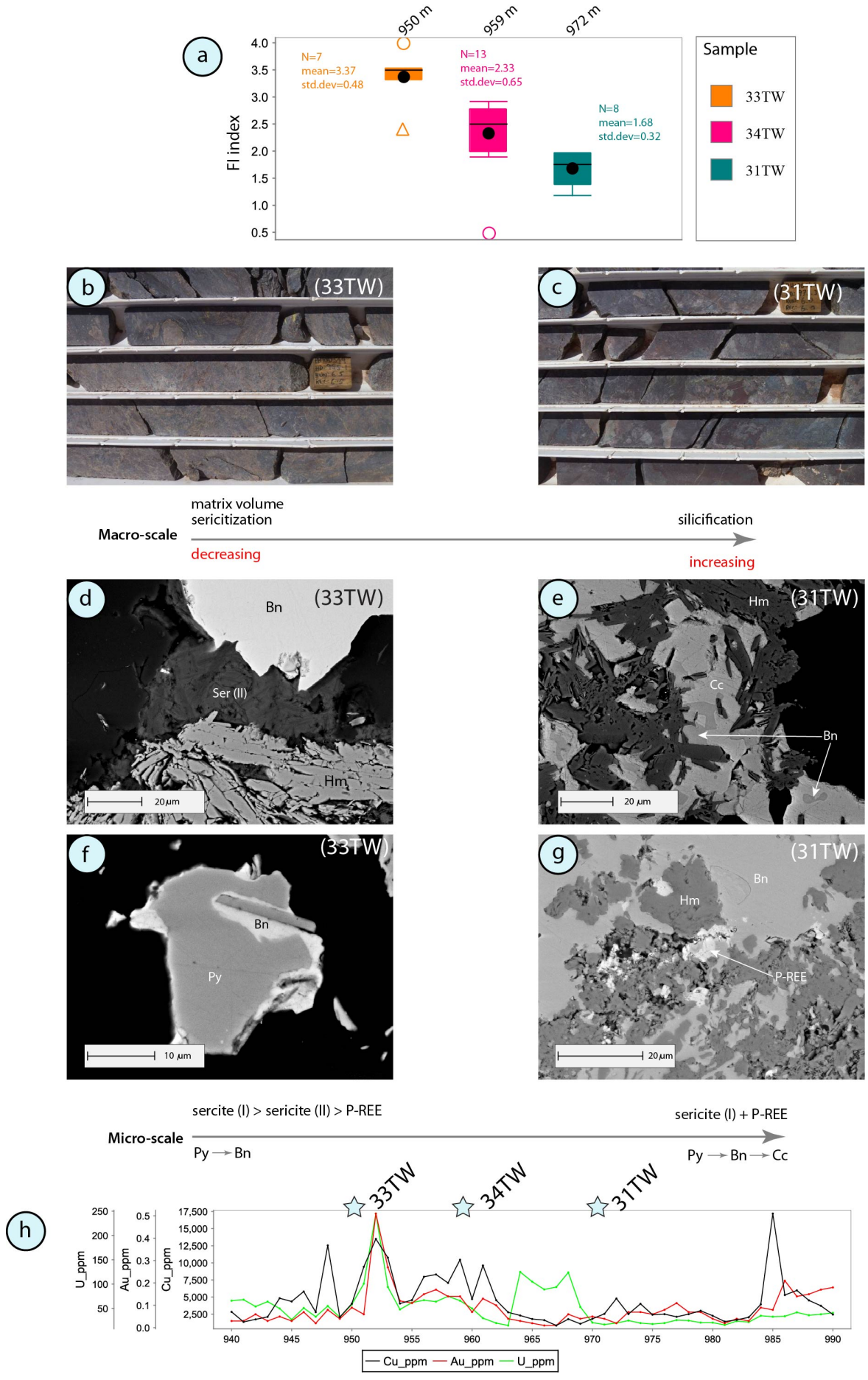
a
950 m
959 m
972 m
FI index
N=7
mean=3.37
std.dev=0.48
N=13
mean=2.33
std.dev=0.65
N=8
mean=1.68
std.dev=0.32
Sample
33TW
34TW
31TW
b
(33TW)
c
(31TW)
Macro-scale
matrix volume
sericitization
decreasing
silicification
increasing
d
(33TW)
Bn
Ser (II)
Hm
20 µm
e
(31TW)
Hm
Cc
Bn
20 µm
f
(33TW)
Bn
Py
10 µm
g
(31TW)
Bn
Hm
P-REE
20 µm
Micro-scale
sercite (I) > sericite (II) > P-REE
Py → Bn
sericite (I) + P-REE
Py → Bn → Cc
h
33TW
34TW
31TW
U_ppm
Au_ppm
Cu_ppm
Cu_ppm
Au_ppm
U_ppm

Figure 20

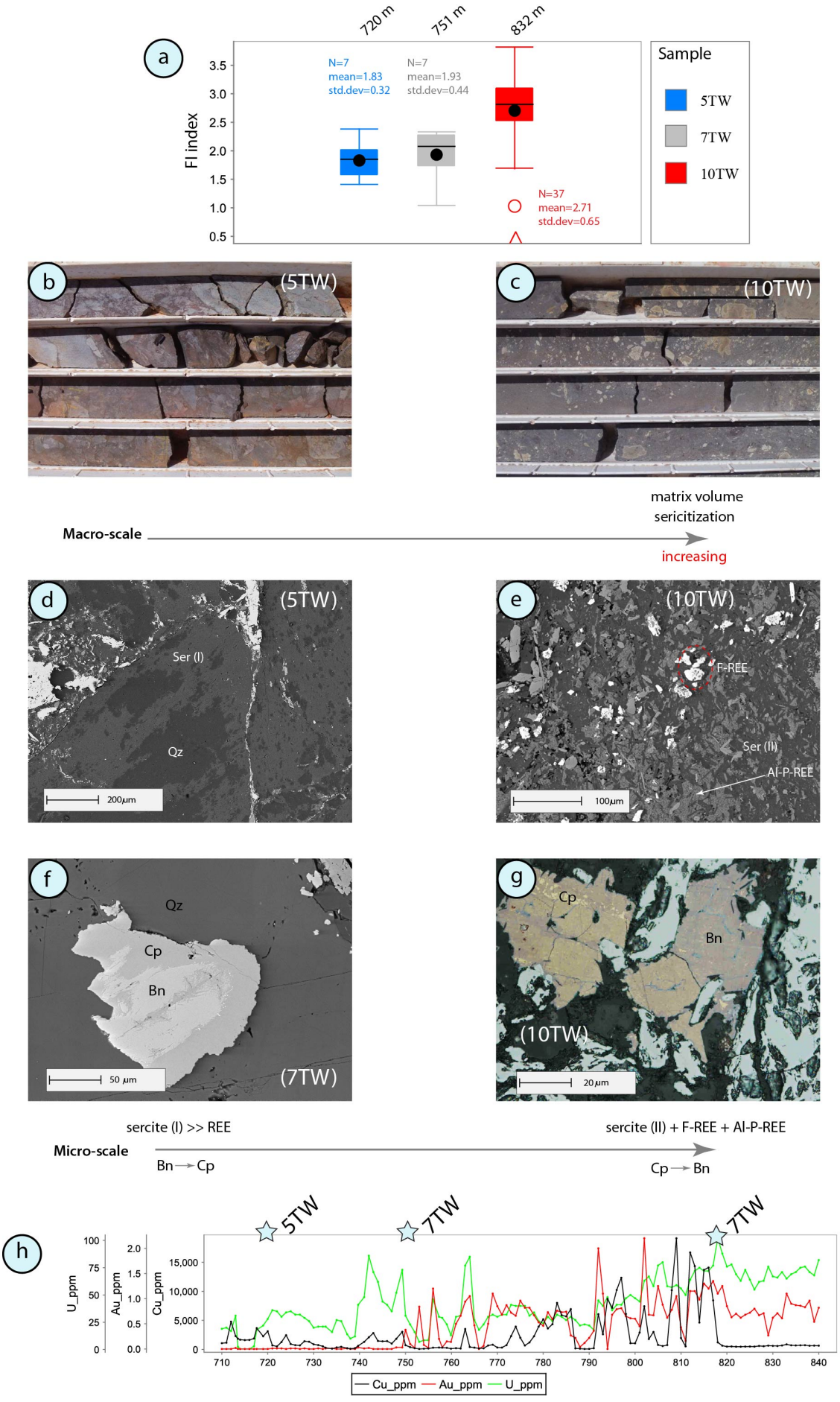
a
720 m
751 m
832 m
FI index
N=7
mean=1.83
std.dev=0.32
N=7
mean=1.93
std.dev=0.44
N=37
mean=2.71
std.dev=0.65
Sample
5TW
7TW
10TW
b
(5TW)
c
(10TW)
matrix volume
sericitization
Macro-scale
increasing
d
(5TW)
Ser (I)
Qz
200µm
e
(10TW)
F-REE
Ser (II)
Al-P-REE
100µm
f
Qz
Cp
Bn
50 µm
(7TW)
g
Cp
Bn
(10TW)
20 µm
sercite (I) >> REE
sercite (II) + F-REE + Al-P-REE
Micro-scale
Bn → Cp
Cp → Bn
h
5TW
7TW
7TW
U_ppm
Au_ppm
Cu_ppm
Cu_ppm
Au_ppm
U_ppm

Figure 21

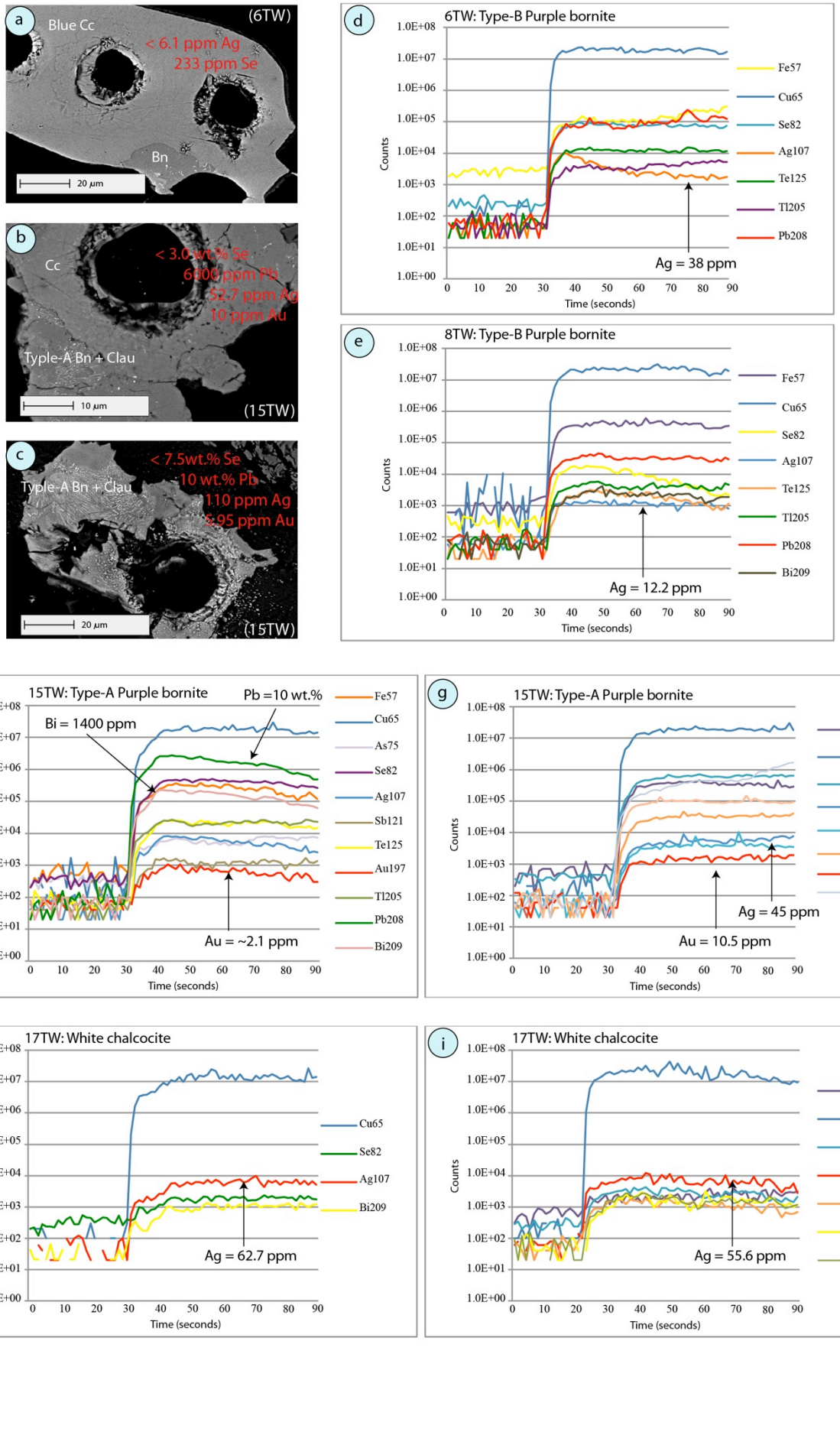
a
Blue Cc
(6TW)
< 6.1 ppm Ag
233 ppm Se
Bn
20 µm
b
Cc
< 3.0 wt.% Se
6000 ppm Pb
52.7 ppm Ag
10 ppm Au
Typle-A Bn + Clau
10 µm
(15TW)
c
< 7.5wt.% Se
10 wt.% Pb
110 ppm Ag
6.95 ppm Au
Typle-A Bn + Clau
20 µm
(15TW)
d
6TW: Type-B Purple bornite
Counts
Time (seconds)
Fe57
Cu65
Se82
Ag107
Te125
Tl205
Pb208
Ag = 38 ppm
e
8TW: Type-B Purple bornite
Counts
Time (seconds)
Fe57
Cu65
Se82
Ag107
Te125
Tl205
Pb208
Bi209
Ag = 12.2 ppm
f
15TW: Type-A Purple bornite
Pb =10 wt.%
Bi = 1400 ppm
Au = ~2.1 ppm
Counts
Time (seconds)
Fe57
Cu65
As75
Se82
Ag107
Sb121
Te125
Au197
Tl205
Pb208
Bi209
g
15TW: Type-A Purple bornite
Ag = 45 ppm
Au = 10.5 ppm
Counts
Time (seconds)
Fe57
Cu65
Se82
Ag107
Sb121
Te125
Au197
Pb208
h
17TW: White chalcocite
Ag = 62.7 ppm
Counts
Time (seconds)
Cu65
Se82
Ag107
Bi209
i
17TW: White chalcocite
Ag = 55.6 ppm
Counts
Time (seconds)
Fe57
Cu65
Se82
Ag107
Te125
Pb208
Bi209

Figure 22

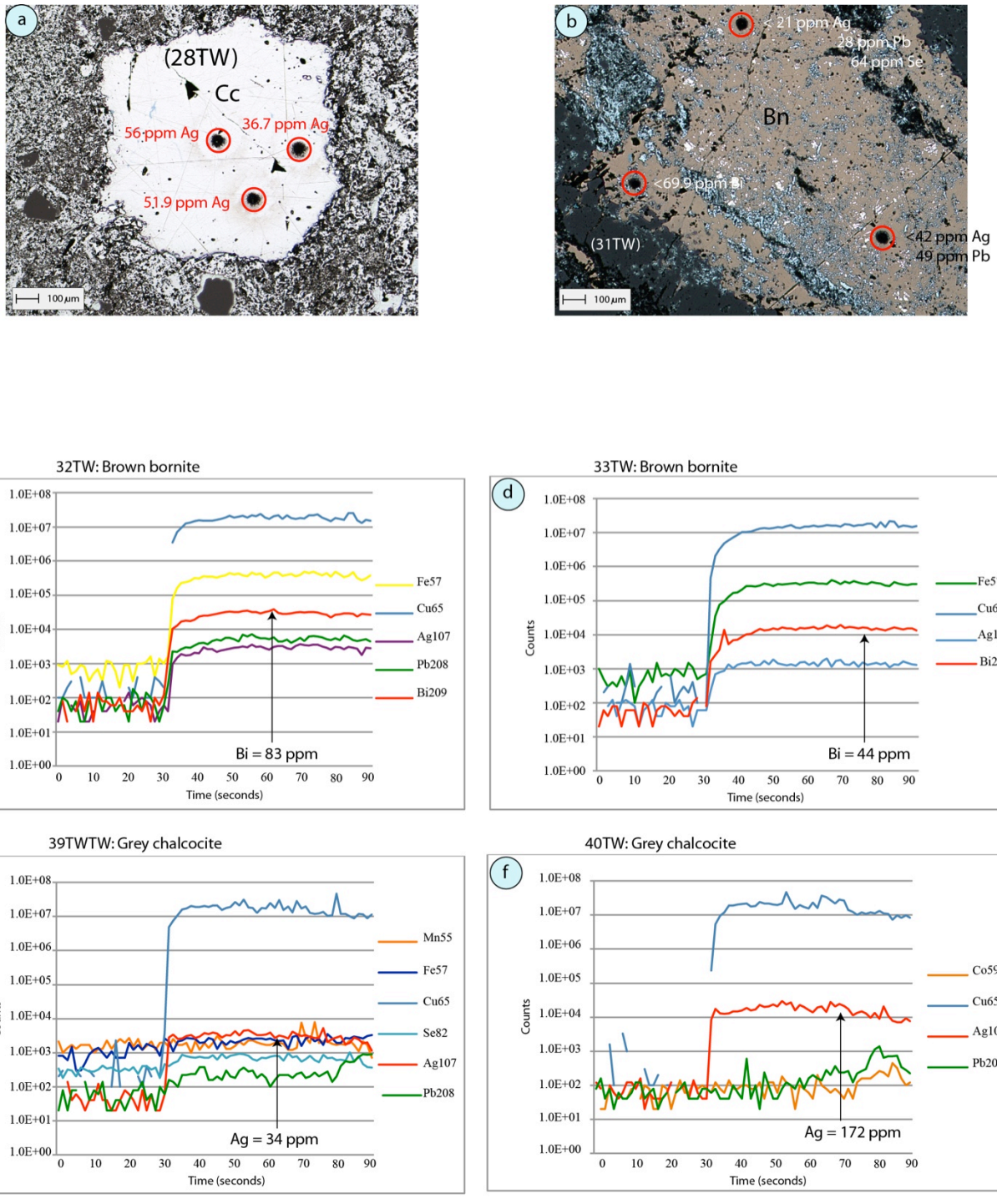
a
(28TW)
Cc
56 ppm Ag
36.7 ppm Ag
51.9 ppm Ag
100 µm
b
< 21 ppm Ag
28 ppm Pb
64 ppm Se
Bn
<69.9 ppm Bi
(31TW)
<42 ppm Ag
49 ppm Pb
100 µm
32TW: Brown bornite
c
Counts
Time (seconds)
Fe57
Cu65
Ag107
Pb208
Bi209
Bi = 83 ppm
33TW: Brown bornite
d
Counts
Time (seconds)
Fe57
Cu65
Ag107
Bi209
Bi = 44 ppm
39TWTW: Grey chalcocite
e
Counts
Time (seconds)
Mn55
Fe57
Cu65
Se82
Ag107
Pb208
Ag = 34 ppm
40TW: Grey chalcocite
f
Counts
Time (seconds)
Co59
Cu65
Ag107
Pb208
Ag = 172 ppm

Figure 23

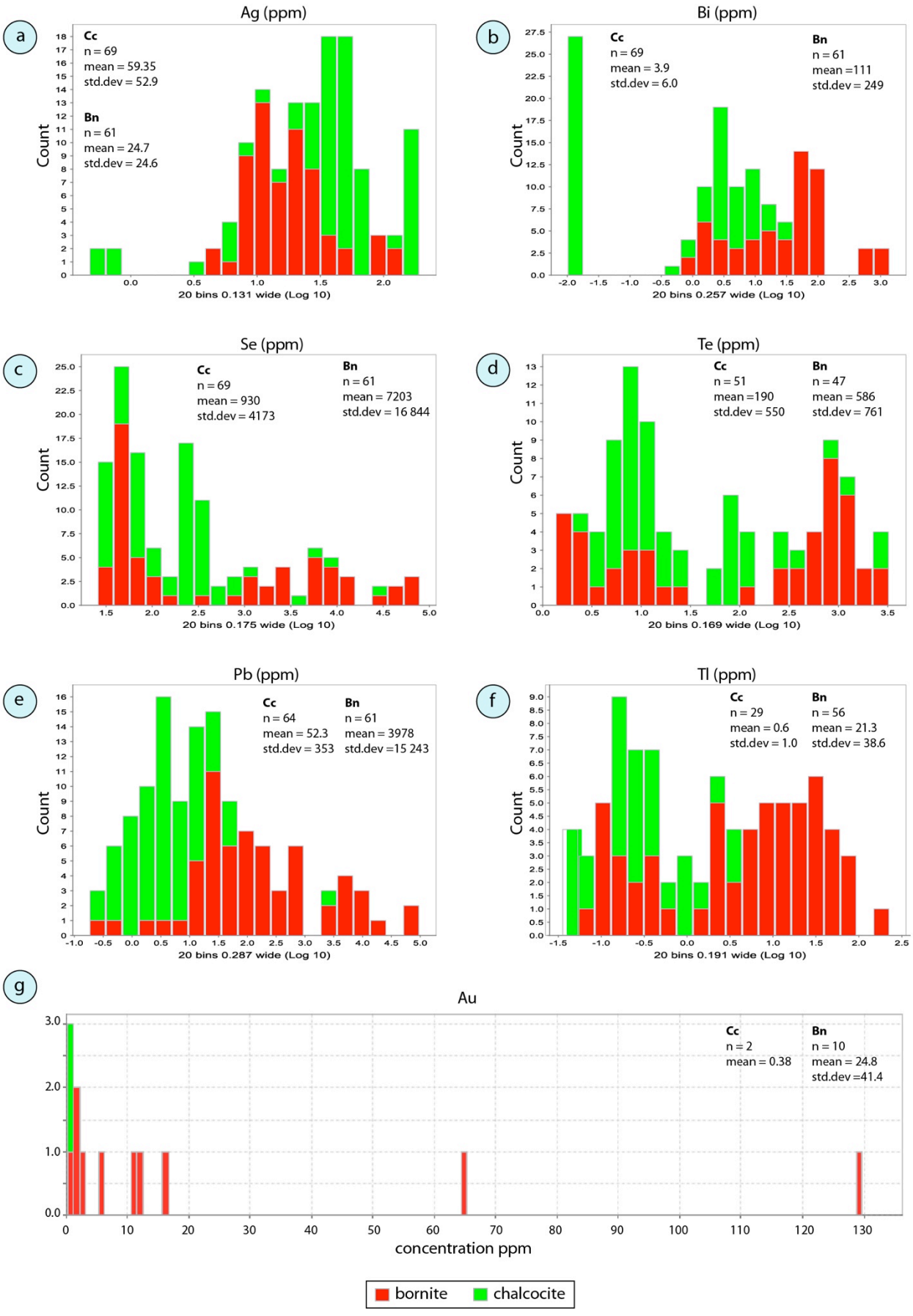
a
Ag (ppm)
Cc
n = 69
mean = 59.35
std.dev = 52.9
Bn
n = 61
mean = 24.7
std.dev = 24.6
Count
20 bins 0.131 wide (Log 10)
b
Bi (ppm)
Cc
n = 69
mean = 3.9
std.dev = 6.0
Bn
n = 61
mean =111
std.dev = 249
Count
20 bins 0.257 wide (Log 10)
c
Se (ppm)
Cc
n = 69
mean = 930
std.dev = 4173
Bn
n = 61
mean = 7203
std.dev = 16 844
Count
20 bins 0.175 wide (Log 10)
d
Te (ppm)
Cc
n = 51
mean =190
std.dev = 550
Bn
n = 47
mean = 586
std.dev = 761
Count
20 bins 0.169 wide (Log 10)
e
Pb (ppm)
Cc
n = 64
mean = 52.3
std.dev = 353
Bn
n = 61
mean = 3978
std.dev =15 243
Count
20 bins 0.287 wide (Log 10)
f
Tl (ppm)
Cc
n = 29
mean = 0.6
std.dev = 1.0
Bn
n = 56
mean = 21.3
std.dev = 38.6
Count
20 bins 0.191 wide (Log 10)
g
Au
Cc
n = 2
mean = 0.38
Bn
n = 10
mean = 24.8
std.dev =41.4
concentration ppm
bornite
chalcocite

Figure 24

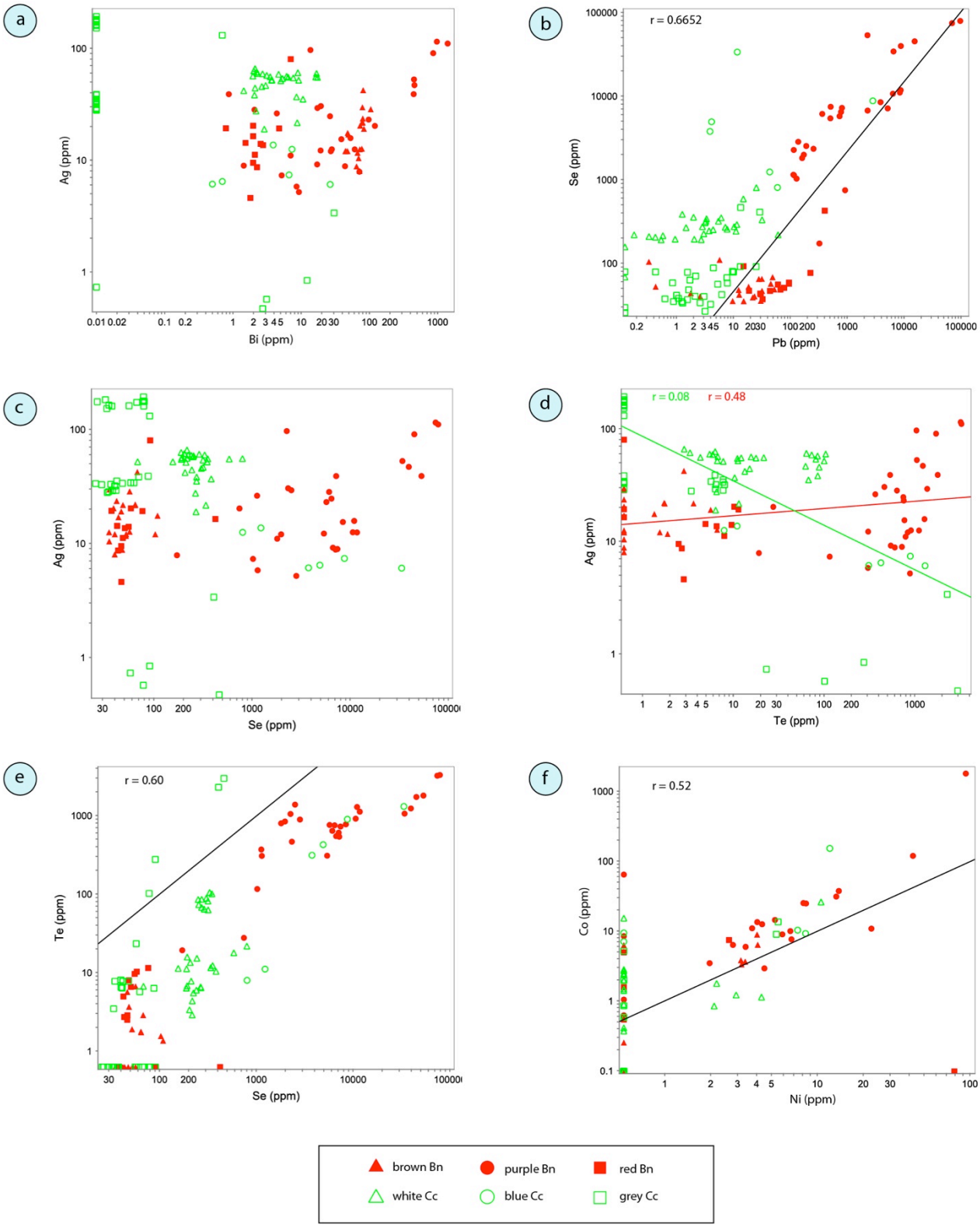
a
Ag (ppm)
Bi (ppm)
b
r = 0.6652
Se (ppm)
Pb (ppm)
c
Ag (ppm)
Se (ppm)
d
r = 0.08
r = 0.48
Ag (ppm)
Te (ppm)
e
r = 0.60
Te (ppm)
Se (ppm)
f
r = 0.52
Co (ppm)
Ni (ppm)
brown Bn
purple Bn
red Bn
white Cc
blue Cc
grey Cc

Figure 25

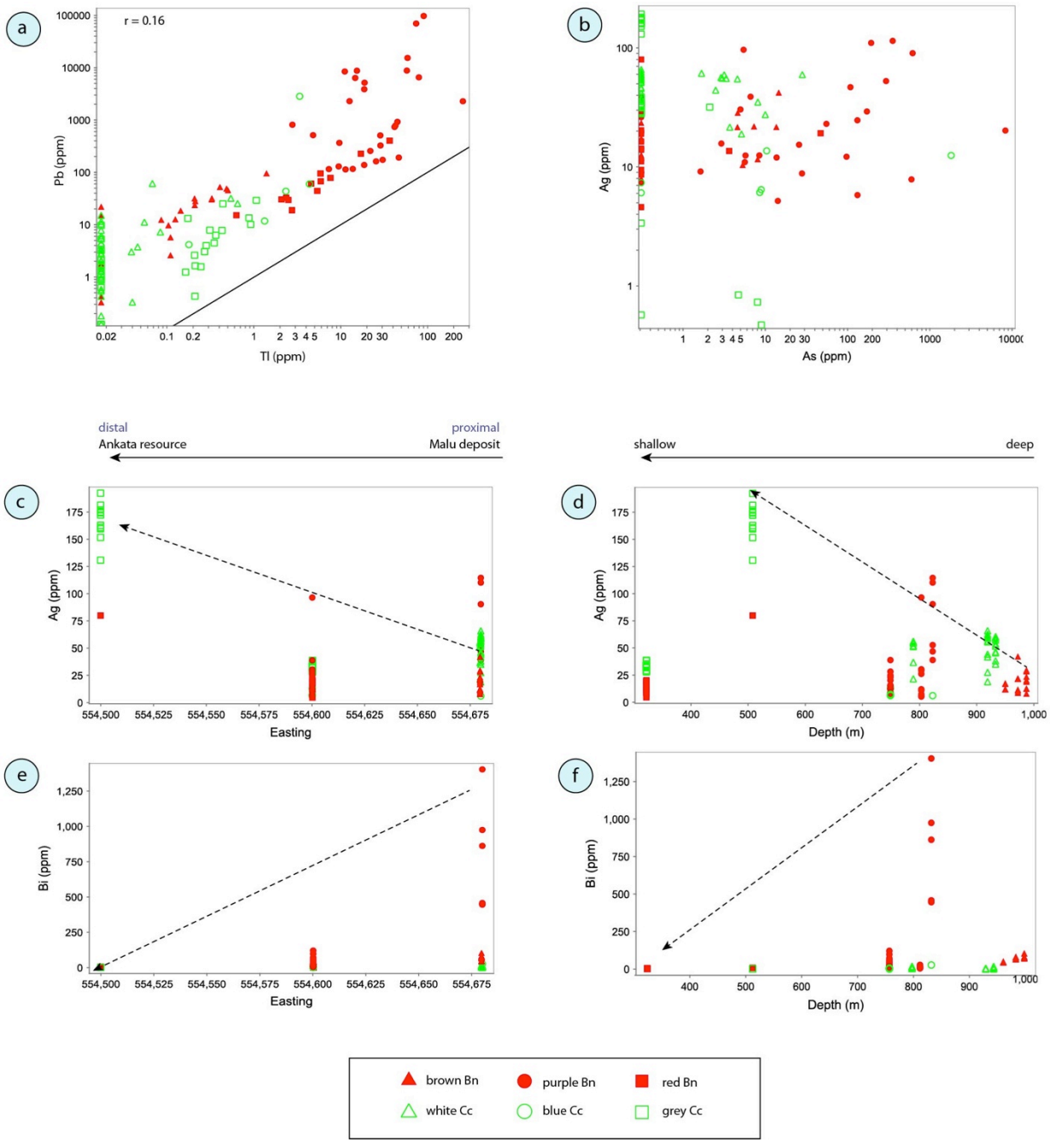
a
r = 0.16
Pb (ppm)
Tl (ppm)
b
Ag (ppm)
As (ppm)
distal
Ankata resource
proximal
Malu deposit
shallow
deep
c
Ag (ppm)
Easting
d
Ag (ppm)
Depth (m)
e
Bi (ppm)
Easting
f
Bi (ppm)
Depth (m)
brown Bn
purple Bn
red Bn
white Cc
blue Cc
grey Cc

Figure 26

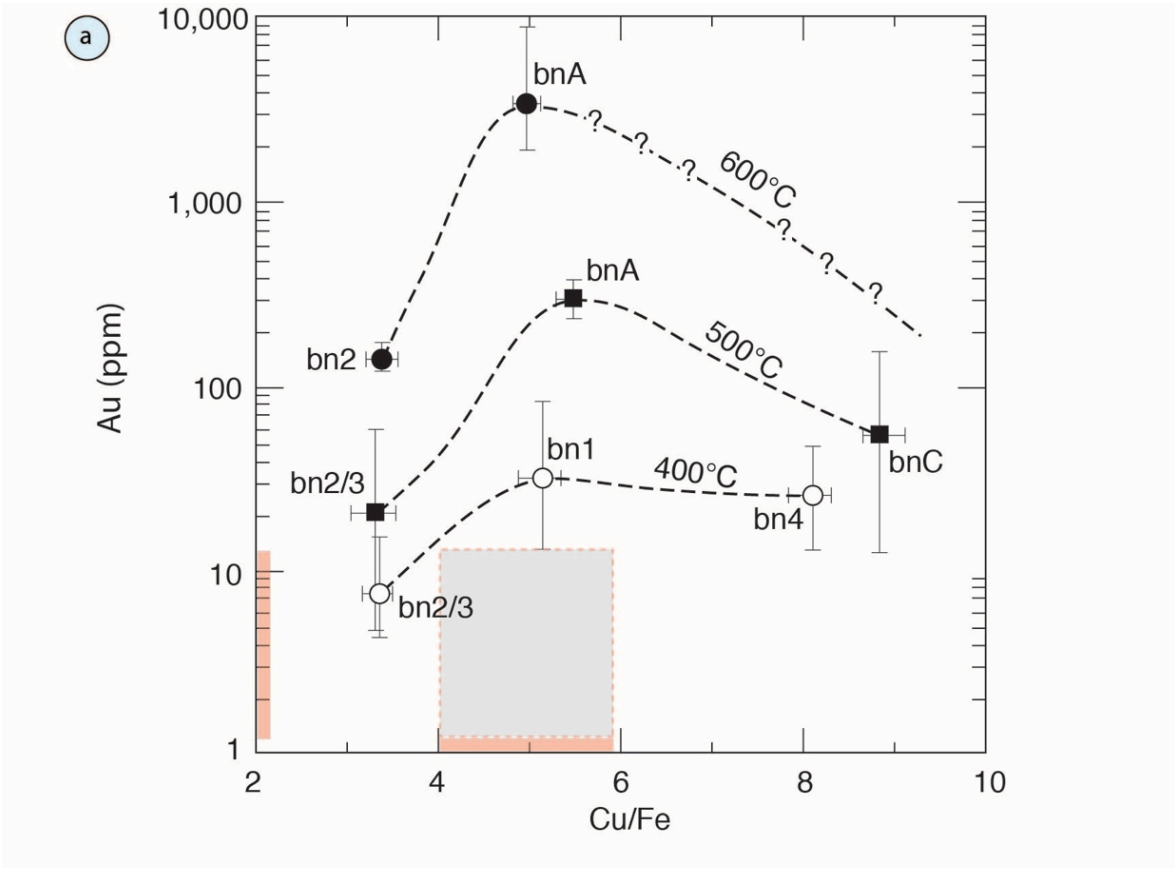
a
10,000
1,000
100
10
1
Au (ppm)
2
4
6
8
10
Cu/Fe
bnA
600°C
bnA
500°C
bn2
bn1
400°C
bnC
bn2/3
bn4
bn2/3

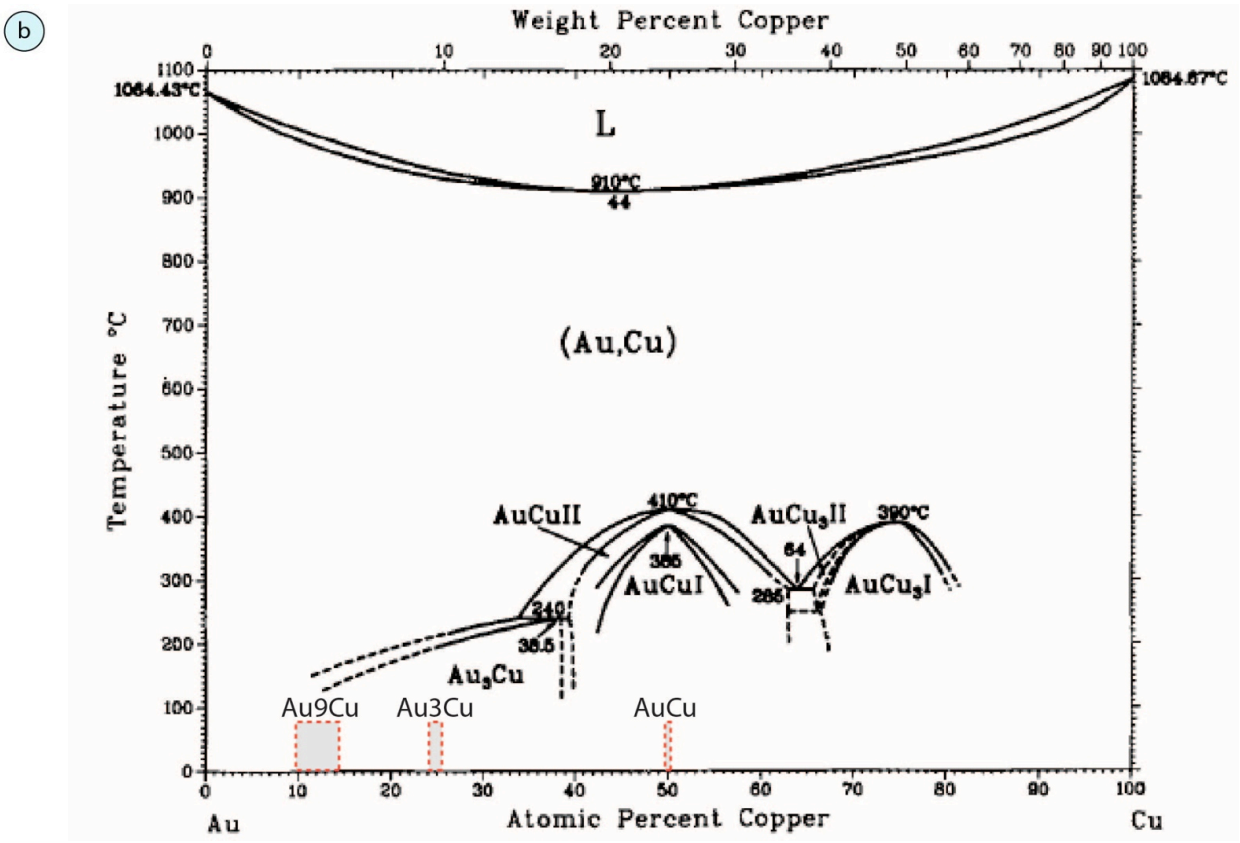
b
Weight Percent Copper
0
10
20
30
40
50
60
70
80
90
100
1100
1084.43°C
1084.87°C
L
910°C
44
1000
900
800
700
600
500
400
300
200
100
0
Temperature °C
(Au,Cu)
AuCuII
410°C
AuCu3II
390°C
64
385
AuCuI
285
AuCu3I
340
355
Au3Cu
Au9Cu
Au3Cu
AuCu
0
10
20
30
40
50
60
70
80
90
100
Au
Atomic Percent Copper
Cu

Table 1: Key to abbreviations used

Rock Types		Rock Textures		Rock Alteration	
BSLT	Basalt	**AC**	Angular clasts	**CH**	Chlorite
SLST	Siltstone	**CR**	Crackle	**HE**	Earthy Hematite
SNST	Sandstone	**FB**	Flow Banded	**HD**	Crystalline Hematite
HMBX	Hematite Breccia	**MP**	Monolithic	**HG**	Steely Hematite
DACT	Dacite	**PM**	Heterolithic	**HR**	Silicified Hematite
DOLM	Dolomite	**PX**	Psudeobrecciated	**HS**	Specular Hematite
HMRK	Hematite rock	**UR**	Subrounded clasts	**SF**	Silica
		UA	Subangular clasts	**SR**	Sericite
		VU	Vuggy		

Gangue minerals		Opaques	
Al-P-REE	Florencite	**Alt**	Altaite
Ap	Apatite	**An**	Anilite
Cal	Calcite	**Au**	Gold
Chl	Chlorite	**Bi**	Native bismuth
Dol	Dolomite	**Bn1**	Brown bornite
F-REE	Fluocerite	**Bn2**	Purple bornite
F-Ap	Fluorapatite	**Bn3**	Red bornite
Hm	Hematite	**Brt**	Barite
Ilm	Ilmenite	**Cas**	Cassiterite
P-REE	Monazite	**Cc1**	White chalcocite
Qz	Quartz	**Cc2**	Blue chalcocite
Ser	Sericite	**Cc3**	Grey chalcocite
		Clau	Clausthalite
		Cof	Coffinite
		Cp	Chalcopyrite
		Dig	Digenite
		Dj	Djurleite
		Dom	Domeykite
		Lo	Loellingite
		Mgt	Magnetite
		Phl	Phlogopite
		Py	Pyrite
		Rt	Rutile
		Saf	Safflorite
		Y-Cof	Yittrium - coffinite
		Xtm	Xenotime
		Zr	Zircon

Table 2: Sample descriptions - whole-rock assays, lithology, alteration

Sample "TW"	Depth (m)	Cu (%)	Au ppm	U ppm	Ce ppm	Rock Type	Texture 1	Texture 2	Alteration 1	Alteration 2	Comments
PH10D550: 555030.9E, 6711641 N											
1	1002	<0.01	0.35	41.0	1810	BSLT	UR	FB	SR	HE	Plag microlaths in bleached zone
2	1007	<0.01	11.30	50.0	2210	SLST	UA	PX?	HE	SR	impure SLST
3	1012	<0.01	179	30.0	780	SLST/SNST	FB		HE	SR	Visual Au
4	1011	<0.01	2.45	42.0	2200	SNST?	FM	GC	SR	HE	
PH10D551: 554600E, 6721535N											
5	720	0.22	0.00	28.0	600	SLST	AC	MP			leucoxcene in micro fractures
6	749	0.30	0.03	73.0	1370	HMBX	UR	UA	CH	SR	SF HE veins X-cutting SLST clasts
7	751	0.07	0.38	23.0	1190	HMBX	MP	UR	HR		
8	803	0.74	2.20	67.0	3220	HMBX	AC		SR	HR	SR overprinting HR
9	831	0.06	0.62	66.0	2320	HMBX	MP	UA	HE	SR	HE overprinting SR
10	832	0.06	0.71	71.0	2280	HMBX	MP	UA	HE	SR	HE overprinting SR
11	840	0.07	0.54	82.0	2600	HMBX		UA	SR	HE	HE overprinting SR
12	865	0.05	0.20	74.0	390	HMBX	MP	UA	SR	HE	HE overprinting SR
PH10D554: 554680E, 6712514N											
13	800	0.02	1.10	25.0	255	UNBX	AC	MP	CH	SR	
14	821	0.04	1.20	73.0	2940	HMRK (SLST?)			HG	SF	>Vcb crackle veining, qz-feldspathic blebs?
15	823	0.03	2.55	59.0	5420	HMRK (SLST?)			HG	SF	Feldspathic veins
16	853	0.01	0.12	28.0	590	HMRK	VU		HG	SF	Feldspathic veins
17	919	3.06	1.15	57.0	3590	HMBX	MP	AC/UA	HE	SF?	Visual Bn Cc
18	922	1.27	1.10	48.0	2910	HMBX	MP	UR/RC	NA?	SR	
19	924	1.96	0.93	58.0	3870	HMBX	PX		HE	HG	Visual Bn Cc
20	926	2.75	0.93	49.0	2610	HMBX	MP	UR/UA	HE		Visual Bn Cc
21	928	4.66	0.55	47.0	2570	HMBX	UA	UR	HE		Visual Bn Cc
22	932	2.00	0.87	39.0	2210	HMBX	UA	UR	HE		Visual Bn Cc
23	933	2.10	0.80	36.0	1910	HMBX	UA	UR	HE		Visual Bn Cc
PH10D549: 554680E, 6712420N											
24	722	0.03	1.35	47.0	1830	HMRK (SLST?)			HG	HE	
25	731	0.04	1.35	50.0	2710	HMRK (SLST?)	VU		HG	HE	HE overprinting HG
26	750	0.06	0.81	58.0	5780	HMBX	FB	UR	SR	HR	
27	758	0.05	0.12	66.0	9720	HMBX	UA	AC/UA	HG	SF	cut by >Vcb
28	789	1.63	0.93	230.0	1780	HMBX (SLST?)	UR		HE	SR	Visual Cc in matrix
29	793	0.05	2.05	43.0	1990	HMRK (SLST?)			HG	HE	
30	830	0.01	4.15	19.0	500	HMRK (SLST?)	VU	AC/UA	HE		clast supported crackle BX
31	972	0.48	0.02	20.0	430	UNBX	AC		HE	HD	SF patchy alteration -Visual Bn in HE matrix
32	987	0.60	0.14	42.0	560	DACT			HE	HG	Visual Bn
33	950	0.40	0.09	58.0	760	SLST / DACT			HE		HE altered siltstone? And HE stained DACT.
34	959	1.05	0.14	66.0	730	DACT	FB	UR	HE		
PH07D339: 554950E, 6712480N											
35	780	0.01	26.60	12.0	1060	HMBX	UA	PM	HG	SF	pervassively replaced and cross cut by >Vcb
36	832	0.16	0.43	350.0	3390	BX			HE	SF	HE replaced moderately sorted BX?
37	835	0.84	1.48	78.0	2390	BX	UR		HE		
	320	8.82	0.08	64.0	18						
PH11D555: 554500E, 6712460N											
38	320	8.2	0.08	64.0	18	DOLM	VU		CH		Vis. Py, Cp, minor Bn
PH10D541: 554600E, 6712430N											
39	322	8.5	0.19	33.0	245	HMRK			HD		Vis. Bn and Cc
PH11D576:554499E, 6712523N											
40	508	21.2	0.07	8.0	34	DOLM	VU		HE		Vis. Cc massive veins (~10%)
PH11D567: 555119E, 6712606N											
41	992	1190	49	345	530	HMBX	UR				Vis. Au in micro fractures

Table 3: Sample descriptions - mineral associations, analytical methodology

	MINERAL ASSOCIATION						ANALYTICAL METHODS				
Sam. ID	**Ore**			**Gangue/Alteration**			**Optical**	**SEM**	**EPMA**		**LA-ICP-MS**
	Oxides	Sulphides	Others	Major	Minor	Others			Gangue	Ore	
PH10D550											
1TW	Hm						x				
2aTW	Hm	Cp > Bn2 > Cc2	Clau, Cass, Coff	Qz > Ser	Chl	P-REE	x	x			
2bTW	Hm	Cp		Qz > Ser			x				
3aTW	Hm	Cc3 > Bn3	AuCu	Qz > Ser (II)		Al-P-REE	x	x	x	x	
3bTW	Hm		Au9Cu, Au3Cu	Qz > Ser (II)	Phl (?)	Al-P-REE	x	x	x	x	x
4TW	Hm	Bn		Qz > Ser			x	x			
PH10D551											
5TW	Hm			Ser (I) > Qz		Ru; Ap	x	x	x		
6TW	Hm	Bn2 >> Cc2	Cau, Cof, Dom	Qz > Ser	Ch,	Ap	x	x		x	x
7TW	Hm	Cp >> Bn	Alt	Qz > Ser	Ca, Chl	P-REE	x	x	x	x	
8TW	Hm	Bn > Cp, Cc1		Qz > Ser		Ru; REE	x	x		x	x
9TW	Hm	Cp > Bn		Qz > Ser			x				
10TW	Hm, Il	Bn2, Cc2 > Cp	Clau	Ser (II) >> Qz	Qz	Al-P-REE, F-REE	x	x	x		
11TW	Hm	Bn2, Cc2 > Cp	Clau, coff	Qz > Ser			x	x			
12TW	Hm	Cp		Qz > Ser	Sr	Ru;	x	x			
PH10D554											
13TW	Hm, Il			Qz			x		x		
14TW	Hm	Cp	Au	Qz	Chl, Sr	Al-P-REE	x	x	x		
15TW	Hm	Bn2 > Cc2	Clau, Lo, Saf, Coff	Qz		Xtm	x	x		x	x
16TW	Hm	Cp		Qz			x				
17TW	Hm	Cc1		Ser (II) > Qz			x	x		x	x
18TW	Hm	Cc1, Cc2, Bn,	Cas	Ser (II) > Qz		P-REE	x	x	x		
19TW	Hm	Cc1, Cc2	Cas	Ser (II) > Qz		F-REE, P-REE, Cu-Si	x	x	x		
20TW	Hm	Cc2		Ser (II) > Qz		F-REE, P-REE	x	x			
21TW	Hm	Cc2					x			x	
22TW	Hm	Cc2 >> Cc1, Bn					x				x
23TW		Cc2 >> Cc1, Bn					x				
PH10D549											
24TW	Hm, il	Cp					x				
25TW	Hm. Il	Cp		Qz, Cal		REE's F-Ap, Ap	x	x			
26TW	Hm. Il	Cc2, Cc1	Dom; Au-Cu, Cu	Qz, Cal	Chl	Al-P-REE	x	x			
27TW	Hm	Cp		Qz, Cal		P-REE	x	x			
28TW	Hm	Cc2, Cc1		Qz, Sr	Chl,	F-REE, P-REE	x	x	x	x	x
29TW											
30TW	Hm. Il	Cp			Cal	F-REE; Cas;	x	x			
31TW	Hm	Bn1	Py	Qz			x	x	x	x	x
32TW	Hm	Bn1 >> Cc	Py	Qz >> Ser		P-REE; F-REE	x	x			x
33TW	Hm	Bn1	Py,	Qz >> Ser		Phl?	x	x			x
34TW	Hm	Bn1 > Cc > Cp	Py, Cas	Qz	Ser	P-REE	x	x	x		
PH07D339											
35TW	Hm			Qz, Cal	Sr, chl,	P-REE; Al-P-REE	x	x	x		
36TW	Hm, Il	Bn, Cp		Qz,	Sr	F-Ap, P-REE	x	x			
37TW	Hm	Cc2 > Cc1, Bn	Coff, F-Ap	Qz >> Ser			x	x	x		x
PH11D555											
38TW	Hm > Mgt	Py >> Cc3		Cal			x				
PH10D541											
39TW	Hm	Cc3 > Bn3 > Py > Cp					x			x	x
PH11D576											
40TW	Hm	Cc3 > Bn3		Cal			x			x	x
PH11D567											
41TW	Hm, Ru	Cp >> Bn2 > Cc2	Au, Lo, Y-Coff, Coff, Saf, Bi	Cal > Qz			x	x		x	

Table 4: Summary of electron microprobe data for Cu-(Fe)-sulphides

Sample	3aTW		3bTW		6TW		8TW (3)		15TW	41aTW		17TW		21TW		28TW	39aTW		39bTW		40TW	
	Mean (n=15)	Std.dev	Mean (n=10)	Std.dev	Mean (n=24)	Std.dev	Mean (n=6)	Std.dev		Mean (n=10)	Std.dev	Mean (n=11)	Std.dev	Mean	Std.dev		Mean (n=30)	Std.dev	Mean (n=9)	Std.dev	Mean (n=20)	Std.dev
	Grey Chalcocite Au-Cu				*Blue Chalcocite*					*Blue chalcocite Au-Cu*		*White Chalcocite*					*Grey Chalcocite*					
Cu	78.6	0.7	79.2	0.7	79.0	0.5	79.1	1.5	74.7	77.2	1.4	81.0	0.9	81.2	0.7	80.3	80.3	0.4	80.5	0.2	80.1	0.3
Ag	<mdl	-	<mdl	-	<mdl	-	0.06	0.06	<mdl	0.03	0.04	0.05	0.05	0.08	0.02	<mdl	0.04	0.04	<mdl	-	0.05	0.06
Fe	0.1	0.2	0.2	0.22	0.14	0.1	0.37	0.22	1.32	0.23	0.22	0.05	0.14	0.35	0.19	0.14	0.05	0.12	0.12	0.12	0.09	0.13
Pb	<mdl	-	<mdl	-	<mdl	-	<mdl	-	0.58	<mdl	-	<mdl	-	<mdl	-	<mdl	<mdl	-	<mdl	-	<mdl	-
Bi	<mdl	-	0.1	0.04	0.11	0.13	**0.05**	0.06	0.12	0.17	0.06	0.07	0.05	<mdl	-	<mdl	0.08	0.08	0.08	0.07	0.08	0.06
S	21.3	0.8	20.7	0.1	20.6	0.4	21.5	1.2	19.0	20.8	0.5	20.1	1.4	19.9	1.1	20.8	20.5	0.3	20.5	0.2	20.5	0.2
Te	0.4	0.3	0.4	0.18	0.06	0.04	<mdl	-	0.17	0.15	0.17	<mdl	-	<mdl	-	<mdl	<mdl	-	<mdl	-	<mdl	-
Se	0.2	0.1	0.2	0.18	0.54	0.15	0.37	0.20	3.53	0.09	0.04	<mdl	-	<mdl	-	<mdl	<mdl	-	<mdl	-	<mdl	-
Total	**100.7**	**0.8**	**100.8**	**0.7**	**100.5**	**0.6**	**101.6**	**0.4**	**99.4**	**98.9**	**0.6**	**101.3**	**1.0**	**101.6**	**0.2**	**101.3**	**101.0**	**0.4**	**101.4**	**0.2**	**101.0**	**0.3**
Formula calculated to 3 a.p.f.u																						
Cu	1.9	0.0	2.0	0.0	2.0	0.0	1.9	0.1	1.9	1.9	0.0	2.0	0.1	2.0	0.0	2.0	2.0	0.0	2.0	0.0	2.0	0.0
Ag	0.00	0.00	0.00	0.00	0.00	0.00	0.00	0.00	0.00	0.00	0.00	0.00	0.00	0.00	0.00	0.00	0.00	0.00	0.00	0.00	0.00	0.00
Fe	0.00	0.00	0.00	0.00	0.00	0.00	0.00	0.00	0.00	0.00	0.00	0.00	0.00	0.00	0.00	0.00	0.00	0.00	0.00	0.00	0.00	0.00
Pb	0.00	0.00	0.00	0.01	0.00	0.00	0.01	0.01	0.04	0.01	0.01	0.00	0.00	0.01	0.01	0.00	0.00	0.00	0.00	0.00	0.00	0.00
Bi	0.00	0.00	0.00	0.00	0.00	0.00	0.00	0.00	0.00	0.00	0.00	0.00	0.00	0.00	0.00	0.00	0.00	0.00	0.00	0.00	0.00	0.00
Total M	**1.9**	**0.0**	**2.0**	**0.01**	**1.97**	**0.0**	**1.95**	**0.05**	**1.96**	**1.95**	**0.03**	**2.01**	**0.05**	**2.02**	**0.04**	**1.98**	**1.99**	**0.01**	**1.99**	**0.01**	**1.99**	**0.01**
S	1.0	0.0	1.0	0.0	1.0	0.0	1.0	0.0	1.0	1.0	0.0	1.0	0.1	1.0	0.0	1.0	1.0	0.0	1.0	0.0	1.0	0.0
Te	0.00	0.00	0.00	0.00	0.00	0.00	0.00	0.00	0.00	0.00	0.00	0.00	0.00	0.00	0.00	0.00	0.00	0.00	0.00	0.00	0.00	0.00
Se	0.00	0.00	0.00	0.00	0.01	0.00	0.01	0.00	0.07	0.00	0.00	0.00	0.00	0.00	0.00	0.00	0.00	0.00	0.00	0.00	0.00	0.00
S(+Te+Se)	**1.1**	**0.0**	**1.0**	**0.01**	**1.03**	**0.01**	**1.05**	**0.05**	**1.04**	**1.04**	**0.02**	**0.99**	**0.05**	**0.98**	**0.04**	**1.02**	**1.01**	**0.01**	**1.01**	**0.01**	**1.01**	**0.01**
Total	3.0	0.0	3.0	0.00	3.00	0.00	3.00	0.00	3.00	3.00	0.01	3.00	0.00	3.00	0.00	3.00	3.00	0.00	3.00	0.00	3.00	0.00
M/S	**1.9**	**0.1**	**1.9**	**0.0**	**1.9**	**0.0**	**1.9**	**0.1**	**1.9**	**1.9**	**0.1**	**2.0**	**0.2**	**2.1**	**0.1**	**1.9**	**2.0**	**0.0**	**2.0**	**0.0**	**2.0**	**0.0**
Cu/Fe	**N/A**	**N/A**	**N/A**	**N/A**	**N/A**	**N/A**	**N/A**	**N/A**	**N/A**	**N/A**	**N/A**	**N/A**	**N/A**	**N/A**	**N/A**	**N/A**	**N/A**	**N/A**	**N/A**	**N/A**	**N/A**	**N/A**

Sample	3aTW	3bTW		6TW		7TW		8TW		15TW		31TW		32TW		34TW	39bTW		39bTW		41aTW		41bTW
	Mean (n=1)	Mean (n=2)	Std.dev	Mean (n=15)	Std.dev	Mean (n=2)	Std.dev	Mean (n=7)	Std.dev	Mean (n=2)	Std.dev	Mean (n=26)	Std.dev	Mean (n=22)	Std.dev	Mean (n=39)	Std.dev	Mean (n=8)	Std.dev	Mean (n=8)	Std.dev	Mean (n=5)	Std.dev	
	Red bornite Au-Cu			*Purple Bornite*								*Brown Bornite*						*Red Bornite*					
Cu	63.1	64.2	0.1	59.7	2.6	63.1	0.3	63.1	1.6	65.2	4.1	64.0	0.4	63.4	0.5	63.5	0.5	63.6	0.1	63.9	0.2	64.7	2.0	62.9
Ag	<mdl	-	0.0	0.0	0.0	<mdl	-	<mdl	-	<mdl	-	<mdl	-	<mdl	-	<mdl	-	<mdl	-	0.06	0.1	<mdl	-	0.1
Fe	11.8	10.7	0.2	11.0	1.2	11.6	0.3	11.2	0.9	7.3	2.9	11.2	0.2	11.3	0.1	11.2	0.1	10.9	0.1	10.5	0.1	8.9	1.6	10.7
Pb	0.0	-	0.0	0.89	1.25	0.2	0.06	<mdl	-	0.78	0.69	<mdl	-	<mdl	-	<mdl	-	<mdl	-	<mdl	-	0.50	0.5	0.1
Bi	<mdl	-	0.0	<mdl	-	<mdl	-	<mdl	-	0.17	0.02	0.10	0.07	<mdl	-	0.07	0.05	0.10	0.08	<mdl	-	<mdl	-	0.3
S	25.9	25.9	0.2	26.4	1.4	26.4	0.2	26.2	0.8	21.5	1.4	26.3	0.4	26.7	0.4	26.6	0.3	25.5	0.1	25.5	0.2	24.4	0.7	26.4
Te	<mdl	-	0.0	0.1	0.1	0.1	0.0	<mdl	-	0.1	0.02	<mdl	-	<mdl	-	<mdl	-	<mdl	-	<mdl	-	0.53	0.4	0.0
Se	<mdl	-	0.0	0.80	0.44	0.08	0.02	0.50	0.21	3.68	0.50	<mdl	-	<mdl	-	<mdl	-	<mdl	-	<mdl	-	0.15	0.1	0.0
Total	**100.8**	**101.0**	**0.2**	**98.9**	**0.5**	**101.4**	**0.1**	**101.2**	**0.7**	**98.8**	**0.1**	**101.7**	**0.3**	**101.6**	**0.5**	**101.5**	**0.4**	**100.2**	**0.1**	**100.1**	**0.3**	**99.2**	**0.4**	**100.5**
Formula calculated to 10 a.p.f.u																								
Cu	4.9	5.0	0.0	4.7	0.2	4.9	0.0	4.9	0.2	5.4	0.4	5.0	0.1	4.9	0.0	4.9	0.0	5.0	0.0	5.0	0.0	5.2	0.2	4.9
Ag	0.00	0.00	0.00	0.00	0.00	0.00	0.00	0.00	0.00	0.00	0.00	0.00	0.00	0.00	0.00	0.00	0.00	0.00	0.00	0.00	0.00	0.00	0.00	0.00
Fe	1.0	1.0	0.0	1.0	0.1	1.0	0.0	1.0	0.1	0.7	0.3	1.0	0.0	1.0	0.0	1.0	0.0	1.0	0.0	0.9	0.0	0.8	0.1	1.0
Pb	0.00	0.00	0.00	0.04	0.06	0.00	0.00	0.00	0.00	0.04	0.03	0.00	0.00	0.00	0.00	0.00	0.00	0.00	0.00	0.00	0.00	0.02	0.03	0.00
Bi	0.00	0.00	0.00	0.00	0.00	0.00	0.00	0.00	0.00	0.00	0.00	0.00	0.00	0.00	0.00	0.00	0.00	0.00	0.00	0.00	0.00	0.00	0.00	0.01
Total M	**6.0**	**6.0**	**0.0**	**5.8**	**0.2**	**5.9**	**0.0**	**5.9**	**0.1**	**6.2**	**0.2**	**6.0**	**0.0**	**5.9**	**0.0**	**5.9**	**0.0**	**6.0**	**0.0**	**6.0**	**0.0**	**6.1**	**0.1**	**5.9**
S	4.0	4.0	0.0	4.2	0.2	4.1	0.0	4.1	0.1	3.6	0.2	4.0	0.0	4.1	0.0	4.1	0.0	4.0	0.0	4.0	0.0	3.9	0.1	4.1
Te	0.00	0.00	0.00	0.00	0.00	0.00	0.00	0.00	0.00	0.00	0.00	0.00	0.00	0.00	0.00	0.00	0.00	0.00	0.00	0.00	0.00	0.02	0.01	0.00
Se	0.00	0.00	0.00	0.05	0.03	0.00	0.00	0.03	0.01	0.25	0.03	0.00	0.00	0.00	0.00	0.00	0.00	0.00	0.00	0.00	0.00	0.01	0.01	0.00
S(+Te+Se)	**4.0**	**4.0**	**0.0**	**4.2**	**0.2**	**4.1**	**0.0**	**4.1**	**0.1**	**3.8**	**0.2**	**4.0**	**0.0**	**4.1**	**0.0**	**4.1**	**0.0**	**4.0**	**0.0**	**4.0**	**0.0**	**3.9**	**0.1**	**4.1**
Total	10.0	10.0	0.0	10.0	0.0	10.0	0.0	10.0	0.0	10.0	0.0	10.0	0.0	10.0	0.0	10.0	0.0	10.0	0.0	10.0	0.0	10.0	0.0	10.0
M/S	**1.5**	**1.5**	**0.0**	**1.4**	**0.1**	**1.5**	**0.0**	**1.4**	**0.1**	**1.6**	**0.1**	**1.5**	**0.0**	**1.4**	**0.0**	**1.4**	**0.0**	**1.5**	**0.0**	**1.5**	**0.0**	**1.5**	**0.0**	**1.4**
Cu/Fe	**4.7**	**5.3**	**0.1**	**4.9**	**0.8**	**4.8**	**0.2**	**5.0**	**0.5**	**8.5**	**3.8**	**5.0**	**0.1**	**4.9**	**0.1**	**5.0**	**0.1**	**5.1**	**0.1**	**5.4**	**0.1**	**6.6**	**1.4**	**5.2**

Table 5: Summary of electron microprobe data for gold phases

drill core PH10D550	3TW					
	Mean (20)	Std.dev	Mean (24)	Std.dev	Mean (33)	Std.dev
	Au9Cu		*Au3Cu*		*AuCu*	
S	0.02	0.02	0.01	0.02	0.02	0.05
Fe	0.02	0.02	0.02	0.03	0.01	0.02
Cu	3.79	0.89	10.13	0.64	24.45	0.36
Ag	0.07	0.04	0.03	0.03	0.02	0.03
Au	96.87	1.01	90.22	0.81	75.49	0.40
Hg	0.00	0.00	0.00	0.00	0.00	0.00
Total	100.76	0.49	100.41	0.49	100.00	0.49
Formulae, calculated to:	**10 a.p.f.u**		**4 a.p.f.u**		**2 a.p.f.u**	
Au	8.90	0.23	4.83	2.27	4.98	0.04
Cu	1.07	0.23	1.66	0.75	5.00	0.04
Ag	0.06	0.04	0.02	0.03	0.00	0.00
Au:Cu	8.58	1.45	2.89	0.20	1.00	0.02

drill core PH10D567	41aTW		41bTW	
	Mean (15)	Std.dev	Mean (31)	Std.dev
	Native Gold			
	0.52	1.02	0.40	0.27
S	0.53	1.21	0.35	0.30
Fe	0.78	1.13	0.65	0.22
Cu	0.73	0.14	0.78	0.16
Ag	97.19	3.49	96.99	1.05
Au	0.00	0.00	0.00	0.00
Hg	0.02	0.04	0.04	0.08
Total	99.8	0.8	99.2	0.8
Formulae, calculated to 1 a.p.f.u				
Au	0.93	0.10	0.93	0.03
Cu	0.02	0.02	0.02	0.01
Fe	0.02	0.03	0.01	0.01
S	0.03	0.05	0.02	0.02
Ag	0.01	0.00	0.01	0.00
Bi	0.00	0.00	0.00	0.00
Total	**1.00**	**0.20**	**1.00**	**0.06**

Table 6: Summary of electron microprobe data for arsenide phases

Label	41aTW		41bTW		41dTW		41aTW		41bTW		41dTW	
	Mean (7)	Std.dev	Mean (2)	Std.dev	Mean (13)	Std.dev	Mean (2)	Std.dev	Mean (3)	Std.dev	Mean (5)	Std.dev
	Co-Safflorite						*Loellingite*					
Cu	0.54	0.83	0.09	0.00	0.38	0.37	1.46	0.72	1.08	0.54	0.76	0.51
Ag	0.02	0.02	0.02	0.02	0.01	0.02	0.06	0.04	0.02	0.03	0.02	0.02
Fe	1.82	1.27	1.37	1.05	2.64	3.24	25.35	0.97	25.42	0.26	25.10	0.51
Pb	0.04	0.07	0.07	0.06	0.03	0.05	0.02	0.03	0.02	0.04	0.07	0.07
Bi	0.17	0.15	0.02	0.03	0.20	0.27	1.28	1.28	0.01	0.01	0.01	0.03
S	0.57	0.82	0.41	0.42	0.25	0.16	0.47	0.42	0.08	0.08	0.19	0.30
Te	0.03	0.04	0.00	0.00	0.00	0.01	0.04	0.01	0.02	0.03	0.01	0.01
Se	0.55	0.11	0.60	0.07	0.54	0.08	0.55	0.05	0.56	0.12	0.57	0.03
Co	24.55	1.86	25.95	2.06	24.37	3.58	0.36	0.09	0.37	0.07	1.05	0.71
Ni	1.79	2.16	0.72	0.61	0.88	1.04	0.07	0.03	0.01	0.01	0.07	0.05
As	69.77	1.47	71.07	1.24	70.27	0.60	69.95	1.87	71.38	0.70	71.33	0.56
Total	**99.9**	**1.0**	**100.3**	**0.5**	**99.6**	**0.5**	**99.6**	**0.6**	**99.0**	**0.3**	**99.2**	**0.2**
Formulae, calculated to 3 a.p.f.u												
Fe	0.07	0.05	0.05	0.04	0.10	0.12	0.94	0.03	0.95	0.01	0.93	0.02
Co	0.86	0.07	0.91	0.07	0.86	0.13	0.01	0.00	0.01	0.00	0.04	0.03
Ni	0.06	0.08	0.03	0.02	0.03	0.04	0.00	0.00	0.00	0.00	0.00	0.00
Cu	0.02	0.03	0.00	0.00	0.01	0.01	0.05	0.02	0.04	0.02	0.02	0.02
Ag	0.00	0.00	0.00	0.00	0.00	0.00	0.00	0.00	0.00	0.00	0.00	0.00
Bi	0.00	0.00	0.00	0.00	0.00	0.00	0.01	0.01	0.00	0.00	0.00	0.00
Pb	0.00	0.00	0.00	0.00	0.00	0.00	0.00	0.00	0.00	0.00	0.00	0.00
Total Metals	**1.02**	**0.02**	**0.99**	**0.01**	**1.01**	**0.01**	**1.02**	**0.01**	**1.00**	**0.02**	**1.00**	**0.01**
As	**1.93**	**0.06**	**1.96**	**0.04**	**1.96**	**0.02**	**1.94**	**0.03**	**1.98**	**0.02**	**1.97**	**0.02**
S	0.04	0.05	0.03	0.03	0.02	0.01	0.03	0.03	0.01	0.01	0.01	0.02
Se	0.01	0.00	0.02	0.00	0.01	0.00	0.01	0.00	0.01	0.00	0.01	0.00
Te	0.00	0.00	0.00	0.00	0.00	0.00	0.00	0.00	0.00	0.00	0.00	0.00
S+Se	0.05	0.05	0.04	0.02	0.03	0.01	0.04	0.03	0.02	0.00	0.03	0.02

Table 7: Summary of electron microprobe data for REE phases

	31TW Mean (2)	Std.dev
	Monazite	
CaO	1.20	0.22
Y2O3	0.08	0.07
La2O3	19.1	2.4
Ce2O3	28.6	3.0
Nd2O3	7.22	0.31
Pr2O3	2.59	0.25
Sm2O3	0.49	0.00
Gd2O3	0.25	0.08
Tb2O3	0.00	0.00
Dy2O3	0.04	0.05
Ho2O3	0.04	0.00
Er2O3	0.04	0.05
Yb2O3		
Lu2O3	0.00	0.00
Sc2O3	0.00	0.00
ZrO2	0.00	0.00
Nb2O5	0.00	0.00
Na2O	0.00	0.00
K2O	0.51	0.61
ThO2	0.29	0.30
UO2	0.18	0.14
SrO		
FeO	4.77	4.17
TiO2	0.00	0.00
MgO	0.23	0.32
SiO2	3.27	4.30
MnO		
Cr2O3		
Al2O3	1.79	2.52
P2O5	24.0	0.5
As2O5		
V2O5		
F (wt.%)	1.56	1.19
Cl (wt.%)	0.04	0.03
Total	96.2	5.2
True total	94.9	6.3
Monazite (LREE…..)PO4		
Ca	0.05	0.02
Y	0.00	0.00
La	0.29	0.08
Ce	0.43	0.11
Nd	0.11	0.02
Pr	0.04	0.01
Sm	0.01	0.00
Gd	0.00	0.00
Tb	0.00	0.00
Dy	0.00	0.00
Ho	0.00	0.00
Er	0.00	0.00
Yb	0.00	0.00
Lu	0.00	0.00
Sc	0.00	0.00
Zr	0.00	0.00
Nb	0.00	0.00
Mg	0.01	0.02
Fe	0.15	0.12
Mn	0.00	0.00
Na	0.00	0.00
K	0.01	0.01
Th	0.00	0.00
U	0.00	0.00
Sr	0.00	0.00
Total	1.12	0.09
P	0.83	0.11
Si	0.12	0.16
Total	0.95	0.05
F	0.21	0.18
Cl	0.00	0.00
Total	0.22	0.19
mol.% Monazite-(La)	25.9	5.1
mol.% Monazite-(Ce)	38.4	6.7
mol.% Monazite-(Nd)	9.5	1.1
mol.% Monazite-(Sm)	0.62	0.04

	15TW Mean(7)	std.dev
	Xenotime	
CaO	0.21	0.05
Y2O3	37.48	3.79
La2O3	0.00	0.01
Ce2O3	0.05	0.03
Nd2O3	0.10	0.06
Pr2O3	0.01	0.02
Sm2O3	0.36	0.17
Gd2O3	8.19	2.82
Tb2O3	0.00	0.00
Dy2O3	7.72	0.84
Ho2O3	0.18	0.13
Er2O3	3.52	0.51
Yb2O3	2.27	0.51
Lu2O3	0.43	0.06
Sc2O3		
ZrO2		
Nb2O5		
Na2O		
K2O		
ThO2	0.15	0.10
UO2	0.40	0.39
SrO		
FeO		
TiO2		
MgO		
SiO2	1.04	0.56
MnO		
Cr2O3		
Al2O3	0.15	0.35
P2O5	28.91	1.04
As2O5		
V2O5		
F (wt.%)	0.98	0.49
Cl (wt.%)	0.01	0.01
Total	93.69	1.09
True total	92.86	1.30
Xenotime (Y,HREE…..)PO4		
Ca	0.01	0.00
Y	0.75	0.08
La	0.00	0.00
Ce	0.00	0.00
Nd	0.00	0.00
Pr	0.00	0.00
Sm	0.00	0.00
Gd	0.10	0.04
Tb	0.00	0.00
Dy	0.09	0.01
Ho	0.00	0.00
Er	0.04	0.01
Yb	0.02	0.01
Lu	0.00	0.00
Sc	0.00	0.00
Zr	0.00	0.00
Nb	0.00	0.00
Mg	0.00	0.00
Fe	0.08	0.11
Mn	0.00	0.00
Na	0.00	0.00
K	0.00	0.00
Th	0.00	0.00
U	0.00	0.00
Sr	0.00	0.00
Total	1.11	0.08
P	0.92	0.02
Si	0.04	0.02
Total	0.96	0.03
F	0.12	0.06
Cl	0.00	0.00
Total	0.12	0.06
mol.% Xenotime-(Y)	68.01	8.43
mol.% 'Xenotime-(Gd)'	9.24	3.09
mol.% 'Xenotime-(Dy)'	8.48	1.07
mol.% Xenotime-(Yb)	1.44	1.42
mol% pretulite	0.11	0.14

	15TW Mean (4)	std.dev
	Florencite	
CaO	0.34	0.03
Y2O3	0.02	0.01
La2O3	7.14	0.47
Ce2O3	12.47	1.14
Nd2O3	3.09	0.65
Pr2O3	1.19	0.19
Sm2O3	0.17	0.10
Gd2O3	0.01	0.01
Tb2O3	0.00	0.00
Dy2O3	0.00	0.00
Ho2O3	0.03	0.06
Er2O3	0.02	0.02
Yb2O3		
Lu2O3	0.01	0.01
Sc2O3	0.00	0.00
ZrO2	0.00	0.00
Nb2O5	0.01	0.01
Na2O	0.02	0.02
K2O	0.04	0.04
ThO2	0.07	0.06
UO2	0.03	0.06
PbO	0.02	0.02
SrO		
FeO	5.50	6.31
TiO2	0.01	0.02
MgO	0.05	0.01
SiO2	0.38	0.13
MnO		
Cr2O3		
Al2O3	28.52	1.93
P2O5	25.91	2.58
As2O5		
V2O5		
F (wt.%)	0.51	0.04
Cl (wt.%)	0.03	0.00
Total	**85.59**	**0.99**
True total	**85.14**	**1.00**
Florencite (LREE…..)Al3(PO4)2(OH)6		
Ca	0.03	0.00
Y	0.00	0.00
La	0.23	0.01
Ce	0.40	0.03
Nd	0.10	0.02
Pr	0.04	0.01
Sm	0.00	0.00
Gd	0.00	0.00
Tb	0.00	0.00
Dy	0.00	0.00
Ho	0.00	0.00
Er	0.00	0.00
Yb	0.00	0.00
Lu	0.00	0.00
Sc	0.00	0.00
Zr	0.00	0.00
Nb	0.00	0.00
Mg	0.01	0.00
Fe	0.42	0.50
Mn	0.00	0.00
Na	0.00	0.00
K	0.00	0.00
Th	0.00	0.00
U	0.00	0.00
Pb	0.00	0.00
Sr	0.00	0.00
Total	**1.24**	**0.47**
Al	**2.97**	**0.10**
P	1.94	0.13
Si	0.03	0.01
Total	**1.97**	**0.13**
F	0.14	0.01
Cl	0.00	0.00
OH (by difference)	5.85	0.01
Total	**6.00**	**0.00**
mol.% Florencite-(La)	20.42	6.30
mol.% Florencite-(Ce)	35.37	10.59
mol.% Florencite-(Nd)	8.63	3.21

Table 8: Summary of electron microprobe data for mica

	51TW		7TW		35TW		28TW	13TW				15TW		13TW			
(Wt.%)	Mean (7)	Std.dev	Mean (7)	Std.dev	Mean (6)	Std.dev		Mean (6)	Std.dev	**Mean (30)**	**std.dev**	Mean (3)	Std.dev	Mean (37)	Std.dev	**Mean (40)**	**std.dev**
	Depth from700 to 820 m											*Depth from 800 to 840 m*					
CaO	<mdl	-	<mdl	-	<mdl	-	<mdl	<mdl	-	**<mdl**	**<mdl**	<mdl	<mdl	<mdl	<mdl	**<mdl**	**<mdl**
Na2O	<mdl	-	<mdl	-	<mdl	-	<mdl	<mdl	-	**<mdl**	**<mdl**	<mdl	<mdl	<mdl	<mdl	**<mdl**	**<mdl**
K2O	10.0	0.3	10.7	0.3	10.4	0.3	10.9	9.6	0.8	**10.2**	**0.6**	9.7	0.9	10.1	2.0	**10.1**	**1.4**
FeO	3.10	0.50	3.85	0.40	3.15	0.36	4.61	3.57	0.65	**3.47**	**0.59**	4.37	1.99	3.98	0.93	**4.01**	**0.90**
TiO2	0.33	<mdl	<mdl	-	<mdl	-	<mdl	<mdl	-	**<mdl**	**<mdl**	<mdl	<mdl	<mdl	<mdl	**<mdl**	**<mdl**
MgO	2.84	0.48	1.30	0.11	2.51	0.20	1.25	1.38	0.09	**1.98**	**0.75**	1.83	0.81	1.79	0.37	**1.79**	**0.35**
SiO2	48.1	1.9	47.7	1.1	49.6	0.9	47.3	45.5	1.9	**47.7**	**2.0**	49.1	4.6	49.6	9.4	**49.6**	**6.6**
MnO	<mdl	-	<mdl	-	<mdl	-	<mdl	<mdl	-	**<mdl**	**<mdl**	<mdl	<mdl	<mdl	<mdl	**<mdl**	**<mdl**
Cr2O3	0.02	0.01	0.01	0.02	<mdl	0.01	<mdl	0.02	0.02	**0.01**	**0.01**	0.02	0.01	0.01	0.01	**0.01**	**0.01**
Al2O3	30.3	2.6	30.1	0.9	28.7	0.4	29.9	29.8	1.7	**29.8**	**1.7**	28.7	1.4	27.9	5.6	**28.0**	**3.9**
F (wt.%)	0.89	0.14	0.90	0.19	1.36	0.14	0.82	0.78	0.23	**0.97**	**0.27**	0.95	0.14	1.22	0.29	**1.20**	**0.24**
Cl (wt.%)	0.26	0.10	<mdl	-	0.05	0.03	0.02	0.16	0.05	**0.12**	**0.12**	<mdl	-	0.09	0.11	**0.09**	**0.11**
Total	**96.2**	**0.8**	**94.8**	**0.9**	**96.0**	**1.4**	**95.0**	**91.4**	**0.6**	**94.7**	**2.1**	**94.8**	**2.8**	**95.2**	**14.4**	**95.2**	**1.7**
Muscovite KAl2(Si3Al)O10(OH,F)2																	
Na	0.04	0.03	0.01	0.01	0.02	0.01	0.01	0.03	0.01	**0.03**	**0.02**	0.01	0.00	0.02	0.01	**0.02**	**0.01**
K	0.86	0.03	0.93	0.03	0.89	0.03	0.95	0.87	0.08	**0.89**	**0.05**	0.84	0.11	0.89	0.17	**0.88**	**0.13**
Total	**0.90**	**0.06**	**0.94**	**0.03**	**0.91**	**0.03**	**0.97**	**0.90**	**0.08**	**0.92**	**0.05**	**0.85**	**0.11**	**0.91**	**0.18**	**0.90**	**0.13**
Total Al	0.3	0.1	2.4	0.1	2.3	0.0	2.4	2.5	0.1	**2.4**	**0.1**	2.3	0.2	2.2	0.4	**2.3**	**0.3**
Si	0.3	0.1	3.3	0.1	3.3	0.0	3.2	3.2	0.1	**3.3**	**0.1**	3.3	0.2	3.4	0.6	**3.4**	**0.3**
Al (iv)	0.26	0.10	0.74	0.06	0.66	0.02	0.76	0.78	0.13	**0.74**	**0.10**	0.67	0.18	0.63	0.30	**0.64**	**0.30**
Total	**0.3**	**0.1**	**4.0**	**0.0**	**4.0**	**0.0**	**4.0**	**4.0**	**0.0**	**4.0**	**0.0**	**4.0**	**0.0**	**4.0**	**0.6**	**4.0**	**0.0**
Al (vi)	0.3	0.1	1.7	0.0	1.6	0.0	1.7	1.7	0.0	**1.7**	**0.1**	1.6	0.1	1.6	0.2	**1.6**	**0.0**
Cr	0.26	0.10	0.00	0.00	0.00	0.00	0.00	0.00	0.00	**0.00**	**0.00**	0.00	0.00	0.00	0.00	**0.00**	**0.00**
Mg	0.26	0.10	0.13	0.01	0.25	0.02	0.13	0.15	0.01	**0.20**	**0.07**	0.19	0.08	0.18	0.04	**0.18**	**0.04**
Fe	0.26	0.10	0.22	0.02	0.18	0.02	0.26	0.21	0.04	**0.20**	**0.03**	0.25	0.12	0.23	0.05	**0.23**	**0.05**
Mn	0.26	0.10	0.00	0.00	0.00	0.00	0.00	0.00	0.00	**0.00**	**0.00**	0.00	0.00	0.00	0.00	**0.00**	**0.00**
Ca	0.26	0.10	0.00	0.00	0.00	0.00	0.00	0.02	0.01	**0.01**	**0.01**	0.01	0.00	0.01	0.01	**0.01**	**0.01**
Ti	0.26	0.10	0.01	0.00	0.00	0.00	0.00	0.01	0.01	**0.01**	**0.01**	0.00	0.00	0.01	0.01	**0.01**	**0.01**
Total	**0.3**	**0.1**	**2.0**	**0.0**	**2.1**	**0.0**	**2.1**	**2.1**	**0.0**	**2.1**	**0.0**	**2.1**	**0.1**	**2.0**	**0.3**	**2.0**	**0.1**
TOTAL	**0.3**	**0.1**	**7.0**	**0.0**	**96.0**	**1.4**	**7.0**	**7.0**	**0.1**	**7.0**	**0.0**	**6.9**	**0.1**	**7.0**	**1.1**	**7.0**	**0.2**
F	**0.26**	**0.10**	**0.19**	**0.04**	**96.02**	**1.38**	**0.18**	**0.17**	**0.05**	**0.21**	**0.06**	**0.20**	**0.03**	**0.26**	**0.06**	**0.26**	**0.05**
Cl	0.26	0.10	0.00	0.00	96.02	1.38	0.00	0.02	0.01	**0.01**	**0.01**	0.00	0.00	0.01	0.01	**0.01**	**0.01**
OH	0.3	0.1	1.8	0.0	96.0	1.4	1.8	1.8	0.1	**1.8**	**0.1**	1.8	0.0	1.7	0.3	**1.7**	**0.1**
Total	0.3	0.1	2.0	0.0	96.0	1.4	2.0	2.0	0.0	**2.0**	**0.0**	2.0	0.0	2.0	0.3	**2.0**	**0.0**
phengite component %	0.3	0.1	17.6	1.3	96.0	1.4	19.4	18.3	1.9	**19.9**	**2.9**	20.9	8.3	20.9	4.2	**20.9**	**3.9**
Fe/(Fe+Mg)	0.26	0.10	0.62	0.02	96.02	1.38	0.67	0.59	0.04	**0.51**	**0.12**	0.57	0.01	0.55	0.09	**0.56**	**0.04**
% F-end-member	0.26	0.10	9.69	2.02	96.02	1.38	8.9	8.68	2.63	**10.43**	**2.89**	10.17	1.46	13.18	3.21	**12.96**	**2.71**
% Cl-end-member	0.26	0.10	0.06	0.08	96.02	1.38	0.1	0.92	0.29	**0.68**	**0.66**	0.07	0.06	0.53	0.63	**0.50**	**0.64**

	37TW		18TW		19TW		33TW		34TW			2aTW		3aTW		31TW			
(Wt.%)	Mean (6)	Std.dev	Mean (4)	Std.dev	Mean (2)	Std.dev	Mean (7)	Std.dev	Mean (13)	**Mean (32)**	**std.dev**	Mean (2)	Std.dev	Mean (10)	Std.dev	Mean (8)	Std.dev	**Mean (20)**	**std.dev**
	Depth from 840 to 950 m											*Depth from 950 to 1010 m*							
CaO	<mdl	<mdl	<mdl	<mdl	<mdl	<mdl	<mdl	<mdl	<mdl	**<mdl**	**<mdl**	0.38	0.21	<mdl	-	<mdl	-	**<mdl**	**<mdl**
Na2O	<mdl	<mdl	<mdl	<mdl	<mdl	<mdl	<mdl	<mdl	<mdl	**<mdl**	**<mdl**	<mdl	<mdl	<mdl	-	<mdl	-	**<mdl**	**<mdl**
K2O	9.4	0.5	10.1	0.7	10.8	0.06	10.2	0.8	10.4	**10.2**	**0.7**	10.4	0.6	10.0	0.5	9.3	0.4	**9.8**	**0.6**
FeO	2.21	0.51	3.50	0.61	4.03	0.36	3.87	0.28	3.96	**3.56**	**0.78**	3.87	0.57	2.00	0.35	3.62	0.44	**2.83**	**0.94**
TiO2	<mdl	<mdl	<mdl	<mdl	<mdl	<mdl	<mdl	<mdl	<mdl	**<mdl**	**<mdl**	<mdl	<mdl	<mdl	-	<mdl	-	**<mdl**	**<mdl**
MgO	1.89	0.05	1.54	0.16	1.57	0.09	1.29	0.10	1.92	**1.71**	**0.29**	1.97	0.08	2.74	0.38	1.58	0.69	**2.20**	**0.75**
SiO2	51.2	2.4	47.7	3.8	49.4	1.28	47.3	1.4	48.0	**48.5**	**2.3**	47.7	0.8	53.5	2.3	49.0	1.5	**51.2**	**3.1**
MnO	<mdl	<mdl	<mdl	<mdl	<mdl	<mdl	<mdl	<mdl	<mdl	**<mdl**	**<mdl**	<mdl	<mdl	<mdl	-	<mdl	-	**<mdl**	**<mdl**
Cr2O3	<mdl	0.01	<mdl	0.01	<mdl	-	0.01	0.01	0.01	**<mdl**	**-**	<mdl	-	<mdl	-	<mdl	-	**<mdl**	**-**
Al2O3	30.0	1.4	28.2	1.7	30.4	0.71	30.8	1.0	28.1	**29.2**	**1.6**	29.5	0.9	28.6	1.5	30.9	1.8	**29.6**	**1.9**
F (wt.%)	1.17	0.05	1.23	0.11	0.91	0.08	1.41	0.16	1.06	**1.17**	**0.24**	1.02	0.18	0.76	0.22	0.82	0.14	**0.81**	**0.20**
Cl (wt.%)	0.03	0.01	0.16	0.05	<mdl	-	0.03	0.02	0.14	**0.09**	**0.15**	0.37	0.38	0.02	0.01	0.03	0.02	**0.06**	**0.14**
Total	**96.3**	**1.4**	**92.9**	**2.0**	**97.2**	2.54	**95.1**	**2.3**	**94.2**	**94.8**	**2.2**	**95.9**	**2.8**	**98.0**	**1.3**	**95.5**	**0.8**	**96.8**	**1.7**
Muscovite KAl2(Si3Al)O10(OH,F)2																			
Na	0.04	0.01	0.03	0.00	0.01	0.00	0.02	0.01	0.02	**0.02**	**0.01**	0.07	0.08	0.02	0.00	0.01	0.00	**0.02**	**0.03**
K	0.79	0.05	0.90	0.08	0.92	0.02	0.89	0.07	0.92	**0.89**	**0.07**	0.90	0.08	0.83	0.05	0.79	0.04	**0.82**	**0.06**
Total	**0.83**	**0.06**	**0.93**	**0.08**	**0.93**	0.02	**0.91**	**0.07**	**0.94**	**0.91**	**0.07**	**0.98**	**0.01**	**0.85**	**0.05**	**0.80**	**0.04**	**0.84**	**0.07**
Total Al	2.3	0.1	2.3	0.2	2.4	0.01	2.5	0.0	2.3	**2.4**	**0.1**	2.4	0.0	2.2	0.1	2.4	0.1	**2.3**	**0.2**
Si	3.4	0.1	3.3	0.2	3.3	0.00	3.2	0.0	3.3	**3.3**	**0.1**	3.3	0.0	3.5	0.1	3.3	0.1	**3.4**	**0.1**
Al (iv)	0.62	0.11	0.67	0.18	0.71	0.00	0.77	0.03	0.68	**0.69**	**0.09**	0.75	0.03	0.54	0.10	0.72	0.08	**0.63**	**0.13**
Total	**4.0**	**0.0**	**4.0**	**0.0**	**4.0**	0.00	**4.0**	**0.0**	**4.0**	**4.0**	**0.0**	**4.0**	**0.0**	**4.0**	**0.0**	**4.0**	**0.0**	**4.0**	**0.0**
Al (vi)	1.7	0.0	1.7	0.0	1.7	0.00	1.7	0.0	1.6	**1.7**	**0.1**	1.6	0.0	1.6	0.0	1.7	0.1	**1.7**	**0.1**
Cr	0.00	0.00	0.00	0.00	0.00	0.00	0.00	0.00	0.00	**0.00**	**0.00**	0.00	0.00	0.00	0.00	0.00	0.00	**0.00**	**0.00**
Mg	0.19	0.00	0.16	0.02	0.16	0.00	0.13	0.01	0.20	**0.17**	**0.03**	0.20	0.00	0.26	0.04	0.16	0.07	**0.21**	**0.07**
Fe	0.12	0.03	0.20	0.04	0.22	0.01	0.22	0.02	0.23	**0.20**	**0.05**	0.22	0.03	0.11	0.02	0.20	0.03	**0.16**	**0.05**
Mn	0.00	0.00	0.00	0.00	0.00	0.00	0.00	0.00	0.00	**0.00**	**0.00**	0.00	0.00	0.00	0.00	0.00	0.00	**0.00**	**0.00**
Ca	0.00	0.00	0.01	0.00	0.00	0.00	0.00	0.00	0.02	**0.01**	**0.01**	0.03	0.01	0.00	0.00	0.00	0.00	**0.01**	**0.01**
Ti	0.00	0.00	0.01	0.00	0.00	0.00	0.00	0.00	0.01	**0.00**	**0.00**	0.01	0.00	0.00	0.00	0.01	0.00	**0.01**	**0.00**
Total	**2.0**	**0.0**	**2.0**	**0.0**	**2.1**	0.01	**2.1**	**0.0**	**2.1**	**2.1**	**0.0**	**2.1**	**0.0**	**2.0**	**0.0**	**2.1**	**0.0**	**2.1**	**0.0**
TOTAL	**6.9**	**0.1**	**7.0**	**0.1**	**7.0**	0.01	**7.0**	**0.0**	**7.0**	**7.0**	**0.1**	**7.0**	**0.0**	**6.9**	**0.1**	**6.9**	**0.0**	**6.9**	**0.1**
F	**0.24**	**0.01**	**0.27**	**0.02**	**0.19**	0.01	**0.31**	**0.04**	**0.23**	**0.25**	**0.05**	**0.22**	**0.05**	**0.16**	**0.05**	**0.17**	**0.03**	**0.17**	**0.04**
Cl	0.00	0.00	0.02	0.01	0.00	0.00	0.00	0.00	0.02	**0.01**	**0.02**	0.04	0.04	0.00	0.00	0.00	0.00	**0.01**	**0.02**
OH	1.8	0.0	1.7	0.0	1.8	0.01	1.7	0.0	1.8	**1.7**	**0.0**	1.7	0.0	1.8	0.0	1.8	0.0	**1.8**	**0.0**
Total	2.0	0.0	2.0	0.0	2.0	0.00	2.0	0.0	2.0	**2.0**	**0.0**	2.0	0.0	2.0	0.0	2.0	0.0	**2.0**	**0.0**
phengite component %	15.5	1.3	18.7	2.3	18.6	0.78	17.2	1.0	21.9	**19.0**	**2.9**	22.0	1.8	18.7	2.1	17.7	2.9	**18.6**	**2.6**
Fe/(Fe+Mg)	0.39	0.05	0.56	0.03	0.59	0.01	0.63	0.02	0.54	**0.54**	**0.08**	0.53	0.02	0.29	0.04	0.58	0.10	**0.43**	**0.16**
% F-end-member	12.20	0.52	13.63	0.89	9.50	0.57	15.27	1.86	11.59	**12.63**	**2.65**	11.00	2.26	7.82	2.50	8.66	1.55	**8.48**	**2.24**
% Cl-end-member	0.15	0.05	0.95	0.31	0.10	0.00	0.20	0.12	0.83	**0.53**	**0.89**	2.10	2.12	0.11	0.06	0.13	0.10	**0.32**	**0.78**

Table 9: Summary of minor and trace elements in chalcocite determined by LA-ICP-MS (ppm)

Samples		Ag	As	Au	Bi	Co	Ni	Pb	Sb	Se	Sn	Te	Tl
White Chalcocite													
28TW	Mean (10)	48.9	3.88	<mdl	8.37	14.0	10.6	6.42	1.99	329	1.11	12.6	0.65
	Std.dev	10.6	0.52	<mdl	4.57	12.0	0.00	8.42	0.00	210	0.39	4.34	0.00
23TW	Mean (10)	50.7	18.1	<mdl	6.6	2.9	4.3	8.7	4.8	296.3	2.7	81.3	0.5
	Std.Dev	8.6	10.0	<mdl	4.5	4.7	0.0	8.3	4.1	31.3	1.3	13.7	0.0
17TW	Mean (11)	50.2	4.05	<mdl	2.32	1.8	2.41	8.30	0.30	225	0.95	7.0	0.06
	Std.dev	15.3	2.82	<mdl	0.55	0.68	0.46	17.8	0.08	27.0	0.95	3.86	0.02
	Mean (31)	**50.0**	**6.35**	**<mdl**	**5.67**	**3.64**	**4.43**	**7.92**	**2.44**	**282**	**1.38**	**32.8**	**0.19**
	Std.dev	**11.9**	**7.28**	**<mdl**	**4.53**	**6.48**	**3.55**	**12.6**	**3.70**	**131**	**1.22**	**35.2**	**0.25**
Blue Chalcocite													
6TW	Mean(5)	9.21	462	0.60	3.82	37.5	9.30	589	8.86	3894	3.98	330	2.56
	Std.dev	3.20	784	0.00	2.87	57.1	2.00	1122	7.83	2873	0.00	327	1.55
15TW		6.06	<mdl	<mdl	26.6	<mdl	<mdl	11.7	<mdl	33522	<mdl	1301	1.33
	Mean (6)	**8.69**	**462**	**0.60**	**7.61**	**37.5**	**9.30**	**493**	**8.86**	**8832**	**3.98**	**492**	**2.32**
	Std.dev	**3.45**	**905**	**<mdl**	**9.73**	**63.8**	**2.45**	**1146**	**11.1**	**12432**	**<mdl**	**514**	**1.65**
Grey Chalcocite													
39TW	Mean (15)	32.7	2.11	<mdl	<mdl	<mdl	<mdl	2.30	<mdl	45.9	<mdl	6.6	0.3
	Std.dev	3.25	-	<mdl	<mdl	<mdl	<mdl	1.55	<mdl	16.89	<mdl	1.45	0.08
40TW	Mean (12)	166	<mdl	<mdl	0.70	<mdl	<mdl	5.45	<mdl	57.8	<mdl	<mdl	0.34
	Std.dev	15.3	<mdl	<mdl	0.00	<mdl	<mdl	15.3	<mdl	15.3	<mdl	<mdl	15.3
	Mean (27)	**92.2**	**2.11**	<mdl	**0.70**	<mdl	<mdl	**3.74**	<mdl	**51.2**	<mdl	**6.61**	**0.29**
	Std.dev	**68.6**	**-**	**<mdl**	**-**	**<mdl**	**<mdl**	**5.14**	**<mdl**	**20.6**	**<mdl**	**1.45**	**0.09**
Grey Chalcocite + Au-Cu													
3bTW	**Mean (5)**	**1.20**	**7.22**	**1185**	**12.1**	**7.38**	**5.47**	**14.8**	**4.10**	**219.7**	**0.89**	**1131**	**0.67**
	Std.dev	**1.22**	**2.22**	**2177**	**12.9**	**4.94**	**0.11**	**8.40**	**6.13**	**199**	**0.08**	**1390**	**0.40**

Table 10: Summary of minor and trace elements in bornite determined by LA-ICP-MS (ppm)

Sample	Element	Ag	As	Au	Bi	Co	Ni	Pb	Sb	Se	Sn	Te	Tl
Purple Bornite Type A													
15TW	Mean (6)	75.6	262	16.2	766	5.53	6.45	33310	19.0	54241	1.35	2046	103
	Std.dev	30.6	196	22.0	355	4.09	0.39	36541	7.71	16905	0.18	883.4	69.1
Purple Bornite Type-B													
8TW	Mean (9)	24.8	49.7	48.9	12.4	14.1	5.9	155	3.3	1892	30.7	688	20.6
	Std.dev	28.7	70.9	70.3	7.6	12.9	4.4	47.0	2.7	663	34.7	403	12.4
6TW	Mean (14)	17.0	841	<mdl	41.5	189	22.0	2845	14.7	6775	2.96	641	21.1
	Std.dev	9.00	2479	<mdl	36.2	530	29.8	3101	41.9	3334	2.09	356	14.0
	Mean (23)	**20.6**	**486**	**53.2**	**28.5**	**110**	**14.3**	**1657**	**8.7**	**4578**	**15.1**	**650**	**20.5**
	Std.dev	**18.3**	**1843**	**50.7**	**30.9**	**395**	**22.8**	**2661**	**28.8**	**3554**	**22.2**	**355**	**12.7**
Brown Bornite													
31TW	Mean (7)	19.7	8.91	<mdl	74.2	5.37	3.56	28.9	1.05	54.4	0.79	2.38	0.24
	Std.dev	11.5	4.22	<mdl	6.82	2.17	0.45	16.9	0.67	11.9	0.26	0.85	0.15
32TW	Mean (8)	19.3	4.62	<mdl	80.19	3.30	<mdl	34.69	0.59	43.9	5.35	6.14	0.48
	Std.dev	7.82	-	<mdl	10.68	2.45	<mdl	26.85	0.09	8.72	-	0.71	0.47
33TW	Mean (5)	14.1	<mdl	<mdl	46.9	0.25	<mdl	2.18	<mdl	69.7	0.55	1.45	0.11
	Std.dev	2.84	<mdl	<mdl	2.01	<mdl	<mdl	2.21	<mdl	33.8	0.18	0.14	0.00
	Mean (20)	**18.1**	**8.29**	**<mdl**	**69.8**	**4.34**	**3.56**	**24.5**	**0.92**	**54.0**	**1.13**	**3.01**	**0.32**
	Std.dev	**8.45**	**4.18**	**<mdl**	**15.7**	**2.62**	**0.45**	**23.2**	**0.59**	**20.5**	**1.50**	**1.93**	**0.33**
Red Bornite													
40TW	Mean (2)	49.5	47.0	2.85	5.90	4.93	<mdl	121	4.78	84.2	3.33	11.4	8.84
39TW	Mean (10)	13.2	3.64	<mdl	1.97	3.18	40.9	86.2	3.11	85.3	1.27	5.92	7.56
	Std.dev	4.84	-	<mdl	0.58	3.71	54.1	114	6.44	119	-	3.14	10.4
	Mean (12)	**19.2**	**25.3**	**2.85**	**2.69**	**3.62**	**40.9**	**92.0**	**3.30**	**85.1**	**2.30**	**6.53**	**7.77**
	Std.dev	**19.7**	**30.7**	**-**	**1.74**	**3.15**	**54.1**	**114**	**6.05**	**108**	**1.46**	**3.46**	**10.0**

APPENDIX FIGURE CAPTIONS

Figure 1A: Backscatter electron and reflected light images showing textural and mineralogical aspects of native gold; (a) native bismuth forming on grain boundary of loellingite. (b) Crustation of loellingite occurring on chalcopyrite grains. (c) Inclusions of gold are present in minor chalcopyrite. (d) Y-coffinite sharing mutual boundaries with safflorite. (e) Crustation of bismuth of safflorite. (f) Gold present as an inclusion in interstitial chalcopyrite. (g) Coexisting grain of purple bornite and blue chalcocite hosted in calcite vein. (h) Loellingite with intergrowths of chalcopyrite on grain boundaries. (i) Fibrous grain of rutile encompassed by interstitial chalcopyrite. (j) Gold hosted within silicate gangue. (k) Fibrous aggregate of bismuth forming on grain boundary of chalcopyrite. (j) Complex intergrowth of Co-arsenides and chalcocite.

Figure A1

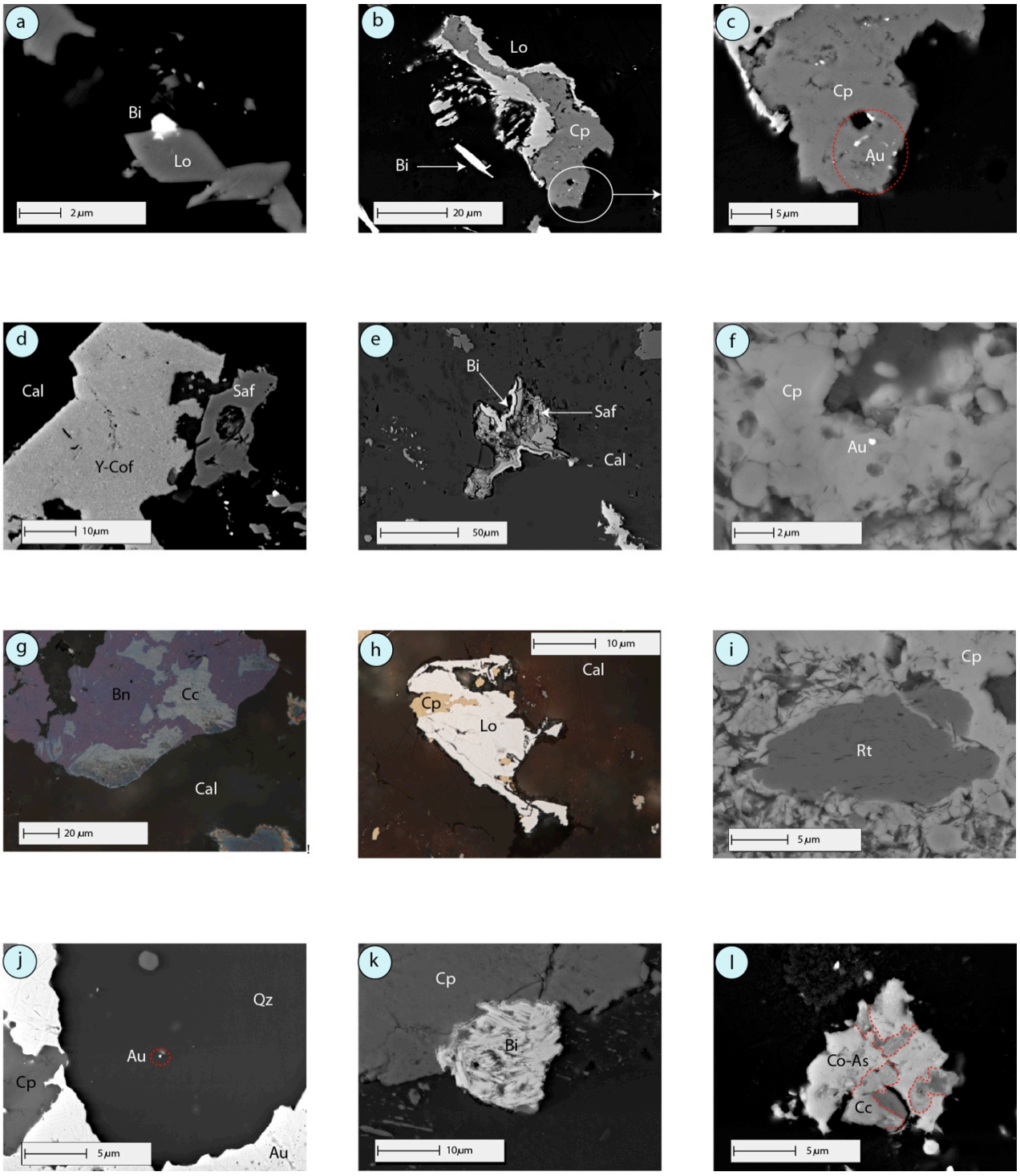
a
Bi
Lo
2 µm
b
Lo
Cp
Bi
20 µm
c
Cp
Au
5 µm
d
Cal
Saf
Y-Cof
10µm
e
Bi
Saf
Cal
50µm
f
Cp
Au
2 µm
g
Bn
Cc
Cal
20 µm
h
10 µm
Cal
Cp
Lo
i
Cp
Rt
5 µm
j
Qz
Au
Cp
5µm
Au
k
Cp
Bi
10µm
l
Co-As
Cc
5µm

Figure A2

Sample 1TW PH10D550

Sample 2TW PH10D550

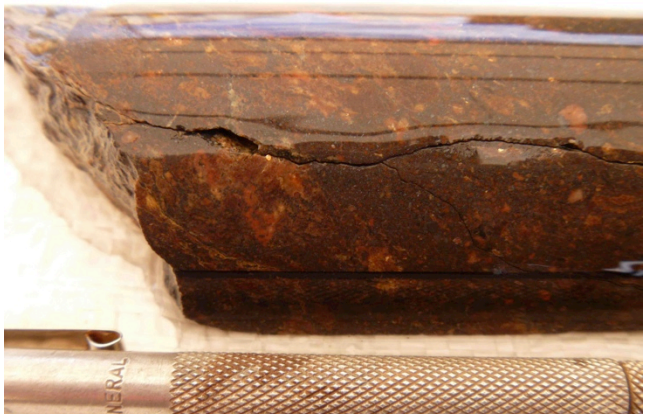

Sample 3TW PH10D550

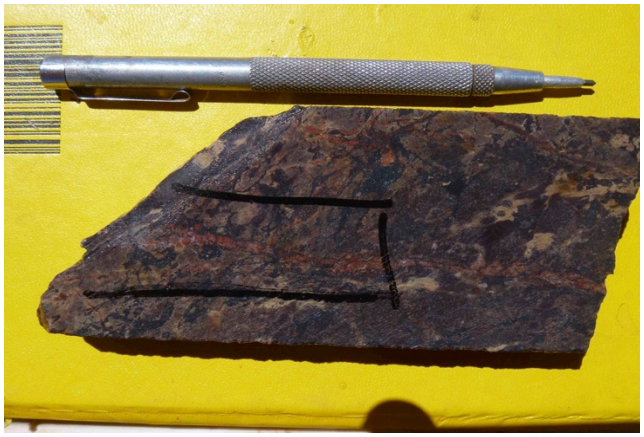

Sample 4TW PH10D550

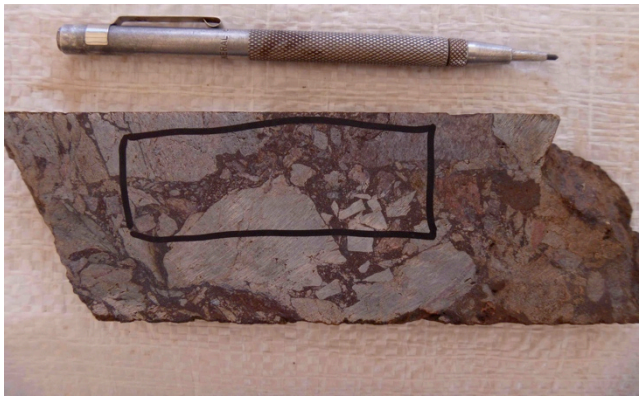

Sample 5TW PH10D551

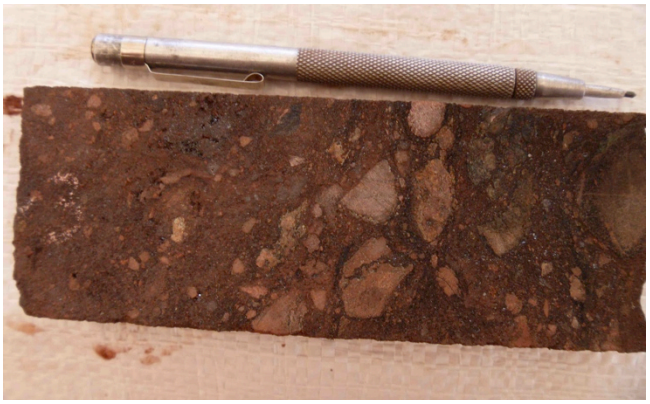

Sample 6TW PH10D551

Sample 7TW PH10D551

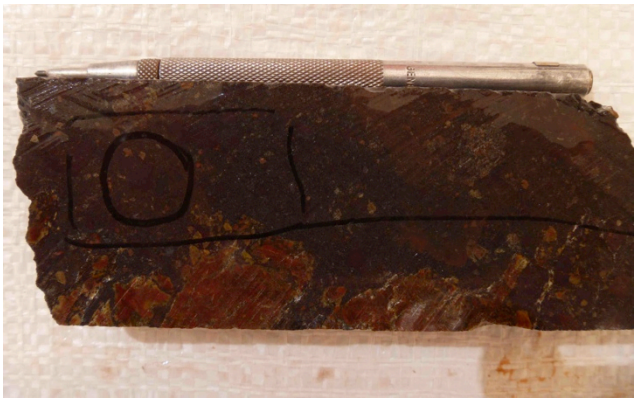

Sample 8TW PH10D551

Figure A3

Sample 9TW PH10D551

Sample 10TW PH10D551

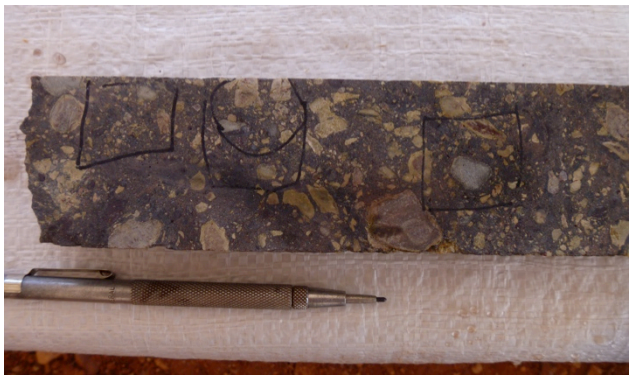

Sample 11TW PH10D551

Sample 12TW PH10D551

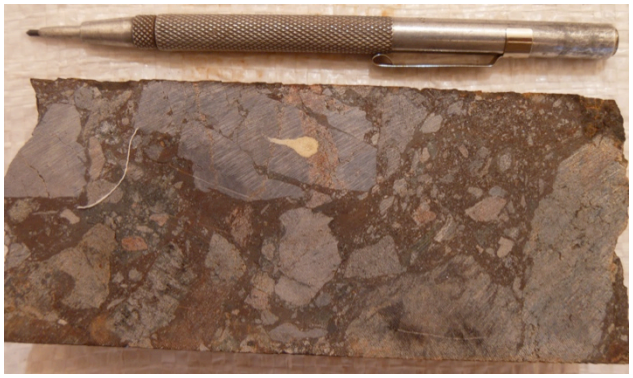

Sample 13TW PH10D554

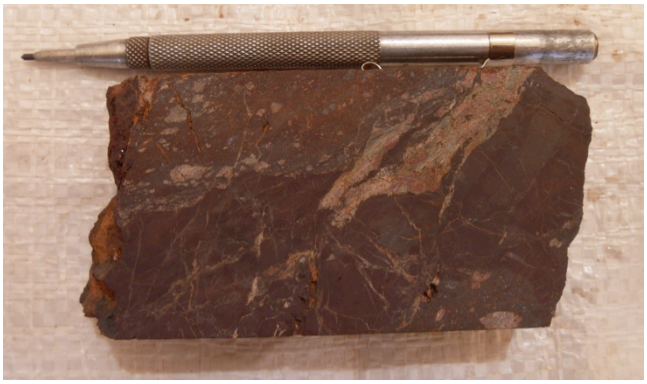

Sample 14TW PH10D554

Sample 15TW PH10D554

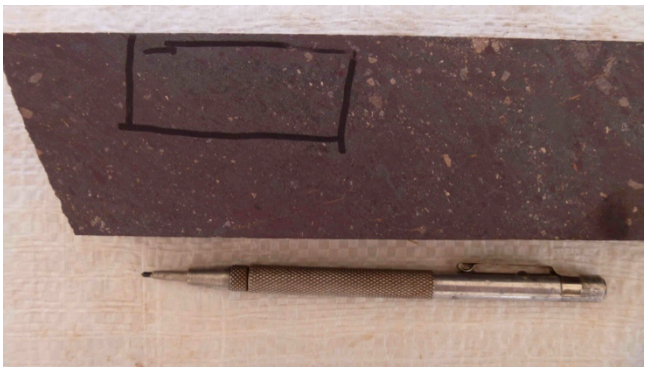

Sample 17TW PH10D554

Figure A4

Sample 18TW PH10D554

Sample 19TW PH10D554

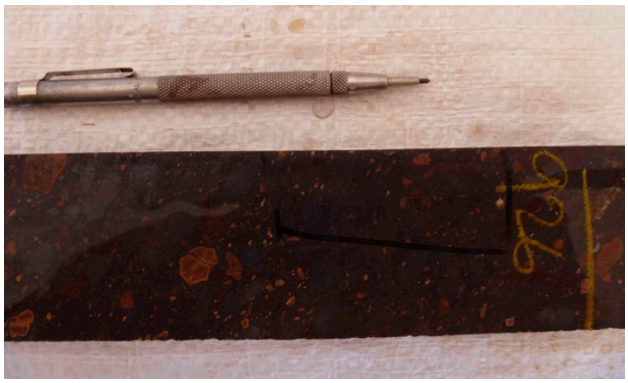

Sample 20TW PH10D554

Sample 21TW PH10D554

Sample 22TW PH10D554

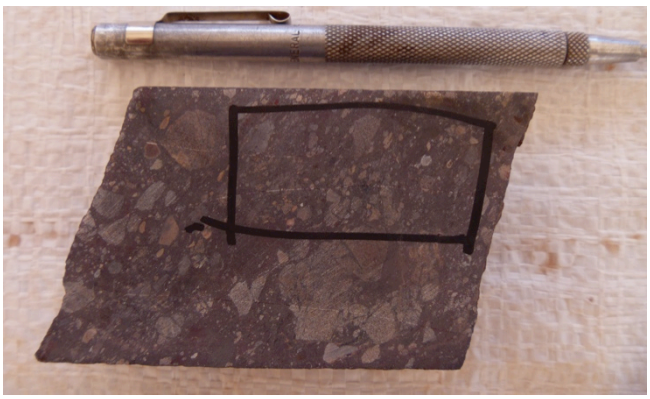

Sample 23TW PH10D554

Sample 24TW PH10D549

Sample 25TW PH10D549

Figure A5

Sample 26TW PH10D549

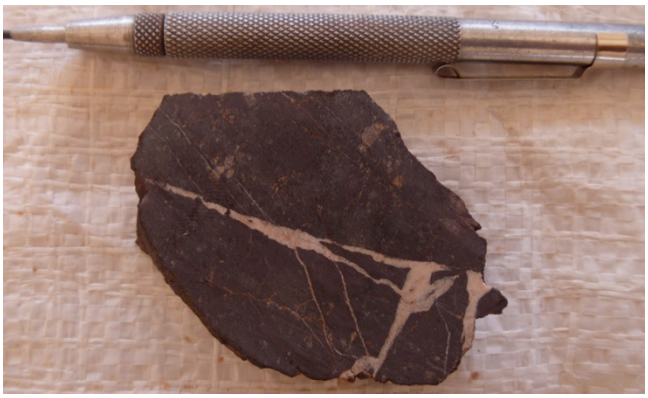

Sample 27TW PH10D549

Sample 28TW PH10D549

Sample 29TW PH10D549

Sample 30TW PH10D549

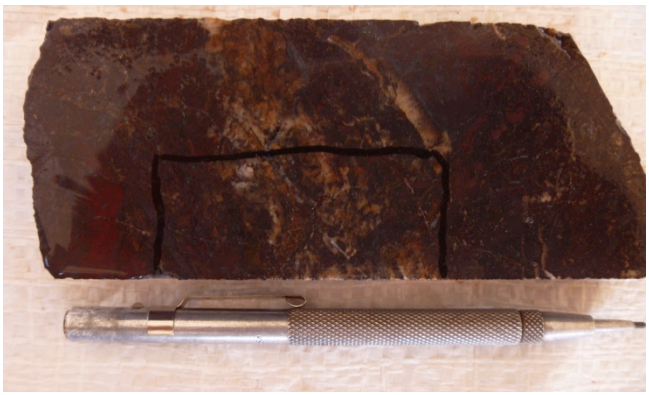

Sample 31TW PH10D549

Sample 32TW PH10D549

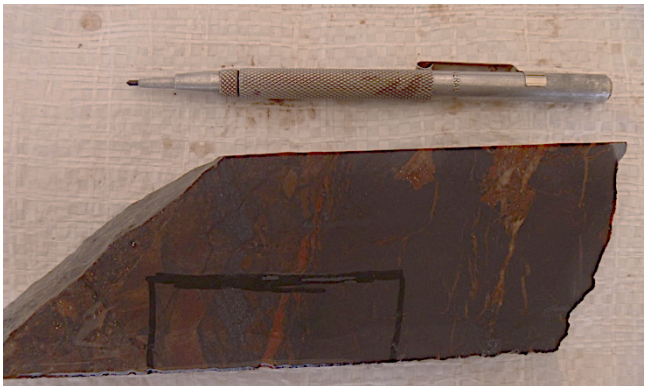

Sample 33TW PH10D549

Figure A6

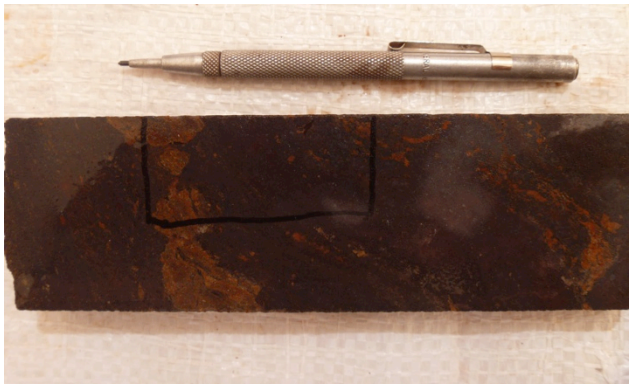

Sample 34TW PH10D549

Sample 35TW PH07D339

Sample 36TW PH07D339

Sample 37TW PH0 339

* samples images for samples 38,39,40,41 N/A

Table A1: Complete electron microanalysis data for chalcocite

Label	Cu	Ag	Fe	Pb	Bi	S	Te	Se	Total	Cu	Ag	Fe	Pb	Bi	Total M	S	Te	Se	S(+Te+Se)	Total	M/S	Cu/Fe
										Flormulae calculated 3 a.p.f.u												
PH10D550																						
3aTW	79.7	0.00	0.12	0.05	0.04	21.5	0.00	0.02	**101.4**	1.95	0.00	0.00	0.00	0.00	**1.96**	1.04	0.00	0.00	**1.04**	**3.00**	**1.87**	**N/A**
	80.1	0.00	0.70	0.03	0.04	20.9	0.45	0.03	**102.3**	1.96	0.00	0.00	0.02	0.00	**1.98**	1.01	0.01	0.00	**1.02**	**3.00**	**1.94**	**N/A**
	80.0	0.00	0.82	0.00	0.11	21.0	0.42	0.08	**102.4**	1.95	0.00	0.00	0.02	0.00	**1.98**	1.02	0.01	0.00	**1.02**	**3.00**	**1.93**	**N/A**
	79.7	0.00	0.59	0.16	0.12	20.9	0.42	0.03	**101.9**	1.96	0.00	0.00	0.02	0.00	**1.98**	1.02	0.01	0.00	**1.02**	**3.00**	**1.93**	**N/A**
	78.6	0.03	0.01	0.03	0.01	21.0	0.26	0.31	**100.3**	1.95	0.00	0.00	0.00	0.00	**1.96**	1.04	0.00	0.01	**1.04**	**3.00**	**1.87**	**N/A**
	78.7	0.06	0.03	0.04	0.00	21.2	0.18	0.31	**100.5**	1.95	0.00	0.00	0.00	0.00	**1.95**	1.04	0.00	0.01	**1.05**	**3.00**	**1.86**	**N/A**
	78.4	0.00	0.01	0.02	0.00	21.0	0.03	0.25	**99.7**	1.96	0.00	0.00	0.00	0.00	**1.96**	1.04	0.00	0.00	**1.04**	**3.00**	**1.87**	**N/A**
	77.8	0.02	0.00	0.01	0.13	20.9	0.55	0.41	**99.8**	1.95	0.00	0.00	0.00	0.00	**1.95**	1.03	0.01	0.01	**1.05**	**3.00**	**1.86**	**N/A**
	78.8	0.02	0.00	0.00	0.08	20.0	0.59	0.31	**99.8**	1.99	0.00	0.00	0.00	0.00	**1.99**	1.00	0.01	0.01	**1.01**	**3.00**	**1.97**	**N/A**
	78.1	0.02	0.00	0.04	0.02	20.7	0.61	0.40	**99.9**	1.95	0.00	0.00	0.00	0.00	**1.96**	1.03	0.01	0.01	**1.04**	**3.00**	**1.87**	**N/A**
	77.7	0.02	0.02	0.10	0.14	22.4	0.88	0.11	**101.3**	1.90	0.00	0.00	0.00	0.00	**1.90**	1.09	0.01	0.00	**1.10**	**3.00**	**1.73**	**N/A**
	78.1	0.00	0.07	0.08	0.08	23.0	0.14	0.03	**101.4**	1.89	0.00	0.00	0.00	0.00	**1.89**	1.10	0.00	0.00	**1.11**	**3.00**	**1.71**	**N/A**
	80.4	0.01	0.11	0.03	0.11	21.2	0.36	0.05	**102.3**	1.96	0.00	0.00	0.00	0.00	**1.97**	1.03	0.00	0.00	**1.03**	**3.00**	**1.90**	**N/A**
	79.5	0.00	0.09	0.00	0.10	21.4	0.50	0.08	**101.7**	1.95	0.00	0.00	0.00	0.00	**1.95**	1.04	0.01	0.00	**1.05**	**3.00**	**1.86**	**N/A**
Mean (n=15)	**79.0**	**0.0**	**0.2**	**0.0**	**0.1**	**21.2**	**0.4**	**0.2**	**101.1**	**1.9**	**0.0**	**0.0**	**0.0**	**0.0**	**2.0**	**1.0**	**0.0**	**0.0**	**1.0**	**3.0**	**1.9**	**N/A**
Std Dev	**0.9**	**0.0**	**0.3**	**0.0**	**0.0**	**0.7**	**0.2**	**0.1**	**1.0**	**0.0**	**0.0**	**0.0**	**0.0**	**0.0**	**0.0**	**0.0**	**0.0**	**0.0**	**0.0**	**0.0**	**0.1**	**N/A**
3bTW	79.0	0.04	0.01	0.00	0.10	20.8	0.26	0.00	**100.2**	1.97	0.00	0.00	0.00	0.00	**1.97**	1.03	0.00	0.00	**1.03**	**3.00**	**1.91**	**N/A**
	77.5	0.02	1.26	0.06	0.11	23.4	0.15	0.04	**102.5**	1.85	0.00	0.00	0.03	0.00	**1.89**	1.11	0.00	0.00	**1.11**	**3.00**	**1.70**	**N/A**
	77.2	0.06	1.79	0.08	0.00	23.6	0.06	0.06	**102.8**	1.84	0.00	0.00	0.05	0.00	**1.89**	1.11	0.00	0.00	**1.11**	**3.00**	**1.69**	**N/A**
	79.6	0.04	0.56	0.06	0.07	20.7	0.02	0.01	**101.1**	1.97	0.00	0.00	0.02	0.00	**1.98**	1.01	0.00	0.00	**1.02**	**3.00**	**1.96**	**N/A**
	80.8	0.01	0.09	0.11	0.03	21.2	0.03	0.00	**102.3**	1.97	0.00	0.00	0.00	0.00	**1.97**	1.03	0.00	0.00	**1.03**	**3.00**	**1.92**	**N/A**
	80.2	0.05	0.36	0.01	0.08	20.7	0.40	0.09	**101.9**	1.97	0.00	0.00	0.01	0.00	**1.99**	1.01	0.00	0.00	**1.01**	**3.00**	**1.96**	**N/A**
	79.6	0.05	0.26	0.01	0.11	20.7	0.47	0.14	**101.4**	1.97	0.00	0.00	0.01	0.00	**1.98**	1.01	0.01	0.00	**1.02**	**3.00**	**1.93**	**N/A**
	78.8	0.01	0.03	0.03	0.00	20.9	0.49	0.48	**100.7**	1.96	0.00	0.00	0.00	0.00	**1.96**	1.03	0.01	0.01	**1.04**	**3.00**	**1.87**	**N/A**
	78.3	0.00	0.00	0.05	0.07	20.7	0.51	0.28	**99.9**	1.96	0.00	0.00	0.00	0.00	**1.96**	1.03	0.01	0.01	**1.04**	**3.00**	**1.89**	**N/A**
	78.7	0.00	0.01	0.05	0.06	20.8	0.50	0.30	**100.4**	1.96	0.00	0.00	0.00	0.00	**1.96**	1.03	0.01	0.01	**1.04**	**3.00**	**1.89**	**N/A**
Mean (n=10)	**79.0**	**0.0**	**0.4**	**0.0**	**0.1**	**21.3**	**0.3**	**0.1**	**101.3**	**1.9**	**0.0**	**0.0**	**0.0**	**0.0**	**2.0**	**1.0**	**0.0**	**0.0**	**1.0**	**3.0**	**1.9**	**N/A**
Std Dev	**1.1**	**0.02**	**0.62**	**0.03**	**0.04**	**1.1**	**0.21**	**0.16**	**1.0**	**0.05**	**0.00**	**0.00**	**0.02**	**0.00**	**0.04**	**0.04**	**0.00**	**0.00**	**0.04**	**0.00**	**0.10**	**N/A**
PH10D551																						
6TW	77.3	0.01	2.32	0.06	0.13	23.8	0.09	0.11	**103.8**	1.82	0.00	0.00	0.06	0.00	**1.89**	1.11	0.00	0.00	**1.11**	**3.00**	**1.69**	**N/A**
	74.5	0.02	1.75	0.10	0.09	27.1	0.07	0.16	**103.8**	1.71	0.00	0.00	0.05	0.00	**1.76**	1.24	0.00	0.00	**1.24**	**3.00**	**1.42**	**N/A**
	75.1	0.00	2.58	0.11	0.13	25.7	0.11	0.16	**104.0**	1.74	0.00	0.00	0.07	0.00	**1.81**	1.18	0.00	0.00	**1.19**	**3.00**	**1.53**	**N/A**
	77.7	0.01	1.95	0.11	0.09	23.7	0.13	0.19	**103.8**	1.83	0.00	0.00	0.05	0.00	**1.89**	1.11	0.00	0.00	**1.11**	**3.00**	**1.69**	**N/A**
	77.5	0.00	3.50	0.00	0.00	22.8	0.20	0.24	**104.3**	1.83	0.00	0.00	0.09	0.00	**1.92**	1.07	0.00	0.00	**1.08**	**3.00**	**1.79**	**N/A**
	78.4	0.00	0.09	0.08	0.26	20.7	0.00	0.58	**100.1**	1.96	0.00	0.00	0.00	0.00	**1.97**	1.02	0.00	0.01	**1.03**	**3.00**	**1.90**	**N/A**
	79.3	0.13	0.06	0.00	0.00	20.7	0.04	0.61	**100.9**	1.97	0.00	0.00	0.00	0.00	**1.97**	1.02	0.00	0.01	**1.03**	**3.00**	**1.91**	**N/A**
	78.0	0.04	0.08	0.01	0.02	21.1	0.12	0.47	**99.8**	1.95	0.00	0.00	0.00	0.00	**1.95**	1.04	0.00	0.01	**1.05**	**3.00**	**1.85**	**N/A**
	79.1	0.01	0.12	0.12	0.05	20.4	0.10	0.71	**100.6**	1.97	0.00	0.00	0.00	0.00	**1.98**	1.01	0.00	0.01	**1.02**	**3.00**	**1.93**	**N/A**
	79.4	0.00	0.28	0.00	0.04	20.5	0.07	0.70	**100.9**	1.97	0.00	0.00	0.01	0.00	**1.98**	1.01	0.00	0.01	**1.02**	**3.00**	**1.94**	**N/A**
	78.0	0.05	0.39	0.02	0.21	19.0	0.10	0.69	**98.5**	2.00	0.00	0.00	0.01	0.00	**2.02**	0.97	0.00	0.01	**0.98**	**3.00**	**2.05**	**N/A**
	79.1	0.00	0.23	0.10	0.09	20.6	0.07	0.34	**100.6**	1.97	0.00	0.00	0.01	0.00	**1.98**	1.01	0.00	0.01	**1.02**	**3.00**	**1.93**	**N/A**
	79.0	0.00	0.11	0.01	0.00	21.1	0.00	0.46	**100.7**	1.95	0.00	0.00	0.00	0.00	**1.96**	1.03	0.00	0.01	**1.04**	**3.00**	**1.88**	**N/A**
	78.8	0.00	0.27	0.00	0.00	20.5	0.02	0.46	**100.0**	1.97	0.00	0.00	0.01	0.00	**1.98**	1.01	0.00	0.01	**1.02**	**3.00**	**1.93**	**N/A**
	79.0	0.00	0.12	0.00	0.17	20.3	0.12	0.73	**100.4**	1.97	0.00	0.00	0.00	0.00	**1.98**	1.00	0.00	0.01	**1.02**	**3.00**	**1.94**	**N/A**
	78.9	0.00	0.13	0.00	0.18	20.7	0.11	0.48	**100.5**	1.96	0.00	0.00	0.00	0.00	**1.97**	1.02	0.00	0.01	**1.03**	**3.00**	**1.91**	**N/A**
	79.6	0.00	0.12	0.00	0.00	20.7	0.01	0.25	**100.7**	1.97	0.00	0.00	0.00	0.00	**1.98**	1.02	0.00	0.00	**1.02**	**3.00**	**1.94**	**N/A**
	78.4	0.00	0.09	0.00	0.00	20.9	0.08	0.38	**99.9**	1.96	0.00	0.00	0.00	0.00	**1.96**	1.03	0.00	0.01	**1.04**	**3.00**	**1.88**	**N/A**
	79.3	0.00	0.06	0.00	0.08	21.1	0.02	0.40	**100.9**	1.96	0.00	0.00	0.00	0.00	**1.96**	1.03	0.00	0.01	**1.04**	**3.00**	**1.89**	**N/A**
	79.5	0.00	0.05	0.00	0.31	20.5	0.03	0.57	**101.0**	1.98	0.00	0.00	0.00	0.00	**1.98**	1.01	0.00	0.01	**1.02**	**3.00**	**1.94**	**N/A**
	78.8	0.04	0.11	0.00	0.32	20.4	0.09	0.83	**100.6**	1.97	0.00	0.00	0.00	0.00	**1.97**	1.01	0.00	0.02	**1.03**	**3.00**	**1.92**	**N/A**
	78.9	0.00	0.12	0.07	0.37	20.5	0.06	0.65	**100.7**	1.97	0.00	0.00	0.00	0.00	**1.97**	1.01	0.00	0.01	**1.03**	**3.00**	**1.93**	**N/A**
	79.7	0.00	0.13	0.12	0.00	20.7	0.11	0.50	**101.2**	1.97	0.00	0.00	0.00	0.00	**1.98**	1.01	0.00	0.01	**1.02**	**3.00**	**1.93**	**N/A**
	79.4	0.00	0.20	0.03	0.00	20.5	0.03	0.46	**100.7**	1.97	0.00	0.00	0.01	0.00	**1.98**	1.01	0.00	0.01	**1.02**	**3.00**	**1.94**	**N/A**
Mean (n=24)	**78.5**	**0.01**	**0.62**	**0.04**	**0.11**	**21.4**	**0.07**	**0.46**	**101.2**	**1.93**	**0.00**	**0.00**	**0.02**	**0.00**	**1.95**	**1.04**	**0.00**	**0.01**	**1.05**	**3.00**	**1.9**	**N/A**
Std Dev	**1.3**	**0.03**	**1.0**	**0.05**	**0.12**	**1.9**	**0.05**	**0.20**	**1.5**	**0.08**	**0.00**	**0.00**	**0.03**	**0.00**	**0.1**	**0.06**	**0.00**	**0.00**	**0.06**	**0.00**	**0.14**	**N/A**
7TW1	80.6	0.00	0.81	0.03	0.00	20.8	0.00	0.11	**102.3**	1.97	0.00	0.00	0.02	0.00	**1.99**	1.00	0.00	0.00	**1.01**	**3.00**	**1.98**	**N/A**
8TW1	77.6	0.08	0.68	0.00	0.01	23.2	0.00	0.50	**102.1**	1.86	0.00	0.00	0.02	0.00	**1.88**	1.11	0.00	0.01	**1.12**	**3.00**	**1.69**	**N/A**
	77.6	0.13	0.55	0.05	0.11	22.9	0.01	0.43	**101.8**	1.88	0.00	0.00	0.02	0.00	**1.90**	1.10	0.00	0.01	**1.10**	**3.00**	**1.72**	**N/A**
	80.5	0.05	0.13	0.14	0.00	20.9	0.00	0.15	**101.9**	1.97	0.00	0.00	0.00	0.00	**1.98**	1.02	0.00	0.00	**1.02**	**3.00**	**1.94**	**N/A**
	80.1	0.02	0.47	0.12	0.11	21.0	0.01	0.46	**102.3**	1.96	0.00	0.00	0.01	0.00	**1.97**	1.02	0.00	0.01	**1.03**	**3.00**	**1.92**	**N/A**
	79.3	0.01	0.42	0.11	0.04	20.8	0.05	0.53	**101.2**	1.96	0.00	0.00	0.01	0.00	**1.97**	1.02	0.00	0.01	**1.03**	**3.00**	**1.92**	**N/A**
	78.6	0.10	0.91	0.10	0.02	22.5	0.00	0.64	**102.9**	1.89	0.00	0.00	0.02	0.00	**1.92**	1.07	0.00	0.01	**1.08**	**3.00**	**1.77**	**N/A**
Mean (n=6)	**79.0**	**0.06**	**0.53**	**0.09**	**0.05**	**21.9**	**0.01**	**0.45**	**102.0**	**1.92**	**0.00**	**0.00**	**0.01**	**0.00**	**1.94**	**1.05**	**0.00**	**0.01**	**1.06**	**3.00**	**1.82**	**N/A**
Std Dev	**1.23**	**0.05**	**0.26**	**0.05**	**0.05**	**1.10**	**0.02**	**0.16**	**0.55**	**0.05**	**0.00**	**0.00**	**0.01**	**0.00**	**0.04**	**0.04**	**0.00**	**0.00**	**0.04**	**0.00**	**0.11**	**N/A**
PH10D554																						
15TW	74.7	0.01	1.32	0.58	0.12	19.0	0.17	3.53	**99.4**	1.92	0.00	0.00	0.04	0.00	**1.96**	0.97	0.00	0.07	**1.04**	**3.00**	**1.88**	**N/A**
Mean (n=1)	**74.7**	**0.01**	**1.32**	**0.58**	**0.12**	**19.0**	**0.17**	**3.53**	**99.4**	**1.92**	**0.00**	**0.00**	**0.04**	**0.00**	**1.96**	**0.97**	**0.00**	**0.07**	**1.04**	**3.00**	**1.88**	**N/A**
17TW	81.3	0.00	0.03	0.12	0.14	20.6	0.06	0.03	**102.3**	2.00	0.00	0.00	0.00	0.00	**2.00**	1.00	0.00	0.00	**1.00**	**3.00**	**1.99**	**N/A**
	80.8	0.04	0.00	0.02	0.10	20.7	0.05	0.06	**101.8**	1.99	0.00	0.00	0.00	0.00	**1.99**	1.01	0.00	0.00	**1.01**	**3.00**	**1.97**	**N/A**
	79.2	0.17	0.47	0.07	0.09	19.7	0.00	0.05	**99.7**	2.00	0.00	0.00	0.01	0.00	**2.02**	0.98	0.00	0.00	**0.98**	**3.00**	**2.05**	**N/A**
	81.1	0.08	0.00	0.04	0.05	20.5	0.00	0.00	**101.8**	2.00	0.00	0.00	0.00	0.00	**2.00**	1.00	0.00	0.00	**1.00**	**3.00**	**2.00**	**N/A**
	81.7	0.00	0.00	0.00	0.06	20.7	0.05	0.01	**102.5**	2.00	0.00	0.00	0.00	0.00	**2.00**	1.00	0.00	0.00	**1.00**	**3.00**	**1.99**	**N/A**
	82.5	0.03	0.00	0.00	0.08	16.2	0.02	0.14	**99.0**	2.16	0.00	0.00	0.00	0.00	**2.16**	0.84	0.00	0.00	**0.84**	**3.00**	**2.56**	**N/A**
	81.0	0.05	0.02	0.09	0.02	21.0	0.08	0.01	**102.2**	1.98	0.00	0.00	0.00	0.00	**1.98**	1.02	0.00	0.00	**1.02**	**3.00**	**1.95**	**N/A**

Table A1: Complete electron microanalysis data for chalcocite (continued)

Label	Cu	Ag	Fe	Pb	Bi	S	Te	Se	Total	Cu	Ag	Fe	Pb	Bi	Total M	S	Te	Se	S(+Te+Se)	Total	M/S	Cu/Fe
										Flormulae calculated 3 a.p.f.u												
	81.6	0.00	0.01	0.00	0.00	20.6	0.00	0.01	**102.3**	2.00	0.00	0.00	0.00	0.00	**2.00**	1.00	0.00	0.00	**1.00**	**3.00**	**2.00**	**N/A**
	81.1	0.02	0.03	0.09	0.00	20.6	0.01	0.01	**101.8**	1.99	0.00	0.00	0.00	0.00	**1.99**	1.01	0.00	0.00	**1.01**	**3.00**	**1.98**	**N/A**
	81.5	0.01	0.02	0.06	0.11	20.7	0.01	0.03	**102.4**	2.00	0.00	0.00	0.00	0.00	**2.00**	1.00	0.00	0.00	**1.00**	**3.00**	**1.99**	**N/A**
	81.4	0.05	0.02	0.00	0.09	20.6	0.02	0.04	**102.2**	2.00	0.00	0.00	0.00	0.00	**2.00**	1.00	0.00	0.00	**1.00**	**3.00**	**2.00**	**N/A**
	81.7	0.00	0.00	0.03	0.00	20.7	0.00	0.01	**102.5**	2.00	0.00	0.00	0.00	0.00	**2.00**	1.00	0.00	0.00	**1.00**	**3.00**	**1.99**	**N/A**
	81.3	0.10	0.00	0.00	0.15	20.3	0.01	0.02	**101.9**	2.01	0.00	0.00	0.00	0.00	**2.01**	0.99	0.00	0.00	**0.99**	**3.00**	**2.02**	**N/A**
	83.8	0.01	0.01	0.00	0.08	18.7	0.02	0.00	**102.6**	2.08	0.00	0.00	0.00	0.00	**2.08**	0.92	0.00	0.00	**0.92**	**3.00**	**2.26**	**N/A**
	82.6	0.05	0.01	0.00	0.06	20.0	0.00	0.03	**102.7**	2.03	0.00	0.00	0.00	0.00	**2.03**	0.97	0.00	0.00	**0.97**	**3.00**	**2.09**	**N/A**
	81.8	0.00	0.00	0.00	0.11	20.9	0.03	0.03	**102.8**	1.99	0.00	0.00	0.00	0.00	**1.99**	1.01	0.00	0.00	**1.01**	**3.00**	**1.97**	**N/A**
	82.5	0.05	0.02	0.07	0.08	19.1	0.01	0.03	**101.9**	2.05	0.00	0.00	0.00	0.00	**2.06**	0.94	0.00	0.00	**0.94**	**3.00**	**2.18**	**N/A**
	81.7	0.06	0.00	0.00	0.12	20.7	0.00	0.02	**102.6**	2.00	0.00	0.00	0.00	0.00	**2.00**	1.00	0.00	0.00	**1.00**	**3.00**	**1.99**	**N/A**
	80.3	0.02	0.05	0.00	0.03	21.5	0.00	0.00	**101.9**	1.96	0.00	0.00	0.00	0.00	**1.96**	1.04	0.00	0.00	**1.04**	**3.00**	**1.89**	**N/A**
	81.4	0.05	0.01	0.10	0.17	20.7	0.02	0.01	**102.5**	1.99	0.00	0.00	0.00	0.00	**2.00**	1.00	0.00	0.00	**1.00**	**3.00**	**1.99**	**N/A**
	81.3	0.03	0.13	0.04	0.16	21.0	0.01	0.05	**102.8**	1.98	0.00	0.00	0.00	0.00	**1.99**	1.01	0.00	0.00	**1.01**	**3.00**	**1.96**	**N/A**
	81.6	0.04	0.02	0.06	0.07	20.6	0.02	0.03	**102.4**	2.00	0.00	0.00	0.00	0.00	**2.00**	1.00	0.00	0.00	**1.00**	**3.00**	**2.00**	**N/A**
	82.1	0.08	0.02	0.00	0.04	20.4	0.04	0.04	**102.7**	2.01	0.00	0.00	0.00	0.00	**2.01**	0.99	0.00	0.00	**0.99**	**3.00**	**2.02**	**N/A**
	81.5	0.00	0.05	0.02	0.06	20.9	0.04	0.05	**102.6**	1.99	0.00	0.00	0.00	0.00	**1.99**	1.01	0.00	0.00	**1.01**	**3.00**	**1.96**	**N/A**
	81.7	0.05	0.06	0.02	0.04	20.9	0.00	0.02	**102.8**	1.99	0.00	0.00	0.00	0.00	**1.99**	1.01	0.00	0.00	**1.01**	**3.00**	**1.97**	**N/A**
	81.2	0.00	0.04	0.05	0.07	21.0	0.02	0.02	**102.4**	1.98	0.00	0.00	0.00	0.00	**1.98**	1.01	0.00	0.00	**1.02**	**3.00**	**1.95**	**N/A**
	82.6	0.06	0.00	0.11	0.13	19.9	0.01	0.04	**102.9**	2.03	0.00	0.00	0.00	0.00	**2.03**	0.97	0.00	0.00	**0.97**	**3.00**	**2.10**	**N/A**
	81.7	0.01	0.01	0.19	0.07	20.5	0.03	0.08	**102.6**	2.00	0.00	0.00	0.00	0.00	**2.00**	0.99	0.00	0.00	**1.00**	**3.00**	**2.01**	**N/A**
	81.4	0.04	0.00	0.00	0.02	20.7	0.00	0.06	**102.1**	1.99	0.00	0.00	0.00	0.00	**1.99**	1.00	0.00	0.00	**1.01**	**3.00**	**1.98**	**N/A**
	81.6	0.00	0.00	0.08	0.10	21.1	0.02	0.00	**102.9**	1.98	0.00	0.00	0.00	0.00	**1.98**	1.02	0.00	0.00	**1.02**	**3.00**	**1.95**	**N/A**
	81.6	0.11	0.00	0.00	0.08	20.4	0.02	0.00	**102.2**	2.01	0.00	0.00	0.00	0.00	**2.01**	0.99	0.00	0.00	**0.99**	**3.00**	**2.02**	**N/A**
	81.9	0.02	0.00	0.09	0.15	20.4	0.03	0.04	**102.7**	2.01	0.00	0.00	0.00	0.00	**2.01**	0.99	0.00	0.00	**0.99**	**3.00**	**2.02**	**N/A**
	80.8	0.00	0.05	0.04	0.12	21.3	0.00	0.01	**102.3**	1.97	0.00	0.00	0.00	0.00	**1.97**	1.03	0.00	0.00	**1.03**	**3.00**	**1.92**	**N/A**
	81.7	0.00	0.04	0.04	0.10	20.8	0.00	0.01	**102.7**	1.99	0.00	0.00	0.00	0.00	**2.00**	1.00	0.00	0.00	**1.00**	**3.00**	**1.99**	**N/A**
	81.6	0.00	0.04	0.02	0.00	20.5	0.00	0.01	**102.3**	2.00	0.00	0.00	0.00	0.00	**2.00**	1.00	0.00	0.00	**1.00**	**3.00**	**2.01**	**N/A**
	81.7	0.08	0.04	0.02	0.05	20.8	0.00	0.02	**102.7**	1.99	0.00	0.00	0.00	0.00	**2.00**	1.00	0.00	0.00	**1.00**	**3.00**	**1.99**	**N/A**
	81.1	0.00	0.00	0.00	0.00	20.8	0.02	0.04	**102.0**	1.99	0.00	0.00	0.00	0.00	**1.99**	1.01	0.00	0.00	**1.01**	**3.00**	**1.96**	**N/A**
	81.2	0.00	0.00	0.00	0.06	20.6	0.01	0.00	**101.8**	2.00	0.00	0.00	0.00	0.00	**2.00**	1.00	0.00	0.00	**1.00**	**3.00**	**1.99**	**N/A**
	81.3	0.08	0.00	0.04	0.07	20.7	0.00	0.00	**102.2**	1.99	0.00	0.00	0.00	0.00	**1.99**	1.01	0.00	0.00	**1.01**	**3.00**	**1.98**	**N/A**
	81.4	0.00	0.01	0.06	0.00	20.9	0.02	0.01	**102.4**	1.99	0.00	0.00	0.00	0.00	**1.99**	1.01	0.00	0.00	**1.01**	**3.00**	**1.96**	**N/A**
	81.2	0.00	0.02	0.00	0.00	20.8	0.02	0.00	**102.1**	1.99	0.00	0.00	0.00	0.00	**1.99**	1.01	0.00	0.00	**1.01**	**3.00**	**1.97**	**N/A**
	80.7	0.02	0.00	0.00	0.11	20.6	0.00	0.04	**101.4**	1.99	0.00	0.00	0.00	0.00	**1.99**	1.01	0.00	0.00	**1.01**	**3.00**	**1.98**	**N/A**
	80.6	0.02	0.02	0.06	0.00	21.0	0.01	0.01	**101.7**	1.98	0.00	0.00	0.00	0.00	**1.98**	1.02	0.00	0.00	**1.02**	**3.00**	**1.94**	**N/A**
	81.2	0.00	0.00	0.07	0.10	20.7	0.00	0.00	**102.1**	1.99	0.00	0.00	0.00	0.00	**1.99**	1.01	0.00	0.00	**1.01**	**3.00**	**1.98**	**N/A**
	81.2	0.00	0.01	0.12	0.15	20.5	0.02	0.01	**102.0**	2.00	0.00	0.00	0.00	0.00	**2.00**	1.00	0.00	0.00	**1.00**	**3.00**	**2.00**	**N/A**
	81.3	0.04	0.00	0.10	0.13	20.8	0.00	0.00	**102.4**	1.99	0.00	0.00	0.00	0.00	**1.99**	1.01	0.00	0.00	**1.01**	**3.00**	**1.98**	**N/A**
Mean (n=46)	**81.5**	**0.03**	**0.03**	**0.04**	**0.07**	**20.5**	**0.02**	**0.02**	**102.2**	**2.00**	**0.00**	**0.00**	**0.00**	**0.00**	2.00	**1.00**	**0.00**	**0.00**	**1.00**	**3.00**	**2.01**	**N/A**
Std Dev	**0.69**	**0.04**	**0.07**	**0.04**	**0.05**	**0.81**	**0.02**	**0.03**	**0.71**	**0.03**	**0.00**	**0.00**	**0.00**	**0.00**	**0.03**	**0.03**	**0.00**	**0.00**	**0.03**	**0.00**	**0.10**	**N/A**
21TW	80.9	0.00	0.27	0.11	0.07	21.5	0.02	0.06	**102.9**	1.96	0.00	0.00	0.01	0.00	**1.97**	1.03	0.00	0.00	**1.03**	**3.00**	**1.91**	**N/A**
	80.9	0.08	0.19	0.02	0.02	21.4	0.06	0.05	**102.7**	1.96	0.00	0.00	0.01	0.00	**1.97**	1.03	0.00	0.00	**1.03**	**3.00**	**1.91**	**N/A**
	80.7	0.11	0.09	0.00	0.02	21.8	0.06	0.02	**102.7**	1.95	0.00	0.00	0.00	0.00	**1.95**	1.04	0.00	0.00	**1.05**	**3.00**	**1.87**	**N/A**
	80.2	0.03	0.27	0.03	0.11	21.8	0.01	0.04	**102.5**	1.94	0.00	0.00	0.01	0.00	**1.95**	1.05	0.00	0.00	**1.05**	**3.00**	**1.87**	**N/A**
	81.1	0.08	0.19	0.05	0.00	21.1	0.00	0.08	**102.7**	1.97	0.00	0.00	0.01	0.00	**1.98**	1.02	0.00	0.00	**1.02**	**3.00**	**1.94**	**N/A**
	80.8	0.00	0.13	0.00	0.15	21.8	0.00	0.04	**102.9**	1.95	0.00	0.00	0.00	0.00	**1.96**	1.04	0.00	0.00	**1.04**	**3.00**	**1.87**	**N/A**
	80.8	0.05	0.11	0.11	0.02	21.5	0.00	0.04	**102.6**	1.96	0.00	0.00	0.00	0.00	**1.97**	1.03	0.00	0.00	**1.03**	**3.00**	**1.90**	**N/A**
	80.4	0.09	0.15	0.07	0.06	21.3	0.05	0.00	**102.2**	1.96	0.00	0.00	0.00	0.00	**1.97**	1.03	0.00	0.00	**1.03**	**3.00**	**1.91**	**N/A**
	80.7	0.08	0.16	0.18	0.10	21.6	0.03	0.05	**102.9**	1.95	0.00	0.00	0.00	0.00	**1.96**	1.04	0.00	0.00	**1.04**	**3.00**	**1.89**	**N/A**
	80.2	0.09	0.20	0.00	0.08	21.4	0.03	0.05	**102.0**	1.96	0.00	0.00	0.01	0.00	**1.96**	1.03	0.00	0.00	**1.04**	**3.00**	**1.90**	**N/A**
	80.7	0.07	0.26	0.00	0.07	21.5	0.00	0.07	**102.6**	1.96	0.00	0.00	0.01	0.00	**1.97**	1.03	0.00	0.00	**1.03**	**3.00**	**1.90**	**N/A**
	80.5	0.17	0.39	0.14	0.04	21.3	0.00	0.09	**102.6**	1.96	0.00	0.00	0.01	0.00	**1.97**	1.03	0.00	0.00	**1.03**	**3.00**	**1.92**	**N/A**
	80.7	0.07	0.22	0.07	0.00	20.6	0.00	0.08	**101.7**	1.98	0.00	0.00	0.01	0.00	**1.99**	1.01	0.00	0.00	**1.01**	**3.00**	**1.98**	**N/A**
	81.6	0.00	0.09	0.11	0.03	21.1	0.00	0.04	**103.0**	1.98	0.00	0.00	0.00	0.00	**1.99**	1.01	0.00	0.00	**1.01**	**3.00**	**1.96**	**N/A**
	81.7	0.06	0.03	0.06	0.17	20.8	0.00	0.01	**102.8**	1.99	0.00	0.00	0.00	0.00	**2.00**	1.00	0.00	0.00	**1.00**	**3.00**	**1.99**	**N/A**
	81.8	0.04	0.03	0.18	0.01	20.9	0.00	0.00	**102.9**	1.99	0.00	0.00	0.00	0.00	**1.99**	1.01	0.00	0.00	**1.01**	**3.00**	**1.98**	**N/A**
	81.2	0.01	0.11	0.00	0.16	21.3	0.00	0.04	**102.8**	1.97	0.00	0.00	0.00	0.00	**1.98**	1.02	0.00	0.00	**1.02**	**3.00**	**1.93**	**N/A**
	81.3	0.01	0.12	0.07	0.12	21.2	0.04	0.02	**102.9**	1.97	0.00	0.00	0.00	0.00	**1.98**	1.02	0.00	0.00	**1.02**	**3.00**	**1.94**	**N/A**
	81.7	0.00	0.33	0.09	0.10	20.6	0.00	0.03	**102.9**	1.99	0.00	0.00	0.01	0.00	**2.00**	1.00	0.00	0.00	**1.00**	**3.00**	**2.01**	**N/A**
	81.4	0.05	0.51	0.01	0.13	20.7	0.00	0.00	**102.8**	1.98	0.00	0.00	0.01	0.00	**2.00**	1.00	0.00	0.00	**1.00**	**3.00**	**2.00**	**N/A**
	81.5	0.00	0.43	0.12	0.03	20.8	0.04	0.00	**102.8**	1.98	0.00	0.00	0.01	0.00	**2.00**	1.00	0.00	0.00	**1.00**	**3.00**	**1.99**	**N/A**
	81.6	0.10	0.49	0.11	0.00	19.1	0.00	0.03	**101.5**	2.04	0.00	0.00	0.01	0.00	**2.05**	0.95	0.00	0.00	**0.95**	**3.00**	**2.17**	**N/A**
	82.0	0.08	0.33	0.06	0.05	20.0	0.00	0.02	**102.6**	2.02	0.00	0.00	0.01	0.00	**2.03**	0.97	0.00	0.00	**0.97**	**3.00**	**2.08**	**N/A**
	83.4	0.00	0.21	0.07	0.13	18.9	0.01	0.08	**102.9**	2.06	0.00	0.00	0.01	0.00	**2.07**	0.93	0.00	0.00	**0.93**	**3.00**	**2.23**	**N/A**
	81.7	0.00	0.02	0.14	0.05	20.8	0.03	0.04	**102.7**	1.99	0.00	0.00	0.00	0.00	**1.99**	1.00	0.00	0.00	**1.01**	**3.00**	**1.98**	**N/A**
	81.6	0.03	0.04	0.05	0.00	21.0	0.05	0.03	**102.8**	1.99	0.00	0.00	0.00	0.00	**1.99**	1.01	0.00	0.00	**1.01**	**3.00**	**1.96**	**N/A**
	81.9	0.00	0.02	0.06	0.09	20.8	0.03	0.02	**102.8**	1.99	0.00	0.00	0.00	0.00	**2.00**	1.00	0.00	0.00	**1.00**	**3.00**	**1.99**	**N/A**
	81.6	0.02	0.05	0.14	0.17	20.8	0.05	0.01	**102.8**	1.99	0.00	0.00	0.00	0.00	**1.99**	1.00	0.00	0.00	**1.01**	**3.00**	**1.98**	**N/A**
Mean (n=28)	**81.2**	**0.05**	**0.20**	**0.07**	**0.07**	**20.97**	**0.02**	**0.04**	**102.6**	**1.98**	**0.00**	**0.00**	**0.01**	**0.00**	1.99	**1.01**	**0.00**	**0.00**	**1.01**	**3.00**	**1.96**	**N/A**
Std Dev	**0.69**	**0.04**	**0.14**	**0.05**	**0.06**	**0.69**	**0.02**	**0.03**	**0.36**	**0.03**	**0.00**	**0.00**	**0.00**	**0.00**	**0.03**	**0.03**	**0.00**	**0.00**	**0.03**	**0.00**	**0.08**	**N/A**
PH10D549																						
28TW	81.5	0.02	0.15	0.03	0.22	21.0	0.04	0.00	**103.0**	1.98	0.00	0.00	0.00	0.00	**1.99**	1.01	0.00	0.00	**1.01**	**3.00**	**1.96**	**N/A**
	81.5	0.04	0.10	0.02	0.00	20.7	0.01	0.00	**102.4**	1.99	0.00	0.00	0.00	0.00	**1.99**	1.01	0.00	0.00	**1.01**	**3.00**	**1.98**	**N/A**
	81.8	0.00	0.02	0.00	0.00	20.9	0.00	0.00	**102.7**	1.99	0.00	0.00	0.00	0.00	**1.99**	1.01	0.00	0.00	**1.01**	**3.00**	**1.97**	**N/A**
	81.6	0.00	0.01	0.08	0.05	20.8	0.00	0.00	**102.5**	1.99	0.00	0.00	0.00	0.00	**1.99**	1.01	0.00	0.00	**1.01**	**3.00**	**1.98**	**N/A**
	81.6	0.02	0.02	0.05	0.04	20.7	0.02	0.06	**102.5**	1.99	0.00	0.00	0.00	0.00	**1.99**	1.00	0.00	0.00	**1.01**	**3.00**	**1.98**	**N/A**
	82.0	0.00	0.01	0.00	0.08	20.5	0.00	0.00	**102.6**	2.00	0.00	0.00	0.00	0.00	**2.01**	0.99	0.00	0.00	**0.99**	**3.00**	**2.02**	**N/A**
	81.4	0.00	0.04	0.09	0.01	20.7	0.01	0.00	**102.3**	1.99	0.00	0.00	0.00	0.00	**1.99**	1.00	0.00	0.00	**1.01**	**3.00**	**1.98**	**N/A**

Table A1: Complete electron microanalysis data for chalcocite (continued)

Label	Cu	Ag	Fe	Pb	Bi	S	Te	Se	Total	Cu	Ag	Fe	Pb	Bi	Total M	S	Te	Se	S(+Te+Se)	Total	M/S	Cu/Fe
										Flormulae calculated 3 a.p.f.u												
	81.5	0.05	0.04	0.09	0.16	21.1	0.00	0.00	**103.0**	1.98	0.00	0.00	0.00	0.00	**1.98**	1.02	0.00	0.00	**1.02**	**3.00**	**1.95**	**N/A**
	81.7	0.00	0.11	0.04	0.00	20.8	0.01	0.00	**102.6**	1.99	0.00	0.00	0.00	0.00	**2.00**	1.00	0.00	0.00	**1.00**	**3.00**	**1.99**	**N/A**
	82.0	0.00	0.06	0.00	0.06	20.7	0.00	0.01	**102.8**	2.00	0.00	0.00	0.00	0.00	**2.00**	1.00	0.00	0.00	**1.00**	**3.00**	**2.00**	**N/A**
	81.9	0.08	0.03	0.02	0.02	20.9	0.02	0.02	**103.0**	1.99	0.00	0.00	0.00	0.00	**1.99**	1.01	0.00	0.00	**1.01**	**3.00**	**1.97**	**N/A**
	81.6	0.03	0.03	0.12	0.00	21.1	0.00	0.00	**102.8**	1.98	0.00	0.00	0.00	0.00	**1.99**	1.01	0.00	0.00	**1.01**	**3.00**	**1.96**	**N/A**
	81.7	0.17	0.00	0.00	0.10	20.3	0.00	0.00	**102.3**	2.01	0.00	0.00	0.00	0.00	**2.01**	0.99	0.00	0.00	**0.99**	**3.00**	**2.04**	**N/A**
	81.4	0.11	0.08	0.01	0.20	20.8	0.05	0.05	**102.7**	1.99	0.00	0.00	0.00	0.00	**1.99**	1.01	0.00	0.00	**1.01**	**3.00**	**1.97**	**N/A**
	81.8	0.00	0.04	0.00	0.07	21.0	0.00	0.03	**102.9**	1.99	0.00	0.00	0.00	0.00	**1.99**	1.01	0.00	0.00	**1.01**	**3.00**	**1.97**	**N/A**
	81.5	0.11	0.02	0.06	0.04	21.2	0.00	0.00	**102.9**	1.98	0.00	0.00	0.00	0.00	**1.98**	1.02	0.00	0.00	**1.02**	**3.00**	**1.94**	**N/A**
	81.5	0.07	0.04	0.00	0.03	21.0	0.01	0.02	**102.7**	1.98	0.00	0.00	0.00	0.00	**1.98**	1.01	0.00	0.00	**1.02**	**3.00**	**1.95**	**N/A**
	81.1	0.01	0.17	0.00	0.03	21.3	0.01	0.05	**102.7**	1.97	0.00	0.00	0.00	0.00	**1.98**	1.02	0.00	0.00	**1.02**	**3.00**	**1.93**	**N/A**
	80.3	0.03	0.14	0.00	0.00	20.8	0.01	0.05	**101.3**	1.98	0.00	0.00	0.00	0.00	**1.98**	1.02	0.00	0.00	**1.02**	**3.00**	**1.95**	**N/A**
	81.7	0.01	0.12	0.00	0.00	20.8	0.00	0.08	**102.7**	1.99	0.00	0.00	0.00	0.00	**1.99**	1.00	0.00	0.00	**1.01**	**3.00**	**1.98**	**N/A**
	81.0	0.04	0.39	0.00	0.00	20.7	0.00	0.07	**102.2**	1.98	0.00	0.00	0.01	0.00	**1.99**	1.00	0.00	0.00	**1.01**	**3.00**	**1.98**	**N/A**
	81.4	0.00	0.09	0.11	0.00	21.0	0.00	0.01	**102.6**	1.98	0.00	0.00	0.00	0.00	**1.98**	1.02	0.00	0.00	**1.02**	**3.00**	**1.95**	**N/A**
	81.7	0.06	0.11	0.03	0.09	21.0	0.00	0.00	**102.9**	1.98	0.00	0.00	0.00	0.00	**1.99**	1.01	0.00	0.00	**1.01**	**3.00**	**1.97**	**N/A**
Mean (n=23)	**81.5**	**0.04**	**0.08**	**0.03**	**0.05**	**20.87**	**0.01**	**0.02**	**102.6**	**1.99**	**0.00**	**0.00**	**0.00**	**0.00**	1.99	**1.01**	**0.00**	**0.00**	**1.01**	**3.00**	**1.97**	**N/A**
Std Dev	**0.36**	**0.04**	**0.08**	**0.04**	**0.07**	**0.22**	**0.01**	**0.03**	**0.36**	**0.01**	**0.00**	**0.00**	**0.00**	**0.00**	**0.01**	**0.01**	**0.00**	**0.00**	**0.01**	**0.00**	**0.02**	**N/A**
31TW	80.6	0.00	0.12	0.11	0.11	21.8	0.01	0.03	**102.7**	1.95	0.00	0.00	0.00	0.00	**1.95**	1.05	0.00	0.00	**1.05**	**3.00**	**1.87**	**N/A**
	81.0	0.00	0.09	0.13	0.23	21.4	0.00	0.00	**102.9**	1.96	0.00	0.00	0.00	0.00	**1.97**	1.03	0.00	0.00	**1.03**	**3.00**	**1.91**	**N/A**
	80.7	0.06	0.11	0.01	0.12	21.6	0.00	0.06	**102.6**	1.96	0.00	0.00	0.00	0.00	**1.96**	1.04	0.00	0.00	**1.04**	**3.00**	**1.89**	**N/A**
	80.9	0.05	0.15	0.12	0.13	21.5	0.00	0.00	**102.9**	1.96	0.00	0.00	0.00	0.00	**1.97**	1.03	0.00	0.00	**1.03**	**3.00**	**1.90**	**N/A**
Mean (n=4)	**77.8**	**0.04**	**0.09**	**0.04**	**0.07**	**20.12**	**0.01**	**0.02**	**98.2**	**1.90**	**0.00**	**0.00**	**0.00**	**0.00**	**1.90**	**0.97**	**0.00**	**0.00**	**0.97**	**2.87**	**1.87**	**N/A**
Std Dev	**0.20**	**0.03**	**0.03**	**0.06**	**0.06**	**0.16**	**0.01**	**0.03**	**0.12**	**0.01**	**0.00**	**0.00**	**0.00**	**0.00**	**0.01**	**0.01**	**0.00**	**0.00**	**0.01**	**0.00**	**0.02**	**N/A**
PH11D541																						
39aTW	80.1	0.00	0.03	0.02	0.09	20.0	0.03	0.04	**100.3**	2.01	0.00	0.00	0.00	0.00	**2.01**	0.99	0.00	0.00	**0.99**	**3.00**	**2.02**	**N/A**
	80.5	0.13	0.01	0.19	0.15	20.6	0.00	0.00	**101.6**	1.98	0.00	0.00	0.00	0.00	**1.99**	1.01	0.00	0.00	**1.01**	**3.00**	**1.98**	**N/A**
	80.4	0.00	0.05	0.00	0.16	20.4	0.01	0.03	**101.1**	1.99	0.00	0.00	0.00	0.00	**2.00**	1.00	0.00	0.00	**1.00**	**3.00**	**1.99**	**N/A**
	80.1	0.04	0.49	0.00	0.27	20.2	0.02	0.03	**101.1**	1.99	0.00	0.00	0.01	0.00	**2.00**	0.99	0.00	0.00	**1.00**	**3.00**	**2.01**	**N/A**
	80.2	0.00	0.01	0.01	0.02	20.5	0.00	0.00	**100.8**	1.99	0.00	0.00	0.00	0.00	**1.99**	1.01	0.00	0.00	**1.01**	**3.00**	**1.97**	**N/A**
	80.5	0.14	0.04	0.10	0.00	20.8	0.03	0.00	**101.6**	1.98	0.00	0.00	0.00	0.00	**1.99**	1.01	0.00	0.00	**1.01**	**3.00**	**1.96**	**N/A**
	80.7	0.00	0.02	0.00	0.00	20.3	0.00	0.12	**101.1**	2.00	0.00	0.00	0.00	0.00	**2.00**	1.00	0.00	0.00	**1.00**	**3.00**	**2.00**	**N/A**
	80.0	0.00	0.02	0.08	0.14	20.3	0.00	0.00	**100.6**	2.00	0.00	0.00	0.00	0.00	**2.00**	1.00	0.00	0.00	**1.00**	**3.00**	**1.99**	**N/A**
	80.5	0.09	0.03	0.08	0.08	20.4	0.02	0.00	**101.2**	1.99	0.00	0.00	0.00	0.00	**2.00**	1.00	0.00	0.00	**1.00**	**3.00**	**1.99**	**N/A**
	80.0	0.00	0.00	0.05	0.08	20.8	0.00	0.00	**100.9**	1.98	0.00	0.00	0.00	0.00	**1.98**	1.02	0.00	0.00	**1.02**	**3.00**	**1.94**	**N/A**
	81.1	0.07	0.01	0.16	0.17	20.3	0.00	0.00	**101.8**	2.00	0.00	0.00	0.00	0.00	**2.01**	0.99	0.00	0.00	**0.99**	**3.00**	**2.02**	**N/A**
	80.1	0.04	0.01	0.00	0.03	20.4	0.01	0.02	**100.7**	1.99	0.00	0.00	0.00	0.00	**1.99**	1.01	0.00	0.00	**1.01**	**3.00**	**1.98**	**N/A**
	79.8	0.05	0.00	0.07	0.27	20.3	0.00	0.00	**100.5**	1.99	0.00	0.00	0.00	0.00	**2.00**	1.00	0.00	0.00	**1.00**	**3.00**	**1.99**	**N/A**
	80.8	0.04	0.00	0.01	0.00	20.7	0.05	0.03	**101.6**	1.99	0.00	0.00	0.00	0.00	**1.99**	1.01	0.00	0.00	**1.01**	**3.00**	**1.97**	**N/A**
	79.8	0.05	0.02	0.03	0.00	20.4	0.00	0.02	**100.3**	1.99	0.00	0.00	0.00	0.00	**1.99**	1.01	0.00	0.00	**1.01**	**3.00**	**1.98**	**N/A**
	80.2	0.08	0.00	0.07	0.00	20.7	0.00	0.00	**101.1**	1.98	0.00	0.00	0.00	0.00	**1.98**	1.02	0.00	0.00	**1.02**	**3.00**	**1.95**	**N/A**
	80.4	0.00	0.00	0.00	0.02	20.8	0.00	0.01	**101.2**	1.98	0.00	0.00	0.00	0.00	**1.99**	1.01	0.00	0.00	**1.01**	**3.00**	**1.96**	**N/A**
	80.3	0.01	0.01	0.12	0.15	20.6	0.00	0.00	**101.2**	1.99	0.00	0.00	0.00	0.00	**1.99**	1.01	0.00	0.00	**1.01**	**3.00**	**1.97**	**N/A**
	80.6	0.03	0.00	0.00	0.00	20.7	0.01	0.00	**101.4**	1.99	0.00	0.00	0.00	0.00	**1.99**	1.01	0.00	0.00	**1.01**	**3.00**	**1.97**	**N/A**
	80.9	0.09	0.00	0.00	0.15	20.0	0.04	0.00	**101.2**	2.01	0.00	0.00	0.00	0.00	**2.01**	0.98	0.00	0.00	**0.98**	**3.00**	**2.05**	**N/A**
	80.3	0.05	0.00	0.20	0.09	20.1	0.01	0.07	**100.9**	2.00	0.00	0.00	0.00	0.00	**2.00**	0.99	0.00	0.00	**0.99**	**3.00**	**2.02**	**N/A**
	80.2	0.00	0.03	0.01	0.07	19.8	0.03	0.01	**100.2**	2.01	0.00	0.00	0.00	0.00	**2.01**	0.98	0.00	0.00	**0.98**	**3.00**	**2.04**	**N/A**
	80.5	0.00	0.01	0.03	0.03	20.7	0.03	0.04	**101.4**	1.98	0.00	0.00	0.00	0.00	**1.99**	1.01	0.00	0.00	**1.01**	**3.00**	**1.96**	**N/A**
	80.0	0.07	0.02	0.06	0.00	20.3	0.00	0.02	**100.5**	1.99	0.00	0.00	0.00	0.00	**2.00**	1.00	0.00	0.00	**1.00**	**3.00**	**1.99**	**N/A**
	80.1	0.00	0.02	0.03	0.00	20.8	0.00	0.00	**101.0**	1.98	0.00	0.00	0.00	0.00	**1.98**	1.02	0.00	0.00	**1.02**	**3.00**	**1.94**	**N/A**
	80.5	0.05	0.02	0.00	0.20	20.5	0.01	0.00	**101.3**	1.99	0.00	0.00	0.00	0.00	**2.00**	1.00	0.00	0.00	**1.00**	**3.00**	**1.99**	**N/A**
	79.4	0.00	0.02	0.15	0.09	21.1	0.09	0.00	**100.9**	1.96	0.00	0.00	0.00	0.00	**1.97**	1.03	0.00	0.00	**1.03**	**3.00**	**1.90**	**N/A**
	80.6	0.02	0.02	0.04	0.00	20.4	0.04	0.02	**101.2**	2.00	0.00	0.00	0.00	0.00	**2.00**	1.00	0.00	0.00	**1.00**	**3.00**	**1.99**	**N/A**
	79.6	0.00	0.14	0.04	0.14	20.6	0.02	0.06	**100.6**	1.98	0.00	0.00	0.00	0.00	**1.98**	1.01	0.00	0.00	**1.02**	**3.00**	**1.95**	**N/A**
	79.4	0.04	0.49	0.00	0.09	20.6	0.02	0.13	**100.8**	1.97	0.00	0.00	0.01	0.00	**1.98**	1.01	0.00	0.00	**1.01**	**3.00**	**1.96**	**N/A**
Mean (n=30)	**80.3**	**0.04**	**0.05**	**0.05**	**0.08**	**20.47**	**0.02**	**0.02**	**101.0**	**1.99**	**0.00**	**0.00**	**0.00**	**0.00**	1.99	**1.01**	**0.00**	**0.00**	**1.01**	**3.00**	**1.98**	**N/A**
Std Dev	**0.40**	**0.04**	**0.12**	**0.06**	**0.08**	**0.29**	**0.02**	**0.03**	**0.42**	**0.01**	**0.00**	**0.00**	**0.00**	**0.00**	**0.01**	**0.01**	**0.00**	**0.00**	**0.01**	**0.00**	**0.03**	**N/A**
39bTW	80.5	0.00	0.24	0.01	0.05	20.5	0.01	0.03	**101.4**	1.99	0.00	0.00	0.01	0.00	**2.00**	1.00	0.00	0.00	**1.00**	**3.00**	**1.99**	**N/A**
	80.2	0.03	0.40	0.04	0.21	20.4	0.00	0.00	**101.4**	1.98	0.00	0.00	0.01	0.00	**2.00**	1.00	0.00	0.00	**1.00**	**3.00**	**1.99**	**N/A**
	80.7	0.00	0.07	0.00	0.12	20.3	0.01	0.02	**101.2**	2.00	0.00	0.00	0.00	0.00	**2.00**	1.00	0.00	0.00	**1.00**	**3.00**	**2.00**	**N/A**
	80.9	0.00	0.11	0.11	0.04	20.3	0.01	0.00	**101.5**	2.00	0.00	0.00	0.00	0.00	**2.00**	1.00	0.00	0.00	**1.00**	**3.00**	**2.01**	**N/A**
	80.5	0.07	0.04	0.00	0.02	20.5	0.00	0.00	**101.2**	1.99	0.00	0.00	0.00	0.00	**1.99**	1.01	0.00	0.00	**1.01**	**3.00**	**1.98**	**N/A**
	80.5	0.00	0.03	0.00	0.06	20.7	0.01	0.02	**101.3**	1.99	0.00	0.00	0.00	0.00	**1.99**	1.01	0.00	0.00	**1.01**	**3.00**	**1.97**	**N/A**
	80.3	0.09	0.04	0.00	0.18	20.5	0.08	0.00	**101.2**	1.99	0.00	0.00	0.00	0.00	**1.99**	1.00	0.00	0.00	**1.01**	**3.00**	**1.98**	**N/A**
	80.8	0.07	0.03	0.00	0.14	20.8	0.06	0.07	**102.0**	1.98	0.00	0.00	0.00	0.00	**1.99**	1.01	0.00	0.00	**1.01**	**3.00**	**1.96**	**N/A**
	80.5	0.01	0.05	0.04	0.05	20.8	0.03	0.00	**101.5**	1.98	0.00	0.00	0.00	0.00	**1.98**	1.02	0.00	0.00	**1.02**	**3.00**	**1.95**	**N/A**
	80.6	0.05	0.15	0.03	0.00	20.8	0.03	0.07	**101.9**	1.98	0.00	0.00	0.00	0.00	**1.98**	1.01	0.00	0.00	**1.01**	**3.00**	**1.95**	**N/A**
Mean (n=10)	**80.5**	**0.03**	**0.12**	**0.02**	**0.09**	**20.56**	**0.02**	**0.02**	**101.5**	**1.99**	**0.00**	**0.00**	**0.00**	**0.00**	1.99	**1.01**	**0.00**	**0.00**	**1.01**	**3.00**	**1.98**	**N/A**
Std Dev	**0.22**	**0.04**	**0.12**	**0.03**	**0.07**	**0.19**	**0.03**	**0.03**	**0.28**	**0.01**	**0.00**	**0.00**	**0.00**	**0.00**	**0.01**	**0.01**	**0.00**	**0.00**	**0.01**	**0.00**	**0.02**	**N/A**
PH11D576																						
40TW	80.0	0.05	0.02	0.00	0.00	20.8	0.02	0.00	**100.9**	1.98	0.00	0.00	0.00	0.00	**1.98**	1.02	0.00	0.00	**1.02**	**3.00**	**1.94**	**N/A**
	80.4	0.00	0.00	0.04	0.03	20.5	0.01	0.02	**101.1**	1.99	0.00	0.00	0.00	0.00	**1.99**	1.01	0.00	0.00	**1.01**	**3.00**	**1.98**	**N/A**
	80.0	0.00	0.00	0.14	0.05	20.6	0.03	0.00	**100.8**	1.99	0.00	0.00	0.00	0.00	**1.99**	1.01	0.00	0.00	**1.01**	**3.00**	**1.97**	**N/A**
	80.5	0.04	0.05	0.00	0.13	20.3	0.00	0.00	**101.2**	2.00	0.00	0.00	0.00	0.00	**2.00**	1.00	0.00	0.00	**1.00**	**3.00**	**2.00**	**N/A**
	79.8	0.07	0.05	0.00	0.11	20.6	0.07	0.05	**100.8**	1.98	0.00	0.00	0.00	0.00	**1.98**	1.01	0.00	0.00	**1.01**	**3.00**	**1.95**	**N/A**
	80.1	0.02	0.08	0.16	0.04	20.4	0.00	0.02	**100.8**	1.99	0.00	0.00	0.00	0.00	**2.00**	1.00	0.00	0.00	**1.00**	**3.00**	**1.99**	**N/A**
	79.9	0.20	0.10	0.16	0.06	20.7	0.08	0.07	**101.3**	1.98	0.00	0.00	0.00	0.00	**1.98**	1.01	0.00	0.00	**1.02**	**3.00**	**1.95**	**N/A**
	80.1	0.07	0.11	0.04	0.05	20.4	0.02	0.03	**100.8**	1.99	0.00	0.00	0.00	0.00	**1.99**	1.00	0.00	0.00	**1.00**	**3.00**	**1.98**	**N/A**

Table A1: Complete electron microanalysis data for chalcocite (continued)

Label	Cu	Ag	Fe	Pb	Bi	S	Te	Se	Total	Cu	Ag	Fe	Pb	Bi	Total M	S	Te	Se	S(+Te+Se)	Total	M/S	Cu/Fe
										Flormulae calculated 3 a.p.f.u												
	79.8	0.02	0.11	0.11	0.11	20.6	0.00	0.00	**100.8**	1.98	0.00	0.00	0.00	0.00	**1.99**	1.01	0.00	0.00	**1.01**	**3.00**	**1.96**	**N/A**
	79.9	0.00	0.28	0.04	0.07	20.6	0.00	0.00	**100.8**	1.98	0.00	0.00	0.01	0.00	**1.99**	1.01	0.00	0.00	**1.01**	**3.00**	**1.97**	**N/A**
	80.3	0.06	0.02	0.21	0.09	20.4	0.00	0.10	**101.3**	1.99	0.00	0.00	0.00	0.00	**1.99**	1.00	0.00	0.00	**1.00**	**3.00**	**1.99**	**N/A**
	80.6	0.04	0.02	0.01	0.09	20.5	0.00	0.03	**101.4**	1.99	0.00	0.00	0.00	0.00	**1.99**	1.00	0.00	0.00	**1.00**	**3.00**	**1.98**	**N/A**
	80.4	0.05	0.00	0.00	0.19	20.6	0.00	0.00	**101.2**	1.99	0.00	0.00	0.00	0.00	**1.99**	1.01	0.00	0.00	**1.01**	**3.00**	**1.97**	**N/A**
	80.6	0.00	0.01	0.00	0.16	20.4	0.03	0.07	**101.3**	2.00	0.00	0.00	0.00	0.00	**2.00**	1.00	0.00	0.00	**1.00**	**3.00**	**1.99**	**N/A**
	79.3	0.17	0.17	0.18	0.17	20.2	0.00	0.03	**100.3**	1.98	0.00	0.00	0.00	0.00	**2.00**	1.00	0.00	0.00	**1.00**	**3.00**	**1.99**	**N/A**
	79.9	0.13	0.01	0.26	0.11	20.6	0.05	0.00	**101.1**	1.98	0.00	0.00	0.00	0.00	**1.99**	1.01	0.00	0.00	**1.01**	**3.00**	**1.96**	**N/A**
	79.9	0.00	0.04	0.26	0.00	20.4	0.00	0.04	**100.7**	1.99	0.00	0.00	0.00	0.00	**1.99**	1.01	0.00	0.00	**1.01**	**3.00**	**1.98**	**N/A**
	80.1	0.00	0.54	0.12	0.14	20.2	0.00	0.00	**101.2**	1.99	0.00	0.00	0.02	0.00	**2.00**	0.99	0.00	0.00	**0.99**	**3.00**	**2.01**	**N/A**
	80.3	0.00	0.02	0.00	0.06	20.6	0.01	0.00	**101.1**	1.99	0.00	0.00	0.00	0.00	**1.99**	1.01	0.00	0.00	**1.01**	**3.00**	**1.97**	**N/A**
	80.0	0.09	0.25	0.10	0.00	20.3	0.00	0.00	**100.8**	1.99	0.00	0.00	0.01	0.00	**2.00**	1.00	0.00	0.00	**1.00**	**3.00**	**2.00**	**N/A**
Mean (n=20)	**80.1**	**0.05**	**0.09**	**0.09**	**0.08**	**20.49**	**0.02**	**0.02**	**100.98**	**1.99**	**0.00**	**0.00**	**0.00**	**0.00**	**1.99**	**1.01**	**0.00**	**0.00**	**1.01**	**3.00**	**1.98**	**N/A**
Std Dev	**0.33**	**0.06**	**0.13**	**0.09**	**0.06**	**0.16**	**0.02**	**0.03**	**0.28**	**0.01**	**0.00**	**0.00**	**0.00**	**0.00**	**0.01**	**0.01**	**0.00**	**0.00**	**0.01**	**0.00**	**0.02**	**N/A**
41aTW	77.6	0.01	0.05	0.24	0.07	20.5	0.13	0.07	**98.6**	1.96	0.00	0.00	0.00	0.00	**1.97**	1.03	0.00	0.00	**1.03**	**3.00**	**1.91**	**N/A**
	77.8	0.04	0.10	0.00	0.25	20.6	0.40	0.12	**99.4**	1.96	0.00	0.00	0.00	0.00	**1.96**	1.03	0.01	0.00	**1.03**	**3.00**	**1.90**	**N/A**
	74.3	0.00	0.69	0.15	0.15	21.2	0.00	0.11	**98.1**	1.88	0.00	0.00	0.02	0.00	**1.90**	1.06	0.00	0.00	**1.07**	**2.97**	**1.79**	**N/A**
	78.2	0.12	0.09	0.00	0.18	20.8	0.00	0.12	**99.6**	1.96	0.00	0.00	0.00	0.00	**1.97**	1.03	0.00	0.00	**1.03**	**3.00**	**1.90**	**N/A**
	77.6	0.00	0.05	0.04	0.22	20.7	0.00	0.02	**98.7**	1.96	0.00	0.00	0.00	0.00	**1.96**	1.03	0.00	0.00	**1.03**	**3.00**	**1.90**	**N/A**
	77.6	0.00	0.11	0.14	0.12	20.3	0.36	0.12	**98.8**	1.97	0.00	0.00	0.00	0.00	**1.97**	1.02	0.00	0.00	**1.03**	**3.00**	**1.93**	**N/A**
	78.8	0.00	0.15	0.18	0.07	20.4	0.34	0.12	**100.1**	1.97	0.00	0.00	0.00	0.00	**1.98**	1.01	0.00	0.00	**1.02**	**3.00**	**1.95**	**N/A**
	78.1	0.02	0.16	0.00	0.19	20.3	0.25	0.05	**99.2**	1.97	0.00	0.00	0.00	0.00	**1.98**	1.01	0.00	0.00	**1.02**	**3.00**	**1.94**	**N/A**
	75.6	0.08	0.51	0.05	0.21	21.6	0.00	0.05	**98.1**	1.90	0.00	0.00	0.01	0.00	**1.92**	1.08	0.00	0.00	**1.08**	**3.00**	**1.78**	**N/A**
	76.4	0.04	0.39	0.21	0.21	21.5	0.00	0.11	**98.9**	1.91	0.00	0.00	0.01	0.00	**1.93**	1.07	0.00	0.00	**1.07**	**3.00**	**1.80**	**N/A**
Mean (n=10)	**77.2**	**0.03**	**0.23**	**0.10**	**0.17**	**20.8**	**0.15**	**0.09**	**98.9**	**1.94**	**0.00**	**0.00**	**0.01**	**0.00**	**1.95**	**1.04**	**0.00**	**0.00**	**1.04**	**3.00**	**1.88**	**N/A**
Std Dev	**1.37**	**0.04**	**0.22**	**0.09**	**0.06**	**0.51**	**0.17**	**0.04**	**0.62**	**0.03**	**0.00**	**0.00**	**0.01**	**0.00**	**0.03**	**0.02**	**0.00**	**0.00**	**0.02**	**0.01**	**0.07**	**N/A**

Table A2: Complete electron microanalysis data for bornite

Label	Cu	Ag	Fe	Pb	Bi	S	Te	Se	Total	Cu	Ag	Fe	Pb	Bi	Total M	S	Te	Se	S(+Te+Se)	Total	M/S	Cu/Fe
										Flormulae calculated 3 a.p.f.u												
PH10D550																						
3aTW	79.7	0.00	0.12	0.05	0.04	21.5	0.00	0.02	**101.4**	1.95	0.00	0.00	0.00	0.00	**1.96**	1.04	0.00	0.00	**1.04**	**3.00**	**1.87**	**N/A**
	80.1	0.00	0.70	0.03	0.04	20.9	0.45	0.03	**102.3**	1.96	0.00	0.00	0.02	0.00	**1.98**	1.01	0.01	0.00	**1.02**	**3.00**	**1.94**	**N/A**
	80.0	0.00	0.82	0.00	0.11	21.0	0.42	0.08	**102.4**	1.95	0.00	0.00	0.02	0.00	**1.98**	1.02	0.01	0.00	**1.02**	**3.00**	**1.93**	**N/A**
	79.7	0.00	0.59	0.16	0.12	20.9	0.42	0.03	**101.9**	1.96	0.00	0.00	0.02	0.00	**1.98**	1.02	0.01	0.00	**1.02**	**3.00**	**1.93**	**N/A**
	78.6	0.03	0.01	0.03	0.01	21.0	0.26	0.31	**100.3**	1.95	0.00	0.00	0.00	0.00	**1.96**	1.04	0.00	0.01	**1.04**	**3.00**	**1.87**	**N/A**
	78.7	0.06	0.03	0.04	0.00	21.2	0.18	0.31	**100.5**	1.95	0.00	0.00	0.00	0.00	**1.95**	1.04	0.00	0.01	**1.05**	**3.00**	**1.86**	**N/A**
	78.4	0.00	0.01	0.02	0.00	21.0	0.03	0.25	**99.7**	1.96	0.00	0.00	0.00	0.00	**1.96**	1.04	0.00	0.00	**1.04**	**3.00**	**1.87**	**N/A**
	77.8	0.02	0.00	0.01	0.13	20.9	0.55	0.41	**99.8**	1.95	0.00	0.00	0.00	0.00	**1.95**	1.03	0.01	0.01	**1.05**	**3.00**	**1.86**	**N/A**
	78.8	0.02	0.00	0.00	0.08	20.0	0.59	0.31	**99.8**	1.99	0.00	0.00	0.00	0.00	**1.99**	1.00	0.01	0.01	**1.01**	**3.00**	**1.97**	**N/A**
	78.1	0.02	0.00	0.04	0.02	20.7	0.61	0.40	**99.9**	1.95	0.00	0.00	0.00	0.00	**1.96**	1.03	0.01	0.01	**1.04**	**3.00**	**1.87**	**N/A**
	77.7	0.02	0.02	0.10	0.14	22.4	0.88	0.11	**101.3**	1.90	0.00	0.00	0.00	0.00	**1.90**	1.09	0.01	0.00	**1.10**	**3.00**	**1.73**	**N/A**
	78.1	0.00	0.07	0.08	0.08	23.0	0.14	0.03	**101.4**	1.89	0.00	0.00	0.00	0.00	**1.89**	1.10	0.00	0.00	**1.11**	**3.00**	**1.71**	**N/A**
	80.4	0.01	0.11	0.03	0.11	21.2	0.36	0.05	**102.3**	1.96	0.00	0.00	0.00	0.00	**1.97**	1.03	0.00	0.00	**1.03**	**3.00**	**1.90**	**N/A**
	79.5	0.00	0.09	0.00	0.10	21.4	0.50	0.08	**101.7**	1.95	0.00	0.00	0.00	0.00	**1.95**	1.04	0.01	0.00	**1.05**	**3.00**	**1.86**	**N/A**
Mean (n=15)	**79.0**	**0.0**	**0.2**	**0.0**	**0.1**	**21.2**	**0.4**	**0.2**	**101.1**	**1.9**	**0.0**	**0.0**	**0.0**	**0.0**	**2.0**	**1.0**	**0.0**	**0.0**	**1.0**	**3.0**	**1.9**	**N/A**
Std Dev	**0.9**	**0.0**	**0.3**	**0.0**	**0.0**	**0.7**	**0.2**	**0.1**	**1.0**	**0.0**	**0.0**	**0.0**	**0.0**	**0.0**	**0.0**	**0.0**	**0.0**	**0.0**	**0.0**	**0.0**	**0.1**	**N/A**
3bTW	79.0	0.04	0.01	0.00	0.10	20.8	0.26	0.00	**100.2**	1.97	0.00	0.00	0.00	0.00	**1.97**	1.03	0.00	0.00	**1.03**	**3.00**	**1.91**	**N/A**
	77.5	0.02	1.26	0.06	0.11	23.4	0.15	0.04	**102.5**	1.85	0.00	0.00	0.03	0.00	**1.89**	1.11	0.00	0.00	**1.11**	**3.00**	**1.70**	**N/A**
	77.2	0.06	1.79	0.08	0.00	23.6	0.06	0.06	**102.8**	1.84	0.00	0.00	0.05	0.00	**1.89**	1.11	0.00	0.00	**1.11**	**3.00**	**1.69**	**N/A**
	79.6	0.04	0.56	0.06	0.07	20.7	0.02	0.01	**101.1**	1.97	0.00	0.00	0.02	0.00	**1.98**	1.01	0.00	0.00	**1.02**	**3.00**	**1.96**	**N/A**
	80.8	0.01	0.09	0.11	0.03	21.2	0.03	0.00	**102.3**	1.97	0.00	0.00	0.00	0.00	**1.97**	1.03	0.00	0.00	**1.03**	**3.00**	**1.92**	**N/A**
	80.2	0.05	0.36	0.01	0.08	20.7	0.40	0.09	**101.9**	1.97	0.00	0.00	0.01	0.00	**1.99**	1.01	0.00	0.00	**1.01**	**3.00**	**1.96**	**N/A**
	79.6	0.05	0.26	0.01	0.11	20.7	0.47	0.14	**101.4**	1.97	0.00	0.00	0.01	0.00	**1.98**	1.01	0.01	0.00	**1.02**	**3.00**	**1.93**	**N/A**
	78.8	0.01	0.03	0.03	0.00	20.9	0.49	0.48	**100.7**	1.96	0.00	0.00	0.00	0.00	**1.96**	1.03	0.01	0.01	**1.04**	**3.00**	**1.87**	**N/A**
	78.3	0.00	0.00	0.05	0.07	20.7	0.51	0.28	**99.9**	1.96	0.00	0.00	0.00	0.00	**1.96**	1.03	0.01	0.01	**1.04**	**3.00**	**1.89**	**N/A**
	78.7	0.00	0.01	0.05	0.06	20.8	0.50	0.30	**100.4**	1.96	0.00	0.00	0.00	0.00	**1.96**	1.03	0.01	0.01	**1.04**	**3.00**	**1.89**	**N/A**
Mean (n=10)	**79.0**	**0.0**	**0.4**	**0.0**	**0.1**	**21.3**	**0.3**	**0.1**	**101.3**	**1.9**	**0.0**	**0.0**	**0.0**	**0.0**	**2.0**	**1.0**	**0.0**	**0.0**	**1.0**	**3.0**	**1.9**	**N/A**
Std Dev	**1.1**	**0.02**	**0.62**	**0.03**	**0.04**	**1.1**	**0.21**	**0.16**	**1.0**	**0.05**	**0.00**	**0.00**	**0.02**	**0.00**	**0.04**	**0.04**	**0.00**	**0.00**	**0.04**	**0.00**	**0.10**	**N/A**
PH10D551																						
6TW	77.3	0.01	2.32	0.06	0.13	23.8	0.09	0.11	**103.8**	1.82	0.00	0.00	0.06	0.00	**1.89**	1.11	0.00	0.00	**1.11**	**3.00**	**1.69**	**N/A**
	74.5	0.02	1.75	0.10	0.09	27.1	0.07	0.16	**103.8**	1.71	0.00	0.00	0.05	0.00	**1.76**	1.24	0.00	0.00	**1.24**	**3.00**	**1.42**	**N/A**
	75.1	0.00	2.58	0.11	0.13	25.7	0.11	0.16	**104.0**	1.74	0.00	0.00	0.07	0.00	**1.81**	1.18	0.00	0.00	**1.19**	**3.00**	**1.53**	**N/A**
	77.7	0.01	1.95	0.11	0.09	23.7	0.13	0.19	**103.8**	1.83	0.00	0.00	0.05	0.00	**1.89**	1.11	0.00	0.00	**1.11**	**3.00**	**1.69**	**N/A**
	77.5	0.00	3.50	0.00	0.00	22.8	0.20	0.24	**104.3**	1.83	0.00	0.00	0.09	0.00	**1.92**	1.07	0.00	0.00	**1.08**	**3.00**	**1.79**	**N/A**
	78.4	0.00	0.09	0.08	0.26	20.7	0.00	0.58	**100.1**	1.96	0.00	0.00	0.00	0.00	**1.97**	1.02	0.00	0.01	**1.03**	**3.00**	**1.90**	**N/A**
	79.3	0.13	0.06	0.00	0.00	20.7	0.04	0.61	**100.9**	1.97	0.00	0.00	0.00	0.00	**1.97**	1.02	0.00	0.01	**1.03**	**3.00**	**1.91**	**N/A**
	78.0	0.04	0.08	0.01	0.02	21.1	0.12	0.47	**99.8**	1.95	0.00	0.00	0.00	0.00	**1.95**	1.04	0.00	0.01	**1.05**	**3.00**	**1.85**	**N/A**
	79.1	0.01	0.12	0.12	0.05	20.4	0.10	0.71	**100.6**	1.97	0.00	0.00	0.00	0.00	**1.98**	1.01	0.00	0.01	**1.02**	**3.00**	**1.93**	**N/A**
	79.4	0.00	0.28	0.00	0.04	20.5	0.07	0.70	**100.9**	1.97	0.00	0.00	0.01	0.00	**1.98**	1.01	0.00	0.01	**1.02**	**3.00**	**1.94**	**N/A**
	78.0	0.05	0.39	0.02	0.21	19.0	0.10	0.69	**98.5**	2.00	0.00	0.00	0.01	0.00	**2.02**	0.97	0.00	0.01	**0.98**	**3.00**	**2.05**	**N/A**
	79.1	0.00	0.23	0.10	0.09	20.6	0.07	0.34	**100.6**	1.97	0.00	0.00	0.01	0.00	**1.98**	1.01	0.00	0.01	**1.02**	**3.00**	**1.93**	**N/A**
	79.0	0.00	0.11	0.01	0.00	21.1	0.00	0.46	**100.7**	1.95	0.00	0.00	0.00	0.00	**1.96**	1.03	0.00	0.01	**1.04**	**3.00**	**1.88**	**N/A**
	78.8	0.00	0.27	0.00	0.00	20.5	0.02	0.46	**100.0**	1.97	0.00	0.00	0.01	0.00	**1.98**	1.01	0.00	0.01	**1.02**	**3.00**	**1.93**	**N/A**
	79.0	0.00	0.12	0.00	0.17	20.3	0.12	0.73	**100.4**	1.97	0.00	0.00	0.00	0.00	**1.98**	1.00	0.00	0.01	**1.02**	**3.00**	**1.94**	**N/A**
	78.9	0.00	0.13	0.00	0.18	20.7	0.11	0.48	**100.5**	1.96	0.00	0.00	0.00	0.00	**1.97**	1.02	0.00	0.01	**1.03**	**3.00**	**1.91**	**N/A**
	79.6	0.00	0.12	0.00	0.00	20.7	0.01	0.25	**100.7**	1.97	0.00	0.00	0.00	0.00	**1.98**	1.02	0.00	0.00	**1.02**	**3.00**	**1.94**	**N/A**
	78.4	0.00	0.09	0.00	0.00	20.9	0.08	0.38	**99.9**	1.96	0.00	0.00	0.00	0.00	**1.96**	1.03	0.00	0.01	**1.04**	**3.00**	**1.88**	**N/A**
	79.3	0.00	0.06	0.00	0.08	21.1	0.02	0.40	**100.9**	1.96	0.00	0.00	0.00	0.00	**1.96**	1.03	0.00	0.01	**1.04**	**3.00**	**1.89**	**N/A**
	79.5	0.00	0.05	0.00	0.31	20.5	0.03	0.57	**101.0**	1.98	0.00	0.00	0.00	0.00	**1.98**	1.01	0.00	0.01	**1.02**	**3.00**	**1.94**	**N/A**
	78.8	0.04	0.11	0.00	0.32	20.4	0.09	0.83	**100.6**	1.97	0.00	0.00	0.00	0.00	**1.97**	1.01	0.00	0.02	**1.03**	**3.00**	**1.92**	**N/A**
	78.9	0.00	0.12	0.07	0.37	20.5	0.06	0.65	**100.7**	1.97	0.00	0.00	0.00	0.00	**1.97**	1.01	0.00	0.01	**1.03**	**3.00**	**1.93**	**N/A**
	79.7	0.00	0.13	0.12	0.00	20.7	0.11	0.50	**101.2**	1.97	0.00	0.00	0.00	0.00	**1.98**	1.01	0.00	0.01	**1.02**	**3.00**	**1.93**	**N/A**
	79.4	0.00	0.20	0.03	0.00	20.5	0.03	0.46	**100.7**	1.97	0.00	0.00	0.01	0.00	**1.98**	1.01	0.00	0.01	**1.02**	**3.00**	**1.94**	**N/A**
Mean (n=24)	**78.5**	**0.01**	**0.62**	**0.04**	**0.11**	**21.4**	**0.07**	**0.46**	**101.2**	**1.93**	**0.00**	**0.00**	**0.02**	**0.00**	**1.95**	**1.04**	**0.00**	**0.01**	**1.05**	**3.00**	**1.9**	**N/A**
Std Dev	**1.3**	**0.03**	**1.0**	**0.05**	**0.12**	**1.9**	**0.05**	**0.20**	**1.5**	**0.08**	**0.00**	**0.00**	**0.03**	**0.00**	**0.1**	**0.06**	**0.00**	**0.00**	**0.06**	**0.00**	**0.14**	**N/A**
7TW1	80.6	0.00	0.81	0.03	0.00	20.8	0.00	0.11	**102.3**	1.97	0.00	0.00	0.02	0.00	**1.99**	1.00	0.00	0.00	**1.01**	**3.00**	**1.98**	**N/A**
8TW1	77.6	0.08	0.68	0.00	0.01	23.2	0.00	0.50	**102.1**	1.86	0.00	0.00	0.02	0.00	**1.88**	1.11	0.00	0.01	**1.12**	**3.00**	**1.69**	**N/A**
	77.6	0.13	0.55	0.05	0.11	22.9	0.01	0.43	**101.8**	1.88	0.00	0.00	0.02	0.00	**1.90**	1.10	0.00	0.01	**1.10**	**3.00**	**1.72**	**N/A**
	80.5	0.05	0.13	0.14	0.00	20.9	0.00	0.15	**101.9**	1.97	0.00	0.00	0.00	0.00	**1.98**	1.02	0.00	0.00	**1.02**	**3.00**	**1.94**	**N/A**
	80.1	0.02	0.47	0.12	0.11	21.0	0.01	0.46	**102.3**	1.96	0.00	0.00	0.01	0.00	**1.97**	1.02	0.00	0.01	**1.03**	**3.00**	**1.92**	**N/A**
	79.3	0.01	0.42	0.11	0.04	20.8	0.05	0.53	**101.2**	1.96	0.00	0.00	0.01	0.00	**1.97**	1.02	0.00	0.01	**1.03**	**3.00**	**1.92**	**N/A**
	78.6	0.10	0.91	0.10	0.02	22.5	0.00	0.64	**102.9**	1.89	0.00	0.00	0.02	0.00	**1.92**	1.07	0.00	0.01	**1.08**	**3.00**	**1.77**	**N/A**
Mean (n=6)	**79.0**	**0.06**	**0.53**	**0.09**	**0.05**	**21.9**	**0.01**	**0.45**	**102.0**	**1.92**	**0.00**	**0.00**	**0.01**	**0.00**	**1.94**	**1.05**	**0.00**	**0.01**	**1.06**	**3.00**	**1.82**	**N/A**
Std Dev	**1.23**	**0.05**	**0.26**	**0.05**	**0.05**	**1.10**	**0.02**	**0.16**	**0.55**	**0.05**	**0.00**	**0.00**	**0.01**	**0.00**	**0.04**	**0.04**	**0.00**	**0.00**	**0.04**	**0.00**	**0.11**	**N/A**
PH10D554																						
15TW	74.7	0.01	1.32	0.58	0.12	19.0	0.17	3.53	**99.4**	1.92	0.00	0.00	0.04	0.00	**1.96**	0.97	0.00	0.07	**1.04**	**3.00**	**1.88**	**N/A**
Mean (n=1)	**74.7**	**0.01**	**1.32**	**0.58**	**0.12**	**19.0**	**0.17**	**3.53**	**99.4**	**1.92**	**0.00**	**0.00**	**0.04**	**0.00**	**1.96**	**0.97**	**0.00**	**0.07**	**1.04**	**3.00**	**1.88**	**N/A**
17TW	81.3	0.00	0.03	0.12	0.14	20.6	0.06	0.03	**102.3**	2.00	0.00	0.00	0.00	0.00	**2.00**	1.00	0.00	0.00	**1.00**	**3.00**	**1.99**	**N/A**
	80.8	0.04	0.00	0.02	0.10	20.7	0.05	0.06	**101.8**	1.99	0.00	0.00	0.00	0.00	**1.99**	1.01	0.00	0.00	**1.01**	**3.00**	**1.97**	**N/A**
	79.2	0.17	0.47	0.07	0.09	19.7	0.00	0.05	**99.7**	2.00	0.00	0.00	0.01	0.00	**2.02**	0.98	0.00	0.00	**0.98**	**3.00**	**2.05**	**N/A**
	81.1	0.08	0.00	0.04	0.05	20.5	0.00	0.00	**101.8**	2.00	0.00	0.00	0.00	0.00	**2.00**	1.00	0.00	0.00	**1.00**	**3.00**	**2.00**	**N/A**
	81.7	0.00	0.00	0.00	0.06	20.7	0.05	0.01	**102.5**	2.00	0.00	0.00	0.00	0.00	**2.00**	1.00	0.00	0.00	**1.00**	**3.00**	**1.99**	**N/A**
	82.5	0.03	0.00	0.00	0.08	16.2	0.02	0.14	**99.0**	2.16	0.00	0.00	0.00	0.00	**2.16**	0.84	0.00	0.00	**0.84**	**3.00**	**2.56**	**N/A**
	81.0	0.05	0.02	0.09	0.02	21.0	0.08	0.01	**102.2**	1.98	0.00	0.00	0.00	0.00	**1.98**	1.02	0.00	0.00	**1.02**	**3.00**	**1.95**	**N/A**

Table A2: Complete electron microanalysis data for bornite (continued)

Label	Cu	Ag	Fe	Pb	Bi	S	Te	Se	Total	Cu	Ag	Fe	Pb	Bi	Total M	S	Te	Se	S(+Te+Se)	Total	M/S	Cu/Fe
										Flormulae calculated 3 a.p.f.u												
	81.6	0.00	0.01	0.00	0.00	20.6	0.00	0.01	**102.3**	2.00	0.00	0.00	0.00	0.00	**2.00**	1.00	0.00	0.00	**1.00**	**3.00**	**2.00**	**N/A**
	81.1	0.02	0.03	0.09	0.00	20.6	0.01	0.01	**101.8**	1.99	0.00	0.00	0.00	0.00	**1.99**	1.01	0.00	0.00	**1.01**	**3.00**	**1.98**	**N/A**
	81.5	0.01	0.02	0.06	0.11	20.7	0.01	0.03	**102.4**	2.00	0.00	0.00	0.00	0.00	**2.00**	1.00	0.00	0.00	**1.00**	**3.00**	**1.99**	**N/A**
	81.4	0.05	0.02	0.00	0.09	20.6	0.02	0.04	**102.2**	2.00	0.00	0.00	0.00	0.00	**2.00**	1.00	0.00	0.00	**1.00**	**3.00**	**2.00**	**N/A**
	81.7	0.00	0.00	0.03	0.00	20.7	0.00	0.01	**102.5**	2.00	0.00	0.00	0.00	0.00	**2.00**	1.00	0.00	0.00	**1.00**	**3.00**	**1.99**	**N/A**
	81.3	0.10	0.00	0.00	0.15	20.3	0.01	0.02	**101.9**	2.01	0.00	0.00	0.00	0.00	**2.01**	0.99	0.00	0.00	**0.99**	**3.00**	**2.02**	**N/A**
	83.8	0.01	0.01	0.00	0.08	18.7	0.02	0.00	**102.6**	2.08	0.00	0.00	0.00	0.00	**2.08**	0.92	0.00	0.00	**0.92**	**3.00**	**2.26**	**N/A**
	82.6	0.05	0.01	0.00	0.06	20.0	0.00	0.03	**102.7**	2.03	0.00	0.00	0.00	0.00	**2.03**	0.97	0.00	0.00	**0.97**	**3.00**	**2.09**	**N/A**
	81.8	0.00	0.00	0.00	0.11	20.9	0.03	0.03	**102.8**	1.99	0.00	0.00	0.00	0.00	**1.99**	1.01	0.00	0.00	**1.01**	**3.00**	**1.97**	**N/A**
	82.5	0.05	0.02	0.07	0.08	19.1	0.01	0.03	**101.9**	2.05	0.00	0.00	0.00	0.00	**2.06**	0.94	0.00	0.00	**0.94**	**3.00**	**2.18**	**N/A**
	81.7	0.06	0.00	0.00	0.12	20.7	0.00	0.02	**102.6**	2.00	0.00	0.00	0.00	0.00	**2.00**	1.00	0.00	0.00	**1.00**	**3.00**	**1.99**	**N/A**
	80.3	0.02	0.05	0.00	0.03	21.5	0.00	0.00	**101.9**	1.96	0.00	0.00	0.00	0.00	**1.96**	1.04	0.00	0.00	**1.04**	**3.00**	**1.89**	**N/A**
	81.4	0.05	0.01	0.10	0.17	20.7	0.02	0.01	**102.5**	1.99	0.00	0.00	0.00	0.00	**2.00**	1.00	0.00	0.00	**1.00**	**3.00**	**1.99**	**N/A**
	81.3	0.03	0.13	0.04	0.16	21.0	0.01	0.05	**102.8**	1.98	0.00	0.00	0.00	0.00	**1.99**	1.01	0.00	0.00	**1.01**	**3.00**	**1.96**	**N/A**
	81.6	0.04	0.02	0.06	0.07	20.6	0.02	0.03	**102.4**	2.00	0.00	0.00	0.00	0.00	**2.00**	1.00	0.00	0.00	**1.00**	**3.00**	**2.00**	**N/A**
	82.1	0.08	0.02	0.00	0.04	20.4	0.04	0.04	**102.7**	2.01	0.00	0.00	0.00	0.00	**2.01**	0.99	0.00	0.00	**0.99**	**3.00**	**2.02**	**N/A**
	81.5	0.00	0.05	0.02	0.06	20.9	0.04	0.05	**102.6**	1.99	0.00	0.00	0.00	0.00	**1.99**	1.01	0.00	0.00	**1.01**	**3.00**	**1.96**	**N/A**
	81.7	0.05	0.06	0.02	0.04	20.9	0.00	0.02	**102.8**	1.99	0.00	0.00	0.00	0.00	**1.99**	1.01	0.00	0.00	**1.01**	**3.00**	**1.97**	**N/A**
	81.2	0.00	0.04	0.05	0.07	21.0	0.02	0.02	**102.4**	1.98	0.00	0.00	0.00	0.00	**1.98**	1.01	0.00	0.00	**1.02**	**3.00**	**1.95**	**N/A**
	82.6	0.06	0.00	0.11	0.13	19.9	0.01	0.04	**102.9**	2.03	0.00	0.00	0.00	0.00	**2.03**	0.97	0.00	0.00	**0.97**	**3.00**	**2.10**	**N/A**
	81.7	0.01	0.01	0.19	0.07	20.5	0.03	0.08	**102.6**	2.00	0.00	0.00	0.00	0.00	**2.00**	0.99	0.00	0.00	**1.00**	**3.00**	**2.01**	**N/A**
	81.4	0.04	0.00	0.00	0.02	20.7	0.00	0.06	**102.1**	1.99	0.00	0.00	0.00	0.00	**1.99**	1.00	0.00	0.00	**1.01**	**3.00**	**1.98**	**N/A**
	81.6	0.00	0.00	0.08	0.10	21.1	0.02	0.00	**102.9**	1.98	0.00	0.00	0.00	0.00	**1.98**	1.02	0.00	0.00	**1.02**	**3.00**	**1.95**	**N/A**
	81.6	0.11	0.00	0.00	0.08	20.4	0.02	0.00	**102.2**	2.01	0.00	0.00	0.00	0.00	**2.01**	0.99	0.00	0.00	**0.99**	**3.00**	**2.02**	**N/A**
	81.9	0.02	0.00	0.09	0.15	20.4	0.03	0.04	**102.7**	2.01	0.00	0.00	0.00	0.00	**2.01**	0.99	0.00	0.00	**0.99**	**3.00**	**2.02**	**N/A**
	80.8	0.00	0.05	0.04	0.12	21.3	0.00	0.01	**102.3**	1.97	0.00	0.00	0.00	0.00	**1.97**	1.03	0.00	0.00	**1.03**	**3.00**	**1.92**	**N/A**
	81.7	0.00	0.04	0.04	0.10	20.8	0.00	0.01	**102.7**	1.99	0.00	0.00	0.00	0.00	**2.00**	1.00	0.00	0.00	**1.00**	**3.00**	**1.99**	**N/A**
	81.6	0.00	0.04	0.02	0.00	20.5	0.00	0.01	**102.3**	2.00	0.00	0.00	0.00	0.00	**2.00**	1.00	0.00	0.00	**1.00**	**3.00**	**2.01**	**N/A**
	81.7	0.08	0.04	0.02	0.05	20.8	0.00	0.02	**102.7**	1.99	0.00	0.00	0.00	0.00	**2.00**	1.00	0.00	0.00	**1.00**	**3.00**	**1.99**	**N/A**
	81.1	0.00	0.00	0.00	0.00	20.8	0.02	0.04	**102.0**	1.99	0.00	0.00	0.00	0.00	**1.99**	1.01	0.00	0.00	**1.01**	**3.00**	**1.96**	**N/A**
	81.2	0.00	0.00	0.00	0.06	20.6	0.01	0.00	**101.8**	2.00	0.00	0.00	0.00	0.00	**2.00**	1.00	0.00	0.00	**1.00**	**3.00**	**1.99**	**N/A**
	81.3	0.08	0.00	0.04	0.07	20.7	0.00	0.00	**102.2**	1.99	0.00	0.00	0.00	0.00	**1.99**	1.01	0.00	0.00	**1.01**	**3.00**	**1.98**	**N/A**
	81.4	0.00	0.01	0.06	0.00	20.9	0.02	0.01	**102.4**	1.99	0.00	0.00	0.00	0.00	**1.99**	1.01	0.00	0.00	**1.01**	**3.00**	**1.96**	**N/A**
	81.2	0.00	0.02	0.00	0.00	20.8	0.02	0.00	**102.1**	1.99	0.00	0.00	0.00	0.00	**1.99**	1.01	0.00	0.00	**1.01**	**3.00**	**1.97**	**N/A**
	80.7	0.02	0.00	0.00	0.11	20.6	0.00	0.04	**101.4**	1.99	0.00	0.00	0.00	0.00	**1.99**	1.01	0.00	0.00	**1.01**	**3.00**	**1.98**	**N/A**
	80.6	0.02	0.02	0.06	0.00	21.0	0.01	0.01	**101.7**	1.98	0.00	0.00	0.00	0.00	**1.98**	1.02	0.00	0.00	**1.02**	**3.00**	**1.94**	**N/A**
	81.2	0.00	0.00	0.07	0.10	20.7	0.00	0.00	**102.1**	1.99	0.00	0.00	0.00	0.00	**1.99**	1.01	0.00	0.00	**1.01**	**3.00**	**1.98**	**N/A**
	81.2	0.00	0.01	0.12	0.15	20.5	0.02	0.01	**102.0**	2.00	0.00	0.00	0.00	0.00	**2.00**	1.00	0.00	0.00	**1.00**	**3.00**	**2.00**	**N/A**
	81.3	0.04	0.00	0.10	0.13	20.8	0.00	0.00	**102.4**	1.99	0.00	0.00	0.00	0.00	**1.99**	1.01	0.00	0.00	**1.01**	**3.00**	**1.98**	**N/A**
Mean (n=46)	**81.5**	**0.03**	**0.03**	**0.04**	**0.07**	**20.5**	**0.02**	**0.02**	**102.2**	**2.00**	**0.00**	**0.00**	**0.00**	**0.00**	2.00	**1.00**	**0.00**	**0.00**	**1.00**	**3.00**	**2.01**	**N/A**
Std Dev	**0.69**	**0.04**	**0.07**	**0.04**	**0.05**	**0.81**	**0.02**	**0.03**	**0.71**	**0.03**	**0.00**	**0.00**	**0.00**	**0.00**	**0.03**	**0.03**	**0.00**	**0.00**	**0.03**	**0.00**	**0.10**	**N/A**
21TW	80.9	0.00	0.27	0.11	0.07	21.5	0.02	0.06	**102.9**	1.96	0.00	0.00	0.01	0.00	**1.97**	1.03	0.00	0.00	**1.03**	**3.00**	**1.91**	**N/A**
	80.9	0.08	0.19	0.02	0.02	21.4	0.06	0.05	**102.7**	1.96	0.00	0.00	0.01	0.00	**1.97**	1.03	0.00	0.00	**1.03**	**3.00**	**1.91**	**N/A**
	80.7	0.11	0.09	0.00	0.02	21.8	0.06	0.02	**102.7**	1.95	0.00	0.00	0.00	0.00	**1.95**	1.04	0.00	0.00	**1.05**	**3.00**	**1.87**	**N/A**
	80.2	0.03	0.27	0.03	0.11	21.8	0.01	0.04	**102.5**	1.94	0.00	0.00	0.01	0.00	**1.95**	1.05	0.00	0.00	**1.05**	**3.00**	**1.87**	**N/A**
	81.1	0.08	0.19	0.05	0.00	21.1	0.00	0.08	**102.7**	1.97	0.00	0.00	0.01	0.00	**1.98**	1.02	0.00	0.00	**1.02**	**3.00**	**1.94**	**N/A**
	80.8	0.00	0.13	0.00	0.15	21.8	0.00	0.04	**102.9**	1.95	0.00	0.00	0.00	0.00	**1.96**	1.04	0.00	0.00	**1.04**	**3.00**	**1.87**	**N/A**
	80.8	0.05	0.11	0.11	0.02	21.5	0.00	0.04	**102.6**	1.96	0.00	0.00	0.00	0.00	**1.97**	1.03	0.00	0.00	**1.03**	**3.00**	**1.90**	**N/A**
	80.4	0.09	0.15	0.07	0.06	21.3	0.05	0.00	**102.2**	1.96	0.00	0.00	0.00	0.00	**1.97**	1.03	0.00	0.00	**1.03**	**3.00**	**1.91**	**N/A**
	80.7	0.08	0.16	0.18	0.10	21.6	0.03	0.05	**102.9**	1.95	0.00	0.00	0.00	0.00	**1.96**	1.04	0.00	0.00	**1.04**	**3.00**	**1.89**	**N/A**
	80.2	0.09	0.20	0.00	0.08	21.4	0.03	0.05	**102.0**	1.96	0.00	0.00	0.01	0.00	**1.96**	1.03	0.00	0.00	**1.04**	**3.00**	**1.90**	**N/A**
	80.7	0.07	0.26	0.00	0.07	21.5	0.00	0.07	**102.6**	1.96	0.00	0.00	0.01	0.00	**1.97**	1.03	0.00	0.00	**1.03**	**3.00**	**1.90**	**N/A**
	80.5	0.17	0.39	0.14	0.04	21.3	0.00	0.09	**102.6**	1.96	0.00	0.00	0.01	0.00	**1.97**	1.03	0.00	0.00	**1.03**	**3.00**	**1.92**	**N/A**
	80.7	0.07	0.22	0.07	0.00	20.6	0.00	0.08	**101.7**	1.98	0.00	0.00	0.01	0.00	**1.99**	1.01	0.00	0.00	**1.01**	**3.00**	**1.98**	**N/A**
	81.6	0.00	0.09	0.11	0.03	21.1	0.00	0.04	**103.0**	1.98	0.00	0.00	0.00	0.00	**1.99**	1.01	0.00	0.00	**1.01**	**3.00**	**1.96**	**N/A**
	81.7	0.06	0.03	0.06	0.17	20.8	0.00	0.01	**102.8**	1.99	0.00	0.00	0.00	0.00	**2.00**	1.00	0.00	0.00	**1.00**	**3.00**	**1.99**	**N/A**
	81.8	0.04	0.03	0.18	0.01	20.9	0.00	0.00	**102.9**	1.99	0.00	0.00	0.00	0.00	**1.99**	1.01	0.00	0.00	**1.01**	**3.00**	**1.98**	**N/A**
	81.2	0.01	0.11	0.00	0.16	21.3	0.00	0.04	**102.8**	1.97	0.00	0.00	0.00	0.00	**1.98**	1.02	0.00	0.00	**1.02**	**3.00**	**1.93**	**N/A**
	81.3	0.01	0.12	0.07	0.12	21.2	0.04	0.02	**102.9**	1.97	0.00	0.00	0.00	0.00	**1.98**	1.02	0.00	0.00	**1.02**	**3.00**	**1.94**	**N/A**
	81.7	0.00	0.33	0.09	0.10	20.6	0.00	0.03	**102.9**	1.99	0.00	0.00	0.01	0.00	**2.00**	1.00	0.00	0.00	**1.00**	**3.00**	**2.01**	**N/A**
	81.4	0.05	0.51	0.01	0.13	20.7	0.00	0.00	**102.8**	1.98	0.00	0.00	0.01	0.00	**2.00**	1.00	0.00	0.00	**1.00**	**3.00**	**2.00**	**N/A**
	81.5	0.00	0.43	0.12	0.03	20.8	0.04	0.00	**102.8**	1.98	0.00	0.00	0.01	0.00	**2.00**	1.00	0.00	0.00	**1.00**	**3.00**	**1.99**	**N/A**
	81.6	0.10	0.49	0.11	0.00	19.1	0.00	0.03	**101.5**	2.04	0.00	0.00	0.01	0.00	**2.05**	0.95	0.00	0.00	**0.95**	**3.00**	**2.17**	**N/A**
	82.0	0.08	0.33	0.06	0.05	20.0	0.00	0.02	**102.6**	2.02	0.00	0.00	0.01	0.00	**2.03**	0.97	0.00	0.00	**0.97**	**3.00**	**2.08**	**N/A**
	83.4	0.00	0.21	0.07	0.13	18.9	0.01	0.08	**102.9**	2.06	0.00	0.00	0.01	0.00	**2.07**	0.93	0.00	0.00	**0.93**	**3.00**	**2.23**	**N/A**
	81.7	0.00	0.02	0.14	0.05	20.8	0.03	0.04	**102.7**	1.99	0.00	0.00	0.00	0.00	**1.99**	1.00	0.00	0.00	**1.01**	**3.00**	**1.98**	**N/A**
	81.6	0.03	0.04	0.05	0.00	21.0	0.05	0.03	**102.8**	1.99	0.00	0.00	0.00	0.00	**1.99**	1.01	0.00	0.00	**1.01**	**3.00**	**1.96**	**N/A**
	81.9	0.00	0.02	0.06	0.09	20.8	0.03	0.02	**102.8**	1.99	0.00	0.00	0.00	0.00	**2.00**	1.00	0.00	0.00	**1.00**	**3.00**	**1.99**	**N/A**
	81.6	0.02	0.05	0.14	0.17	20.8	0.05	0.01	**102.8**	1.99	0.00	0.00	0.00	0.00	**1.99**	1.00	0.00	0.00	**1.01**	**3.00**	**1.98**	**N/A**
Mean (n=28)	**81.2**	**0.05**	**0.20**	**0.07**	**0.07**	**20.97**	**0.02**	**0.04**	**102.6**	**1.98**	**0.00**	**0.00**	**0.01**	**0.00**	1.99	**1.01**	**0.00**	**0.00**	**1.01**	**3.00**	**1.96**	**N/A**
Std Dev	**0.69**	**0.04**	**0.14**	**0.05**	**0.06**	**0.69**	**0.02**	**0.03**	**0.36**	**0.03**	**0.00**	**0.00**	**0.00**	**0.00**	**0.03**	**0.03**	**0.00**	**0.00**	**0.03**	**0.00**	**0.08**	**N/A**
PH10D549																						
28TW	81.5	0.02	0.15	0.03	0.22	21.0	0.04	0.00	**103.0**	1.98	0.00	0.00	0.00	0.00	**1.99**	1.01	0.00	0.00	**1.01**	**3.00**	**1.96**	**N/A**
	81.5	0.04	0.10	0.02	0.00	20.7	0.01	0.00	**102.4**	1.99	0.00	0.00	0.00	0.00	**1.99**	1.01	0.00	0.00	**1.01**	**3.00**	**1.98**	**N/A**
	81.8	0.00	0.02	0.00	0.00	20.9	0.00	0.00	**102.7**	1.99	0.00	0.00	0.00	0.00	**1.99**	1.01	0.00	0.00	**1.01**	**3.00**	**1.97**	**N/A**
	81.6	0.00	0.01	0.08	0.05	20.8	0.00	0.00	**102.5**	1.99	0.00	0.00	0.00	0.00	**1.99**	1.01	0.00	0.00	**1.01**	**3.00**	**1.98**	**N/A**
	81.6	0.02	0.02	0.05	0.04	20.7	0.02	0.06	**102.5**	1.99	0.00	0.00	0.00	0.00	**1.99**	1.00	0.00	0.00	**1.01**	**3.00**	**1.98**	**N/A**
	82.0	0.00	0.01	0.00	0.08	20.5	0.00	0.00	**102.6**	2.00	0.00	0.00	0.00	0.00	**2.01**	0.99	0.00	0.00	**0.99**	**3.00**	**2.02**	**N/A**
	81.4	0.00	0.04	0.09	0.01	20.7	0.01	0.00	**102.3**	1.99	0.00	0.00	0.00	0.00	**1.99**	1.00	0.00	0.00	**1.01**	**3.00**	**1.98**	**N/A**

Table A2: Complete electron microanalysis data for bornite (continued)

Label	Cu	Ag	Fe	Pb	Bi	S	Te	Se	Total	Cu	Ag	Fe	Pb	Bi	Total M	S	Te	Se	S(+Te+Se)	Total	M/S	Cu/Fe
										Flormulae calculated 3 a.p.f.u												
	81.5	0.05	0.04	0.09	0.16	21.1	0.00	0.00	**103.0**	1.98	0.00	0.00	0.00	0.00	**1.98**	1.02	0.00	0.00	**1.02**	**3.00**	**1.95**	**N/A**
	81.7	0.00	0.11	0.04	0.00	20.8	0.01	0.00	**102.6**	1.99	0.00	0.00	0.00	0.00	**2.00**	1.00	0.00	0.00	**1.00**	**3.00**	**1.99**	**N/A**
	82.0	0.00	0.06	0.00	0.06	20.7	0.00	0.01	**102.8**	2.00	0.00	0.00	0.00	0.00	**2.00**	1.00	0.00	0.00	**1.00**	**3.00**	**2.00**	**N/A**
	81.9	0.08	0.03	0.02	0.02	20.9	0.02	0.02	**103.0**	1.99	0.00	0.00	0.00	0.00	**1.99**	1.01	0.00	0.00	**1.01**	**3.00**	**1.97**	**N/A**
	81.6	0.03	0.03	0.12	0.00	21.1	0.00	0.00	**102.8**	1.98	0.00	0.00	0.00	0.00	**1.99**	1.01	0.00	0.00	**1.01**	**3.00**	**1.96**	**N/A**
	81.7	0.17	0.00	0.00	0.10	20.3	0.00	0.00	**102.3**	2.01	0.00	0.00	0.00	0.00	**2.01**	0.99	0.00	0.00	**0.99**	**3.00**	**2.04**	**N/A**
	81.4	0.11	0.08	0.01	0.20	20.8	0.05	0.05	**102.7**	1.99	0.00	0.00	0.00	0.00	**1.99**	1.01	0.00	0.00	**1.01**	**3.00**	**1.97**	**N/A**
	81.8	0.00	0.04	0.00	0.07	21.0	0.00	0.03	**102.9**	1.99	0.00	0.00	0.00	0.00	**1.99**	1.01	0.00	0.00	**1.01**	**3.00**	**1.97**	**N/A**
	81.5	0.11	0.02	0.06	0.04	21.2	0.00	0.00	**102.9**	1.98	0.00	0.00	0.00	0.00	**1.98**	1.02	0.00	0.00	**1.02**	**3.00**	**1.94**	**N/A**
	81.5	0.07	0.04	0.00	0.03	21.0	0.01	0.02	**102.7**	1.98	0.00	0.00	0.00	0.00	**1.98**	1.01	0.00	0.00	**1.02**	**3.00**	**1.95**	**N/A**
	81.1	0.01	0.17	0.00	0.03	21.3	0.01	0.05	**102.7**	1.97	0.00	0.00	0.00	0.00	**1.98**	1.02	0.00	0.00	**1.02**	**3.00**	**1.93**	**N/A**
	80.3	0.03	0.14	0.00	0.00	20.8	0.01	0.05	**101.3**	1.98	0.00	0.00	0.00	0.00	**1.98**	1.02	0.00	0.00	**1.02**	**3.00**	**1.95**	**N/A**
	81.7	0.01	0.12	0.00	0.00	20.8	0.00	0.08	**102.7**	1.99	0.00	0.00	0.00	0.00	**1.99**	1.00	0.00	0.00	**1.01**	**3.00**	**1.98**	**N/A**
	81.0	0.04	0.39	0.00	0.00	20.7	0.00	0.07	**102.2**	1.98	0.00	0.00	0.01	0.00	**1.99**	1.00	0.00	0.00	**1.01**	**3.00**	**1.98**	**N/A**
	81.4	0.00	0.09	0.11	0.00	21.0	0.00	0.01	**102.6**	1.98	0.00	0.00	0.00	0.00	**1.98**	1.02	0.00	0.00	**1.02**	**3.00**	**1.95**	**N/A**
	81.7	0.06	0.11	0.03	0.09	21.0	0.00	0.00	**102.9**	1.98	0.00	0.00	0.00	0.00	**1.99**	1.01	0.00	0.00	**1.01**	**3.00**	**1.97**	**N/A**
Mean (n=23)	**81.5**	**0.04**	**0.08**	**0.03**	**0.05**	**20.87**	**0.01**	**0.02**	**102.6**	**1.99**	**0.00**	**0.00**	**0.00**	**0.00**	1.99	**1.01**	**0.00**	**0.00**	**1.01**	**3.00**	**1.97**	**N/A**
Std Dev	**0.36**	**0.04**	**0.08**	**0.04**	**0.07**	**0.22**	**0.01**	**0.03**	**0.36**	**0.01**	**0.00**	**0.00**	**0.00**	**0.00**	**0.01**	**0.01**	**0.00**	**0.00**	**0.01**	**0.00**	**0.02**	**N/A**
31TW	80.6	0.00	0.12	0.11	0.11	21.8	0.01	0.03	**102.7**	1.95	0.00	0.00	0.00	0.00	**1.95**	1.05	0.00	0.00	**1.05**	**3.00**	**1.87**	**N/A**
	81.0	0.00	0.09	0.13	0.23	21.4	0.00	0.00	**102.9**	1.96	0.00	0.00	0.00	0.00	**1.97**	1.03	0.00	0.00	**1.03**	**3.00**	**1.91**	**N/A**
	80.7	0.06	0.11	0.01	0.12	21.6	0.00	0.06	**102.6**	1.96	0.00	0.00	0.00	0.00	**1.96**	1.04	0.00	0.00	**1.04**	**3.00**	**1.89**	**N/A**
	80.9	0.05	0.15	0.12	0.13	21.5	0.00	0.00	**102.9**	1.96	0.00	0.00	0.00	0.00	**1.97**	1.03	0.00	0.00	**1.03**	**3.00**	**1.90**	**N/A**
Mean (n=4)	**77.8**	**0.04**	**0.09**	**0.04**	**0.07**	**20.12**	**0.01**	**0.02**	**98.2**	**1.90**	**0.00**	**0.00**	**0.00**	**0.00**	**1.90**	**0.97**	**0.00**	**0.00**	**0.97**	**2.87**	**1.87**	**N/A**
Std Dev	**0.20**	**0.03**	**0.03**	**0.06**	**0.06**	**0.16**	**0.01**	**0.03**	**0.12**	**0.01**	**0.00**	**0.00**	**0.00**	**0.00**	**0.01**	**0.01**	**0.00**	**0.00**	**0.01**	**0.00**	**0.02**	**N/A**
PH11D541																						
39aTW	80.1	0.00	0.03	0.02	0.09	20.0	0.03	0.04	**100.3**	2.01	0.00	0.00	0.00	0.00	**2.01**	0.99	0.00	0.00	**0.99**	**3.00**	**2.02**	**N/A**
	80.5	0.13	0.01	0.19	0.15	20.6	0.00	0.00	**101.6**	1.98	0.00	0.00	0.00	0.00	**1.99**	1.01	0.00	0.00	**1.01**	**3.00**	**1.98**	**N/A**
	80.4	0.00	0.05	0.00	0.16	20.4	0.01	0.03	**101.1**	1.99	0.00	0.00	0.00	0.00	**2.00**	1.00	0.00	0.00	**1.00**	**3.00**	**1.99**	**N/A**
	80.1	0.04	0.49	0.00	0.27	20.2	0.02	0.03	**101.1**	1.99	0.00	0.00	0.01	0.00	**2.00**	0.99	0.00	0.00	**1.00**	**3.00**	**2.01**	**N/A**
	80.2	0.00	0.01	0.01	0.02	20.5	0.00	0.00	**100.8**	1.99	0.00	0.00	0.00	0.00	**1.99**	1.01	0.00	0.00	**1.01**	**3.00**	**1.97**	**N/A**
	80.5	0.14	0.04	0.10	0.00	20.8	0.03	0.00	**101.6**	1.98	0.00	0.00	0.00	0.00	**1.99**	1.01	0.00	0.00	**1.01**	**3.00**	**1.96**	**N/A**
	80.7	0.00	0.02	0.00	0.00	20.3	0.00	0.12	**101.1**	2.00	0.00	0.00	0.00	0.00	**2.00**	1.00	0.00	0.00	**1.00**	**3.00**	**2.00**	**N/A**
	80.0	0.00	0.02	0.08	0.14	20.3	0.00	0.00	**100.6**	2.00	0.00	0.00	0.00	0.00	**2.00**	1.00	0.00	0.00	**1.00**	**3.00**	**1.99**	**N/A**
	80.5	0.09	0.03	0.08	0.08	20.4	0.02	0.00	**101.2**	1.99	0.00	0.00	0.00	0.00	**2.00**	1.00	0.00	0.00	**1.00**	**3.00**	**1.99**	**N/A**
	80.0	0.00	0.00	0.05	0.08	20.8	0.00	0.00	**100.9**	1.98	0.00	0.00	0.00	0.00	**1.98**	1.02	0.00	0.00	**1.02**	**3.00**	**1.94**	**N/A**
	81.1	0.07	0.01	0.16	0.17	20.3	0.00	0.00	**101.8**	2.00	0.00	0.00	0.00	0.00	**2.01**	0.99	0.00	0.00	**0.99**	**3.00**	**2.02**	**N/A**
	80.1	0.04	0.01	0.00	0.03	20.4	0.01	0.02	**100.7**	1.99	0.00	0.00	0.00	0.00	**1.99**	1.01	0.00	0.00	**1.01**	**3.00**	**1.98**	**N/A**
	79.8	0.05	0.00	0.07	0.27	20.3	0.00	0.00	**100.5**	1.99	0.00	0.00	0.00	0.00	**2.00**	1.00	0.00	0.00	**1.00**	**3.00**	**1.99**	**N/A**
	80.8	0.04	0.00	0.01	0.00	20.7	0.05	0.03	**101.6**	1.99	0.00	0.00	0.00	0.00	**1.99**	1.01	0.00	0.00	**1.01**	**3.00**	**1.97**	**N/A**
	79.8	0.05	0.02	0.03	0.00	20.4	0.00	0.02	**100.3**	1.99	0.00	0.00	0.00	0.00	**1.99**	1.01	0.00	0.00	**1.01**	**3.00**	**1.98**	**N/A**
	80.2	0.08	0.00	0.07	0.00	20.7	0.00	0.00	**101.1**	1.98	0.00	0.00	0.00	0.00	**1.98**	1.02	0.00	0.00	**1.02**	**3.00**	**1.95**	**N/A**
	80.4	0.00	0.00	0.00	0.02	20.8	0.00	0.01	**101.2**	1.98	0.00	0.00	0.00	0.00	**1.99**	1.01	0.00	0.00	**1.01**	**3.00**	**1.96**	**N/A**
	80.3	0.01	0.01	0.12	0.15	20.6	0.00	0.00	**101.2**	1.99	0.00	0.00	0.00	0.00	**1.99**	1.01	0.00	0.00	**1.01**	**3.00**	**1.97**	**N/A**
	80.6	0.03	0.00	0.00	0.00	20.7	0.01	0.00	**101.4**	1.99	0.00	0.00	0.00	0.00	**1.99**	1.01	0.00	0.00	**1.01**	**3.00**	**1.97**	**N/A**
	80.9	0.09	0.00	0.00	0.15	20.0	0.04	0.00	**101.2**	2.01	0.00	0.00	0.00	0.00	**2.01**	0.98	0.00	0.00	**0.98**	**3.00**	**2.05**	**N/A**
	80.3	0.05	0.00	0.20	0.09	20.1	0.01	0.07	**100.9**	2.00	0.00	0.00	0.00	0.00	**2.00**	0.99	0.00	0.00	**0.99**	**3.00**	**2.02**	**N/A**
	80.2	0.00	0.03	0.01	0.07	19.8	0.03	0.01	**100.2**	2.01	0.00	0.00	0.00	0.00	**2.01**	0.98	0.00	0.00	**0.98**	**3.00**	**2.04**	**N/A**
	80.5	0.00	0.01	0.03	0.03	20.7	0.03	0.04	**101.4**	1.98	0.00	0.00	0.00	0.00	**1.99**	1.01	0.00	0.00	**1.01**	**3.00**	**1.96**	**N/A**
	80.0	0.07	0.02	0.06	0.00	20.3	0.00	0.02	**100.5**	1.99	0.00	0.00	0.00	0.00	**2.00**	1.00	0.00	0.00	**1.00**	**3.00**	**1.99**	**N/A**
	80.1	0.00	0.02	0.03	0.00	20.8	0.00	0.00	**101.0**	1.98	0.00	0.00	0.00	0.00	**1.98**	1.02	0.00	0.00	**1.02**	**3.00**	**1.94**	**N/A**
	80.5	0.05	0.02	0.00	0.20	20.5	0.01	0.00	**101.3**	1.99	0.00	0.00	0.00	0.00	**2.00**	1.00	0.00	0.00	**1.00**	**3.00**	**1.99**	**N/A**
	79.4	0.00	0.02	0.15	0.09	21.1	0.09	0.00	**100.9**	1.96	0.00	0.00	0.00	0.00	**1.97**	1.03	0.00	0.00	**1.03**	**3.00**	**1.90**	**N/A**
	80.6	0.02	0.02	0.04	0.00	20.4	0.04	0.02	**101.2**	2.00	0.00	0.00	0.00	0.00	**2.00**	1.00	0.00	0.00	**1.00**	**3.00**	**1.99**	**N/A**
	79.6	0.00	0.14	0.04	0.14	20.6	0.02	0.06	**100.6**	1.98	0.00	0.00	0.00	0.00	**1.98**	1.01	0.00	0.00	**1.02**	**3.00**	**1.95**	**N/A**
	79.4	0.04	0.49	0.00	0.09	20.6	0.02	0.13	**100.8**	1.97	0.00	0.00	0.01	0.00	**1.98**	1.01	0.00	0.00	**1.01**	**3.00**	**1.96**	**N/A**
Mean (n=30)	**80.3**	**0.04**	**0.05**	**0.05**	**0.08**	**20.47**	**0.02**	**0.02**	**101.0**	**1.99**	**0.00**	**0.00**	**0.00**	**0.00**	1.99	**1.01**	**0.00**	**0.00**	**1.01**	**3.00**	**1.98**	**N/A**
Std Dev	**0.40**	**0.04**	**0.12**	**0.06**	**0.08**	**0.29**	**0.02**	**0.03**	**0.42**	**0.01**	**0.00**	**0.00**	**0.00**	**0.00**	**0.01**	**0.01**	**0.00**	**0.00**	**0.01**	**0.00**	**0.03**	**N/A**
39bTW	80.5	0.00	0.24	0.01	0.05	20.5	0.01	0.03	**101.4**	1.99	0.00	0.00	0.01	0.00	**2.00**	1.00	0.00	0.00	**1.00**	**3.00**	**1.99**	**N/A**
	80.2	0.03	0.40	0.04	0.21	20.4	0.00	0.00	**101.4**	1.98	0.00	0.00	0.01	0.00	**2.00**	1.00	0.00	0.00	**1.00**	**3.00**	**1.99**	**N/A**
	80.7	0.00	0.07	0.00	0.12	20.3	0.01	0.02	**101.2**	2.00	0.00	0.00	0.00	0.00	**2.00**	1.00	0.00	0.00	**1.00**	**3.00**	**2.00**	**N/A**
	80.9	0.00	0.11	0.11	0.04	20.3	0.01	0.00	**101.5**	2.00	0.00	0.00	0.00	0.00	**2.00**	1.00	0.00	0.00	**1.00**	**3.00**	**2.01**	**N/A**
	80.5	0.07	0.04	0.00	0.02	20.5	0.00	0.00	**101.2**	1.99	0.00	0.00	0.00	0.00	**1.99**	1.01	0.00	0.00	**1.01**	**3.00**	**1.98**	**N/A**
	80.5	0.00	0.03	0.00	0.06	20.7	0.01	0.02	**101.3**	1.99	0.00	0.00	0.00	0.00	**1.99**	1.01	0.00	0.00	**1.01**	**3.00**	**1.97**	**N/A**
	80.3	0.09	0.04	0.00	0.18	20.5	0.08	0.00	**101.2**	1.99	0.00	0.00	0.00	0.00	**1.99**	1.00	0.00	0.00	**1.01**	**3.00**	**1.98**	**N/A**
	80.8	0.07	0.03	0.00	0.14	20.8	0.06	0.07	**102.0**	1.98	0.00	0.00	0.00	0.00	**1.99**	1.01	0.00	0.00	**1.01**	**3.00**	**1.96**	**N/A**
	80.5	0.01	0.05	0.04	0.05	20.8	0.03	0.00	**101.5**	1.98	0.00	0.00	0.00	0.00	**1.98**	1.02	0.00	0.00	**1.02**	**3.00**	**1.95**	**N/A**
	80.6	0.05	0.15	0.03	0.00	20.8	0.03	0.07	**101.9**	1.98	0.00	0.00	0.00	0.00	**1.98**	1.01	0.00	0.00	**1.01**	**3.00**	**1.95**	**N/A**
Mean (n=10)	**80.5**	**0.03**	**0.12**	**0.02**	**0.09**	**20.56**	**0.02**	**0.02**	**101.5**	**1.99**	**0.00**	**0.00**	**0.00**	**0.00**	1.99	**1.01**	**0.00**	**0.00**	**1.01**	**3.00**	**1.98**	**N/A**
Std Dev	**0.22**	**0.04**	**0.12**	**0.03**	**0.07**	**0.19**	**0.03**	**0.03**	**0.28**	**0.01**	**0.00**	**0.00**	**0.00**	**0.00**	**0.01**	**0.01**	**0.00**	**0.00**	**0.01**	**0.00**	**0.02**	**N/A**
PH11D576																						
40TW	80.0	0.05	0.02	0.00	0.00	20.8	0.02	0.00	**100.9**	1.98	0.00	0.00	0.00	0.00	**1.98**	1.02	0.00	0.00	**1.02**	**3.00**	**1.94**	**N/A**
	80.4	0.00	0.00	0.04	0.03	20.5	0.01	0.02	**101.1**	1.99	0.00	0.00	0.00	0.00	**1.99**	1.01	0.00	0.00	**1.01**	**3.00**	**1.98**	**N/A**
	80.0	0.00	0.00	0.14	0.05	20.6	0.03	0.00	**100.8**	1.99	0.00	0.00	0.00	0.00	**1.99**	1.01	0.00	0.00	**1.01**	**3.00**	**1.97**	**N/A**
	80.5	0.04	0.05	0.00	0.13	20.3	0.00	0.00	**101.2**	2.00	0.00	0.00	0.00	0.00	**2.00**	1.00	0.00	0.00	**1.00**	**3.00**	**2.00**	**N/A**
	79.8	0.07	0.05	0.00	0.11	20.6	0.07	0.05	**100.8**	1.98	0.00	0.00	0.00	0.00	**1.98**	1.01	0.00	0.00	**1.01**	**3.00**	**1.95**	**N/A**
	80.1	0.02	0.08	0.16	0.04	20.4	0.00	0.02	**100.8**	1.99	0.00	0.00	0.00	0.00	**2.00**	1.00	0.00	0.00	**1.00**	**3.00**	**1.99**	**N/A**
	79.9	0.20	0.10	0.16	0.06	20.7	0.08	0.07	**101.3**	1.98	0.00	0.00	0.00	0.00	**1.98**	1.01	0.00	0.00	**1.02**	**3.00**	**1.95**	**N/A**
	80.1	0.07	0.11	0.04	0.05	20.4	0.02	0.03	**100.8**	1.99	0.00	0.00	0.00	0.00	**1.99**	1.00	0.00	0.00	**1.00**	**3.00**	**1.98**	**N/A**

Table A2: Complete electron microanalysis data for bornite (continued)

Label	Cu	Ag	Fe	Pb	Bi	S	Te	Se	Total	Cu	Ag	Fe	Pb	Bi	Total M	S	Te	Se	S(+Te+Se)	Total	M/S	Cu/Fe
										Flormulae calculated 3 a.p.f.u												
	79.8	0.02	0.11	0.11	0.11	20.6	0.00	0.00	**100.8**	1.98	0.00	0.00	0.00	0.00	**1.99**	1.01	0.00	0.00	**1.01**	**3.00**	**1.96**	**N/A**
	79.9	0.00	0.28	0.04	0.07	20.6	0.00	0.00	**100.8**	1.98	0.00	0.00	0.01	0.00	**1.99**	1.01	0.00	0.00	**1.01**	**3.00**	**1.97**	**N/A**
	80.3	0.06	0.02	0.21	0.09	20.4	0.00	0.10	**101.3**	1.99	0.00	0.00	0.00	0.00	**1.99**	1.00	0.00	0.00	**1.00**	**3.00**	**1.99**	**N/A**
	80.6	0.04	0.02	0.01	0.09	20.5	0.00	0.03	**101.4**	1.99	0.00	0.00	0.00	0.00	**1.99**	1.00	0.00	0.00	**1.00**	**3.00**	**1.98**	**N/A**
	80.4	0.05	0.00	0.00	0.19	20.6	0.00	0.00	**101.2**	1.99	0.00	0.00	0.00	0.00	**1.99**	1.01	0.00	0.00	**1.01**	**3.00**	**1.97**	**N/A**
	80.6	0.00	0.01	0.00	0.16	20.4	0.03	0.07	**101.3**	2.00	0.00	0.00	0.00	0.00	**2.00**	1.00	0.00	0.00	**1.00**	**3.00**	**1.99**	**N/A**
	79.3	0.17	0.17	0.18	0.17	20.2	0.00	0.03	**100.3**	1.98	0.00	0.00	0.00	0.00	**2.00**	1.00	0.00	0.00	**1.00**	**3.00**	**1.99**	**N/A**
	79.9	0.13	0.01	0.26	0.11	20.6	0.05	0.00	**101.1**	1.98	0.00	0.00	0.00	0.00	**1.99**	1.01	0.00	0.00	**1.01**	**3.00**	**1.96**	**N/A**
	79.9	0.00	0.04	0.26	0.00	20.4	0.00	0.04	**100.7**	1.99	0.00	0.00	0.00	0.00	**1.99**	1.01	0.00	0.00	**1.01**	**3.00**	**1.98**	**N/A**
	80.1	0.00	0.54	0.12	0.14	20.2	0.00	0.00	**101.2**	1.99	0.00	0.00	0.02	0.00	**2.00**	0.99	0.00	0.00	**0.99**	**3.00**	**2.01**	**N/A**
	80.3	0.00	0.02	0.00	0.06	20.6	0.01	0.00	**101.1**	1.99	0.00	0.00	0.00	0.00	**1.99**	1.01	0.00	0.00	**1.01**	**3.00**	**1.97**	**N/A**
	80.0	0.09	0.25	0.10	0.00	20.3	0.00	0.00	**100.8**	1.99	0.00	0.00	0.01	0.00	**2.00**	1.00	0.00	0.00	**1.00**	**3.00**	**2.00**	**N/A**
Mean (n=20)	**80.1**	**0.05**	**0.09**	**0.09**	**0.08**	**20.49**	**0.02**	**0.02**	**100.98**	**1.99**	**0.00**	**0.00**	**0.00**	**0.00**	**1.99**	**1.01**	**0.00**	**0.00**	**1.01**	**3.00**	**1.98**	**N/A**
Std Dev	**0.33**	**0.06**	**0.13**	**0.09**	**0.06**	**0.16**	**0.02**	**0.03**	**0.28**	**0.01**	**0.00**	**0.00**	**0.00**	**0.00**	**0.01**	**0.01**	**0.00**	**0.00**	**0.01**	**0.00**	**0.02**	**N/A**
41aTW	77.6	0.01	0.05	0.24	0.07	20.5	0.13	0.07	**98.6**	1.96	0.00	0.00	0.00	0.00	**1.97**	1.03	0.00	0.00	**1.03**	**3.00**	**1.91**	**N/A**
	77.8	0.04	0.10	0.00	0.25	20.6	0.40	0.12	**99.4**	1.96	0.00	0.00	0.00	0.00	**1.96**	1.03	0.01	0.00	**1.03**	**3.00**	**1.90**	**N/A**
	74.3	0.00	0.69	0.15	0.15	21.2	0.00	0.11	**98.1**	1.88	0.00	0.00	0.02	0.00	**1.90**	1.06	0.00	0.00	**1.07**	**2.97**	**1.79**	**N/A**
	78.2	0.12	0.09	0.00	0.18	20.8	0.00	0.12	**99.6**	1.96	0.00	0.00	0.00	0.00	**1.97**	1.03	0.00	0.00	**1.03**	**3.00**	**1.90**	**N/A**
	77.6	0.00	0.05	0.04	0.22	20.7	0.00	0.02	**98.7**	1.96	0.00	0.00	0.00	0.00	**1.96**	1.03	0.00	0.00	**1.03**	**3.00**	**1.90**	**N/A**
	77.6	0.00	0.11	0.14	0.12	20.3	0.36	0.12	**98.8**	1.97	0.00	0.00	0.00	0.00	**1.97**	1.02	0.00	0.00	**1.03**	**3.00**	**1.93**	**N/A**
	78.8	0.00	0.15	0.18	0.07	20.4	0.34	0.12	**100.1**	1.97	0.00	0.00	0.00	0.00	**1.98**	1.01	0.00	0.00	**1.02**	**3.00**	**1.95**	**N/A**
	78.1	0.02	0.16	0.00	0.19	20.3	0.25	0.05	**99.2**	1.97	0.00	0.00	0.00	0.00	**1.98**	1.01	0.00	0.00	**1.02**	**3.00**	**1.94**	**N/A**
	75.6	0.08	0.51	0.05	0.21	21.6	0.00	0.05	**98.1**	1.90	0.00	0.00	0.01	0.00	**1.92**	1.08	0.00	0.00	**1.08**	**3.00**	**1.78**	**N/A**
	76.4	0.04	0.39	0.21	0.21	21.5	0.00	0.11	**98.9**	1.91	0.00	0.00	0.01	0.00	**1.93**	1.07	0.00	0.00	**1.07**	**3.00**	**1.80**	**N/A**
Mean (n=10)	**77.2**	**0.03**	**0.23**	**0.10**	**0.17**	**20.8**	**0.15**	**0.09**	**98.9**	**1.94**	**0.00**	**0.00**	**0.01**	**0.00**	**1.95**	**1.04**	**0.00**	**0.00**	**1.04**	**3.00**	**1.88**	**N/A**
Std Dev	**1.37**	**0.04**	**0.22**	**0.09**	**0.06**	**0.51**	**0.17**	**0.04**	**0.62**	**0.03**	**0.00**	**0.00**	**0.01**	**0.00**	**0.03**	**0.02**	**0.00**	**0.00**	**0.02**	**0.01**	**0.07**	**N/A**

Table A3: Complete electron microanalysis data for Au-Cu phases

	Au9Cu 3aTW	Au9Cu 3aTW	Au9Cu 3aTW	Au9Cu 3aTW	Au9Cu 3aTW	Au9Cu 3aTW	Au9Cu 3aTW	Au9Cu 3aTW	Au9Cu 3bTW	Au9Cu 3bTW	Au9Cu 3bTW	Au9Cu 3bTW	Au9Cu 3bTW	Au9Cu 3bTW	Au9Cu 3bTW	Au9Cu 3bTW	Au9Cu 3bTW	**Au9Cu Mean**	**n=20 Std.dev**
S	0.03	0.01	0.02	0.03	0.00	0.04	0.01	0.06	0.00	0.00	0.00	0.00	0.03	0.00	0.04	0.02	0.02	**0.02**	**0.02**
Fe	0.03	0.02	0.00	0.03	0.01	0.00	0.01	0.00	0.04	0.00	0.00	0.00	0.04	0.04	0.00	0.07	0.00	**0.02**	**0.02**
Cu	3.3	3.4	3.5	3.3	3.5	3.6	3.7	3.9	3.2	3.3	3.3	3.4	3.3	3.4	3.5	3.4	3.6	**3.8**	**0.9**
Ag	0.02	0.07	0.00	0.20	0.03	0.11	0.08	0.00	0.09	0.06	0.05	0.08	0.06	0.10	0.06	0.08	0.07	**0.07**	**0.04**
Au	96.8	97.8	98.1	97.3	96.7	97.1	97.4	96.9	96.5	97.2	97.4	97.9	97.0	97.1	97.2	96.7	98.0	**96.9**	**1.0**
Hg	0.00	0.00	0.00	0.00	0.00	0.00	0.00	0.00	0.00	0.00	0.00	0.00	0.00	0.00	0.00	0.00	0.00	**0.00**	**0.00**
Total	100.2	101.3	101.6	100.9	100.3	100.9	101.1	100.8	99.8	100.5	100.7	101.4	100.4	100.6	100.7	100.3	101.7	**100.8**	**0.5**
	calculated to 10 a.p.f.u																		
Au	9.0	9.0	9.0	9.0	9.0	8.9	8.9	8.9	9.0	9.0	9.0	9.0	9.0	9.0	9.0	9.0	9.0	**8.9**	**0.2**
Cu	0.96	0.98	0.99	0.95	1.01	1.02	1.04	1.10	0.93	1.0	0.96	0.96	0.94	0.97	0.99	0.98	1.01	**1.07**	**0.23**
Ag	0.02	0.07	0.00	0.19	0.03	0.10	0.07	0.00	0.09	0.06	0.05	0.08	0.06	0.09	0.06	0.08	0.07	**0.06**	**0.04**
Au:Cu	9.4	9.2	9.1	9.5	8.9	8.8	8.6	8.1	9.7	9.5	9.4	9.4	9.6	9.3	9.0	9.1	8.9	**8.6**	**1.5**

	Au3Cu 3aTW	Au3Cu 3aTW	Au3Cu 3aTW	Au3Cu 3aTW	Au3Cu 3aTW	Au3Cu 3aTW	Au3Cu 3aTW	Au3Cu 3aTW	Au3Cu 3aTW	Au3Cu 3bTW	Au3Cu 3bTW	Au3Cu 3bTW	Au3Cu 3bTW	Au3Cu 3bTW	Au3Cu 3bTW	Au3Cu 3bTW	Au3Cu 3bTW	Au3Cu 3bTW	Au3Cu 3bTW
S	0.00	0.01	0.01	0.02	0.00	0.05	0.00	0.00	0.05	0.00	0.02	0.00	0.03	0.02	0.04	0.01	0.00	0.00	0.00
Fe	0.00	0.00	0.02	0.03	0.00	0.04	0.01	0.02	0.00	0.03	0.04	0.07	0.04	0.13	0.00	0.00	0.04	0.02	0.00
Cu	9.4	9.5	9.5	9.5	9.8	9.7	10.0	10.3	11.0	11.1	11.1	11.0	11.2	11.1	9.4	9.5	9.5	9.7	9.8
Ag	0.06	0.01	0.07	0.00	0.00	0.00	0.04	0.00	0.04	0.00	0.11	0.05	0.05	0.05	0.00	0.08	0.11	0.00	0.00
Au	91.3	90.8	90.7	89.7	90.6	90.6	91.3	90.6	89.7	89.4	89.5	88.7	89.6	88.4	91.3	91.2	90.3	90.7	90.7
Hg	0.00	0.00	0.00	0.00	0.00	0.00	0.00	0.00	0.00	0.00	0.00	0.00	0.00	0.00	0.00	0.00	0.00	0.00	0.00
Total	100.8	100.3	100.3	99.2	100.4	100.4	101.3	100.9	100.8	100.5	100.7	99.8	101.0	99.7	100.8	100.8	99.9	100.4	100.6
	calculated to 4 a.p.f.u																		
Au	3.0	3.0	3.0	3.0	3.0	3.0	3.0	3.0	2.9	2.9	2.9	2.9	2.9	2.9	7.6	7.6	7.5	7.5	7.5
Cu	0.97	0.97	0.98	0.98	1.01	0.99	1.01	1.04	1.10	1.11	1.10	1.11	1.12	1.11	2.42	2.43	2.44	2.48	2.52
Ag	0.06	0.01	0.07	0.00	0.00	0.00	0.04	0.00	0.04	0.00	0.09	0.04	0.05	0.04	0.00	0.03	0.04	0.00	0.00
Au:Cu	3.1	3.1	3.1	3.1	3.0	3.0	2.9	2.8	2.6	2.6	2.6	2.6	2.6	2.6	3.1	3.1	3.1	3.0	3.0

	Au3Cu 3bTW	Au3Cu 3bTW	Au3Cu 3bTW	Au3Cu 3bTW	Au3Cu 3bTW	**Au9Cu Mean**	**n=24 Std.dev**	3aTW AuCu	3aTW AuCu	3aTW AuCu	3aTW AuCu	3aTW AuCu	3aTW AuCu	3aTW AuCu	3aTW AuCu	3aTW AuCu	3aTW AuCu	3aTW AuCu	3aTW AuCu
S	0.01	0.04	0.00	0.02	0.00	**0.01**	**0.02**	0.03	0.00	0.00	0.00	0.02	0.00	0.00	0.00	0.00	0.03	0.00	0.01
Fe	0.02	0.00	0.00	0.04	0.00	**0.02**	**0.03**	0.00	0.00	0.02	0.04	0.01	0.00	0.00	0.02	0.00	0.00	0.00	0.03
Cu	10.0	10.0	10.2	10.3	10.4	**10.1**	**0.6**	24.2	24.4	24.4	24.3	24.6	24.5	24.9	24.7	24.6	24.6	24.6	24.5
Ag	0.03	0.00	0.01	0.03	0.03	**0.03**	**0.03**	0.00	0.02	0.00	0.01	0.00	0.03	0.02	0.00	0.00	0.03	0.07	0.07
Au	90.4	90.7	89.7	90.0	89.2	**90.2**	**0.8**	76.2	75.9	75.3	75.1	75.6	75.2	76.2	75.5	75.1	75.4	75.3	75.1
Hg	0.00	0.00	0.00	0.00	0.00	**0.00**	**0.00**	0.00	0.00	0.00	0.00	0.00	0.00	0.00	0.00	0.00	0.00	0.00	0.00
Total	100.5	100.7	100.0	100.4	99.7	**100.4**	**0.5**	100.5	100.3	99.7	99.5	100.2	99.8	101.2	100.1	99.7	100.1	100.0	99.7
	calculated to 4 a.p.f.u							**calculated to 2 a.p.f.u**											
Au	7.4	7.4	7.4	7.4	7.3	**4.8**	**2.3**	5.0	5.0	5.0	5.0	5.0	5.0	5.0	5.0	5.0	5.0	5.0	5.0
Cu	2.54	2.55	2.61	2.61	2.66	**1.66**	**0.75**	4.96	4.99	5.01	5.01	5.02	5.02	5.03	5.03	5.04	5.02	5.03	5.02
Ag	0.01	0.00	0.00	0.01	0.01	**0.02**	**0.03**	0.00	0.00	0.00	0.00	0.00	0.01	0.00	0.00	0.00	0.01	0.01	0.01
Au:Cu	2.9	2.9	2.8	2.8	2.8	**2.9**	**0.2**	1.0	1.0	1.0	1.0	1.0	1.0	1.0	1.0	1.0	1.0	1.0	1.0

	3aTW AuCu	3aTW AuCu	3aTW AuCu	3aTW AuCu	3aTW AuCu	3aTW AuCu	3aTW AuCu	3aTW AuCu	3aTW AuCu	3aTW AuCu	3aTW AuCu	3bTW AuCu	3bTW AuCu	3bTW AuCu	3bTW AuCu	3bTW AuCu	3bTW AuCu	3bTW AuCu	3bTW AuCu	3bTW AuCu	3bTW AuCu	**Mean AuCu**	**Std.dev n=33**
S	0.04	0.01	0.00	0.00	0.00	0.03	0.00	0.00	0.02	0.04	0.03	0.00	0.00	0.01	0.00	0.04	0.02	0.02	0.00	0.03	0.27	**0.02**	**0.05**
Fe	0.00	0.00	0.07	0.01	0.00	0.00	0.04	0.03	0.01	0.05	0.01	0.03	0.01	0.03	0.02	0.00	0.02	0.02	0.02	0.00	0.00	**0.01**	**0.02**
Cu	24.5	24.8	24.7	24.8	24.9	24.8	24.8	24.9	24.6	24.6	24.7	23.3	24.1	23.8	24.1	24.1	24.0	24.1	24.4	24.3	24.0	**24.4**	**0.4**
Ag	0.05	0.00	0.02	0.00	0.06	0.08	0.03	0.02	0.00	0.02	0.03	0.00	0.00	0.03	0.00	0.02	0.00	0.05	0.06	0.07	0.00	**0.02**	**0.03**
Au	75.1	75.6	75.5	75.5	75.9	75.5	75.4	75.5	74.7	74.8	74.9	75.2	76.3	75.5	76.0	75.9	75.4	75.7	75.9	75.4	75.6	**75.5**	**0.4**
Hg	0.00	0.00	0.00	0.00	0.00	0.00	0.00	0.00	0.00	0.00	0.00	0.00	0.00	0.00	0.00	0.00	0.00	0.00	0.00	0.00	0.00	**0.00**	**0.00**
Total	99.8	100.4	100.3	100.3	100.8	100.4	100.2	100.4	99.3	99.5	99.7	98.5	100.4	99.4	100.0	100.0	99.5	99.9	100.4	99.8	99.9	**100.0**	**0.5**
Au	5.0	5.0	5.0	5.0	5.0	4.9	4.9	4.9	4.9	4.9	4.9	5.1	5.1	5.0	5.0	5.0	5.0	5.0	5.0	5.0	5.0	**5.0**	**0.0**
Cu	5.02	5.04	5.03	5.04	5.04	5.03	5.04	5.05	5.05	5.04	5.05	4.90	4.94	4.94	4.95	4.95	4.96	4.99	4.98	4.90	**5.00**	**0.04**
Ag	0.01	0.00	0.00	0.00	0.01	0.02	0.00	0.00	0.00	0.00	0.01	0.00	0.00	0.01	0.00	0.00	0.00	0.01	0.01	0.01	0.00	**0.00**	**0.00**
Au:Cu	1.0	1.0	1.0	1.0	1.0	1.0	1.0	1.0	1.0	1.0	1.0	1.0	1.0	1.0	1.0	1.0	1.0	1.0	1.0	1.0	1.0	**1.0**	**0.0**

Table A4: Complete electron microanalysis data for native gold

Phase	Native Au	Native Au	Native Au	Native Au	Native Au	Native Au	Native Au	Native Au	Native Au	Native Au	Native Au	Native Au	Native Au	Native Au	Native Au		
Sample	41bTW	41bTW	41bTW	41bTW	41bTW	41bTW	41bTW	41bTW	41bTW	41bTW	41bTW	41bTW	41bTW	41bTW	41bTW	Mean (15)	Std.dev
S	0.12	2.52	0.06	0.50	0.09	0.23	0.18	3.47	0.18	0.07	0.08	0.09	0.11	0.06	0.09	**0.52**	**1.02**
Fe	0.07	1.55	0.25	0.29	0.06	0.11	0.10	4.70	0.12	0.17	0.02	0.16	0.16	0.21	0.05	**0.53**	**1.21**
Cu	0.38	1.89	0.44	0.73	0.26	0.42	0.49	4.59	0.42	0.30	0.18	0.49	0.43	0.43	0.28	**0.78**	**1.13**
Ag	0.77	0.88	0.56	0.74	0.64	0.78	0.74	0.44	0.93	0.85	0.82	0.73	0.65	0.60	0.87	**0.73**	**0.14**
Au	97.6	94.1	98.8	97.2	98.8	98.0	98.1	85.5	97.1	99.6	99.1	99.2	97.7	99.3	98.0	**97.19**	**3.49**
Hg	0.00	0.00	0.00	0.00	0.00	0.00	0.00	0.00	0.00	0.00	0.00	0.00	0.00	0.00	0.00	**0.00**	**0.00**
Bi	0.00	0.00	0.00	0.00	0.09	0.00	0.03	0.05	0.00	0.00	0.03	0.00	0.00	0.00	0.13	**0.02**	**0.04**
Total	98.9	100.9	100.1	99.4	99.9	99.5	99.6	98.8	98.7	101.0	100.2	100.6	99.1	100.6	99.4	**99.79**	**0.76**
calculated to 1 a.p.f.u																	
Au	0.96	0.77	0.97	0.93	0.97	0.96	0.96	0.62	0.96	0.97	0.97	0.96	0.96	0.97	0.97	**0.93**	**0.10**
Cu	0.01	0.05	0.01	0.02	0.01	0.01	0.01	0.10	0.01	0.01	0.01	0.01	0.01	0.01	0.01	**0.02**	**0.02**
Fe	0.00	0.04	0.01	0.01	0.00	0.00	0.00	0.12	0.00	0.01	0.00	0.01	0.01	0.01	0.00	**0.02**	**0.03**
S	0.01	0.13	0.00	0.03	0.01	0.01	0.01	0.15	0.01	0.00	0.01	0.01	0.01	0.00	0.01	**0.03**	**0.05**
Ag	0.01	0.01	0.01	0.01	0.01	0.01	0.01	0.01	0.02	0.02	0.01	0.01	0.01	0.01	0.02	**0.01**	**0.00**
Bi	0.00	0.00	0.00	0.00	0.00	0.00	0.00	0.00	0.00	0.00	0.00	0.00	0.00	0.00	0.00	**0.00**	**0.00**

Phase	Native Au	Native Au	Native Au	Native Au	Native Au	Native Au	Native Au	Native Au	Native Au	Native Au	Native Au	Native Au	Native Au	Native Au	Native Au	Native Au	Native Au
Sample	41aTW	41aTW	41aTW	41aTW	41aTW	41aTW	41aTW	41aTW	41aTW	41aTW	41aTW	41aTW	41aTW	41aTW	41aTW	41aTW	41aTW
S	0.64	0.42	1.22	0.48	0.76	0.14	0.20	0.19	0.16	0.24	0.23	0.21	0.79	0.64	0.48	0.14	0.12
Fe	0.59	0.36	0.67	0.33	0.78	0.36	0.12	0.13	0.01	0.64	0.07	0.11	0.44	0.51	0.39	0.07	0.08
Cu	0.92	0.75	1.28	0.63	1.06	0.42	0.52	0.57	0.53	0.55	0.64	0.48	0.94	0.79	0.74	0.26	0.37
Ag	0.84	1.45	0.84	0.69	0.80	0.66	0.93	0.70	0.90	0.79	0.68	0.67	0.80	0.77	0.99	0.66	0.63
Au	96.1	96.5	94.5	96.2	95.2	96.8	97.1	97.7	97.3	96.2	98.1	97.6	96.5	96.4	96.2	98.2	97.2
Hg	0.00	0.00	0.00	0.00	0.00	0.00	0.00	0.00	0.00	0.00	0.00	0.00	0.00	0.00	0.00	0.00	0.00
Bi	0.00	0.09	0.03	0.00	0.00	0.13	0.00	0.12	0.00	0.00	0.00	0.00	0.00	0.00	0.00	0.01	0.00
Total	99.1	99.5	98.5	98.3	98.6	98.5	98.8	99.4	98.9	98.5	99.7	99.0	99.5	99.1	98.8	99.4	98.4
calculated to 1 a.p.f.u																	
Au	0.90	0.92	0.86	0.93	0.89	0.95	0.95	0.95	0.96	0.93	0.95	0.96	0.90	0.91	0.92	0.97	0.97
Cu	0.03	0.02	0.04	0.02	0.03	0.01	0.02	0.02	0.02	0.02	0.02	0.01	0.03	0.02	0.02	0.01	0.01
Fe	0.02	0.01	0.02	0.01	0.03	0.01	0.00	0.00	0.00	0.02	0.00	0.00	0.01	0.02	0.01	0.00	0.00
S	0.04	0.02	0.07	0.03	0.04	0.01	0.01	0.01	0.01	0.01	0.01	0.01	0.05	0.04	0.03	0.01	0.01
Ag	0.01	0.03	0.01	0.01	0.01	0.01	0.02	0.01	0.02	0.01	0.01	0.01	0.01	0.01	0.02	0.01	0.01
Bi	0.00	0.00	0.00	0.00	0.00	0.00	0.00	0.00	0.00	0.00	0.00	0.00	0.00	0.00	0.00	0.00	0.00

Phase	Native Au	Native Au	Native Au	Native Au	Native Au	Native Au	Native Au	Native Au	Native Au	Native Au	Native Au	Native Au	Native Au	Native Au	Native Au		
Sample	41aTW	41aTW	41aTW	41aTW	41aTW	41aTW	41aTW	41aTW	41aTW	41aTW	41aTW	41aTW	41aTW	41aTW	41aTW	Mean (31)	Std.dev
S	0.49	0.40	0.33	0.46	0.24	0.41	0.37	0.09	0.92	0.38	0.21	0.19	0.74	0.20	**0.40**	**0.27**	
Fe	0.26	0.22	0.17	0.68	1.32	0.15	0.26	0.01	0.48	0.18	0.14	0.15	0.92	0.14	**0.35**	**0.30**	
Cu	0.51	0.71	0.69	0.68	0.75	0.80	0.53	0.41	0.79	0.64	0.53	0.38	0.82	0.48	**0.65**	**0.22**	
Ag	0.65	0.82	0.86	0.75	0.70	0.64	0.80	0.82	0.76	0.80	0.46	0.81	0.81	0.82	**0.78**	**0.16**	
Au	96.2	96.0	96.4	97.5	95.8	97.1	98.2	98.6	96.9	96.6	98.2	98.7	98.1	98.8	**96.99**	**1.05**	
Hg	0.00	0.00	0.00	0.00	0.00	0.00	0.00	0.00	0.00	0.00	0.00	0.00	0.00	0.00	**0.00**	**0.00**	
Bi	0.14	0.00	0.00	0.00	0.00	0.12	0.00	0.20	0.00	0.00	0.00	0.00	0.36	0.00	**0.04**	**0.08**	
Total	98.3	98.2	98.4	100.1	98.8	99.2	100.1	100.1	99.9	98.5	99.5	100.2	101.7	100.4	**99.21**	**0.80**	
calculated to 1 a.p.f.u																	
Au	0.93	0.93	0.94	0.92	0.91	0.93	0.94	0.97	0.90	0.94	0.96	0.96	0.89	0.95	**0.93**	**0.03**	
Cu	0.02	0.02	0.02	0.02	0.02	0.02	0.02	0.01	0.02	0.02	0.02	0.01	0.02	0.01	**0.02**	**0.01**	
Fe	0.01	0.01	0.01	0.02	0.04	0.01	0.01	0.00	0.02	0.01	0.00	0.01	0.03	0.00	**0.01**	**0.01**	
S	0.03	0.02	0.02	0.03	0.01	0.02	0.02	0.01	0.05	0.02	0.01	0.01	0.04	0.01	**0.02**	**0.02**	
Ag	0.01	0.01	0.02	0.01	0.01	0.01	0.01	0.01	0.01	0.01	0.01	0.01	0.01	0.01	**0.01**	**0.00**	
Bi	0.00	0.00	0.00	0.00	0.00	0.00	0.00	0.00	0.00	0.00	0.00	0.00	0.00	0.00	**0.00**	**0.00**	

Table A5: Complete electron microanalysis for Co-safflorite

	41aTW							Mean (7)	Std.dev	41bTW		Mean (2)	Std.dev	41dTW												Mean (13)	Std.dev
	Co-Safflorite																										
Cu	0.24	0.11	0.19	0.40	0.27	0.18	2.40	0.54	0.83	0.09	0.09	0.09	0.00	0.52	0.15	0.12	1.04	0.63	0.19	0.11	0.11	0.04	1.08	0.67	0.09	0.16	0.38	0.37
Ag	0.00	0.01	0.00	0.06	0.00	0.01	0.04	0.02	0.02	0.00	0.03	0.02	0.02	0.00	0.06	0.00	0.00	0.00	0.00	0.00	0.03	0.00	0.00	0.00	0.00	0.01	0.01	0.02
Fe	0.51	0.45	0.49	2.52	2.71	2.76	3.30	1.82	1.27	2.10	0.63	1.37	1.05	0.36	0.15	0.21	0.28	0.76	6.55	3.59	2.42	0.38	3.68	11.41	2.14	2.44	2.64	3.24
Pb	0.20	0.00	0.00	0.00	0.00	0.05	0.00	0.04	0.07	0.11	0.02	0.07	0.06	0.00	0.14	0.05	0.00	0.05	0.00	0.11	0.00	0.00	0.01	0.00	0.00	0.00	0.03	0.05
Bi	0.14	0.09	0.02	0.08	0.14	0.46	0.29	0.17	0.15	0.00	0.04	0.02	0.03	0.99	0.00	0.05	0.00	0.12	0.20	0.12	0.33	0.20	0.41	0.03	0.09	0.00	0.20	0.27
S	0.47	0.34	0.11	0.25	0.14	0.25	2.41	0.57	0.82	0.12	0.71	0.41	0.42	0.63	0.14	0.12	0.44	0.08	0.19	0.22	0.17	0.39	0.16	0.30	0.16	0.31	0.25	0.16
Te	0.00	0.00	0.00	0.00	0.03	0.11	0.06	0.03	0.04	0.00	0.00	0.00	0.00	0.00	0.00	0.00	0.00	0.00	0.00	0.00	0.00	0.00	0.00	0.00	0.02	0.00	0.00	0.01
Se	0.59	0.48	0.44	0.41	0.57	0.70	0.68	0.55	0.11	0.65	0.55	0.60	0.07	0.52	0.55	0.59	0.58	0.47	0.51	0.59	0.53	0.54	0.45	0.62	0.38	0.68	0.54	0.08
Co	27.51	23.54	21.67	25.10	25.53	25.04	23.48	24.55	1.86	24.49	27.41	25.95	2.06	25.03	25.74	25.20	27.78	27.07	20.70	23.99	25.26	28.25	22.72	14.58	26.27	24.17	24.37	3.58
Ni	0.76	4.38	5.39	0.59	0.33	0.00	1.05	1.79	2.16	1.15	0.29	0.72	0.61	2.10	2.43	2.90	0.19	0.11	0.04	0.06	0.74	0.05	0.70	0.20	0.15	1.77	0.88	1.04
As	70.50	71.13	71.29	69.42	68.66	70.21	67.19	69.77	1.47	71.95	70.19	71.07	1.24	68.81	70.56	70.57	69.58	70.36	70.53	70.02	70.48	70.36	70.50	71.36	70.36	70.06	70.27	0.60
Total	**100.9**	**100.5**	**99.6**	**98.8**	**98.4**	**99.8**	**100.9**	**99.9**	**1.0**	**100.7**	**99.9**	**100.3**	**0.5**	**99.0**	**99.9**	**99.8**	**99.9**	**99.6**	**98.9**	**98.8**	**100.1**	**100.2**	**99.7**	**99.2**	**99.7**	**99.6**	**99.6**	**0.5**
Formulae, calculated to 3 a.p.f.u																												
Fe	0.02	0.02	0.02	0.09	0.10	0.10	0.12	0.07	0.05	0.08	0.02	0.05	0.04	0.01	0.01	0.01	0.01	0.03	0.25	0.14	0.09	0.01	0.14	0.43	0.08	0.09	0.10	0.12
Co	0.96	0.83	0.77	0.89	0.91	0.89	0.80	0.86	0.07	0.86	0.96	0.91	0.07	0.89	0.91	0.89	0.98	0.96	0.74	0.86	0.89	0.99	0.81	0.52	0.93	0.85	0.86	0.13
Ni	0.03	0.15	0.19	0.02	0.01	0.00	0.04	0.06	0.08	0.04	0.01	0.03	0.02	0.08	0.09	0.10	0.01	0.00	0.00	0.00	0.03	0.00	0.02	0.01	0.01	0.06	0.03	0.04
Cu	0.01	0.00	0.01	0.01	0.01	0.01	0.08	0.02	0.03	0.00	0.00	0.00	0.00	0.02	0.00	0.00	0.03	0.02	0.01	0.00	0.00	0.00	0.04	0.02	0.00	0.01	0.01	0.01
Ag	0.00	0.00	0.00	0.00	0.00	0.00	0.00	0.00	0.00	0.00	0.00	0.00	0.00	0.00	0.00	0.00	0.00	0.00	0.00	0.00	0.00	0.00	0.00	0.00	0.00	0.00	0.00	0.00
Bi	0.00	0.00	0.00	0.00	0.00	0.00	0.00	0.00	0.00	0.00	0.00	0.00	0.00	0.01	0.00	0.00	0.00	0.00	0.00	0.00	0.00	0.00	0.00	0.00	0.00	0.00	0.00	0.00
Pb	0.00	0.00	0.00	0.00	0.00	0.00	0.00	0.00	0.00	0.00	0.00	0.00	0.00	0.00	0.00	0.00	0.00	0.00	0.00	0.00	0.00	0.00	0.00	0.00	0.00	0.00	0.00	0.00
Total Metal	**1.02**	**1.00**	**0.99**	**1.03**	**1.04**	**1.00**	**1.03**	**1.02**	**0.02**	**0.98**	**1.00**	**0.99**	**0.01**	**1.01**	**1.01**	**1.01**	**1.03**	**1.02**	**0.99**	**1.00**	**1.02**	**1.01**	**1.01**	**0.97**	**1.02**	**1.01**	**1.01**	**0.01**
As	**1.94**	**1.96**	**1.99**	**1.95**	**1.93**	**1.96**	**1.80**	**1.93**	**0.06**	**1.99**	**1.94**	**1.96**	**0.04**	**1.93**	**1.97**	**1.97**	**1.93**	**1.97**	**1.98**	**1.97**	**1.96**	**1.95**	**1.97**	**1.99**	**1.96**	**1.95**	**1.96**	**0.02**
S	0.03	0.02	0.01	0.02	0.01	0.02	0.15	0.04	0.05	0.01	0.05	0.03	0.03	0.04	0.01	0.01	0.03	0.01	0.01	0.01	0.01	0.02	0.01	0.02	0.01	0.02	0.02	0.01
Se	0.02	0.01	0.01	0.01	0.02	0.02	0.02	0.01	0.00	0.02	0.01	0.02	0.00	0.01	0.01	0.02	0.02	0.01	0.01	0.02	0.01	0.01	0.01	0.02	0.01	0.02	0.01	0.00
Te	0.00	0.00	0.00	0.00	0.00	0.00	0.00	0.00	0.00	0.00	0.00	0.00	0.00	0.00	0.00	0.00	0.00	0.00	0.00	0.00	0.00	0.00	0.00	0.00	0.00	0.00	0.00	0.00
S+Se	0.05	0.03	0.02	0.03	0.02	0.03	0.17	0.05	0.05	0.02	0.06	0.04	0.02	0.06	0.02	0.02	0.04	0.02	0.03	0.03	0.03	0.04	0.02	0.04	0.02	0.04	0.03	0.01

Table A6: Complete electron microanalysis for Loellingite

	41aTW		Mean (2)	Std.dev	41bTW			Mean (3)	Std.dev	41dTW					Mean (5)	Std.dev
Loellingite			41aTW													
0.62	1.97	0.95	1.46	0.72	0.46	1.43	1.36	1.08	0.54	0.53	0.48	1.66	0.60	0.50	0.76	0.51
0.00	0.03	0.09	0.06	0.04	0.01	0.00	0.06	0.02	0.03	0.05	0.00	0.00	0.00	0.04	0.02	0.02
25.22	24.66	26.04	25.35	0.97	25.28	25.26	25.72	25.42	0.26	24.55	24.82	24.93	25.84	25.35	25.10	0.51
0.00	0.05	0.00	0.02	0.03	0.00	0.06	0.00	0.02	0.04	0.14	0.14	0.00	0.00	0.08	0.07	0.07
0.04	2.18	0.37	1.28	1.28	0.01	0.00	0.02	0.01	0.01	0.00	0.01	0.00	0.00	0.06	0.01	0.03
0.80	0.77	0.17	0.47	0.42	0.03	0.04	0.17	0.08	0.08	0.01	0.73	0.04	0.10	0.07	0.19	0.30
0.00	0.05	0.03	0.04	0.01	0.06	0.00	0.00	0.02	0.03	0.02	0.03	0.00	0.02	0.00	0.01	0.01
0.66	0.51	0.59	0.55	0.05	0.70	0.50	0.48	0.56	0.12	0.57	0.59	0.56	0.53	0.58	0.57	0.03
1.33	0.30	0.42	0.36	0.09	0.40	0.42	0.29	0.37	0.07	1.86	1.65	0.14	0.63	0.96	1.05	0.71
0.01	0.05	0.09	0.07	0.03	0.00	0.00	0.03	0.01	0.01	0.03	0.11	0.02	0.05	0.12	0.07	0.05
71.16	68.63	71.27	69.95	1.87	71.95	71.59	70.60	71.38	0.70	71.59	70.49	72.00	71.35	71.24	71.33	0.56
99.8	**99.2**	**100.0**	**99.6**	**0.6**	**98.9**	**99.3**	**98.7**	**99.0**	**0.3**	**99.4**	**99.1**	**99.4**	**99.1**	**99.0**	**99.2**	**0.2**
0.92	0.92	0.96	0.94	0.03	0.94	0.94	0.96	0.95	0.01	0.91	0.92	0.93	0.96	0.94	0.93	0.02
0.05	0.01	0.01	0.01	0.00	0.01	0.01	0.01	0.01	0.00	0.07	0.06	0.00	0.02	0.03	0.04	0.03
0.00	0.00	0.00	0.00	0.00	0.00	0.00	0.00	0.00	0.00	0.00	0.00	0.00	0.00	0.00	0.00	0.00
0.02	0.06	0.03	0.05	0.02	0.02	0.05	0.04	0.04	0.02	0.02	0.02	0.05	0.02	0.02	0.02	0.02
0.00	0.00	0.00	0.00	0.00	0.00	0.00	0.00	0.00	0.00	0.00	0.00	0.00	0.00	0.00	0.00	0.00
0.00	0.02	0.00	0.01	0.01	0.00	0.00	0.00	0.00	0.00	0.00	0.00	0.00	0.00	0.00	0.00	0.00
0.00	0.00	0.00	0.00	0.00	0.00	0.00	0.00	0.00	0.00	0.00	0.00	0.00	0.00	0.00	0.00	0.00
0.99	**1.02**	**1.01**	**1.02**	**0.01**	**0.97**	**1.00**	**1.02**	**1.00**	**0.02**	**1.00**	**1.00**	**0.99**	**1.00**	**1.00**	**1.00**	**0.01**
1.94	**1.91**	**1.96**	**1.94**	**0.03**	**2.00**	**1.98**	**1.96**	**1.98**	**0.02**	**1.98**	**1.94**	**2.00**	**1.98**	**1.98**	**1.97**	**0.02**
0.05	0.05	0.01	0.03	0.03	0.00	0.00	0.01	0.01	0.01	0.00	0.05	0.00	0.01	0.00	0.01	0.02
0.02	0.01	0.02	0.01	0.00	0.02	0.01	0.01	0.01	0.00	0.01	0.02	0.01	0.01	0.02	0.01	0.00
0.00	0.00	0.00	0.00	0.00	0.00	0.00	0.00	0.00	0.00	0.00	0.00	0.00	0.00	0.00	0.00	0.00
0.07	0.06	0.03	0.04	0.03	0.02	0.02	0.02	0.02	0.00	0.02	0.06	0.02	0.02	0.02	0.03	0.02

Table A7: Complete electron microanalysis for Monazite

Monazite microprobe analysis template

(Wt.%)	32TW	31TW	Mean	Std.dev
	Monazite			
CaO	1.36	1.04	1.20	0.22
Y2O3	0.13	0.03	0.08	0.07
La2O3	20.8	17.4	19.1	2.4
Ce2O3	30.7	26.4	28.6	3.0
Nd2O3	7.44	7.01	7.22	0.31
Pr2O3	2.77	2.41	2.59	0.25
Sm2O3	0.49	0.49	0.49	0.00
Gd2O3	0.31	0.19	0.25	0.08
Tb2O3	0.00	0.00	0.00	0.00
Dy2O3	0.00	0.07	0.04	0.05
Ho2O3	0.05	0.04	0.04	0.00
Er2O3	0.07	0.00	0.04	0.05
Yb2O3				
Lu2O3	0.00	0.00	0.00	0.00
Sc2O3	0.00	0.00	0.00	0.00
ZrO2	0.00	0.00	0.00	0.00
Nb2O5	0.00	0.00	0.00	0.00
Na2O	0.00	0.00	0.00	0.00
K2O	0.08	0.94	0.51	0.61
ThO2	0.08	0.50	0.29	0.30
UO2	0.08	0.27	0.18	0.14
SrO				
FeO	1.82	7.72	4.77	4.17
TiO2	0.00	0.00	0.00	0.00
MgO	0.00	0.45	0.23	0.32
SiO2	0.23	6.31	3.27	4.30
MnO				
Cr2O3				
Al2O3	0.01	3.57	1.79	2.52
P2O5	23.6	24.3	24.0	0.5
As2O5				
V2O5				
F (wt.%)	2.40	0.72	1.56	1.19
Cl (wt.%)	0.06	0.02	0.04	0.03
Total	**92.5**	**99.9**	96.2	5.2
True total	**90.5**	**99.3**	94.9	6.3
Monazite (LREE…..)PO4				
Ca	0.07	0.04	0.05	0.02
Y	0.00	0.00	0.00	0.00
La	0.35	0.23	0.29	0.08
Ce	0.51	0.35	0.43	0.11
Nd	0.12	0.09	0.11	0.02
Pr	0.05	0.03	0.04	0.01
Sm	0.01	0.01	0.01	0.00
Gd	0.00	0.00	0.00	0.00
Tb	0.00	0.00	0.00	0.00
Dy	0.00	0.00	0.00	0.00
Ho	0.00	0.00	0.00	0.00
Er	0.00	0.00	0.00	0.00
Yb	0.00	0.00	0.00	0.00
Lu	0.00	0.00	0.00	0.00
Sc	0.00	0.00	0.00	0.00
Zr	0.00	0.00	0.00	0.00
Nb	0.00	0.00	0.00	0.00
Mg	0.00	0.02	0.01	0.02
Fe	0.07	0.24	0.15	0.12
Mn	0.00	0.00	0.00	0.00
Na	0.00	0.00	0.00	0.00
K	0.00	0.02	0.01	0.01
Th	0.00	0.00	0.00	0.00
U	0.00	0.00	0.00	0.00
Sr	0.00	0.00	0.00	0.00
Total	**1.18**	**1.05**	1.12	0.09
P	0.91	0.75	0.83	0.11
Si	0.01	0.23	0.12	0.16
Total	**0.92**	**0.98**	0.95	0.05
F	0.34	0.08	0.21	0.18
Cl	0.00	0.00	0.00	0.00
Total	**0.35**	**0.08**	0.22	0.19
mol.% Monazite-(La)	29.5	22.3	25.9	5.1
mol.% Monazite-(Ce)	43.1	33.6	38.4	6.7
mol.% Monazite-(Nd)	10.2	8.7	9.5	1.1
mol.% Monazite-(Sm)	0.65	0.59	0.62	0.04

Table A8: Complete electron microanalysis for Xenotime

Xenotime microprobe analysis template

	15TW	15TW	15TW	15TW	15TW	15TW	15TW	**Mean(7)**	**std.dev**
(Wt.%)	*Xenotime*								
CaO	0.19	0.16	0.27	0.23	0.23	0.14	0.28	0.21	0.05
Y2O3	39.08	40.88	29.38	39.30	39.20	37.24	37.30	37.48	3.79
La2O3	0.03	0.00	0.00	0.00	0.00	0.00	0.00	0.00	0.01
Ce2O3	0.06	0.00	0.01	0.08	0.06	0.07	0.08	0.05	0.03
Nd2O3	0.13	0.06	0.11	0.01	0.07	0.20	0.10	0.10	0.06
Pr2O3	0.00	0.00	0.00	0.00	0.00	0.04	0.00	0.01	0.02
Sm2O3	0.10	0.34	0.58	0.28	0.22	0.55	0.42	0.36	0.17
Gd2O3	6.02	5.70	13.72	6.96	6.97	7.93	10.00	8.19	2.82
Tb2O3	0.00	0.00	0.00	0.00	0.00	0.00	0.00	0.00	0.00
Dy2O3	7.08	7.31	8.51	7.85	7.66	6.61	9.04	7.72	0.84
Ho2O3	0.25	0.09	0.00	0.18	0.33	0.09	0.32	0.18	0.13
Er2O3	3.75	4.21	2.65	3.79	3.72	3.21	3.27	3.52	0.51
Yb2O3				2.33	2.33	2.83	1.59	2.27	0.51
Lu2O3	0.49	0.51	0.34	0.46	0.40	0.41	0.40	0.43	0.06
Sc2O3	0.07	0.10	0.10						
ZrO2	0.00	0.00	0.00						
Nb2O5	0.04	0.02	0.03						
Na2O	0.01	0.01	0.05						
K2O	0.01	0.02	0.00						
ThO2	0.18	0.19	0.05	0.14	0.12	0.34	0.07	0.15	0.10
UO2	0.14	0.21	0.96	0.10	0.24	0.98	0.17	0.40	0.39
SrO									
FeO	6.68	2.92	7.37						
TiO2	0.06	0.00	0.08						
MgO	0.00	0.00	0.00						
SiO2	1.02	1.07	0.15	0.97	0.98	2.08	0.99	1.04	0.56
MnO									
Cr2O3									
Al2O3	0.00	0.00	0.00	0.00	0.00	0.94	0.10	0.15	0.35
P2O5	27.42	28.94	29.18	28.25	28.27	30.47	29.85	28.91	1.04
As2O5									
V2O5									
F (wt.%)	1.42	1.38	0.26	1.29	1.29	0.36	0.89	0.98	0.49
Cl (wt.%)	0.01	0.02	0.01	0.00	0.00	0.00	0.00	0.01	0.01
Total	94.23	94.11	93.80	92.22	92.11	94.49	94.85	93.69	1.09
True total	93.03	92.94	93.58	91.14	91.02	94.19	94.10	92.86	1.30
Xenotime (Y,HREE…..)PO4									
Ca	0.01	0.01	0.01	0.01	0.01	0.01	0.01	0.01	0.00
Y	0.78	0.81	0.59	0.80	0.80	0.71	0.74	0.75	0.08
La	0.00	0.00	0.00	0.00	0.00	0.00	0.00	0.00	0.00
Ce	0.00	0.00	0.00	0.00	0.00	0.00	0.00	0.00	0.00
Nd	0.00	0.00	0.00	0.00	0.00	0.00	0.00	0.00	0.00
Pr	0.00	0.00	0.00	0.00	0.00	0.00	0.00	0.00	0.00
Sm	0.00	0.00	0.01	0.00	0.00	0.01	0.01	0.00	0.00
Gd	0.08	0.07	0.17	0.09	0.09	0.09	0.12	0.10	0.04
Tb	0.00	0.00	0.00	0.00	0.00	0.00	0.00	0.00	0.00
Dy	0.09	0.09	0.10	0.10	0.09	0.08	0.11	0.09	0.01
Ho	0.00	0.00	0.00	0.00	0.00	0.00	0.00	0.00	0.00
Er	0.04	0.05	0.03	0.05	0.04	0.04	0.04	0.04	0.01
Yb	0.00	0.00	0.00	0.03	0.03	0.03	0.02	0.02	0.01
Lu	0.01	0.01	0.00	0.01	0.00	0.00	0.00	0.00	0.00
Sc	0.00	0.00	0.00	0.00	0.00	0.00	0.00	0.00	0.00
Zr	0.00	0.00	0.00	0.00	0.00	0.00	0.00	0.00	0.00
Nb	0.00	0.00	0.00	0.00	0.00	0.00	0.00	0.00	0.00
Mg	0.00	0.00	0.00	0.00	0.00	0.00	0.00	0.00	0.00
Fe	0.21	0.09	0.23	0.00	0.00	0.00	0.00	0.08	0.11
Mn	0.00	0.00	0.00	0.00	0.00	0.00	0.00	0.00	0.00
Na	0.00	0.00	0.00	0.00	0.00	0.00	0.00	0.00	0.00
K	0.00	0.00	0.00	0.00	0.00	0.00	0.00	0.00	0.00
Th	0.00	0.00	0.00	0.00	0.00	0.00	0.00	0.00	0.00
U	0.00	0.00	0.01	0.00	0.00	0.01	0.00	0.00	0.00
Sr	0.00	0.00	0.00	0.00	0.00	0.00	0.00	0.00	0.00
Total	1.23	1.13	1.17	1.09	1.08	0.98	1.05	1.11	0.08
P	0.87	0.91	0.94	0.92	0.92	0.93	0.94	0.92	0.02
Si	0.04	0.04	0.01	0.04	0.04	0.07	0.04	0.04	0.02
Total	0.91	0.95	0.94	0.96	0.96	1.00	0.97	0.96	0.03
F	0.17	0.16	0.03	0.16	0.16	0.04	0.10	0.12	0.06
Cl	0.00	0.00	0.00	0.00	0.00	0.00	0.00	0.00	0.00
Total	0.17	0.16	0.03	0.16	0.16	0.04	0.10	0.12	0.06
mol.% Xenotime-(Y)	63.88	71.43	50.55	73.93	73.94	72.43	69.94	68.01	8.43
mol.% 'Xenotime-(Gd)'	6.13	6.21	14.71	8.16	8.20	9.61	11.68	9.24	3.09
mol.% 'Xenotime-(Dy)'	7.00	7.73	8.86	8.94	8.75	7.78	10.26	8.48	1.07
mol.% Xenotime-(Yb)	0.00	0.00	0.00	2.57	2.57	3.23	1.74	1.44	1.42
mol% pretulite	0.18	0.27	0.29	0.00	0.00	0.00	0.00	0.11	0.14

Table A9: Complete electron microanalysis for Florencite

Florencite microprobe analysis template

(Wt.%)	15TW	15TW	15TW	15TW	Mean (4)	std.dev
	Florencite					
CaO	0.32	0.31	0.37	0.36	0.34	0.03
Y2O3	0.01	0.02	0.02	0.03	0.02	0.01
La2O3	7.77	6.65	7.07	7.08	7.14	0.47
Ce2O3	11.90	11.20	13.73	13.07	12.47	1.14
Nd2O3	2.732	2.477	3.947	3.199	3.09	0.65
Pr2O3	1.1174	1.0203	1.4634	1.146	1.19	0.19
Sm2O3	0.164	0.033	0.281	0.185	0.17	0.10
Gd2O3	0.000	0.000	0.028	0.012	0.01	0.01
Tb2O3	0.000	0.000	0.000	0.000	0.00	0.00
Dy2O3	-	-	-	0.004	0.00	0.00
Ho2O3	0.000	0.005	0.114	0.006	0.03	0.06
Er2O3	0.023	0.000	0.045	0.000	0.02	0.02
Yb2O3						
Lu2O3	0.000	0.024	0.014	0.000	0.01	0.01
Sc2O3	0.00	0.00	0.00	0.00	0.00	0.00
ZrO2	0.00	0.00	0.00	0.00	0.00	0.00
Nb2O5	0.00	0.00	0.01	0.02	0.01	0.01
Na2O	0.02	0.05	0.01	0.00	0.02	0.02
K2O	0.02	0.02	0.02	0.09	0.04	0.04
ThO2	0.1008	0.1343	0.0508	0.0002	0.07	0.06
UO2	0	0	0	0.115	0.03	0.06
PbO	0.051	0.000	0.036	0.007	0.02	0.02
SrO						
FeO	1.79	14.89	1.79	3.52	5.50	6.31
TiO2	0.00	0.03	0.00	0.00	0.01	0.02
MgO	0.06	0.03	0.05	0.05	0.05	0.01
SiO2	0.28	0.33	0.34	0.58	0.38	0.13
MnO						
Cr2O3						
Al2O3	30.32	25.89	29.50	28.38	28.52	1.93
P2O5	27.46	22.09	27.51	26.59	25.91	2.58
As2O5						
V2O5						
F (wt.%)	0.57	0.52	0.49	0.47	0.51	0.04
Cl (wt.%)	0.03	0.03	0.03	0.02	0.03	0.00
Total	**84.73**	**85.74**	**86.92**	**84.95**	**85.59**	**0.99**
True total	**84.24**	**85.29**	**86.49**	**84.54**	**85.14**	**1.00**
Florencite (LREE…..)Al3(PO4)2(OH)6						
Ca	0.029	0.031	0.034	0.034	0.03	0.00
Y	0.000	0.001	0.001	0.001	0.00	0.00
La	0.248	0.229	0.224	0.230	0.23	0.01
Ce	0.376	0.382	0.433	0.422	0.40	0.03
Nd	0.084	0.083	0.121	0.101	0.10	0.02
Pr	0.035	0.035	0.046	0.037	0.04	0.01
Sm	0.005	0.001	0.008	0.006	0.00	0.00
Gd	0.000	0.000	0.001	0.000	0.00	0.00
Tb	0.000	0.000	0.000	0.000	0.00	0.00
Dy	0.000	0.000	0.000	0.000	0.00	0.00
Ho	0.000	0.000	0.003	0.000	0.00	0.00
Er	0.001	0.000	0.001	0.000	0.00	0.00
Yb	0.000	0.000	0.000	0.000	0.00	0.00
Lu	0.000	0.001	0.000	0.000	0.00	0.00
Sc	0.000	0.000	0.000	0.000	0.00	0.00
Zr	0.000	0.000	0.000	0.000	0.00	0.00
Nb	0.000	0.000	0.001	0.001	0.00	0.00
Mg	0.008	0.005	0.006	0.007	0.01	0.00
Fe	0.129	1.161	0.129	0.260	0.42	0.50
Mn	0.000	0.000	0.000	0.000	0.00	0.00
Na	0.002	0.004	0.001	0.000	0.00	0.00
K	0.001	0.001	0.001	0.005	0.00	0.00
Th	0.002	0.003	0.001	0.000	0.00	0.00
U	0.000	0.000	0.000	0.002	0.00	0.00
Pb	0.000	0.000	0.000	0.000	0.00	0.00
Sr	0.000	0.000	0.000	0.000	0.00	0.00
Total	**0.921**	**1.936**	**1.012**	**1.106**	**1.24**	**0.47**
Al	**3.088**	**2.846**	**2.995**	**2.951**	**2.97**	**0.10**
P	2.009	1.744	2.006	1.985	1.94	0.13
Si	0.024	0.030	0.029	0.051	0.03	0.01
Total	**2.033**	**1.775**	**2.035**	**2.036**	**1.97**	**0.13**
F	0.156	0.152	0.134	0.132	0.14	0.01
Cl	0.005	0.005	0.005	0.004	0.00	0.00
OH (by difference)	5.840	5.843	5.861	5.864	5.85	0.01
Total	**6.000**	**6.000**	**6.000**	**6.000**	**6.00**	**0.00**
mol.% Florencite-(La)	26.89	11.81	22.18	20.81	20.42	6.30
mol.% Florencite-(Ce)	40.86	19.75	42.76	38.12	35.37	10.59
mol.% Florencite-(Nd)	9.15	4.26	11.99	9.11	8.63	3.21

Table A10: Complete electron microanalysis for mica

(Wt.%)	5TW	5TW	5TW	5TW	5TW	5TW	5TW	Mean (7)	Std.dev	7TW	7TW	7TW	7TW	7TW	7TW	7TW	Mean (7)	Std.dev	35TW	35TW	35TW	35TW	35TW	35TW	Mean (6)	Std.dev
CaO	0.05	0.06	0.04	0.00	0.02	0.03	0.01	0.03	0.02	0.01	0.01	0.07	0.08	0.01	0.01	0.03	0.03	0.03	0.02	0.01	0.04	0.06	0.01	0.01	0.03	0.02
Na2O	0.51	0.68	0.45	0.22	0.09	0.14	0.09	0.31	0.23	0.06	0.07	0.03	0.19	0.14	0.10	0.13	0.10	0.05	0.16	0.12	0.19	0.19	0.09	0.05	0.13	0.06
K2O	10.4	10.4	9.5	9.8	9.9	10.1	9.9	10.0	0.3	10.8	11.0	10.9	10.0	10.7	10.5	10.8	10.7	0.3	9.9	10.6	10.4	10.2	10.7	10.6	10.4	0.3
FeO	3.19	3.61	3.69	3.32	2.93	2.61	2.36	3.10	0.50	4.62	4.01	3.92	3.61	3.53	3.84	3.43	3.85	0.40	3.07	3.02	2.84	2.91	3.25	3.82	3.15	0.36
TiO2	0.20	0.30	0.50	0.40	0.25	0.33	0.30	0.33	0.10	0.08	0.12	0.07	0.09	0.06	0.12	0.13	0.10	0.03	0.04	0.08	0.06	0.10	0.07	0.13	0.08	0.03
MgO	2.53	2.99	3.11	3.72	2.27	2.69	2.60	2.84	0.48	1.32	1.34	1.23	1.31	1.26	1.49	1.13	1.30	0.11	2.55	2.41	2.71	2.43	2.20	2.74	2.51	0.20
SiO2	49.5	49.0	49.3	45.4	50.5	46.5	46.5	48.1	1.9	48.3	47.9	46.7	49.6	46.9	48.4	46.4	47.7	1.1	49.2	49.1	49.7	49.7	48.8	51.2	49.6	0.9
MnO	0.04	0.00	0.02	0.02	0.00	0.01	0.01	0.01	0.01	0.00	0.01	0.03	0.04	0.00	0.00	0.04	0.02	0.02	0.03	0.00	0.00	0.01	0.04	0.01	0.02	0.02
Cr2O3	0.00	0.03	0.03	0.00	0.01	0.02	0.02	0.02	0.01	0.00	0.00	0.00	0.00	0.00	0.04	0.02	0.01	0.02	0.02	0.00	0.00	0.01	0.00	0.01	0.01	0.01
Al2O3	28.7	26.9	27.7	32.9	30.2	33.1	32.9	30.3	2.6	29.7	30.5	29.8	28.9	30.5	29.6	31.7	30.1	0.9	29.3	28.9	28.3	28.6	28.2	29.0	28.7	0.4
F (wt.%)	0.80	0.98	1.14	0.88	0.73	0.90	0.77	0.89	0.14	1.05	0.99	0.93	0.91	0.81	1.07	0.52	0.90	0.19	1.50	1.49	1.32	1.30	1.39	1.13	1.36	0.14
Cl (wt.%)	0.25	0.26	0.24	0.46	0.17	0.27	0.18	0.26	0.10	0.00	0.01	0.00	0.00	0.01	0.04	0.01	0.01	0.01	0.10	0.01	0.06	0.06	0.03	0.03	0.05	0.03
Total	**96.3**	**95.2**	**95.7**	**97.1**	**97.0**	**96.6**	**95.5**	**96.2**	**0.8**	**95.9**	**95.9**	**93.7**	**94.8**	**93.9**	**95.2**	**94.3**	94.8	0.9	**95.9**	**95.7**	**95.6**	**95.5**	**94.7**	**98.7**	96.0	1.4
Muscovite KAl2(Si3Al)O10(OH,F)2																										
Na	0.07	0.09	0.06	0.03	0.01	0.02	0.01	0.04	0.03	0.01	0.01	0.00	0.03	0.02	0.01	0.02	0.01	0.01	0.02	0.02	0.03	0.03	0.01	0.01	0.02	0.01
K	0.89	0.91	0.82	0.83	0.84	0.86	0.84	0.86	0.03	0.93	0.95	0.96	0.87	0.94	0.92	0.94	0.93	0.03	0.85	0.92	0.89	0.88	0.93	0.88	0.89	0.03
Total	**0.96**	**1.00**	**0.88**	**0.86**	**0.85**	**0.88**	**0.86**	**0.90**	**0.06**	**0.94**	**0.96**	**0.97**	**0.89**	**0.96**	**0.93**	**0.96**	0.94	0.03	**0.87**	**0.93**	**0.92**	**0.91**	**0.94**	**0.89**	0.91	0.03
Total Al	2.3	2.2	2.2	2.6	2.3	2.6	2.6	0.3	0.1	2.4	2.4	2.4	2.3	2.5	2.4	2.6	2.4	0.1	2.3	2.3	2.3	2.3	2.3	2.2	2.3	0.0
Si	3.3	3.4	3.3	3.0	3.3	3.1	3.1	0.3	0.1	3.3	3.2	3.2	3.4	3.2	3.3	3.2	3.3	0.1	3.3	3.3	3.4	3.4	3.3	3.4	3.3	0.0
Al (iv)	0.68	0.65	0.67	0.96	0.68	0.90	0.88	0.26	0.10	0.72	0.76	0.76	0.64	0.77	0.71	0.82	0.74	0.06	0.68	0.67	0.64	0.65	0.66	0.65	0.66	0.02
Total	**4.0**	**4.0**	**4.0**	**4.0**	**4.0**	**4.0**	**4.0**	**0.3**	**0.1**	**4.0**	**4.0**	**4.0**	**4.0**	**4.0**	**4.0**	**4.0**	4.0	0.0	**4.0**	**4.0**	**4.0**	**4.0**	**4.0**	**4.0**	4.0	0.0
Al (vi)	1.6	1.5	1.5	1.6	1.7	1.7	1.7	0.3	0.1	1.7	1.7	1.7	1.7	1.7	1.7	1.7	1.7	0.0	1.6	1.6	1.6	1.6	1.6	1.6	1.6	0.0
Cr	0.00	0.00	0.00	0.00	0.00	0.00	0.00	0.26	0.10	0.00	0.00	0.00	0.00	0.00	0.00	0.00	0.00	0.00	0.00	0.00	0.00	0.00	0.00	0.00	0.00	0.00
Mg	0.25	0.31	0.31	0.37	0.22	0.27	0.26	0.26	0.10	0.13	0.14	0.13	0.13	0.13	0.15	0.12	0.13	0.01	0.26	0.24	0.27	0.25	0.23	0.27	0.25	0.02
Fe	0.18	0.21	0.21	0.19	0.16	0.15	0.13	0.26	0.10	0.26	0.23	0.23	0.21	0.20	0.22	0.20	0.22	0.02	0.17	0.17	0.16	0.17	0.19	0.21	0.18	0.02
Mn	0.00	0.00	0.00	0.00	0.00	0.00	0.00	0.26	0.10	0.00	0.00	0.00	0.00	0.00	0.00	0.00	0.00	0.00	0.00	0.00	0.00	0.00	0.00	0.00	0.00	0.00
Ca	0.00	0.00	0.00	0.00	0.00	0.00	0.00	0.26	0.10	0.00	0.00	0.01	0.01	0.00	0.00	0.00	0.00	0.00	0.00	0.00	0.00	0.00	0.00	0.00	0.00	0.00
Ti	0.01	0.02	0.03	0.02	0.01	0.02	0.02	0.26	0.10	0.00	0.01	0.00	0.01	0.00	0.01	0.01	0.01	0.00	0.00	0.00	0.00	0.01	0.00	0.01	0.00	0.00
Total	**2.0**	**2.1**	**2.1**	**2.2**	**2.1**	**2.1**	**2.1**	**0.3**	**0.1**	**2.1**	**2.1**	**2.1**	**2.0**	**2.0**	**2.0**	**2.1**	2.0	0.0	**2.1**	**2.1**	**2.1**	**2.1**	**2.0**	**2.1**	2.1	0.0
TOTAL	**7.0**	**7.0**	**7.0**	**7.1**	**6.9**	**7.0**	**7.0**	**0.3**	**0.1**	**7.0**	**7.0**	**7.0**	**6.9**	**7.0**	**7.0**	**7.0**	7.0	0.0	**7.0**	**7.0**	**7.0**	**7.0**	**7.0**	**7.0**	96.0	1.4
F	0.17	0.21	0.24	0.19	0.15	0.19	0.16	0.26	0.10	0.23	0.21	0.21	0.20	0.18	0.23	0.11	0.19	0.04	0.32	0.32	0.28	0.28	0.30	0.23	96.02	1.38
Cl	0.03	0.03	0.03	0.05	0.02	0.03	0.02	0.26	0.10	0.00	0.00	0.00	0.00	0.00	0.00	0.00	0.00	0.00	0.01	0.00	0.01	0.01	0.00	0.00	96.02	1.38
OH	1.8	1.8	1.7	1.8	1.8	1.8	1.8	0.3	0.1	1.8	1.8	1.8	1.8	1.8	1.8	1.9	1.8	0.0	1.7	1.7	1.7	1.7	1.7	1.8	96.0	1.4
Total	2.0	2.0	2.0	2.0	2.0	2.0	2.0	0.3	0.1	2.0	2.0	2.0	2.0	2.0	2.0	2.0	2.0	0.0	2.0	2.0	2.0	2.0	2.0	2.0	96.0	1.4
phengite component %	21.9	25.9	26.3	26.1	19.3	20.2	19.2	0.3	0.1	19.5	18.0	17.8	17.2	16.4	18.4	15.7	17.6	1.3	20.9	20.4	21.4	20.5	20.5	23.4	96.0	1.4
Fe/(Fe+Mg)	0.41	0.40	0.40	0.33	0.42	0.35	0.34	0.26	0.10	0.66	0.63	0.64	0.61	0.61	0.59	0.63	0.62	0.02	0.40	0.41	0.37	0.40	0.45	0.44	96.02	1.38
% F-end-member	8.5	10.6	12.2	9.3	7.6	9.5	8.2	0.26	0.10	11.3	10.6	10.3	9.7	8.8	11.5	5.6	9.69	2.02	16.0	16.0	14.1	13.9	15.1	11.7	96.02	1.38
% Cl-end-member	1.4	1.5	1.4	2.6	0.9	1.6	1.0	0.26	0.10	0.0	0.1	0.0	0.0	0.1	0.2	0.0	0.06	0.08	0.6	0.1	0.4	0.4	0.2	0.2	96.02	1.38

Table A10: Complete electron microanalysis for mica (continued)

(Wt.%)	28TW	13TW	13TW	13TW	13TW	13TW	13TW	Mean (6)	Std.dev	15TW	15TW	15TW	Mean (3)	Std.dev	10TW	10TW	10TW	10TW	10TW	10TW	10TW	10TW	10TW	10TW	10TW	10TW
CaO	0.04	0.30	0.22	0.29	0.09	0.31	0.19	0.23	0.09	0.11	0.03	0.07	0.07	0.04	0.10	0.46	0.48	0.17	0.09	0.06	0.04	0.05	0.08	0.03	0.08	0.11	0.02	0.06
Na2O	0.11	0.16	0.26	0.29	0.19	0.26	0.33	0.25	0.06	0.07	0.11	0.07	0.08	0.02	0.10	0.17	0.19	0.42	0.25	0.19	0.10	0.16	0.20	0.23	0.14	0.27	0.14	0.16
K2O	10.9	8.2	9.7	10.2	10.4	9.9	9.5	9.6	0.8	8.9	9.4	10.7	9.7	0.9	10.9	10.3	10.0	10.2	9.5	10.1	10.8	9.1	10.4	10.0	9.4	10.4	10.6	10.1
FeO	4.61	4.18	3.27	3.64	2.92	2.94	4.47	3.57	0.65	6.66	3.44	3.01	4.37	1.99	4.35	3.90	3.80	3.84	3.98	3.45	3.33	3.88	4.21	4.62	2.78	4.99	5.29	3.54
TiO2	0.07	0.06	0.05	0.01	0.05	0.08	0.53	0.13	0.20	0.00	0.04	0.06	0.03	0.03	0.11	0.13	0.04	0.07	0.17	0.24	0.08	0.23	0.12	0.18	0.10	0.16	0.17	0.13
MgO	1.25	1.29	1.40	1.54	1.36	1.37	1.33	1.38	0.09	2.75	1.52	1.22	1.83	0.81	1.66	2.18	2.10	1.88	1.77	1.49	1.53	1.92	1.74	1.95	1.71	1.80	2.33	1.53
SiO2	47.3	49.3	44.3	44.4	45.2	45.5	44.1	45.5	1.9	47.5	54.3	45.4	49.1	4.6	47.4	47.8	45.4	48.7	52.2	49.1	47.9	54.4	47.4	50.6	53.5	48.2	48.1	51.3
MnO	0.01	0.01	0.03	0.00	0.00	0.00	0.00	0.01	0.01	0.06	0.00	0.01	0.02	0.03	0.03	0.02	0.00	0.00	0.00	0.01	0.10	0.00	0.00	0.04	0.00	0.01	0.10	0.00
Cr2O3	0.00	0.01	0.00	0.05	0.02	0.01	0.00	0.02	0.02	0.03	0.01	0.01	0.02	0.01	0.00	0.01	0.02	0.01	0.00	0.01	0.00	0.03	0.00	0.01	0.03	0.00	0.00	0.03
Al2O3	29.9	26.6	31.6	29.9	29.5	30.0	31.2	29.8	1.7	28.1	27.7	30.4	28.7	1.4	29.3	28.3	27.2	30.0	26.1	28.9	31.3	29.1	29.4	27.5	27.1	28.5	27.5	26.8
F (wt.%)	0.82	0.53	0.77	1.15	0.91	0.70	0.59	0.78	0.23	0.79	1.05	1.01	0.95	0.14	1.35	1.14	0.95	0.83	1.16	1.36	1.20	1.55	1.15	1.41	1.13	1.20	1.66	0.98
Cl (wt.%)	0.02	0.10	0.15	0.19	0.11	0.24	0.14	0.16	0.05	0.00	0.02	0.01	0.01	0.01	0.06	0.08	0.12	0.35	0.03	0.02	0.00	0.02	0.01	0.00	0.01	0.04	0.02	0.01
Total	**95.0**	**90.7**	**91.7**	**91.6**	**90.7**	**91.3**	**92.3**	91.4	0.6	**94.9**	**97.6**	**92.0**	94.8	2.8	**95.3**	**94.5**	**90.2**	**96.5**	**95.3**	**94.9**	**96.5**	**100.4**	**94.6**	**96.6**	**95.9**	**95.7**	**95.8**	**94.6**
Muscovite KAl2(Si3Al)O10																												
Na	0.01	0.02	0.04	0.04	0.03	0.04	0.05	0.03	0.01	0.01	0.01	0.01	0.01	0.00	0.01	0.02	0.03	0.06	0.03	0.03	0.01	0.02	0.03	0.03	0.02	0.04	0.02	0.02
K	0.95	0.73	0.87	0.93	0.95	0.90	0.85	0.87	0.08	0.78	0.78	0.96	0.84	0.11	0.96	0.90	0.92	0.88	0.82	0.88	0.93	0.74	0.91	0.86	0.80	0.91	0.93	0.88
Total	**0.97**	**0.76**	**0.90**	**0.97**	**0.97**	**0.93**	**0.89**	0.90	0.08	**0.79**	**0.80**	**0.97**	0.85	0.11	**0.97**	**0.92**	**0.94**	**0.93**	**0.85**	**0.90**	**0.94**	**0.76**	**0.94**	**0.89**	**0.81**	**0.95**	**0.95**	**0.90**
Total Al	2.4	2.2	2.6	2.5	2.5	2.5	2.6	2.5	0.1	2.3	2.1	2.5	2.3	0.2	2.4	2.3	2.3	2.4	2.1	2.3	2.5	2.2	2.4	2.2	2.1	2.3	2.2	2.1
Si	3.2	3.5	3.1	3.2	3.2	3.2	3.1	3.2	0.1	3.3	3.5	3.2	3.3	0.2	3.3	3.3	3.3	3.3	3.5	3.3	3.2	3.5	3.3	3.4	3.5	3.3	3.3	3.5
Al (iv)	0.76	0.55	0.88	0.83	0.78	0.78	0.90	0.78	0.13	0.74	0.47	0.80	0.67	0.18	0.74	0.71	0.72	0.73	0.48	0.65	0.78	0.54	0.74	0.60	0.46	0.71	0.69	0.52
Total	**4.0**	**4.0**	**4.0**	**4.0**	**4.0**	**4.0**	**4.0**	4.0	0.0	**4.0**	**4.0**	**4.0**	4.0	0.0	**4.0**	**4.0**	**4.0**	**4.0**	**4.0**	**4.0**	**4.0**	**4.0**	**4.0**	**4.0**	**4.0**	**4.0**	**4.0**	**4.0**
Al (vi)	1.7	1.7	1.7	1.7	1.7	1.7	1.7	1.7	0.0	1.5	1.7	1.7	1.6	0.1	1.6	1.6	1.6	1.7	1.6	1.7	1.7	1.6	1.6	1.6	1.7	1.6	1.5	1.6
Cr	0.00	0.00	0.00	0.00	0.00	0.00	0.00	0.00	0.00	0.00	0.00	0.00	0.00	0.00	0.00	0.00	0.00	0.00	0.00	0.00	0.00	0.00	0.00	0.00	0.00	0.00	0.00	0.00
Mg	0.13	0.14	0.15	0.16	0.15	0.15	0.14	0.15	0.01	0.28	0.15	0.13	0.19	0.08	0.17	0.22	0.23	0.19	0.18	0.15	0.15	0.18	0.18	0.20	0.17	0.18	0.24	0.16
Fe	0.26	0.25	0.19	0.22	0.18	0.17	0.26	0.21	0.04	0.38	0.19	0.18	0.25	0.12	0.25	0.23	0.23	0.22	0.22	0.20	0.19	0.21	0.24	0.26	0.15	0.29	0.31	0.20
Mn	0.00	0.00	0.00	0.00	0.00	0.00	0.00	0.00	0.00	0.00	0.00	0.00	0.00	0.00	0.00	0.00	0.00	0.00	0.00	0.00	0.01	0.00	0.00	0.00	0.00	0.00	0.01	0.00
Ca	0.00	0.02	0.02	0.02	0.01	0.02	0.01	0.02	0.01	0.01	0.00	0.01	0.01	0.00	0.01	0.03	0.04	0.01	0.01	0.01	0.00	0.00	0.01	0.00	0.01	0.01	0.00	0.01
Ti	0.00	0.00	0.00	0.00	0.00	0.00	0.03	0.01	0.01	0.00	0.00	0.00	0.00	0.00	0.01	0.01	0.00	0.00	0.01	0.01	0.00	0.01	0.01	0.01	0.01	0.01	0.01	0.01
Total	**2.1**	**2.1**	**2.1**	**2.1**	**2.0**	**2.1**	**2.1**	2.1	0.0	**2.2**	**2.0**	**2.0**	2.1	0.1	**2.1**	**2.1**	**2.1**	**2.1**	**2.0**	**2.0**	**2.1**	**2.1**	**2.1**	**2.1**	**2.0**	**2.1**	**2.1**	**2.0**
TOTAL	**7.0**	**6.8**	**7.0**	**7.1**	**7.0**	**7.0**	**7.0**	7.0	0.1	**7.0**	**6.8**	**7.0**	6.9	0.1	**7.0**	**7.0**	**7.0**	**7.0**	**6.9**	**6.9**	**7.0**	**6.8**	**7.0**	**6.9**	**6.8**	**7.0**	**7.0**	**6.9**
F	0.18	0.12	0.17	0.26	0.21	0.16	0.13	0.17	0.05	0.17	0.22	0.22	0.20	0.03	0.29	0.25	0.22	0.18	0.25	0.29	0.25	0.31	0.25	0.30	0.24	0.26	0.36	0.21
Cl	0.00	0.01	0.02	0.02	0.01	0.03	0.02	0.02	0.01	0.00	0.00	0.00	0.00	0.00	0.01	0.01	0.02	0.04	0.00	0.00	0.00	0.00	0.00	0.00	0.00	0.01	0.00	0.00
OH	1.8	1.9	1.8	1.7	1.8	1.8	1.9	1.8	0.1	1.8	1.8	1.8	1.8	0.0	1.7	1.7	1.8	1.8	1.7	1.7	1.7	1.7	1.7	1.7	1.8	1.7	1.6	1.8
Total	2.0	2.0	2.0	2.0	2.0	2.0	2.0	2.0	0.0	2.0	2.0	2.0	2.0	0.0	2.0	2.0	2.0	2.0	2.0	2.0	2.0	2.0	2.0	2.0	2.0	2.0	2.0	2.0
phengite component %	19.4	19.7	17.1	19.3	16.1	16.8	20.8	18.3	1.9	30.5	16.9	15.4	20.9	8.3	21.1	23.5	23.7	20.3	20.7	18.0	17.2	19.6	20.9	22.8	16.7	23.4	26.7	18.4
Fe/(Fe+Mg)	0.67	0.64	0.57	0.57	0.55	0.55	0.65	0.59	0.04	0.58	0.56	0.58	0.57	0.01	0.59	0.50	0.50	0.53	0.56	0.57	0.55	0.53	0.58	0.57	0.48	0.61	0.56	0.56
% F-end-member	8.9	5.8	8.6	13.0	10.3	7.8	6.6	8.68	2.63	8.5	10.8	11.2	10.17	1.46	14.6	12.4	10.8	8.8	12.4	14.6	12.7	15.6	12.5	15.0	11.9	13.0	18.0	10.5
% Cl-end-member	0.1	0.6	0.9	1.1	0.7	1.4	0.8	0.92	0.29	0.0	0.1	0.1	0.07	0.06	0.4	0.5	0.7	2.0	0.2	0.1	0.0	0.1	0.1	0.0	0.0	0.3	0.1	0.1

Table A10: Complete electron microanalysis for mica (continued)

(Wt.%)	10TW	10TW	10TW	10TW	10TW	10TW	10TW	10TW	10TW	10TW	10TW	10TW	10TW	10TW	10TW	10TW	10TW	10TW	10TW	10TW	10TW	10TW	10TW	Mean (37)	Std.dev	37TW	37TW	37TW
CaO	0.04	0.08	0.09	0.04	0.15	0.12	0.10	0.19	0.68	0.07	0.09	0.06	0.03	0.13	0.48	0.21	0.20	0.21	0.10	0.04	0.07	0.06	0.02	0.14	0.14	0.03	0.00	0.01
Na2O	0.18	0.18	0.16	0.18	0.18	0.23	0.12	0.11	0.35	0.08	0.09	0.09	0.13	0.11	0.46	0.33	0.13	0.17	0.12	0.09	0.12	0.15	0.06	0.18	0.09	0.42	0.16	0.26
K2O	9.6	10.3	10.5	10.8	10.4	10.4	10.9	10.9	10.3	2.3	11.0	11.0	10.9	10.8	10.7	10.9	10.8	10.9	11.0	10.0	10.3	9.8	9.2	10.1	2.0	9.6	8.4	9.9
FeO	4.39	4.08	2.93	3.66	3.88	4.02	4.14	4.09	3.73	1.02	3.69	3.91	4.08	3.85	4.49	4.66	4.56	4.05	4.00	4.38	3.36	6.32	3.91	3.98	0.93	3.07	2.62	1.86
TiO2	0.16	1.75	0.11	0.11	0.12	0.06	0.10	0.13	0.07	0.07	0.11	0.14	0.11	0.07	0.03	0.12	0.08	0.12	0.08	0.12	0.10	0.12	0.03	0.16	0.26	0.07	0.02	0.09
MgO	1.80	1.69	1.54	1.58	1.99	2.00	1.78	1.87	2.07	0.38	1.80	1.79	1.76	1.87	1.80	1.70	1.73	1.77	1.75	2.17	1.86	1.88	2.06	1.79	0.37	1.95	1.88	1.92
SiO2	53.4	47.1	48.7	47.6	48.5	48.7	48.1	48.8	47.3	87.7	46.4	47.2	47.2	47.5	46.5	48.1	47.0	47.8	46.8	48.0	47.3	47.4	50.5	49.6	9.4	50.4	56.0	50.0
MnO	0.02	0.00	0.07	0.00	0.00	0.03	0.05	0.01	0.02	0.01	0.05	0.03	0.00	0.00	0.04	0.00	0.08	0.00	0.07	0.02	0.01	0.01	0.00	0.02	0.03	0.00	0.01	0.00
Cr2O3	0.00	0.02	0.01	0.00	0.00	0.00	0.05	0.01	0.03	0.03	0.01	0.03	0.02	0.00	0.00	0.00	0.00	0.00	0.01	0.00	0.00	0.00	0.01	0.01	0.01	0.00	0.00	0.02
Al2O3	24.5	29.0	29.5	30.0	28.4	28.7	29.7	29.7	27.7	5.6	28.7	29.7	29.5	29.9	27.6	29.1	28.4	29.1	29.1	26.3	27.8	27.5	30.4	27.9	5.6	30.5	27.6	32.0
F (wt.%)	1.51	1.24	1.33	1.29	1.17	1.24	1.23	1.21	1.14	0.44	1.56	1.36	1.36	1.24	1.24	1.17	1.34	1.27	1.43	1.39	1.25	1.12	0.57	1.22	0.29	1.21	1.15	1.26
Cl (wt.%)	0.00	0.00	0.00	0.00	0.27	0.25	0.08	0.06	0.29	0.04	0.04	0.03	0.05	0.08	0.43	0.29	0.11	0.19	0.16	0.12	0.03	0.07	0.01	0.09	0.11	0.03	0.04	0.03
Total	**95.6**	**95.4**	**95.0**	**95.2**	**95.1**	**95.8**	**96.3**	**97.1**	**93.7**	**97.7**	**93.6**	**95.4**	**95.1**	**95.5**	**93.7**	**96.6**	**94.4**	**95.6**	**94.6**	**92.6**	**92.2**	**94.5**	**96.8**	95.2	14.4	**97.3**	**98.0**	**97.4**
Muscovite KAl2(Si3Al)O10																												
Na	0.02	0.02	0.02	0.02	0.02	0.03	0.02	0.02	0.05	0.01	0.01	0.01	0.02	0.02	0.06	0.04	0.02	0.02	0.02	0.01	0.02	0.02	0.01	0.02	0.01	0.05	0.02	0.03
K	0.83	0.90	0.91	0.94	0.91	0.91	0.94	0.93	0.92	0.17	0.99	0.96	0.96	0.94	0.96	0.94	0.96	0.95	0.97	0.90	0.92	0.87	0.78	0.89	0.17	0.81	0.69	0.83
Total	**0.85**	**0.92**	**0.94**	**0.96**	**0.93**	**0.94**	**0.96**	**0.95**	**0.96**	**0.18**	**1.00**	**0.97**	**0.98**	**0.95**	**1.02**	**0.99**	**0.98**	**0.98**	**0.99**	**0.91**	**0.94**	**0.89**	**0.78**	0.91	0.18	**0.86**	**0.71**	**0.87**
Total Al	1.9	2.3	2.4	2.4	2.3	2.3	2.4	2.4	2.3	0.4	2.4	2.4	2.4	2.4	2.3	2.3	2.3	2.4	2.4	2.2	2.3	2.3	2.4	2.2	0.4	2.4	2.1	2.5
Si	3.6	3.2	3.3	3.3	3.3	3.3	3.3	3.3	3.3	5.1	3.3	3.2	3.2	3.2	3.3	3.3	3.3	3.3	3.2	3.4	3.3	3.3	3.3	3.4	0.6	3.3	3.6	3.3
Al (iv)	0.40	0.78	0.68	0.74	0.68	0.69	0.74	0.72	0.70	-1.12	0.75	0.76	0.75	0.76	0.72	0.73	0.73	0.73	0.75	0.62	0.67	0.70	0.68	0.63	0.30	0.68	0.41	0.72
Total	**4.0**	**4.0**	**4.0**	**4.0**	**4.0**	**4.0**	**4.0**	**4.0**	**4.0**	**4.0**	**4.0**	**4.0**	**4.0**	**4.0**	**4.0**	**4.0**	**4.0**	**4.0**	**4.0**	**4.0**	**4.0**	**4.0**	**4.0**	4.0	0.6	**4.0**	**4.0**	**4.0**
Al (vi)	1.6	1.6	1.7	1.7	1.6	1.6	1.6	1.6	1.6	1.5	1.6	1.6	1.6	1.7	1.6	1.6	1.6	1.6	1.6	1.6	1.6	1.6	1.7	1.6	0.2	1.7	1.7	1.8
Cr	0.00	0.00	0.00	0.00	0.00	0.00	0.00	0.00	0.00	0.00	0.00	0.00	0.00	0.00	0.00	0.00	0.00	0.00	0.00	0.00	0.00	0.00	0.00	0.00	0.00	0.00	0.00	0.00
Mg	0.18	0.17	0.16	0.16	0.20	0.20	0.18	0.19	0.22	0.03	0.19	0.18	0.18	0.19	0.19	0.17	0.18	0.18	0.18	0.23	0.20	0.20	0.20	0.18	0.04	0.19	0.18	0.19
Fe	0.25	0.23	0.17	0.21	0.22	0.23	0.23	0.23	0.22	0.05	0.22	0.22	0.24	0.22	0.26	0.27	0.27	0.23	0.23	0.26	0.20	0.37	0.22	0.23	0.05	0.17	0.14	0.10
Mn	0.00	0.00	0.00	0.00	0.00	0.00	0.00	0.00	0.00	0.00	0.00	0.00	0.00	0.00	0.00	0.00	0.01	0.00	0.00	0.00	0.00	0.00	0.00	0.00	0.00	0.00	0.00	0.00
Ca	0.00	0.01	0.01	0.00	0.01	0.01	0.01	0.01	0.05	0.01	0.01	0.01	0.00	0.01	0.04	0.02	0.02	0.02	0.01	0.00	0.01	0.01	0.00	0.01	0.01	0.00	0.00	0.00
Ti	0.01	0.09	0.01	0.01	0.01	0.00	0.01	0.01	0.00	0.00	0.01	0.01	0.01	0.00	0.00	0.01	0.00	0.01	0.00	0.01	0.01	0.01	0.00	0.01	0.01	0.00	0.00	0.00
Total	**2.0**	**2.1**	**2.0**	**2.0**	**2.1**	**2.1**	**2.1**	**2.1**	**2.1**	**1.6**	**2.1**	**2.1**	**2.1**	**2.1**	**2.1**	**2.1**	**2.1**	**2.1**	**2.1**	**2.1**	**2.0**	**2.1**	**2.1**	2.0	0.3	**2.1**	**2.0**	**2.0**
TOTAL	**6.8**	**7.0**	**7.0**	**7.0**	**7.0**	**7.0**	**7.0**	**7.0**	**7.0**	**5.8**	**7.1**	**7.0**	**7.0**	**7.0**	**7.1**	**7.0**	**7.0**	**7.0**	**7.1**	**7.0**	**7.0**	**7.0**	**6.9**	7.0	1.1	**6.9**	**6.7**	**6.9**
F	0.32	0.27	0.29	0.28	0.25	0.27	0.26	0.26	0.25	0.08	0.35	0.30	0.30	0.27	0.28	0.25	0.30	0.28	0.31	0.31	0.28	0.25	0.12	0.26	0.06	0.25	0.23	0.26
Cl	0.00	0.00	0.00	0.00	0.03	0.03	0.01	0.01	0.03	0.00	0.01	0.00	0.01	0.01	0.05	0.03	0.01	0.02	0.02	0.01	0.00	0.01	0.00	0.01	0.01	0.00	0.00	0.00
OH	1.7	1.7	1.7	1.7	1.7	1.7	1.7	1.7	1.7	1.9	1.7	1.7	1.7	1.7	1.7	1.7	1.7	1.7	1.7	1.7	1.7	1.7	1.9	1.7	0.3	1.7	1.8	1.7
Total	2.0	2.0	2.0	2.0	2.0	2.0	2.0	2.0	2.0	2.0	2.0	2.0	2.0	2.0	2.0	2.0	2.0	2.0	2.0	2.0	2.0	2.0	2.0	2.0	0.3	2.0	2.0	2.0
phengite component %	22.1	24.3	16.8	18.5	21.5	21.6	20.8	21.2	23.6	5.7	20.4	20.4	20.5	20.4	23.9	22.2	22.7	21.1	20.8	24.1	19.8	27.0	20.0	20.9	4.2	17.8	16.1	14.4
Fe/(Fe+Mg)	0.58	0.57	0.52	0.57	0.52	0.53	0.57	0.55	0.50	0.60	0.54	0.55	0.57	0.54	0.58	0.61	0.60	0.56	0.56	0.53	0.50	0.65	0.51	0.55	0.09	0.47	0.44	0.35
% F-end-member	16.1	13.4	14.3	13.9	12.6	13.4	13.2	12.9	12.6	4.1	17.3	14.7	14.8	13.4	13.8	12.6	14.7	13.8	15.7	15.5	13.9	12.3	5.9	13.18	3.21	12.6	11.6	13.0
% Cl-end-member	0.0	0.0	0.0	0.0	1.6	1.4	0.4	0.3	1.7	0.2	0.2	0.2	0.3	0.5	2.6	1.7	0.6	1.1	0.9	0.7	0.2	0.4	0.0	0.53	0.63	0.1	0.2	0.2

Table A10: Complete electron microanalysis for mica (continued)

(Wt.%)	37TW	37TW	37TW	Mean (6)	Std.dev	18TW	18TW	18TW	18TW	Mean (4)	Std.dev	19TW	19TW	Mean (2)	33TW	33TW	33TW	33TW	33TW	33TW	33TW	Mean (7)	Std.dev	34TW	34TW	34TW	34TW	34TW
CaO	0.04	0.06	0.05	0.03	0.02	0.09	0.17	0.11	0.11	0.12	0.03	0.00	0.02	0.01	0.01	0.02	0.05	0.03	0.00	0.00	0.00	0.02	0.02	0.34	0.23	0.44	0.37	0.76
Na2O	0.32	0.41	0.44	0.34	0.11	0.20	0.23	0.25	0.24	0.23	0.02	0.06	0.08	0.07	0.20	0.16	0.07	0.18	0.10	0.10	0.15	0.14	0.05	0.11	0.09	0.16	0.16	0.12
K2O	9.4	9.7	9.2	9.4	0.5	10.7	10.7	9.4	9.7	10.1	0.7	10.9	10.8	10.8	10.8	10.7	8.8	10.8	10.8	9.4	10.4	10.2	0.8	9.8	10.6	9.3	10.6	10.4
FeO	1.87	2.02	1.84	2.21	0.51	3.76	3.86	2.59	3.77	3.50	0.61	4.28	3.77	4.03	3.63	4.05	4.02	3.86	3.38	4.18	3.95	3.87	0.28	4.45	4.06	4.31	3.46	3.83
TiO2	0.08	0.06	0.10	0.07	0.03	0.12	0.12	0.06	0.17	0.12	0.05	0.01	0.04	0.03	0.07	0.07	0.08	0.02	0.07	0.03	0.04	0.05	0.02	0.07	0.10	0.12	0.09	0.14
MgO	1.84	1.82	1.92	1.89	0.05	1.50	1.60	1.34	1.73	1.54	0.16	1.63	1.50	1.57	1.34	1.24	1.30	1.21	1.23	1.22	1.48	1.29	0.10	1.97	1.62	2.01	1.75	1.83
SiO2	50.5	49.6	50.9	51.2	2.4	44.8	44.4	49.2	52.3	47.7	3.8	50.3	48.5	49.4	48.6	47.1	48.5	47.3	46.9	44.4	48.1	47.3	1.4	45.2	45.2	49.3	47.5	47.8
MnO	0.00	0.00	0.00	0.00	0.00	0.02	0.01	0.02	0.02	0.02	0.00	0.00	0.00	0.00	0.02	0.00	0.00	0.02	0.00	0.03	0.00	0.01	0.01	0.01	0.00	0.00	0.05	0.06
Cr2O3	0.01	0.01	0.00	0.01	0.01	0.01	0.02	0.00	0.00	0.01	0.01	0.00	0.00	0.00	0.00	0.01	0.00	0.03	0.02	0.00	0.00	0.01	0.01	0.00	0.00	0.03	0.02	0.00
Al2O3	29.8	29.9	29.9	30.0	1.4	29.4	29.9	27.2	26.4	28.2	1.7	30.9	29.9	30.4	32.5	30.7	31.2	30.7	31.1	29.7	29.6	30.8	1.0	27.0	27.6	29.8	29.1	28.6
F (wt.%)	1.13	1.15	1.13	1.17	0.05	1.13	1.23	1.18	1.39	1.23	0.11	0.96	0.85	0.91	1.43	1.47	1.50	1.07	1.45	1.55	1.43	1.41	0.16	0.86	0.85	0.29	1.12	1.17
Cl (wt.%)	0.02	0.03	0.02	0.03	0.01	0.19	0.20	0.17	0.09	0.16	0.05	0.01	0.02	0.02	0.00	0.04	0.05	0.05	0.01	0.04	0.04	0.03	0.02	0.65	0.19	0.58	0.03	0.03
Total	**94.9**	**94.7**	**95.5**	96.3	1.4	**91.9**	**92.4**	**91.5**	**95.8**	92.9	2.0	**99.0**	**95.4**	97.2	**98.6**	**95.5**	**95.6**	**95.3**	**95.1**	**90.7**	**95.2**	95.1	2.3	**90.4**	**90.5**	**96.5**	**94.2**	**94.7**
Muscovite KAl2(Si3Al)O10																												
Na	0.04	0.05	0.06	0.04	0.01	0.03	0.03	0.03	0.03	0.03	0.00	0.01	0.01	0.01	0.03	0.02	0.01	0.02	0.01	0.01	0.02	0.02	0.01	0.02	0.01	0.02	0.02	0.02
K	0.80	0.83	0.78	0.79	0.05	0.97	0.97	0.84	0.83	0.90	0.08	0.91	0.93	0.92	0.91	0.94	0.76	0.94	0.94	0.87	0.90	0.89	0.07	0.91	0.98	0.79	0.94	0.91
Total	**0.84**	**0.89**	**0.83**	0.83	0.06	**1.00**	**1.00**	**0.87**	**0.86**	0.93	0.08	**0.91**	**0.94**	0.93	**0.93**	**0.96**	**0.77**	**0.97**	**0.96**	**0.88**	**0.92**	0.91	0.07	**0.92**	**0.99**	**0.82**	**0.96**	**0.93**
Total Al	2.3	2.4	2.3	2.3	0.1	2.5	2.5	2.2	2.1	2.3	0.2	2.4	2.4	2.4	2.5	2.5	2.5	2.5	2.5	2.5	2.4	2.5	0.0	2.3	2.3	2.3	2.4	2.3
Si	3.4	3.3	3.4	3.4	0.1	3.2	3.2	3.4	3.5	3.3	0.2	3.3	3.3	3.3	3.2	3.2	3.3	3.2	3.2	3.2	3.3	3.2	0.0	3.3	3.3	3.3	3.3	3.3
Al (iv)	0.62	0.66	0.62	0.62	0.11	0.81	0.84	0.55	0.49	0.67	0.18	0.71	0.72	0.71	0.80	0.78	0.73	0.77	0.79	0.80	0.71	0.77	0.03	0.72	0.73	0.71	0.72	0.71
Total	**4.0**	**4.0**	**4.0**	4.0	0.0	**4.0**	**4.0**	**4.0**	**4.0**	4.0	0.0	**4.0**	**4.0**	4.0	**4.0**	**4.0**	**4.0**	**4.0**	**4.0**	**4.0**	**4.0**	4.0	0.0	**4.0**	**4.0**	**4.0**	**4.0**	**4.0**
Al (vi)	1.7	1.7	1.7	1.7	0.0	1.7	1.7	1.7	1.6	1.7	0.0	1.7	1.7	1.7	1.7	1.7	1.7	1.7	1.7	1.7	1.7	1.7	0.0	1.6	1.6	1.6	1.6	1.6
Cr	0.00	0.00	0.00	0.00	0.00	0.00	0.00	0.00	0.00	0.00	0.00	0.00	0.00	0.00	0.00	0.00	0.00	0.00	0.00	0.00	0.00	0.00	0.00	0.00	0.00	0.00	0.00	0.00
Mg	0.18	0.18	0.19	0.19	0.00	0.16	0.17	0.14	0.17	0.16	0.02	0.16	0.15	0.16	0.13	0.13	0.13	0.12	0.13	0.13	0.15	0.13	0.01	0.21	0.17	0.20	0.18	0.19
Fe	0.11	0.11	0.10	0.12	0.03	0.22	0.23	0.15	0.21	0.20	0.04	0.23	0.21	0.22	0.20	0.23	0.23	0.22	0.19	0.25	0.23	0.22	0.02	0.27	0.25	0.24	0.20	0.22
Mn	0.00	0.00	0.00	0.00	0.00	0.00	0.00	0.00	0.00	0.00	0.00	0.00	0.00	0.00	0.00	0.00	0.00	0.00	0.00	0.00	0.00	0.00	0.00	0.00	0.00	0.00	0.00	0.00
Ca	0.00	0.00	0.00	0.00	0.00	0.01	0.01	0.01	0.01	0.01	0.00	0.00	0.00	0.00	0.00	0.00	0.00	0.00	0.00	0.00	0.00	0.00	0.00	0.03	0.02	0.03	0.03	0.06
Ti	0.00	0.00	0.01	0.00	0.00	0.01	0.01	0.00	0.01	0.01	0.00	0.00	0.00	0.00	0.00	0.00	0.00	0.00	0.00	0.00	0.00	0.00	0.00	0.00	0.01	0.01	0.01	0.01
Total	**2.0**	**2.0**	**2.0**	2.0	0.0	**2.1**	**2.1**	**2.0**	**2.0**	2.0	0.0	**2.1**	**2.0**	2.1	**2.1**	**2.1**	**2.1**	**2.0**	**2.0**	**2.1**	**2.1**	2.1	0.0	**2.1**	**2.1**	**2.1**	**2.1**	**2.1**
TOTAL	**6.9**	**6.9**	**6.9**	6.9	0.1	**7.1**	**7.1**	**6.9**	**6.9**	7.0	0.1	**7.0**	**7.0**	7.0	**7.0**	**7.0**	**6.9**	**7.0**	**7.0**	**7.0**	**7.0**	7.0	0.0	**7.0**	**7.0**	**6.9**	**7.0**	**7.0**
F	0.24	0.24	0.24	0.24	0.01	0.26	0.28	0.26	0.30	0.27	0.02	0.20	0.18	0.19	0.30	0.32	0.32	0.23	0.31	0.35	0.31	0.31	0.04	0.20	0.20	0.06	0.25	0.25
Cl	0.00	0.00	0.00	0.00	0.00	0.02	0.02	0.02	0.01	0.02	0.01	0.00	0.00	0.00	0.00	0.00	0.01	0.01	0.00	0.01	0.01	0.00	0.00	0.08	0.02	0.07	0.00	0.00
OH	1.8	1.8	1.8	1.8	0.0	1.7	1.7	1.7	1.7	1.7	0.0	1.8	1.8	1.8	1.7	1.7	1.7	1.8	1.7	1.6	1.7	1.7	0.0	1.7	1.8	1.9	1.8	1.7
Total	2.0	2.0	2.0	2.0	0.0	2.0	2.0	2.0	2.0	2.0	0.0	2.0	2.0	2.0	2.0	2.0	2.0	2.0	2.0	2.0	2.0	2.0	0.0	2.0	2.0	2.0	2.0	2.0
phengite component %	14.6	15.0	14.9	15.5	1.3	19.3	20.1	15.2	20.1	18.7	2.3	19.1	18.0	18.6	16.3	17.6	17.3	16.9	15.8	18.3	18.4	17.2	1.0	24.5	21.5	22.6	20.1	22.8
Fe/(Fe+Mg)	0.36	0.38	0.35	0.39	0.05	0.59	0.58	0.52	0.55	0.56	0.03	0.60	0.58	0.59	0.60	0.65	0.63	0.64	0.61	0.66	0.60	0.63	0.02	0.56	0.59	0.55	0.53	0.54
% F-end-member	11.9	12.2	11.9	12.20	0.52	12.8	13.8	13.1	14.8	13.63	0.89	9.9	9.1	9.50	14.9	15.9	15.9	11.5	15.7	17.6	15.4	15.27	1.86	9.9	9.7	3.1	12.3	12.7
% Cl-end-member	0.1	0.2	0.1	0.15	0.05	1.1	1.2	1.0	0.5	0.95	0.31	0.1	0.1	0.10	0.0	0.2	0.3	0.3	0.1	0.3	0.2	0.20	0.12	4.0	1.2	3.3	0.2	0.2

Table A10: Complete electron microanalysis for mica (continued)

(Wt.%)	34TW	34TW	34TW	34TW	34TW	34TW	34TW	34TW	Mean (13)	Std.dev	2aTW	2aTW	Mean (2)	Std.dev	3aTW	3aTW	3aTW	3aTW	3aTW	3aTW	3aTW	3aTW
CaO	0.01	0.40	0.15	0.08	0.06	0.02	0.05	0.05	0.23	0.22	0.23	0.52	0.38	0.21	0.07	0.11	0.07	0.11	0.01	0.03	0.05	0.00
Na2O	0.07	0.13	0.09	0.10	0.14	0.22	0.06	0.13	0.12	0.04	0.11	1.01	0.56	0.64	0.12	0.18	0.12	0.18	0.10	0.11	0.13	0.12
K2O	11.0	10.5	10.5	10.6	10.6	10.7	10.5	10.8	10.4	0.4	10.8	10.0	10.4	0.6	10.0	9.6	10.0	9.6	10.7	10.7	9.3	10.4
FeO	3.59	3.64	3.34	4.43	4.13	4.17	4.23	3.80	3.96	0.37	3.47	4.27	3.87	0.57	2.10	1.89	2.10	1.89	1.94	2.44	1.49	1.51
TiO2	0.09	0.10	0.12	0.14	0.10	0.11	0.08	0.15	0.11	0.02	0.20	0.14	0.17	0.04	0.04	0.01	0.04	0.01	0.08	0.05	0.23	0.03
MgO	2.03	2.00	1.73	2.19	1.94	2.00	2.07	1.84	1.92	0.16	1.91	2.03	1.97	0.08	2.64	2.74	2.64	2.74	2.20	2.27	2.65	2.87
SiO2	48.4	48.0	48.0	49.5	49.3	48.9	48.8	48.4	48.0	1.4	47.2	48.3	47.7	0.8	53.9	53.6	53.9	53.6	49.4	51.4	58.3	54.4
MnO	0.02	0.03	0.00	0.08	0.00	0.06	0.00	0.00	0.02	0.03	0.00	0.01	0.01	0.01	0.00	0.03	0.00	0.03	0.00	0.00	0.02	0.02
Cr2O3	0.00	0.00	0.00	0.02	0.02	0.00	0.00	0.02	0.01	0.01	0.00	0.00	0.00	0.00	0.00	0.00	0.00	0.00	0.01	0.01	0.01	0.01
Al2O3	28.6	28.1	29.0	27.0	28.1	27.1	27.1	28.6	28.1	0.9	28.8	30.1	29.5	0.9	29.7	29.2	29.7	29.2	29.4	29.8	25.6	29.6
F (wt.%)	1.29	0.97	1.10	1.32	1.24	1.29	1.14	1.14	1.06	0.28	1.15	0.89	1.02	0.18	0.61	0.63	0.61	0.63	1.26	0.89	0.56	0.60
Cl (wt.%)	0.02	0.03	0.04	0.04	0.02	0.13	0.04	0.02	0.14	0.22	0.10	0.64	0.37	0.38	0.02	0.02	0.02	0.02	0.02	0.02	0.03	0.01
Total	**95.1**	**93.9**	**94.0**	**95.4**	**95.7**	**94.7**	**94.1**	**95.0**	94.2	1.8	**93.9**	**97.9**	95.9	2.8	**99.2**	**98.0**	**99.2**	**98.0**	**95.1**	**97.7**	**98.4**	**99.6**
Muscovite KAl2(Si3Al)O10																						
Na	0.01	0.02	0.01	0.01	0.02	0.03	0.01	0.02	0.02	0.01	0.02	0.13	0.07	0.08	0.02	0.02	0.02	0.02	0.01	0.01	0.02	0.01
K	0.96	0.92	0.92	0.92	0.92	0.94	0.93	0.94	0.92	0.04	0.96	0.85	0.90	0.08	0.81	0.79	0.81	0.79	0.93	0.89	0.75	0.84
Total	**0.97**	**0.94**	**0.93**	**0.94**	**0.94**	**0.97**	**0.93**	**0.96**	0.94	0.04	**0.97**	**0.98**	0.98	0.01	**0.83**	**0.81**	**0.83**	**0.81**	**0.94**	**0.90**	**0.77**	**0.86**
Total Al	2.3	2.3	2.4	2.2	2.3	2.2	2.2	2.3	2.3	0.1	2.4	2.4	2.4	0.0	2.2	2.2	2.2	2.2	2.3	2.3	1.9	2.2
Si	3.3	3.3	3.3	3.4	3.4	3.4	3.4	3.3	3.3	0.0	3.3	3.2	3.3	0.0	3.4	3.4	3.4	3.4	3.3	3.4	3.7	3.4
Al (iv)	0.69	0.68	0.70	0.62	0.65	0.63	0.63	0.68	0.68	0.04	0.73	0.77	0.75	0.03	0.57	0.55	0.57	0.55	0.66	0.63	0.30	0.55
Total	**4.0**	**4.0**	**4.0**	**4.0**	**4.0**	**4.0**	**4.0**	**4.0**	4.0	0.0	**4.0**	**4.0**	4.0	0.0	**4.0**	**4.0**	**4.0**	**4.0**	**4.0**	**4.0**	**4.0**	**4.0**
Al (vi)	1.6	1.6	1.7	1.6	1.6	1.6	1.6	1.6	1.6	0.0	1.6	1.6	1.6	0.0	1.7	1.7	1.7	1.7	1.7	1.7	1.6	1.7
Cr	0.00	0.00	0.00	0.00	0.00	0.00	0.00	0.00	0.00	0.00	0.00	0.00	0.00	0.00	0.00	0.00	0.00	0.00	0.00	0.00	0.00	0.00
Mg	0.21	0.21	0.18	0.22	0.20	0.21	0.21	0.19	0.20	0.02	0.20	0.20	0.20	0.00	0.25	0.26	0.25	0.26	0.22	0.22	0.25	0.27
Fe	0.21	0.21	0.19	0.25	0.24	0.24	0.24	0.22	0.23	0.02	0.20	0.24	0.22	0.03	0.11	0.10	0.11	0.10	0.11	0.13	0.08	0.08
Mn	0.00	0.00	0.00	0.00	0.00	0.00	0.00	0.00	0.00	0.00	0.00	0.00	0.00	0.00	0.00	0.00	0.00	0.00	0.00	0.00	0.00	0.00
Ca	0.00	0.03	0.01	0.01	0.01	0.00	0.00	0.00	0.02	0.02	0.02	0.04	0.03	0.01	0.01	0.01	0.01	0.01	0.00	0.00	0.00	0.00
Ti	0.01	0.01	0.01	0.01	0.01	0.01	0.00	0.01	0.01	0.00	0.01	0.01	0.01	0.00	0.00	0.00	0.00	0.00	0.00	0.00	0.01	0.00
Total	**2.0**	**2.1**	**2.0**	**2.1**	**2.0**	**2.0**	**2.0**	**2.0**	2.1	0.0	**2.1**	**2.1**	2.1	0.0	**2.0**	**2.0**	**2.0**	**2.0**	**2.0**	**2.0**	**2.0**	**2.0**
TOTAL	**7.0**	**7.0**	**7.0**	**7.0**	**7.0**	**7.0**	**7.0**	**7.0**	7.0	0.0	**7.0**	**7.1**	7.0	0.0	**6.9**	**6.8**	**6.9**	**6.8**	**7.0**	**6.9**	**6.7**	**6.9**
F	0.28	0.21	0.24	0.29	0.27	0.28	0.25	0.25	0.23	0.06	0.25	0.19	0.22	0.05	0.12	0.13	0.12	0.13	0.27	0.19	0.11	0.12
Cl	0.00	0.00	0.01	0.01	0.00	0.02	0.01	0.00	0.02	0.03	0.01	0.07	0.04	0.04	0.00	0.00	0.00	0.00	0.00	0.00	0.00	0.00
OH	1.7	1.8	1.8	1.7	1.7	1.7	1.7	1.8	1.8	0.0	1.7	1.7	1.7	0.0	1.9	1.9	1.9	1.9	1.7	1.8	1.9	1.9
Total	2.0	2.0	2.0	2.0	2.0	2.0	2.0	2.0	2.0	0.0	2.0	2.0	2.0	0.0	2.0	2.0	2.0	2.0	2.0	2.0	2.0	2.0
phengite component %	20.5	21.9	18.9	24.1	21.6	22.5	22.7	20.4	21.9	1.6	20.7	23.3	22.0	1.8	18.2	18.3	18.2	18.3	16.7	17.8	17.7	17.5
Fe/(Fe+Mg)	0.50	0.51	0.52	0.53	0.54	0.54	0.53	0.54	0.54	0.02	0.51	0.54	0.53	0.02	0.31	0.28	0.31	0.28	0.33	0.38	0.24	0.23
% F-end-member	14.0	10.6	12.0	14.3	13.3	14.1	12.4	12.3	11.59	2.96	12.6	9.4	11.00	2.26	6.2	6.4	6.2	6.4	13.5	9.3	5.6	6.0
% Cl-end-member	0.1	0.2	0.2	0.2	0.1	0.7	0.3	0.1	0.83	1.30	0.6	3.6	2.10	2.12	0.1	0.1	0.1	0.1	0.1	0.1	0.2	0.1

Table A10: Complete electron microanalysis for mica (continued)

(Wt.%)	3aTW	3aTW	Mean (10)	Std.dev	31TW	31TW	31TW	31TW	31TW	31TW	31TW	31TW	Mean (8)	Std.dev
CaO	0.07	0.05	0.06	0.04	0.02	0.05	0.01	0.03	0.00	0.02	0.00	0.00	0.02	0.02
Na2O	0.07	0.15	0.13	0.03	0.05	0.07	0.05	0.09	0.07	0.08	0.09	0.07	0.07	0.02
K2O	10.1	10.1	10.0	0.5	9.3	9.2	9.7	9.1	9.4	8.4	9.6	9.6	9.3	0.4
FeO	2.60	2.02	2.00	0.35	3.20	4.09	3.52	4.16	4.13	3.17	3.51	3.19	3.62	0.44
TiO2	0.05	0.00	0.05	0.07	0.17	0.22	0.14	0.26	0.18	0.07	0.13	0.16	0.17	0.06
MgO	3.49	3.13	2.74	0.38	1.14	1.24	1.34	1.40	1.54	3.25	1.23	1.49	1.58	0.69
SiO2	53.5	53.6	53.5	2.3	47.9	47.9	48.9	48.6	49.1	52.6	49.1	48.3	49.0	1.5
MnO	0.01	0.00	0.01	0.01	0.00	0.01	0.05	0.01	0.00	0.00	0.00	0.05	0.02	0.02
Cr2O3	0.00	0.01	0.01	0.01	0.00	0.01	0.01	0.02	0.00	0.01	0.00	0.00	0.01	0.01
Al2O3	26.4	27.8	28.6	1.5	32.7	30.3	31.5	31.1	30.2	27.2	32.4	31.9	30.9	1.8
F (wt.%)	0.91	0.89	0.76	0.22	0.72	0.89	0.93	0.93	0.79	1.02	0.61	0.67	0.82	0.14
Cl (wt.%)	0.00	0.03	0.02	0.01	0.04	0.06	0.00	0.02	0.01	0.04	0.01	0.02	0.03	0.02
Total	**97.2**	**97.7**	98.0	1.3	**95.2**	**94.0**	**96.1**	**95.6**	**95.4**	**95.8**	**96.6**	**95.4**	95.5	0.8
Muscovite KAl2(Si3Al)O10														
Na	0.01	0.02	0.02	0.00	0.01	0.01	0.01	0.01	0.01	0.01	0.01	0.01	0.01	0.00
K	0.85	0.84	0.83	0.05	0.79	0.81	0.82	0.78	0.80	0.71	0.81	0.82	0.79	0.04
Total	**0.86**	**0.86**	0.85	0.05	**0.80**	**0.82**	**0.83**	**0.79**	**0.81**	**0.72**	**0.82**	**0.83**	0.80	0.04
Total Al	2.0	2.1	2.2	0.1	2.6	2.4	2.5	2.5	2.4	2.1	2.5	2.5	2.4	0.1
Si	3.5	3.5	3.5	0.1	3.2	3.3	3.3	3.3	3.3	3.5	3.2	3.2	3.3	0.1
Al (iv)	0.49	0.52	0.54	0.10	0.79	0.73	0.74	0.74	0.70	0.52	0.76	0.77	0.72	0.08
Total	**4.0**	**4.0**	4.0	0.0	**4.0**	**4.0**	**4.0**	**4.0**	**4.0**	**4.0**	**4.0**	**4.0**	4.0	0.0
Al (vi)	1.5	1.6	1.6	0.0	1.8	1.7	1.7	1.7	1.7	1.6	1.8	1.7	1.7	0.1
Cr	0.00	0.00	0.00	0.00	0.00	0.00	0.00	0.00	0.00	0.00	0.00	0.00	0.00	0.00
Mg	0.34	0.30	0.26	0.04	0.11	0.13	0.13	0.14	0.15	0.32	0.12	0.15	0.16	0.07
Fe	0.14	0.11	0.11	0.02	0.18	0.23	0.20	0.23	0.23	0.18	0.19	0.18	0.20	0.03
Mn	0.00	0.00	0.00	0.00	0.00	0.00	0.00	0.00	0.00	0.00	0.00	0.00	0.00	0.00
Ca	0.01	0.00	0.00	0.00	0.00	0.00	0.00	0.00	0.00	0.00	0.00	0.00	0.00	0.00
Ti	0.00	0.00	0.00	0.00	0.01	0.01	0.01	0.01	0.01	0.00	0.01	0.01	0.01	0.00
Total	**2.0**	**2.0**	2.0	0.0	**2.1**	**2.1**	**2.1**	**2.1**	**2.1**	**2.1**	**2.1**	**2.1**	2.1	0.0
TOTAL	**6.9**	**6.9**	6.9	0.1	**6.9**	**6.9**	**6.9**	**6.9**	**6.9**	**6.8**	**6.9**	**6.9**	6.9	0.0
F	0.19	0.18	0.16	0.05	0.15	0.19	0.20	0.20	0.17	0.21	0.13	0.14	0.17	0.03
Cl	0.00	0.00	0.00	0.00	0.00	0.01	0.00	0.00	0.00	0.01	0.00	0.00	0.00	0.00
OH	1.8	1.8	1.8	0.0	1.8	1.8	1.8	1.8	1.8	1.8	1.9	1.9	1.8	0.0
Total	2.0	2.0	2.0	0.0	2.0	2.0	2.0	2.0	2.0	2.0	2.0	2.0	2.0	0.0
phengite component %	24.1	20.6	18.7	2.1	14.5	18.0	16.3	18.4	18.9	23.8	15.4	16.2	17.7	2.9
Fe/(Fe+Mg)	0.30	0.27	0.29	0.04	0.61	0.65	0.60	0.63	0.60	0.35	0.62	0.55	0.58	0.10
% F-end-member	9.4	9.2	7.82	2.50	7.6	9.6	9.8	9.8	8.4	10.7	6.3	7.1	8.66	1.55
% Cl-end-member	0.0	0.2	0.11	0.06	0.2	0.3	0.0	0.1	0.0	0.2	0.1	0.1	0.13	0.10

Table A11: Complete data for trace and minor element (ppm) concentrations in bornite determined by LA-ICP-MS

Element	Ag	As	Au	Bi	Co	Ni	Pb	Sb	Se	Sn	Te	Tl
Purple Bornite Type A												
15TW	115	354	1.88	975	9.94	6.66	69667	13.62	74281	1.53	3208	74.0
15TW	110	194	2.10	1404	0.62	<2.06	97232	14.80	78951	<0.79	3275	90.3
15TW	46.8	108	5.93	458	<0.35	<2.04	8789	8.70	39625	<0.65	1229	57.7
15TW	52.7	294	10.7	451	8.93	5.90	6531	18.70	34121	<0.94	1055	79.4
15TW	38.9	6.61	12.1	446	0.59	<1.83	2278	28.55	53354	<0.65	1792	255
15TW	90.4	618	64.6	862	7.58	6.78	15364	29.63	45115	1.17	1718	58.81
Mean (6)	75.6	262	16.2	766	5.53	6.45	33310	19.0	54241	1.35	2046	103
Std.dev	30.6	196	22.0	355	4.09	0.39	36541	7.71	16905	0.18	883.4	69.1
Purple Bornite Type-B												
8TW	30.4	4.98	1.06	19.5	1.04	<1.50	256	5.34	2334	1.15	463	21.9
8TW	12.0	13.7	16.0	27.2	25.00	8.11	173	1.71	1982	2.50	838	30.4
8TW	96.5	5.44	130	13.7	3.45	1.97	115	1.37	2261	<0.62	1045	7.32
8TW	5.80	132	<0.33	8.56	12.46	4.35	114	3.68	1143	71.24	305	11.4
8TW	5.18	14.21	<0.40	9.27	13.37	4.04	138	1.44	2832	<0.72	887	18.7
8TW	7.30	<1.38	<0.43	5.18	<0.36	<2.06	130	2.58	1025	<0.81	116	9.49
8TW	11.0	5.64	<0.44	7.01	6.30	2.80	162	2.18	1808	<0.80	793	25.5
8TW	26.2	<1.69	<0.47	4.39	<0.45	<2.26	116	1.53	1128	<1.01	368	13.8
8TW	29.2	172	<0.48	17.3	37.28	13.84	191	9.69	2519	47.90	1373	46.7
Mean (9)	24.8	49.7	48.9	12.4	14.1	5.9	155	3.3	1892	30.7	688	20.6
Std.dev	28.7	70.9	70.3	7.6	12.9	4.4	47.0	2.7	663	34.7	403	12.4
6TW	7.86	598	<0.29	71.3	63.97	<4.76	326	4.13	172	<0.87	19	28.7
6TW	12.2	97.11	<0.34	19.3	24.68	8.44	508	1.73	5406	3.18	307	28.6
6TW	15.7	2.92	<0.35	52.8	2.91	4.50	8447	<0.49	11001	<0.82	1280	11.2
6TW	9.15	1.63	<0.36	17.2	14.34	5.28	2291	0.66	6685	6.45	545	12.6
6TW	23.0	55.30	<0.37	97.3	8.41	<4.36	737.10	1.64	5726	<0.88	757	41.7
6TW	15.4	25.71	<0.39	38.8	10.91	3.74	3866	0.58	8433	1.15	771	18.7
6TW	12.5	5.74	<0.39	60.9	10.78	22.63	8729	0.51	11749	1.13	1115	15.4
6TW	8.92	<1.66	<0.40	1.44	<0.51	<2.13	514	<0.37	7423	<0.84	723	4.81
6TW	8.81	27.93	<0.41	43.9	119	42.34	5158	0.62	7111	0.94	603	18.82
6TW	28.2	<1.40	<0.41	2.07	<0.45	<1.91	366	<0.37	6109	<0.81	637	9.66
6TW	12.5	8.46	<0.42	28.1	5.91	3.39	6364	0.46	10641	5.22	910	14.7
6TW	38.8	<1.49	<0.42	0.87	<0.37	<2.09	812	<0.41	7203	<0.81	536	2.8
6TW	20.2	8297	<0.47	120	1784.56	94.02	923	133.95	746	1.70	28	45.0
6TW	24.7	132	<0.48	26.47	31.00	13.32	784	2.23	6451	3.90	749	42.7
Mean (14)	17.0	841	<mdl	41.5	189	22.0	2845	14.7	6775	2.96	641	21.1
Std.dev	9.00	2479	<mdl	36.2	530	29.8	3101	41.9	3334	2.09	356	14.0
Mean (23)	**20.6**	**486**	**53.2**	**28.5**	**110**	**14.3**	**1657**	**8.7**	**4578**	**15.1**	**650**	**20.5**
Std.dev	**18.3**	**1843**	**50.7**	**30.9**	**395**	**22.8**	**2661**	**28.8**	**3554**	**22.2**	**355**	**12.7**
Brown Bornite												
31TW	10.4	5.31	<0.133	69.4	3.80	3.16	9.74	<0.194	35.2	<0.40	<1.53	0.10
31TW	8.78	<2.23	<0.161	64.8	<0.98	<2.56	12.4	<0.183	47.7	<0.44	<1.74	0.09
31TW	21.7	13.6	<0.165	79.5	8.86	4.03	52.6	0.97	48.5	0.48	3.65	0.41
31TW	21.6	4.59	<0.168	78.6	3.63	3.37	28.1	1.56	64.5	<0.52	1.76	0.21
31TW	21.9	7.29	<0.169	78.9	6.25	<2.42	31.73	0.47	64.7	0.95	1.73	0.21
31TW	11.6	8.07	<0.171	67.0	3.31	3.19	18.53	0.35	52.1	0.68	1.89	0.14
31TW	42.2	14.56	<0.174	81.0	6.34	4.07	49.0	1.89	68.0	1.04	2.86	0.49
Mean (7)	19.7	8.91	<mdl	74.2	5.37	3.56	28.9	1.05	54.4	0.79	2.38	0.24
Std.dev	11.5	4.22	<mdl	6.82	2.17	0.45	16.9	0.67	11.9	0.26	0.85	0.15
33TW	16.9	<0.67	<0.200	49.2	<0.205	<1.16	1.79	<0.203	43.7	0.43	<1.25	<0.078
33TW	12.0	<0.62	<0.210	45.2	0.25	<1.11	0.33	<0.181	104	0.40	1.55	<0.072
33TW	17.5	<0.74	<0.229	48.0	<0.209	<1.13	5.74	<0.182	109	0.86	1.35	0.11
33TW	12.0	<0.75	<0.235	44.4	<0.195	<1.08	0.43	<0.215	52.3	0.55	<1.65	<0.074
33TW	12.0	<0.73	<0.257	47.8	<0.226	<1.26	2.61	<0.213	40.0	0.51	<1.48	0.11
Mean (5)	14.1	<mdl	<mdl	46.9	0.25	<mdl	2.18	<mdl	69.7	0.55	1.45	0.11
Std.dev	2.84	<mdl	<mdl	2.01	<mdl	<mdl	2.21	<mdl	33.8	0.18	0.14	0.00
32TW	7.99	<1.37	<0.42	71.8	<0.43	<1.84	23.7	<0.33	40.0	<0.77	<2.36	0.21
32TW	20.3	<1.83	<0.42	73.1	<0.34	<2.24	22.0	<0.38	38.9	<0.79	<2.84	<0.139
32TW	29.6	<1.72	<0.44	79.1	<0.36	<2.11	30.4	<0.45	35.4	<0.87	<2.78	0.33
32TW	19.0	<1.85	<0.45	83.1	1.57	<2.85	32.0	0.52	46.6	<0.87	5.64	0.33
32TW	12.6	<1.67	<0.46	77.5	<0.39	<1.91	45.6	<0.42	56.7	<0.82	6.64	0.50
32TW	23.5	<1.77	<0.48	79.9	<0.36	<1.91	12.7	<0.39	41.9	<0.79	<2.88	0.13
32TW	12.5	<1.62	<0.51	72.3	<0.39	<2.24	15.2	<0.43	35.1	<0.80	<3.12	<0.144
32TW	28.5	4.62	<0.56	104.67	5.03	<2.52	95.97	0.65	56.8	5.35	<3.25	1.40
Mean (8)	19.26	4.62	<mdl	80.19	3.30	<mdl	34.69	0.59	43.92	5.35	6.14	0.48
Std.dev	7.82	-	<mdl	10.68	2.45	<mdl	26.85	0.09	8.72	-	0.71	0.47
Mean (20)	**18.1**	**8.29**	**<mdl**	**69.8**	**4.34**	**3.56**	**24.5**	**0.92**	**54.0**	**1.13**	**3.01**	**0.32**
Std.dev	**8.45**	**4.18**	**<mdl**	**15.7**	**2.62**	**0.45**	**23.2**	**0.59**	**20.5**	**1.50**	**1.93**	**0.33**

Table A11: Complete data for trace and minor element (ppm) concentrations in bornite determined by LA-ICP-MS (continued)

Red Bornite												
40TW	19.2	47.0	2.85	4.76	4.93	<3.16	227	4.78	76.6	3.33	11.4	17.0
40TW	79.9	<1.12	<0.32	7.03	<0.35	<1.77	15.2	<0.31	91.8	<0.73	<2.23	0.63
Mean (2)	49.5	47.04	2.85	5.90	4.93	<mdl	121	4.78	84.2	3.33	11.4	8.84
39TW	9.46	<1.69	<0.38	1.98	<0.35	<1.49	44.2	0.75	46.6	<0.66	2.50	5.38
39TW	8.65	<1.83	<0.38	2.26	<0.35	<1.84	29.7	0.53	43.3	<0.65	2.71	2.50
39TW	4.59	<1.92	<0.45	1.80	<0.36	<1.88	18.9	<0.46	46.7	<0.76	2.85	2.75
39TW	19.3	<1.73	<0.45	0.79	<0.39	<1.68	32.8	0.47	37.1	<0.78	<2.45	2.36
39TW	14.0	<1.79	<0.54	2.55	7.42	2.64	60.8	0.78	55.5	<0.91	9.58	4.57
39TW	14.2	<1.96	<0.60	1.53	<0.47	<2.49	30.4	0.50	42.4	<1.08	4.94	2.08
39TW	11.2	<1.93	<0.61	2.10	0.54	<2.64	67.5	1.02	48.4	<1.08	7.96	5.90
39TW	13.6	3.64	<0.64	2.76	1.57	<2.62	78.2	1.83	50.8	1.27	6.56	7.62
39TW	20.3	<2.23	<0.67	1.98	<0.58	<2.72	95.3	<0.50	58.4	<1.21	10.2	5.84
39TW	16.3	<47.65	<15.69	<3.95	<12.36	79.14	404	19.00	424	<28.21	<94.32	36.6
Mean (10)	13.15	3.64	<mdl	1.97	3.18	40.89	86.20	3.11	85.29	1.27	5.92	7.56
Std.dev	4.84	-	<mdl	0.58	3.71	54.09	114.30	6.44	119.14	-	3.14	10.36
Mean (12)	**19.22**	**25.3**	**2.85**	**2.69**	**3.62**	**40.9**	**92.0**	**3.30**	**85.1**	**2.30**	**6.53**	**7.77**
Std.dev	**19.68**	**30.7**	**-**	**1.74**	**3.15**	**54.1**	**114**	**6.05**	**108**	**1.46**	**3.46**	**10.0**

Table A12: Complete data for trace and minor element (ppm) concentrations in chalcocite determined by LA-ICP-MS

Element	Ag	As	Au	Bi	Co	Ni	Pb	Sb	Se	Sn	Te	Tl
Blue Chalcocite												
6TW	6.44	8.91	0.6	0.7	7.04	<mdl	4.15	<mdl	4916	<mdl	424	0.179
6TW	6.1	8.56	<mdl	0.5	10.2	7.44	3.89	<mdl	3770	<mdl	311	<mdl
6TW	7.37	<mdl	<mdl	6.65	9.18	8.38	2832	<mdl	8749	<mdl	895	3.37
6TW	13.7	10.4	<mdl	3.89	9.35	<mdl	43.57	1.03	1233	3.98	11.0	2.34
6TW	12.5	1819	<mdl	7.34	152	12.08	59.77	16.69	804	<mdl	7.9	4.37
Mean(5)	9.21	462	0.60	3.82	37.5	9.30	589	8.86	3894	3.98	330	2.56
Std.dev	3.20	784	0.00	2.87	57.1	2.00	1122	7.83	2873	0.00	327	1.55
15TW	6.06	<mdl	<mdl	26.6	<mdl	<mdl	11.74	<mdl	33522	<mdl	1301	1.33
Mean (6)	**8.69**	**462**	**0.60**	**7.61**	**37.5**	**9.30**	**493**	**8.86**	**8832**	**3.98**	**492**	**2.32**
Std.dev	**3.45**	**905**	**<mdl**	**9.73**	**63.8**	**2.45**	**1146**	**11.1**	**12432**	**<mdl**	**514**	**1.65**
Grey Chalcocite												
39TW	27.9	<mdl	<mdl	<mdl	<mdl	<mdl	2.61	<mdl	33.6	<mdl	3.45	0.21
39TW	35.2	<mdl	<mdl	<mdl	<mdl	<mdl	6.28	<mdl	42.0	<mdl	7.75	0.37
39TW	33.6	<mdl	<mdl	<mdl	<mdl	<mdl	1.64	<mdl	47.9	<mdl	7.71	0.21
39TW	28.4	<mdl	<mdl	<mdl	<mdl	<mdl	1.24	<mdl	34.7	<mdl	7.73	0.16
39TW	28.9	<mdl	<mdl	<mdl	<mdl	<mdl	1.09	<mdl	38.0	<mdl	<mdl	<mdl
39TW	31.9	<mdl	<mdl	<mdl	<mdl	<mdl	2.12	<mdl	40.2	<mdl	6.46	<mdl
39TW	32.7	<mdl	<mdl	<mdl	<mdl	<mdl	<mdl	<mdl	29.4	<mdl	<3.54	<mdl
39TW	31.8	2.11	<mdl	<mdl	<mdl	<mdl	3.05	<mdl	39.9	<mdl	8.03	0.271
39TW	29.2	<mdl	<mdl	<mdl	<mdl	<mdl	1.01	<mdl	41.3	<mdl	6.34	<mdl
39TW	33.9	<mdl	<mdl	<mdl	<mdl	<mdl	1.73	<mdl	62.7	<mdl	5.69	<mdl
39TW	33.4	<mdl	<mdl	<mdl	<mdl	<mdl	<mdl	<mdl	25.5	<mdl	<mdl	<mdl
39TW	32.9	<mdl	<mdl	<mdl	<mdl	<mdl	1.57	<mdl	36.6	<mdl	<mdl	0.246
39TW	34.0	<mdl	<mdl	<mdl	<mdl	<mdl	0.86	<mdl	58.1	<mdl	<mdl	<mdl
39TW	38.2	<mdl	<mdl	<mdl	<mdl	<mdl	2.18	<mdl	70.2	<mdl	<mdl	<mdl
39TW	38.8	<mdl	<mdl	<mdl	<mdl	<mdl	4.48	<mdl	87.8	<mdl	6.29	0.35
Mean (15)	32.7	2.11	<mdl	<mdl	<mdl	<mdl	2.30	<mdl	45.9	<mdl	6.6	0.3
Std.dev	3.25	-	<mdl	<mdl	<mdl	<mdl	1.55	<mdl	16.89	<mdl	1.45	0.08
Grey Chalcocite												
40TW	160	<mdl	<mdl	<mdl	<mdl	<mdl	0.63	<mdl	37.5	<mdl	<mdl	<mdl
40TW	181	<mdl	<mdl	<mdl	<mdl	<mdl	3.99	<mdl	32.2	<mdl	<mdl	0.28
40TW	163	<mdl	<mdl	<mdl	<mdl	<mdl	0.89	<mdl	34.8	<mdl	<mdl	<mdl
40TW	152	<mdl	<mdl	<mdl	<mdl	<mdl	1.29	<mdl	33.3	<mdl	<mdl	<mdl
40TW	175	<mdl	<mdl	<mdl	<mdl	<mdl	9.69	<mdl	80.0	<mdl	<mdl	<mdl
40TW	131	<mdl	<mdl	0.70	<mdl	<mdl	25.1	<mdl	90.7	<mdl	<mdl	0.44
40TW	174	<mdl	<mdl	<mdl	<mdl	<mdl	3.2	<mdl	26.6	<mdl	<mdl	<mdl
40TW	177	<mdl	<mdl	<mdl	<mdl	<mdl	1.57	<mdl	77.7	<mdl	<mdl	<mdl
40TW	172	<mdl	<mdl	<mdl	<mdl	<mdl	7.74	<mdl	66.9	<mdl	<mdl	0.43
40TW	192	<mdl	<mdl	<mdl	<mdl	<mdl	0.43	<mdl	78.7	<mdl	<mdl	0.21
40TW	161	<mdl	<mdl	<mdl	<mdl	<mdl	5.33	<mdl	55.9	<mdl	<mdl	<mdl
40TW	160	<mdl	<mdl	<mdl	<mdl	<mdl	<mdl	<mdl	79.0	<mdl	<mdl	<mdl
Mean (12)	166	<mdl	<mdl	0.70	<mdl	<mdl	5.45	<mdl	57.8	<mdl	<mdl	0.34
Std.dev	15.3	<mdl	<mdl	0.00	<mdl	<mdl	15.3	<mdl	15.3	<mdl	<mdl	15.3
Mean (27)	**92.2**	**2.11**	<mdl	**0.70**	<mdl	<mdl	**3.74**	<mdl	**51.2**	<mdl	**6.61**	**0.29**
Std.dev	**68.6**	**-**	**<mdl**	**-**	**<mdl**	**<mdl**	**5.14**	**<mdl**	**20.6**	**<mdl**	**1.45**	**0.09**
Grey Chalcocite + Au-Cu												
3bTW	0.47	8.94	12.1	2.73	8.95	5.39	13.5	2.06	464	0.95	2967.46	0.88
3bTW	0.73	8.02	18.0	<mdl	5.16	<mdl	7.86	0.3	57.69	0.83	23.23	0.3
3bTW	0.57	<mdl	28.96	3.11	1.98	<5.14	10.08	<mdl	78.3	<mdl	101.43	0.9
3bTW	0.84	4.71	837	12.21	<mdl	<mdl	13.2	0.8	90.8	<mdl	274.99	0.174
3bTW	3.37	<mdl	5027	30.4	13.44	5.54	29.2	13.23	408	<mdl	2286.55	1.07
Mean (5)	**1.20**	**7.22**	**1185**	**12.1**	**7.38**	**5.47**	**14.76**	**4.10**	**219.7**	**0.89**	**1131**	**0.67**
Std.dev	**1.22**	**2.22**	**2177**	**12.94**	**4.94**	**0.11**	**8.40**	**6.13**	**199**	**0.08**	**1389.95**	**0.40**

Table A12: Complete data for trace and minor element (ppm) concentrations in chalcocite determined by LA-ICP-MS (continued)

Element	Ag	As	Au	Bi	Co	Ni	Pb	Sb	Se	Sn	Te	Tl
White Chalcocite												
28TW	55.1	<mdl	<mdl	6.45	25.97	10.58	2	<mdl	355	<mdl	12.2	<mdl
28TW	54.9	4.58	<mdl	17.4	1.98	<mdl	15.02	<mdl	587	0.72	17.8	<mdl
28TW	36.7	<mdl	<mdl	8.55	<mdl	<mdl	1.27	<mdl	385	<mdl	10.4	<mdl
28TW	51.2	<mdl	<mdl	5.03	<mdl	<mdl	0.58	<mdl	213	<mdl	7.76	<mdl
28TW	56.2	<mdl	<mdl	6.11	<mdl	<mdl	0.95	<mdl	194	<mdl	15.7	<mdl
28TW	51.9	<mdl	<mdl	3.74	<mdl	<mdl	<mdl	<mdl	156	<mdl	11.3	<mdl
28TW	54.4	<mdl	<mdl	7.67	<mdl	<mdl	2.73	<mdl	191	<mdl	11.1	<mdl
28TW	55.4	3.35	<mdl	16.4	<mdl	<mdl	25.4	1.99	800	<mdl	21.7	0.65
28TW	52.0	<mdl	<mdl	3.67	<mdl	<mdl	<mdl	<mdl	68	<mdl	6.67	<mdl
28TW	21.6	3.7	<mdl	8.76	<mdl	<mdl	3.38	<mdl	340	1.5	11.5	<mdl
Mean (10)	48.9	3.88	<mdl	8.37	14.0	10.6	6.42	1.99	329	1.11	12.6	0.65
Std.dev	10.6	0.52	<mdl	4.57	12.0	0.00	8.42	0.00	210	0.39	4.34	0.00
23TW	38.1	<mdl	<mdl	2.07	0.37	<mdl	2.87	<mdl	273	<mdl	85.5	<mdl
23TW	35.1	8.11	<mdl	10.6	1.13	4.31	10.3	<mdl	273	1.39	67.5	<mdl
23TW	45.6	<mdl	<mdl	2.65	<mdl	<mdl	3.2	<mdl	305	<mdl	88.5	<mdl
23TW	60.4	<mdl	<mdl	8.94	2.68	<mdl	11.6	0.67	290	<mdl	64.1	<mdl
23TW	57.3	<mdl	<mdl	3.13	0.41	<mdl	4.42	<mdl	251	<mdl	85.1	<mdl
23TW	58.6	<mdl	<mdl	4.68	<mdl	<mdl	7.81	<mdl	255	<mdl	73.2	<mdl
23TW	59.6	28.17	<mdl	16.8	1.95	<mdl	32.0	8.94	330	4.02	104	0.54
23TW	53.7	<mdl	<mdl	5.33	0.58	<mdl	5.48	<mdl	318	<mdl	81.3	<mdl
23TW	46.5	<mdl	<mdl	3.02	15.23	<mdl	3.3	<mdl	319	<mdl	62.7	<mdl
23TW	51.8	<mdl	<mdl	9.2	0.89	<mdl	6.12	<mdl	349	<mdl	100	<0.23
Mean (10)	50.7	18.1	<mdl	6.6	2.9	4.3	8.7	4.8	296.3	2.7	81.3	0.5
Std.Dev	8.6	10.0	<mdl	4.5	4.7	0.0	8.3	4.1	31.3	1.3	13.7	0.0
17TW	44.2	2.49	<mdl	2.11	1.21	2.94	3.76	<mdl	244	<mdl	15.2	0.05
17TW	56.5	2.89	<mdl	1.96	<mdl	<mdl	2.06	<mdl	193	<mdl	6.76	<mdl
17TW	55.6	2.99	<mdl	3.52	2.35	<mdl	61.1	0.24	219	0.37	4.34	0.068
17TW	62.7	<mdl	<mdl	2.02	<mdl	<mdl	0.54	<mdl	190	<mdl	6.32	<mdl
17TW	61.2	1.68	<mdl	2.22	1.48	<mdl	0.43	<mdl	205	0.68	3.34	<mdl
17TW	27.5	9.99	<mdl	2.18	2.47	<mdl	1.48	0.36	266	2.63	6.55	<mdl
17TW	59.5	3.16	<mdl	2.32	1.77	2.19	3.03	<mdl	225	<mdl	5.49	0.039
17TW	41.8	<mdl	<mdl	1.44	0.84	2.11	0.33	<mdl	208	<0.46	13.4	0.04
17TW	59.0	<mdl	<mdl	2.72	<mdl	<mdl	11.17	<mdl	241	0.49	5.95	0.06
17TW	65.9	<mdl	<mdl	2.11	1.4	<mdl	0.18	<mdl	218	0.58	2.88	<mdl
17TW	18.9	5.13	<mdl	2.88	2.8	<mdl	7.24	<mdl	269	<mdl	6.39	0.08
Mean (11)	50.2	4.05	<mdl	2.32	1.8	2.41	8.30	0.30	225	0.95	7.0	0.06
Std.dev	15.3	2.82	<mdl	0.55	0.68	0.46	17.8	0.08	27.0	0.95	3.86	0.02
Mean (31)	**50.0**	**6.35**	**<mdl**	**5.67**	**3.64**	**4.43**	**7.92**	**2.44**	**282**	**1.38**	**32.8**	**0.19**
Std.dev	**11.9**	**7.28**	**<mdl**	**4.53**	**6.48**	**3.55**	**12.6**	**3.70**	**131**	**1.22**	**35.2**	**0.25**